

IAEA Nuclear Energy Series

No. NF-T-2.2

Basic
Principles

Objectives

Guides

Technical
Reports

Accelerator Simulation and Theoretical Modelling of Radiation Effects in Structural Materials



IAEA

International Atomic Energy Agency

IAEA NUCLEAR ENERGY SERIES PUBLICATIONS

STRUCTURE OF THE IAEA NUCLEAR ENERGY SERIES

Under the terms of Articles III.A and VIII.C of its Statute, the IAEA is authorized to foster the exchange of scientific and technical information on the peaceful uses of atomic energy. The publications in the **IAEA Nuclear Energy Series** provide information in the areas of nuclear power, nuclear fuel cycle, radioactive waste management and decommissioning, and on general issues that are relevant to all of the above mentioned areas. The structure of the IAEA Nuclear Energy Series comprises three levels: **1 – Basic Principles and Objectives**; **2 – Guides**; and **3 – Technical Reports**.

The **Nuclear Energy Basic Principles** publication describes the rationale and vision for the peaceful uses of nuclear energy.

Nuclear Energy Series Objectives publications explain the expectations to be met in various areas at different stages of implementation.

Nuclear Energy Series Guides provide high level guidance on how to achieve the objectives related to the various topics and areas involving the peaceful uses of nuclear energy.

Nuclear Energy Series Technical Reports provide additional, more detailed information on activities related to the various areas dealt with in the IAEA Nuclear Energy Series.

The IAEA Nuclear Energy Series publications are coded as follows: **NG** – general; **NP** – nuclear power; **NF** – nuclear fuel; **NW** – radioactive waste management and decommissioning. In addition, the publications are available in English on the IAEA Internet site:

<http://www.iaea.org/Publications/index.html>

For further information, please contact the IAEA at PO Box 100, Vienna International Centre, 1400 Vienna, Austria.

All users of the IAEA Nuclear Energy Series publications are invited to inform the IAEA of experience in their use for the purpose of ensuring that they continue to meet user needs. Information may be provided via the IAEA Internet site, by post, at the address given above, or by email to Official.Mail@iaea.org.

ACCELERATOR SIMULATION
AND THEORETICAL MODELLING
OF RADIATION EFFECTS IN
STRUCTURAL MATERIALS

The following States are Members of the International Atomic Energy Agency:

AFGHANISTAN	GERMANY	PALAU
ALBANIA	GHANA	PANAMA
ALGERIA	GREECE	PAPUA NEW GUINEA
ANGOLA	GRENADA	PARAGUAY
ANTIGUA AND BARBUDA	GUATEMALA	PERU
ARGENTINA	GUYANA	PHILIPPINES
ARMENIA	HAITI	POLAND
AUSTRALIA	HOLY SEE	PORTUGAL
AUSTRIA	HONDURAS	QATAR
AZERBAIJAN	HUNGARY	REPUBLIC OF MOLDOVA
BAHAMAS	ICELAND	ROMANIA
BAHRAIN	INDIA	RUSSIAN FEDERATION
BANGLADESH	INDONESIA	RWANDA
BARBADOS	IRAN, ISLAMIC REPUBLIC OF	SAINT VINCENT AND THE GRENADINES
BELARUS	IRAQ	SAN MARINO
BELGIUM	IRELAND	SAUDI ARABIA
BELIZE	ISRAEL	SENEGAL
BENIN	ITALY	SERBIA
BOLIVIA, PLURINATIONAL STATE OF	JAMAICA	SEYCHELLES
BOSNIA AND HERZEGOVINA	JAPAN	SIERRA LEONE
BOTSWANA	JORDAN	SINGAPORE
BRAZIL	KAZAKHSTAN	SLOVAKIA
BRUNEI DARUSSALAM	KENYA	SLOVENIA
BULGARIA	KOREA, REPUBLIC OF	SOUTH AFRICA
BURKINA FASO	KUWAIT	SPAIN
BURUNDI	KYRGYZSTAN	SRI LANKA
CAMBODIA	LAO PEOPLE'S DEMOCRATIC REPUBLIC	SUDAN
CAMEROON	LATVIA	SWEDEN
CANADA	LEBANON	SWITZERLAND
CENTRAL AFRICAN REPUBLIC	LESOTHO	SYRIAN ARAB REPUBLIC
CHAD	LIBERIA	TAJIKISTAN
CHILE	LIBYA	THAILAND
CHINA	LIECHTENSTEIN	THE FORMER YUGOSLAV REPUBLIC OF MACEDONIA
COLOMBIA	LITHUANIA	TOGO
CONGO	LUXEMBOURG	TRINIDAD AND TOBAGO
COSTA RICA	MADAGASCAR	TUNISIA
CÔTE D'IVOIRE	MALAWI	TURKEY
CROATIA	MALAYSIA	TURKMENISTAN
CUBA	MALI	UGANDA
CYPRUS	MALTA	UKRAINE
CZECH REPUBLIC	MARSHALL ISLANDS	UNITED ARAB EMIRATES
DEMOCRATIC REPUBLIC OF THE CONGO	MAURITANIA	UNITED KINGDOM OF GREAT BRITAIN AND NORTHERN IRELAND
DENMARK	MAURITIUS	UNITED REPUBLIC OF TANZANIA
DJIBOUTI	MEXICO	UNITED STATES OF AMERICA
DOMINICA	MONACO	URUGUAY
DOMINICAN REPUBLIC	MONGOLIA	UZBEKISTAN
ECUADOR	MONTENEGRO	VANUATU
EGYPT	MOROCCO	VENEZUELA, BOLIVARIAN REPUBLIC OF
EL SALVADOR	MOZAMBIQUE	VIET NAM
ERITREA	MYANMAR	YEMEN
ESTONIA	NAMIBIA	ZAMBIA
ESWATINI	NEPAL	ZIMBABWE
ETHIOPIA	NETHERLANDS	
FIJI	NEW ZEALAND	
FINLAND	NICARAGUA	
FRANCE	NIGER	
GABON	NIGERIA	
GEORGIA	NORWAY	
	OMAN	
	PAKISTAN	

The Agency's Statute was approved on 23 October 1956 by the Conference on the Statute of the IAEA held at United Nations Headquarters, New York; it entered into force on 29 July 1957. The Headquarters of the Agency are situated in Vienna. Its principal objective is "to accelerate and enlarge the contribution of atomic energy to peace, health and prosperity throughout the world".

IAEA NUCLEAR ENERGY SERIES No. NF-T-2.2

ACCELERATOR SIMULATION
AND THEORETICAL MODELLING
OF RADIATION EFFECTS IN
STRUCTURAL MATERIALS

INTERNATIONAL ATOMIC ENERGY AGENCY
VIENNA, 2018

COPYRIGHT NOTICE

All IAEA scientific and technical publications are protected by the terms of the Universal Copyright Convention as adopted in 1952 (Berne) and as revised in 1972 (Paris). The copyright has since been extended by the World Intellectual Property Organization (Geneva) to include electronic and virtual intellectual property. Permission to use whole or parts of texts contained in IAEA publications in printed or electronic form must be obtained and is usually subject to royalty agreements. Proposals for non-commercial reproductions and translations are welcomed and considered on a case-by-case basis. Enquiries should be addressed to the IAEA Publishing Section at:

Marketing and Sales Unit, Publishing Section
International Atomic Energy Agency
Vienna International Centre
PO Box 100
1400 Vienna, Austria
fax: +43 1 2600 29302
tel.: +43 1 2600 22417
email: sales.publications@iaea.org
<http://www.iaea.org/books>

© IAEA, 2018

Printed by the IAEA in Austria

September 2018

STI/PUB/1732

IAEA Library Cataloguing in Publication Data

Names: International Atomic Energy Agency.

Title: Accelerator simulation and theoretical modelling of radiation effects in structural materials / International Atomic Energy Agency.

Description: Vienna : International Atomic Energy Agency, 2018. | Series: IAEA nuclear energy series, ISSN 1995-7807 ; no. NF-T-2.2 | Includes bibliographical references.

Identifiers: IAEAL 18-01158 | ISBN 978-92-0-107415-7 (paperback : alk. paper)

Subjects: LCSH: Nuclear reactors — Materials — Testing. | Materials — Effect of radiation on. | Alloys — Testing.

Classification: UDC 621.039.526:620.1 | STI/PUB/1732

FOREWORD

One of the IAEA's statutory objectives is to "seek to accelerate and enlarge the contribution of atomic energy to peace, health and prosperity throughout the world." One way this objective is achieved is through the publication of a range of technical series. Two of these are the IAEA Nuclear Energy Series and the IAEA Safety Standards Series.

According to Article III.A.6 of the IAEA Statute, the safety standards establish "standards of safety for protection of health and minimization of danger to life and property". The safety standards include the Safety Fundamentals, Safety Requirements and Safety Guides. These standards are written primarily in a regulatory style, and are binding on the IAEA for its own programmes. The principal users are the regulatory bodies in Member States and other national authorities.

The IAEA Nuclear Energy Series comprises reports designed to encourage and assist R&D on, and application of, nuclear energy for peaceful uses. This includes practical examples to be used by owners and operators of utilities in Member States, implementing organizations, academia, and government officials, among others. This information is presented in guides, reports on technology status and advances, and best practices for peaceful uses of nuclear energy based on inputs from international experts. The IAEA Nuclear Energy Series complements the IAEA Safety Standards Series.

This report addresses how to test and ensure the reliability of next generation structural alloys for use in fuel cladding and in-core components of fast reactors and other advanced nuclear power systems that will experience very high neutron doses. These new alloys are currently under development and will most likely be ferritic and ferritic–martensitic alloys, as well as oxide dispersion strengthened versions of the alloys.

The neutron induced damage levels experienced by the new alloys during high exposures will exceed those previously attained during exposures of alloys currently in use. To reach these higher exposures requires decades of use of a very limited number of high flux test reactors with equally limited test volumes. Such high flux spectrum material test reactors currently in operation are BOR-60 in the Russian Federation, the Fast Breeder Test Reactor (FBTR) in India and JOYO in Japan; more are under development, including the Multi-purpose hYbrid Research Reactor (MYRRHA) in Belgium, the Advanced Sodium Technological Reactor for Industrial Development (ASTRID) in France and the Multipurpose Fast-neutron Research Reactor (MBIR) in the Russian Federation. It is obvious that the shorter time frame associated with alloy development and testing is incompatible with the longer time frame involved in the design and construction of next generation advanced reactors within the coming decades. To proceed with design and construction, designers must be able to predict the behaviour and possible degradation of alloy properties throughout the lifetime of each structural component. As the issue of limited test volume cannot be overcome, surrogate irradiation techniques can be used to simulate the damage generation process, exploring the physical origins of damage generation and accumulation, as well as the consequences of such damage as expressed in changes in mechanical properties, especially embrittlement and strength, and in dimensional instabilities arising from void swelling and irradiation creep.

Currently, a promising surrogate experimental technique that allows for attainment of sufficiently high levels of radiation damage in a reasonably short time involves the use of charged particle accelerators operating at damage rates that are orders of magnitude larger than those characteristic of typical test reactors. However, simulation by accelerators involves some well-known, neutron atypical phenomena that must be taken into account. Additionally, such simulations cannot explore all relevant damage processes or cover all required material and environmental parameters. Therefore, multiscale theoretical and computer modelling must be employed to partially bridge these gaps. To meet this dual experimental–calculational need, the IAEA Technical Working Group on Fuel Performance and Technology recommended the initiation of a coordinated research project (CRP) entitled Accelerator Simulation and Theoretical Modelling of Radiation Effects (SMoRE), which has combined the efforts of 19 leading nuclear research and development organizations from 15 Member States. The first research coordination meeting was held in November 2008 at the IAEA Headquarters in Vienna, followed by the second meeting in June 2010 in Paris and the final meeting in December 2011, again at IAEA Headquarters.

This publication contains the results of the SMoRE CRP, including the discussion and conclusions, and also four state of the art reviews of the major research areas under consideration: analysis of critical high dose neutron irradiation data; description of accelerator simulation methodologies used for materials research; presentation of multiscale modelling tools for predicting the evolution of materials under irradiation; and overview of advanced

experimental testing and characterization techniques. Reports from the individual CRP member organizations are compiled in the attached CD-ROM. These individual reports present the current status of experimental and theoretical efforts aimed towards development of new radiation resistant structural alloys for advanced nuclear power applications.

The IAEA wishes to thank all the participants for their contributions to this CRP, with particular gratitude to F.A. Garner (United States of America), who provided technical advice throughout the project. The IAEA officers responsible for this publication were V. Inozemtsev of the Division of Nuclear Fuel Cycle and Waste Technology, and A. Zeman of the Division of Physical and Chemical Sciences.

EDITORIAL NOTE

This publication has been edited by the editorial staff of the IAEA to the extent considered necessary for the reader's assistance. It does not address questions of responsibility, legal or otherwise, for acts or omissions on the part of any person.

Although great care has been taken to maintain the accuracy of information contained in this publication, neither the IAEA nor its Member States assume any responsibility for consequences which may arise from its use.

Guidance provided here, describing good practices, represents expert opinion but does not constitute recommendations made on the basis of a consensus of Member States.

The use of particular designations of countries or territories does not imply any judgement by the publisher, the IAEA, as to the legal status of such countries or territories, of their authorities and institutions or of the delimitation of their boundaries.

The mention of names of specific companies or products (whether or not indicated as registered) does not imply any intention to infringe proprietary rights, nor should it be construed as an endorsement or recommendation on the part of the IAEA.

The IAEA has no responsibility for the persistence or accuracy of URLs for external or third party Internet web sites referred to in this book and does not guarantee that any content on such web sites is, or will remain, accurate or appropriate.

CONTENTS

1.	INTRODUCTION	1
1.1.	Background	1
1.2.	Objective	2
1.3.	Scope	2
1.4.	Structure	2
2.	THE CHALLENGE OF USING ION IRRADIATION TO DEVELOP AND TEST ADVANCED ALLOYS FOR APPLICATION TO VERY HIGH NEUTRON EXPOSURES IN FUTURE REACTOR CONCEPTS	4
2.1.	Introduction	4
2.2.	Materials problems of irradiated austenitic alloys relevant to this coordinated research project	5
2.3.	Void swelling of ferritic–martensitic steels	13
2.4.	Early ion irradiation results for comparison with neutron examples	17
2.5.	Conclusions	20
	References to Chapter 2	21
3.	ACCELERATORS FOR SIMULATION OF RADIATION DAMAGE	23
3.1.	Introduction	23
3.2.	Simulation experiments	24
3.3.	Selection of irradiation characteristics for simulation experiments	27
3.4.	Electron accelerators and high voltage electron microscopes	32
3.5.	Light ion accelerators: Cyclotrons	34
3.6.	Heavy ion irradiation	36
3.7.	Multibeam techniques	39
3.8.	Correlation of results of reactor and accelerator experiments on radiation swelling of materials	41
3.9.	Predicting results for practical applications	43
3.10.	Radiation resistance of stainless steels	44
3.11.	Conclusions	44
	References to Chapter 3	44
4.	MULTISCALE MODELLING IN NUCLEAR MATERIALS SCIENCE	49
4.1.	Introduction	49
4.1.1.	Radiation effects on materials as a multiscale problem	49
4.1.2.	What is multiscale modelling?	50
4.2.	Atomic level modelling	51
4.2.1.	Density functional theory calculations and interatomic potentials	51
4.2.2.	Molecular dynamics	52
4.3.	Nanostructural and microchemical evolution modelling	53
4.3.1.	Metropolis and atomistic kinetic Monte Carlo methods	53
4.3.2.	Rate theory	55
4.4.	Mechanical property modelling	58
4.4.1.	Molecular dynamics simulations of dislocation–defect interactions	58
4.4.2.	Dislocation dynamics and a bridge from molecular to dislocation dynamics	59
4.4.3.	A bridge to finite element methods	60

4.5. Concluding remarks	62
Acknowledgements	63
References to Chapter 4	63
5. PRE- AND POST-IRRADIATION EXAMINATION TECHNIQUES ON ION BEAM IRRADIATED SPECIMENS.....	73
5.1. Introduction	73
5.2. Some techniques used to perform post-irradiation examination.....	74
5.2.1. Focused ion beam specimen preparation for atom probe tomography, micromechanical specimens and transmission electron microscopy	74
5.2.2. Microstructural characterization techniques	76
5.2.3. Microscale and mesoscale mechanical testing	81
5.2.4. Swelling measurements on ion beam irradiated materials	84
5.2.5. Positron annihilation spectroscopy	85
5.2.6. Ion beam analysis	86
5.3. Summary	88
References to Chapter 5	88
6. SUMMARIES AND DISCUSSION OF THE RESULTS OF THE ACCELERATOR SIMULATION AND THEORETICAL MODELLING OF RADIATION EFFECTS COORDINATED RESEARCH PROJECT	91
6.1. Summaries of participant subprojects.....	91
6.2. Discussion and summary.....	97
6.2.1. Structural materials for present and future reactor designs: Trends and challenges	97
6.2.2. Summary of overall results and the path forwards	98
6.3. Conclusions and recommendations.....	99
6.3.1. Assessment of the results.....	99
6.3.2. Recommendations for future activities	101
Reference to Chapter 6.....	102
ANNEX: CONTENTS OF THE ATTACHED CD-ROM: REPORTS FROM THE INDIVIDUAL COORDINATED RESEARCH PROJECT MEMBER ORGANIZATIONS.....	103
ABBREVIATIONS	105
CONTRIBUTORS TO DRAFTING AND REVIEW	107
STRUCTURE OF THE IAEA NUCLEAR ENERGY SERIES.....	108

1. INTRODUCTION

1.1. BACKGROUND

This report addresses an issue of growing importance to the nuclear energy sector. Throughout the international nuclear reactor community, there is a well-recognized need to provide new structural alloys that are capable of reaching much higher neutron doses than those experienced by currently used alloys. This need is especially important for fast reactors and some accelerator driven systems, both of which operate at much higher flux levels and harder neutron spectra than conventional light water cooled reactors that supply the majority of current nuclear power plants. The recent interest in developing long life small modular reactors that are fuelled only once in their lifetime also requires the use of structural materials that are capable of reaching very high exposures without failure. The immediate benefit of reaching these much higher neutron exposures will be to attain much higher burnup of the fuel, a factor that strongly affects the economic viability of nuclear power.

Furthermore, in the post-Fukushima era, there is also a strong need to ensure that all nuclear systems are inherently robust in their ability to withstand both normal and severe conditions. Such robustness is especially important for fuel cladding and structural materials for reactor internals. Concerns about robustness become increasingly important as the structural and cladding materials reach very high doses and thereby suffer higher levels of degradation in their properties.

Development of advanced alloys is usually an iterative three step process in which advanced alloy concepts of new composition and production technology must be first developed and produced. The candidate alloys are then irradiated in either prototypical or surrogate neutron spectra up to significant exposures, and finally, irradiated specimens of these alloys are tested out of the reactor. Lessons learned from the first three step iteration are then used to further optimize composition and production technology, and the improved alloys are again irradiated and tested. Each three step iteration process can take a decade. Usually, three series of three step iterations are necessary, at a minimum, to converge on a fully acceptable candidate alloy. Once such convergence has been attained, an additional time frame of one to two decades is required to attain regulatory and fuel performance code acceptance before the new alloy can be employed in a reactor.

Such a 40–50 year process is, in itself, a daunting task, but the real problem is that there are very few high flux fast spectrum material test reactors currently operating to conduct neutron irradiation studies. Those that are available are very expensive to use and often difficult to access. More importantly, these reactors are either heavily used (e.g. BOR-60) or unavailable for materials testing (e.g. BN-600, a power generation facility). New reactors coming on-line in India and China will also hardly be available to conduct extensive testing in the near future.

One approach previously utilized to shorten the 40–50 year cycle is to use ion bombardment at greatly accelerated damage rates to complete the first several iterations of alloy development and testing. Such techniques have been employed in various national fast reactor programmes to generate the necessary data on void swelling, irradiation creep and phase stability of austenitic alloys, while waiting for the then available but now decommissioned fast reactors to slowly move towards target neutron fluences. Although such ion based surrogate techniques had not been previously thought to be useful for developing data on irradiation induced changes in mechanical properties, both experimental techniques and theoretical modelling have been sufficiently enhanced during recent years, and there are many programmes currently proceeding to develop mechanical property data using ion irradiated specimens.

However, there is another very relevant issue that must be addressed. It is well known that there are some facets of ion bombardment that are atypical of neutron irradiation. These neutron atypical aspects may have some influences on the results, and the impact of these issues must be understood. While some of the atypical aspects can be addressed experimentally to validate the use of the ion results, another widely used complementary approach is to use computer simulation as a bridge for ion–neutron correlations. Computer simulation can also be used to explore some fundamental issues not easily investigated using ion irradiation.

1.2. OBJECTIVE

At present, there are many, mostly independent, national or private institutional efforts to provide new alloys for high dose nuclear service and to forecast their behaviour using either ion or neutron irradiation. Some efforts focus on experimental exploration, while others focus on modelling and simulation. A few groups have hybrid programmes involving both types of activities. In general, however, no single group has sufficient funding and testing resources to successfully conduct a programme that will yield success on a time frame compatible with the need of the nuclear power industry. There is also no international system of coordinated research in place to integrate and focus the various individual efforts towards an efficient and timely execution of an international advanced alloy development programme.

For these reasons, in 2007, the IAEA Technical Working Group on Fuel Performance and Technology recommended the initiation of a coordinated research project (CRP) entitled Accelerator Simulation and Theoretical Modelling of Radiation Effects (SMoRE) that combined the efforts of 19 leading nuclear research and development organizations from 15 Member States towards the study of high dose radiation damage. It was envisioned that this CRP would serve as a model and nucleus for ambitious international collaborative efforts in the future, leveraging and extending international community resources to develop and deploy advanced alloys and structural materials for new generation nuclear systems.

1.3. SCOPE

This publication is aimed at providing support to Member States in the development of advanced radiation resistant structural materials for implementation in future innovative nuclear systems. This aim can be achieved through enhancing experimental simulation capabilities of ion accelerators and improving the predictive performance of theoretical models and computer codes. Such *coupling* is challenging, but necessary, because, on the one hand, outputs of accelerator simulation experiments need adequate theoretical interpretation, and, on the other hand, theoretical models and codes need high dose experimental data as input. Both accelerator simulation and computer modelling have been the specific subjects of the SMoRE CRP, and the results of these studies are analysed, summarized and presented in this report. Additionally, the CRP emphasized post-irradiation analysis techniques needed to efficiently extract the data from ion simulations.

1.4. STRUCTURE

This publication summarizes the findings and conclusions of the SMoRE CRP carried out in 2008–2011 within a work plan jointly agreed on by the following member organizations:

- Belgian Nuclear Research Centre, Belgium;
- China National Nuclear Corporation and China Institute of Atomic Energy, China;
- Saclay Nuclear Research Centre, Commissariat à l'énergie atomique, France;
- Électricité de France, France;
- Bhabha Atomic Research Centre, India;
- Institute of Advanced Energy, Kyoto University, Japan;
- Material Research Laboratory, Institute of Atomic Energy, Poland;
- Institute of Nuclear Physics, National Nuclear Center, Kazakhstan;
- Korea Atomic Energy Research Institute, Republic of Korea;
- Institute of General and Nuclear Physics, Kurchatov Institute National Research Center (KI NRC), Russian Federation;
- Institute for Physics and Power Engineering, Russian Federation;
- Faculty of Electrical Engineering and Information Technology, Slovak University of Technology of Bratislava, Slovakia;
- Institute of Nuclear Fusion, Technical University of Madrid, Spain;
- Department of Nuclear Energy and Safety Research, Paul Scherrer Institute, Switzerland;

- Kharkov Institute of Physics and Technology National Science Center (KI NSC), Ukraine;
- Radiation Effects Consulting, USA;
- Los Alamos National Laboratory, University of California, USA;
- Lawrence Livermore National Laboratory, University of California, USA.

A list of chief scientific investigators who represented these organizations within the CRP is given at the end of this report.

Upon finalization of the planned works in 2012, the CRP charter was amended to provide comprehensive reviews of four important areas of relevance to this CRP: (i) fast neutron irradiation effects, (ii) accelerator simulation techniques, (iii) multiscale modelling tools and (iv) advanced materials characterization methodologies. Specially assigned CRP Members compiled the following state of the art review chapters in this report:

- Challenge of Using Ion Irradiation to Develop and Test Advanced Alloys for Application to Verify High Neutron Exposures in Future Reactor Concepts, by F.A. Garner (USA);
- Accelerators for Simulation of Radiation Damage, by V.N. Voyevodin (Ukraine);
- Multiscale Modelling in Nuclear Materials Science, by L. Malerba (Belgium);
- Pre- and Post-irradiation Examination Techniques on Ion Beam Irradiated Specimens, by P. Hosemann (USA), E. Stegar (Belgium) and O. Anderoglu (USA).

In addition to the above listed review chapters, the final chapter of this report briefly summarizes the subproject reports from each of the CRP participants. The full reports (provided in the accompanying CD-ROM) are relatively self-contained comprehensive studies representing, when taken together, the best current practices of simulation and modelling of radiation effects. Chapter 6 also addresses the challenges and trends in the development of structural materials for present and future reactor designs, as assessed on the basis of the CRP results, followed by assessment of the CRP results and recommendations for future activities.

2. THE CHALLENGE OF USING ION IRRADIATION TO DEVELOP AND TEST ADVANCED ALLOYS FOR APPLICATION TO VERY HIGH NEUTRON EXPOSURES IN FUTURE REACTOR CONCEPTS

F.A. GARNER
Radiation Effects Consulting, Richland, WA,
United States of America

Abstract

This chapter reviews the materials issues that prevent the use of austenitic steels as fuel cladding for doses above 100–150 displacements per atom (dpa) and thereby preclude an increase in fuel burnup. The limited neutron data on ferritic and ferritic–martensitic alloys and their oxide dispersion strengthened (ODS) variants is then presented, which shows promise that these alloys can be subjected to much higher exposures, thereby allowing higher fuel burnups. Finally, the results of recent ion irradiations are presented, demonstrating that ion irradiation can be used successfully as a surrogate to explore void swelling at much higher dpa levels, in the range 300–600 dpa. However, there are enough differences in the neutron and ion environments that modelling assistance is required to extrapolate ion results to neutron conditions, especially for the effects of displacement rate and temperature.

2.1. INTRODUCTION

The SMORE CRP was proposed to assist the nuclear materials community in the development and testing of materials such as advanced ferritic and ferritic–martensitic alloys to be used as structural components, both in currently used reactor types and in advanced reactor concepts such as fusion devices, accelerator driven subcritical reactors or various hybrid devices. A particular aspect of this CRP is the focus on the ability of these materials to withstand very high exposure levels ranging from 200 dpa to perhaps 600 dpa.

Light water cooled or heavy water cooled reactors are not likely candidates to use such alloys because these high dose levels are incompatible with their current power producing role and especially with the constraints imposed by the regulatory and licensing environment. The most probable immediate application lies in liquid metal reactors (LMRs), particularly those cooled by sodium, but possibly also advanced concepts cooled by lead or lead bismuth eutectic. The desire to use LMRs as burners to transmute actinides or as travelling wave reactors to use depleted uranium as fuel makes them the next most likely area where such high dpa levels might be encountered.

In fast reactors, in particular, the driving force to reach higher dpa levels is to reverse the current situation in which the fuel must be removed from the reactor when the cladding containing the fuel reaches some limit that imperils the integrity of the fuel assembly. Optimally, the fuel assembly is removed when the fuel has reached a burnup level that maximizes its integrated power production but is just reaching a neutronic response state where further burnup is no longer efficient. Such an optimal condition lies at ~30% burnup for typical LMR enrichment levels.

Currently, burnup levels of only ~10–11% are attainable using austenitic stainless steels as fuel cladding for typical mixed oxide fuels. As will be shown in the following sections, this non-optimal burnup is dictated by the fuel cladding, which experiences very high levels of distortion due to void swelling and irradiation creep, accompanied by a severe form of embrittlement, arising primarily from void swelling.

In the waning days of various LMR programmes in the United States of America, there was a shift away from austenitic stainless steels to ferritic and ferritic–martensitic steels, which resist swelling to much higher dpa levels. The maximum dose attained in HT9 steel in the US programme was only ~155 dpa in fuelled assemblies and ~200 dpa in experimental specimens, both reached in the Fast Flux Test Facility (FFTF) reactor many years ago. Until recently, there has been no examination of the fuelled assemblies constructed from HT9, but these are now receiving experimental attention.

Ferritic–martensitic alloys have a well-known deficiency in that their strength decreases significantly with increasing temperature, requiring that the FFTF core power level be decreased from 400 to 280 MW in order to avoid loss of strength. Recognizing the economic penalties associated with dropping the power level and maximum temperatures, many countries are striving to develop variants of ferritic or ferritic–martensitic alloys that are strengthened by nano dispersoids or nano features that resist creep deformation at higher temperatures. These alloys are frequently referred to as ODS alloys. In one early ODS alloy, designated MA957, doses of ~100 dpa were reached in the FFTF before the reactor was shut down.

However, in order to reach dpa levels of 200 and beyond, in either alloys such as HT9 or various ODS variants, it is necessary to use a high flux reactor, preferably a fast reactor. Various fast reactors in the USA and Western Europe have been shut down (e.g. the Experimental Breeder Reactor (EBR)-II, FFTF, the Dounreay Fast Reactor (DFR), the Prototype Fast Reactor (PFR) and Phénix). The use of high flux mixed spectrum reactors such as the High Flux Isotope Reactor (HFIR) and the Advanced Test Reactor (ATR) in the USA is impractical for several reasons, which include neutron spectral issues, competition for limited testing space with other programmes and, especially, the inability to reach even 10 dpa/year. Currently, the only possibility of reaching just ~20 dpa/year exists in the Russian BOR-60 fast reactor. Approximately 40 dpa/year could be reached in the Russian BN-600 fast reactor, but the operator deems materials testing missions to be incompatible with its primary mission of power generation. Currently, only limited materials tests are being conducted in Russian domestic programmes, and it is unlikely that additional international programmes might be considered. There are other much more remote possibilities involving the Indian and Chinese fast reactors, but there is little likelihood that such opportunities would arise in less than a decade.

High dpa rate irradiations available on timescales much shorter than decades are desired, but are not possible to achieve. This inability has forced the materials community to turn to surrogate irradiation techniques.

The only viable surrogate technique is that of ion irradiation as a simulation tool. In the very early days of various international LMR programmes, there was a strong reliance on this technique while waiting for reactor tests to be completed and specimens and assemblies to be delivered for examination. While there were some rather remarkable accomplishments using ion bombardment, which were validated by subsequent neutron irradiated specimens, it gradually became apparent that there were limitations and deficiencies arising from aspects of this technique that were atypical of the neutron situation. In addition to the effects associated with surface influences, injected interstitial effects, atypical stress states and gradients in dpa rate, the much higher dpa rates available with ions introduced new phenomena in both simple metals (temperature shift of void swelling) and more complex alloys, where phase stability considerations exhibited other competing dependencies on dpa rate. These factors are covered in Chapter 3.

Therefore, it is necessary to use ion simulation as a surrogate irradiation tool while knowing that it has deficiencies which require interpretation for extrapolation to the desired neutron doses. This CRP was therefore organized as a first step in providing both irradiation data and analytical modelling tools to aid in data interpretation and extrapolation.

2.2. MATERIALS PROBLEMS OF IRRADIATED AUSTENITIC ALLOYS RELEVANT TO THIS COORDINATED RESEARCH PROJECT

As the overwhelming majority of the data on austenitic steels was derived from fast reactors, fast reactor observations and data will be relied upon almost exclusively in this section. Figure 2.1 shows a typical fuelled subassembly from FFTF. Austenitic steels such as American Iron and Steel Institute (AISI) 316 and a titanium modified variant called D9 were used in mostly cold worked condition to construct the fuel wrapper, fuel pins and the wire wrap that separates the pins. Earlier assemblies in the EBR-II reactor were constructed from AISI 304, but with a grid rather than a wire wrap. The fuel pins experienced a higher range of temperatures than the duct, but both had the same range of displacement rates.

There are three primary phenomena of interest in the radiation induced evolution of austenitic alloys (but they are not uniquely separate processes): evolution in mechanical properties, irradiation creep and void swelling. While the first two initially proceed in the absence of void swelling, they eventually become strongly linked and dominated by it. The reader is referred to a recent review on these and other radiation induced phenomena [2.1].

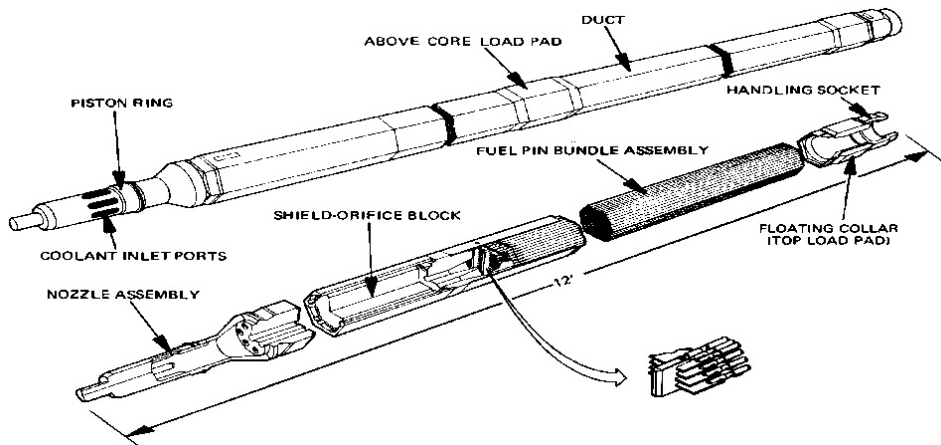


FIG. 2.1. Typical fuelled subassembly in FFTF showing the variety of components, all constructed from austenitic stainless steel.

When metals and alloys are exposed to neutron or ion irradiation at elevated temperatures, they develop a range of microstructural features, most of which are uncharacteristic of the unirradiated state. These features are Frank interstitial loops, enhanced or altered dislocation lines developing into a network, and new or altered precipitates and cavities (white features), which will be addressed in more detail later (see Fig. 2.2).

Even in the simplest annealed solute free model alloys that have no opportunity to change matrix composition or to develop precipitates, there is a radiation induced evolution that leads to a reduction in elongation and an increase in yield strength, as shown in Fig. 2.3.

In general, this process is referred to as irradiation embrittlement, implying a loss of plasticity, but it will be shown below that this is a misnomer, especially compared with a real embrittlement effect that arises later from void swelling. As these alloys were originally in an annealed soft state the alloy hardened and increased in strength as a result of radiation induced microstructure. Complex alloys exhibit the same behaviour, as shown in Fig. 2.4.

However, most austenitic steels are irradiated in the harder cold worked condition, allowing not only hardening but also softening to occur, which depends primarily on temperature but secondarily on dpa rate (see Fig. 2.5).

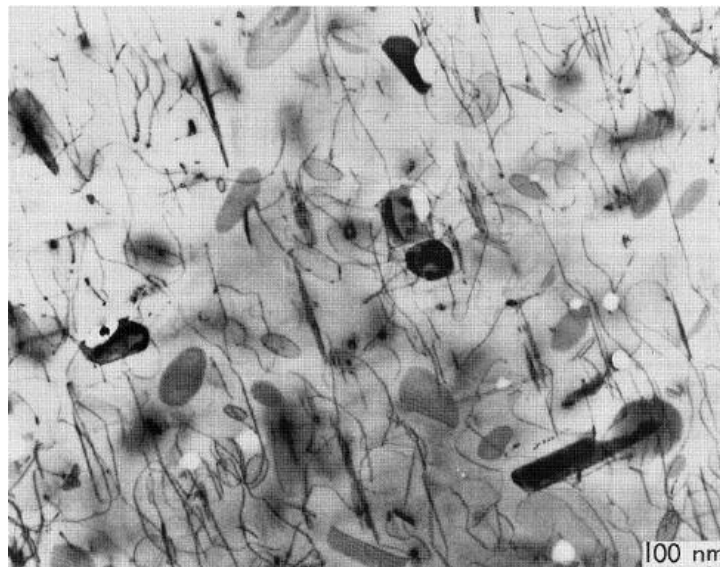


FIG. 2.2. Radiation induced changes in the microstructure of annealed 316 stainless steel after 10 dpa in HFIR at 500°C (micrograph supplied by P.J. Maziasz and J. Stiegler of Oak Ridge National Laboratory).

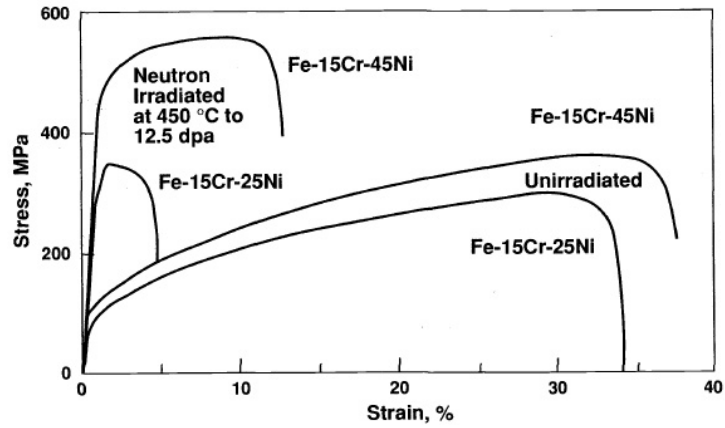


FIG. 2.3. Engineering stress–strain curves generated in tensile tests on two Fe–Cr–Ni model alloys, in the annealed condition, which were irradiated in EBR-II to 12.5 dpa at 450°C [2.2].

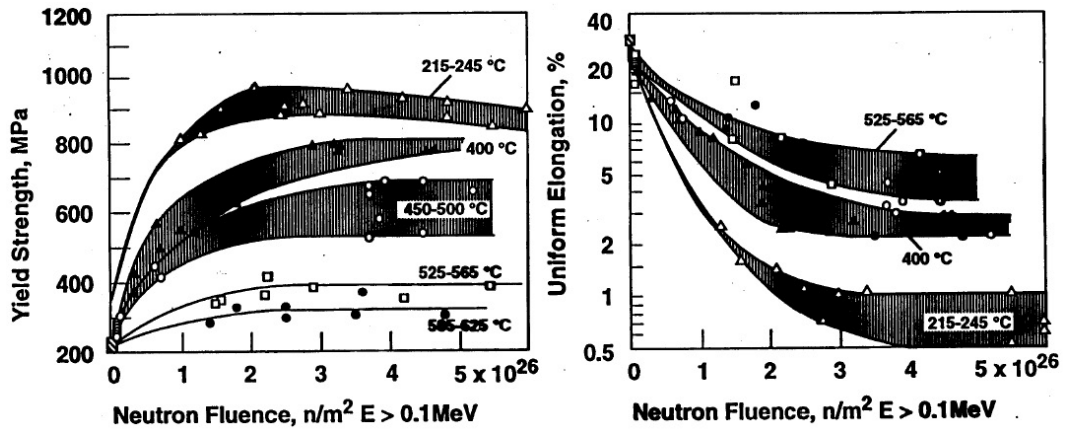


FIG. 2.4. Radiation induced changes in tensile properties of annealed 1.4988 stainless steel in DFR. Tensile tests were conducted at the irradiation temperature [2.3].

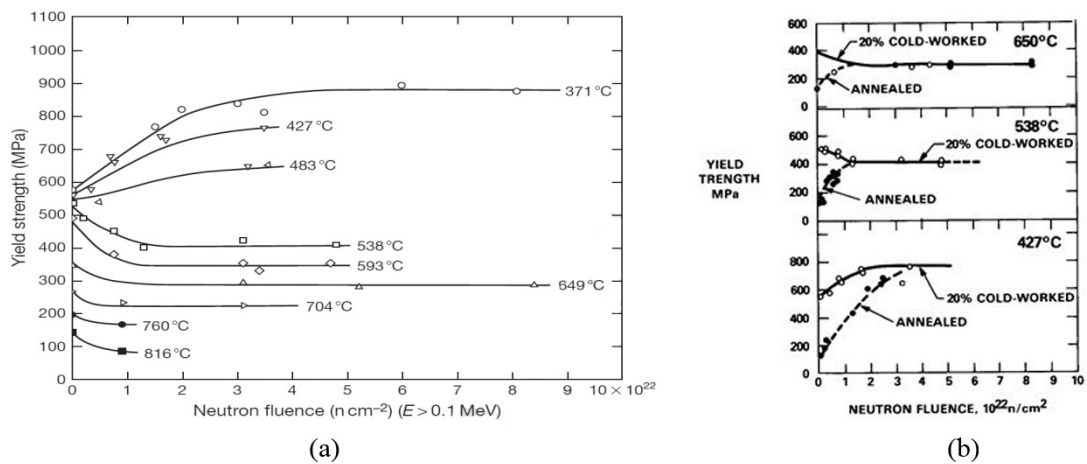


FIG. 2.5. Radiation induced changes in yield strength of (a) 20% cold worked 316 following irradiation in EBR-II, and (b) later tests involving side by side irradiation of both annealed and cold worked steel [2.4]. Tensile tests were conducted at the irradiation temperature.

Interestingly, both annealed and cold worked steel converge during irradiation not only to essentially identical microstructures but also to identical tensile properties. In effect, the material forgets its starting state and converges to a semi-equilibrium state dictated by temperature and dpa rate. As the dose increases, however, the failure surface undergoes a significant transformation, as shown in Fig. 2.6. The failure surfaces eventually develop a faceted appearance that appears to be indicative of cleavage fracture, and therefore embrittlement; in actuality, these facets are the result of flow localization, indicating significant plasticity that is constrained to very narrow bands. If the area beneath the failure surface is studied, it can be seen that intense localized deformation has left a microstructural record in the deformed voids (Fig. 2.7). Therefore, true embrittlement is not yet being observed.

As voids continue to grow, however, the situation begins to change. While void volumes of several percent or less strengthen the material a little, as swelling passes ~5%, a new phenomenon of extreme embrittlement begins to assert itself. Examples of void distributions are shown in Fig. 2.8.

The swelling levels shown in Fig. 2.9 at the fracture points are: (a) 6–10%, (b) 14%, (c) 30% and (d) as noted. Note that the tubes in Fig. 2.9(a) are bent by irradiation creep as a result of being enclosed in a can where sufficient room was not available to accommodate an increase in length. The tubes in Fig. 2.9(a) were used to produce the micrograph in Fig. 2.8(a).

Abrupt failure is a consequence of a series of void related events involving stress concentration between voids, segregation of nickel and export of chromium from void surfaces, resulting in a decrease in stacking fault energy and a change in the martensite start temperature. These factors result in a martensite instability that occurs at a crack tip, producing brittle alpha martensite just ahead of the moving crack, thereby producing a tearing modulus of 0, especially at lower deformation temperatures. Aspects of this phenomenon, as expressed in tensile or Charpy impact tests, are shown in Fig. 2.10.

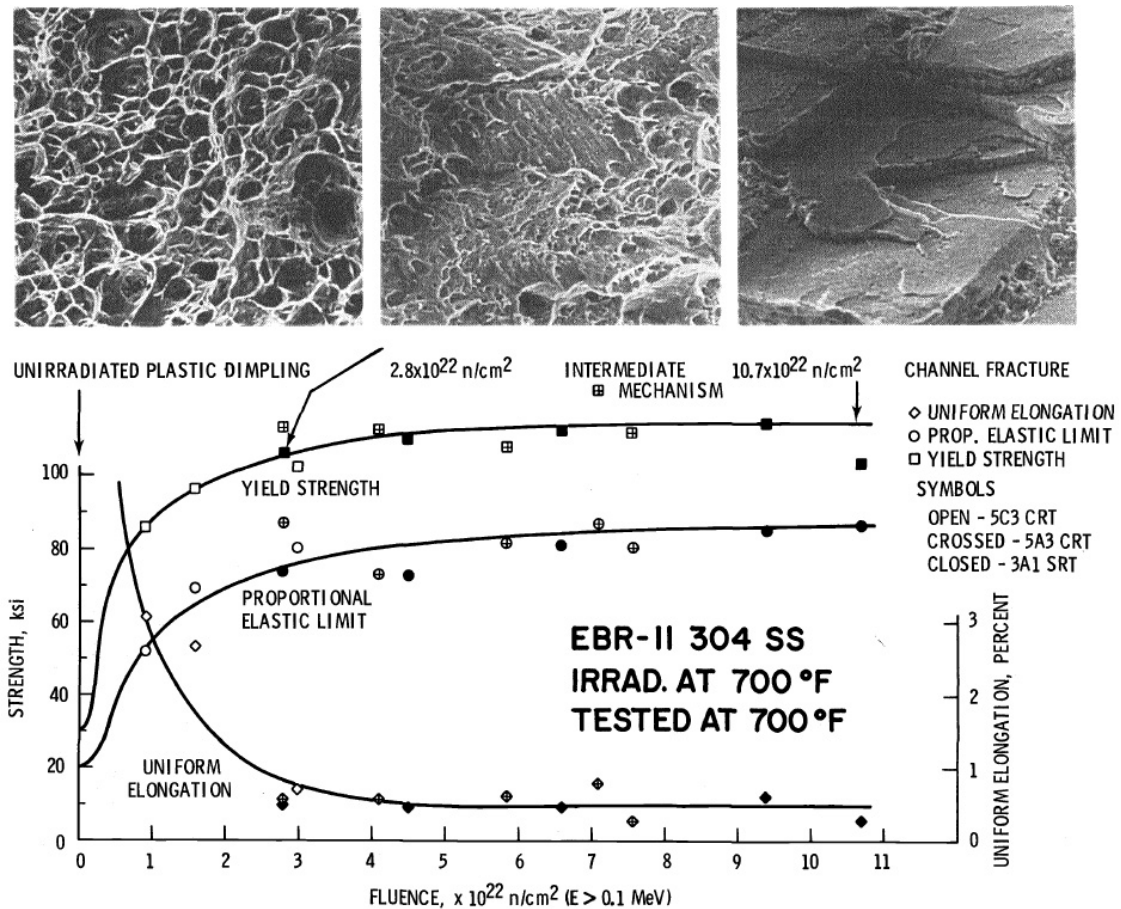


FIG. 2.6. Radiation induced changes in fracture mode of annealed American Iron and Steel Institute 304 stainless steel after irradiation at 370°C in EBR-II [2.5]. 1 ksi = 6.9 MPa; CRT — control rod thimble; SRT — safety rod thimble; SS — stainless steel.

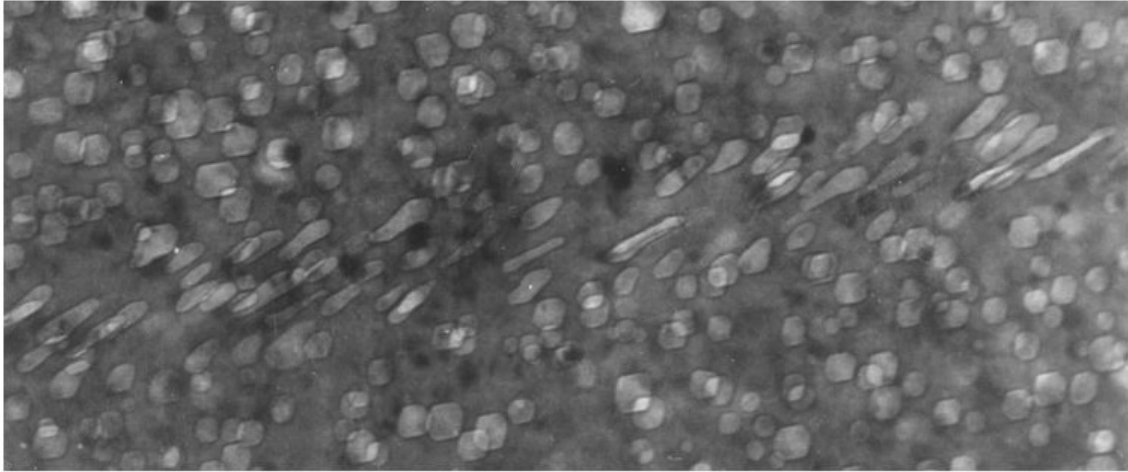


FIG. 2.7. Deformation induced elongation of voids observed under the fracture surface of annealed 304 stainless steel after irradiation at 54 dpa and ~400°C; 200–300% strain has occurred in the deformed volume. The width of the void shear zone is ~0.1 micron [2.5].

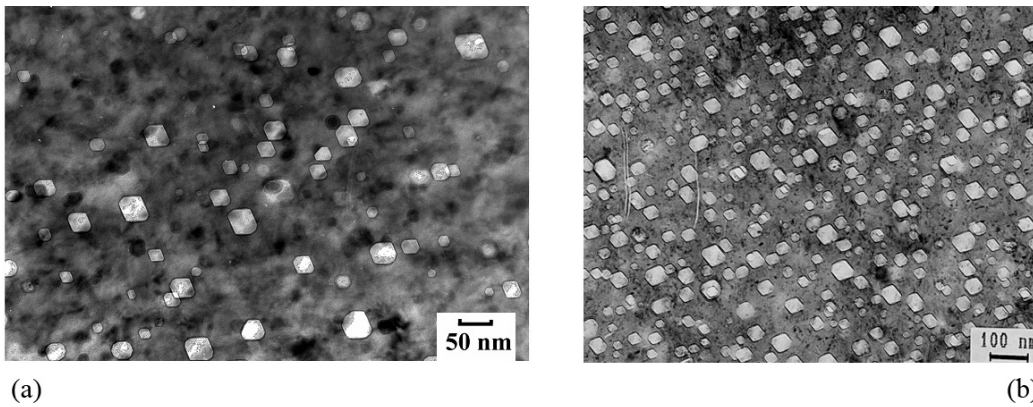


FIG. 2.8. Voids observed at: (a) ~1% in annealed 304 steel at 380°C to 21.7 dpa in EBR-II [2.6] and (b) ~6.2% in austenitic stainless steel EI-847 after 73 dpa at 335°C in a BN-350 fast reactor [2.7]. Note different scales in (a) and (b).

Void swelling can considerably increase the dimensions of a component; two common examples are shown in Fig. 2.11. When swelling is unconstrained, the resulting strains are distributed isotropically, but if constraints exist, then mass will be redirected towards the unconstrained directions by the process of irradiation creep. Examples of these are shown in Fig. 2.12. When the wire swells more than the cladding, a very different distortional result is produced, as shown in Fig. 2.13.

When swelling is constrained in any manner, it activates irradiation creep as described by Eq. (2.1), and the two processes provide the spectacular distortions shown above (Figs 2.12, 2.13). This equation states that the strain rate per unit stress is relatively large compared with thermal creep in the absence of swelling but is accelerated by as much as two additional orders of magnitude as swelling proceeds [2.1]. In effect, the creep rate becomes directly proportional to the swelling rate. The net result is that all local stresses generated by swelling are nearly instantly relaxed by irradiation creep, leading to no internal stresses of consequence during irradiation:

$$\frac{\dot{\epsilon}}{\sigma} = A[1 - \exp(-dpa / \tau)] + B_0 + D\dot{S} \quad (2.1)$$

where

$D\dot{S}$ is the swelling enhanced creep;

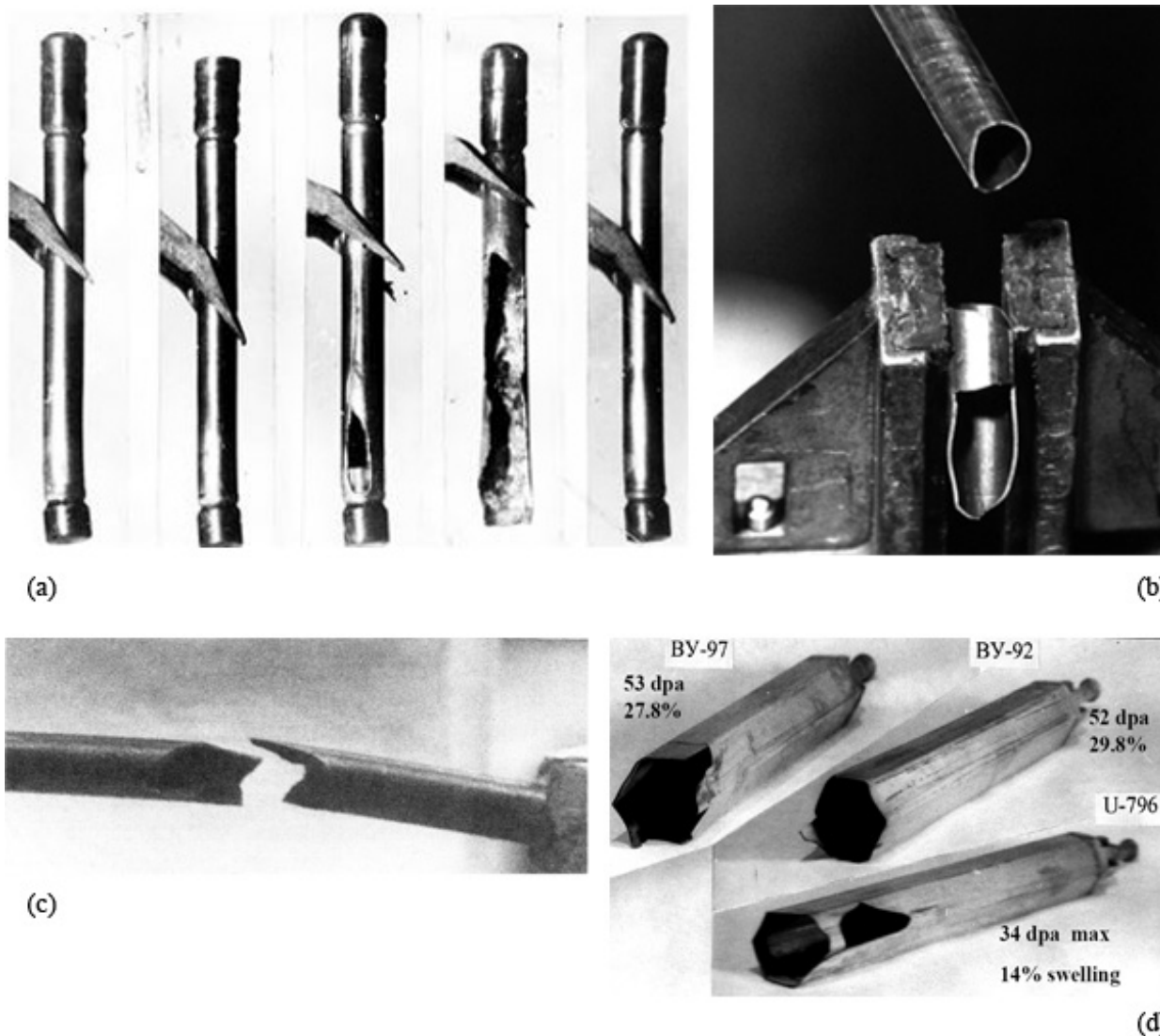


FIG. 2.9. Four examples of extreme embrittlement resulting from void swelling [2.8–2.11]. Swelling levels of: (a) 6–10%, (b) 14%, (c) 30% and (d) as noted.

B_0 is the creep in the absence of void swelling;

$\dot{\epsilon}$ is the rate of strain;

σ is the stress;

and $A[1 - \exp(-\text{dpa} / \tau)]$ is the transient contribution.

As a consequence of swelling induced changes in the volume, swelling–creep interactions to produce distortion and the resultant swelling induced embrittlement, swelling of important reactor components should be kept at ~5% or less in austenitic stainless steels. All stainless steels eventually swell at ~1%/dpa at all relevant fast reactor conditions (e.g. Fig. 2.14), which requires that any compositional or fabrication improvements to resist swelling must be focused on extending the low swelling rate transient or incubation period that precedes the onset of steady state swelling. To date, all the various improved stainless steel variants have been observed to transition to steady state swelling at maximum doses of 100–150 dpa, with high rate swelling immediately following. Therefore, ~150 dpa is effectively the maximum attainable dose for austenitic steels.

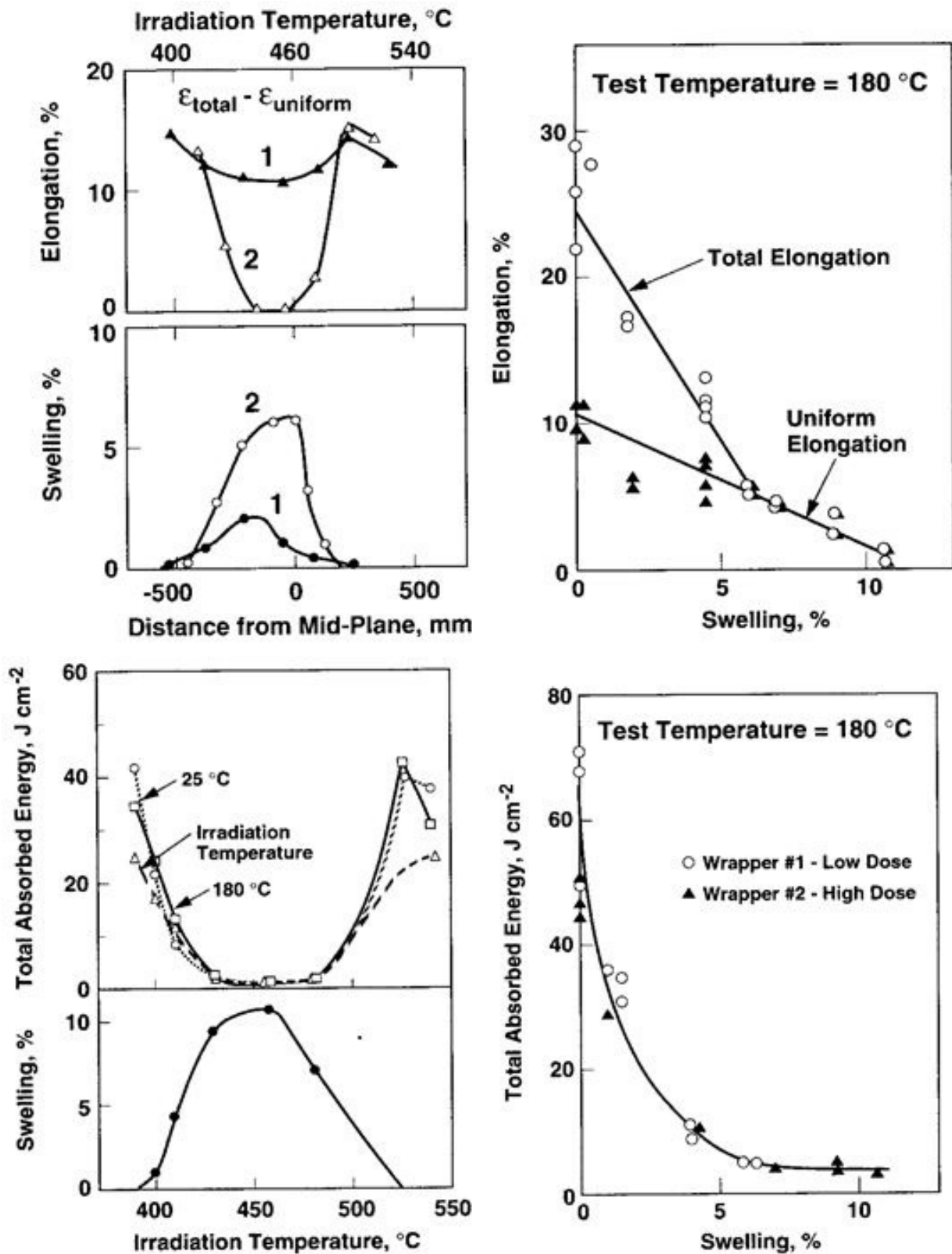


FIG. 2.10. Influence of increasing void swelling to reduce the ductility of 20% cold worked titanium modified 316 steel stainless steel under tensile or impact conditions [2.12].

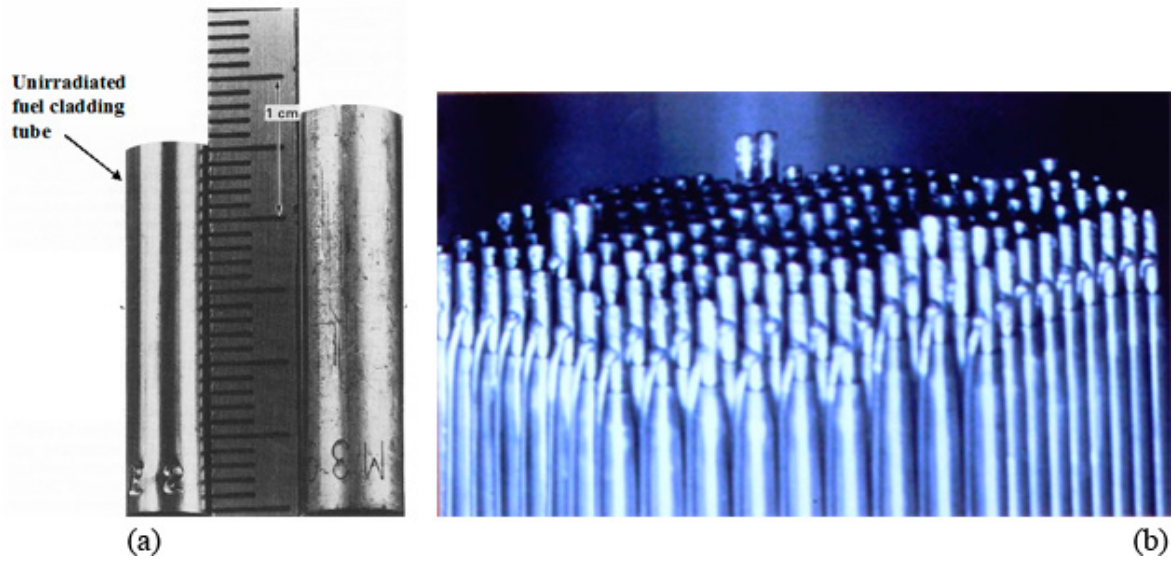


FIG. 2.11. (a) Swelling of 20% cold worked 316 open tube at 510°C and 80 dpa in EBR-II [2.13]. (b) Variable increases in length of fuel pins in D9 stainless steel in an FFTF fuel assembly in response to local variations in temperature, dpa rate and minor differences in phosphorous content in two heats [2.14].

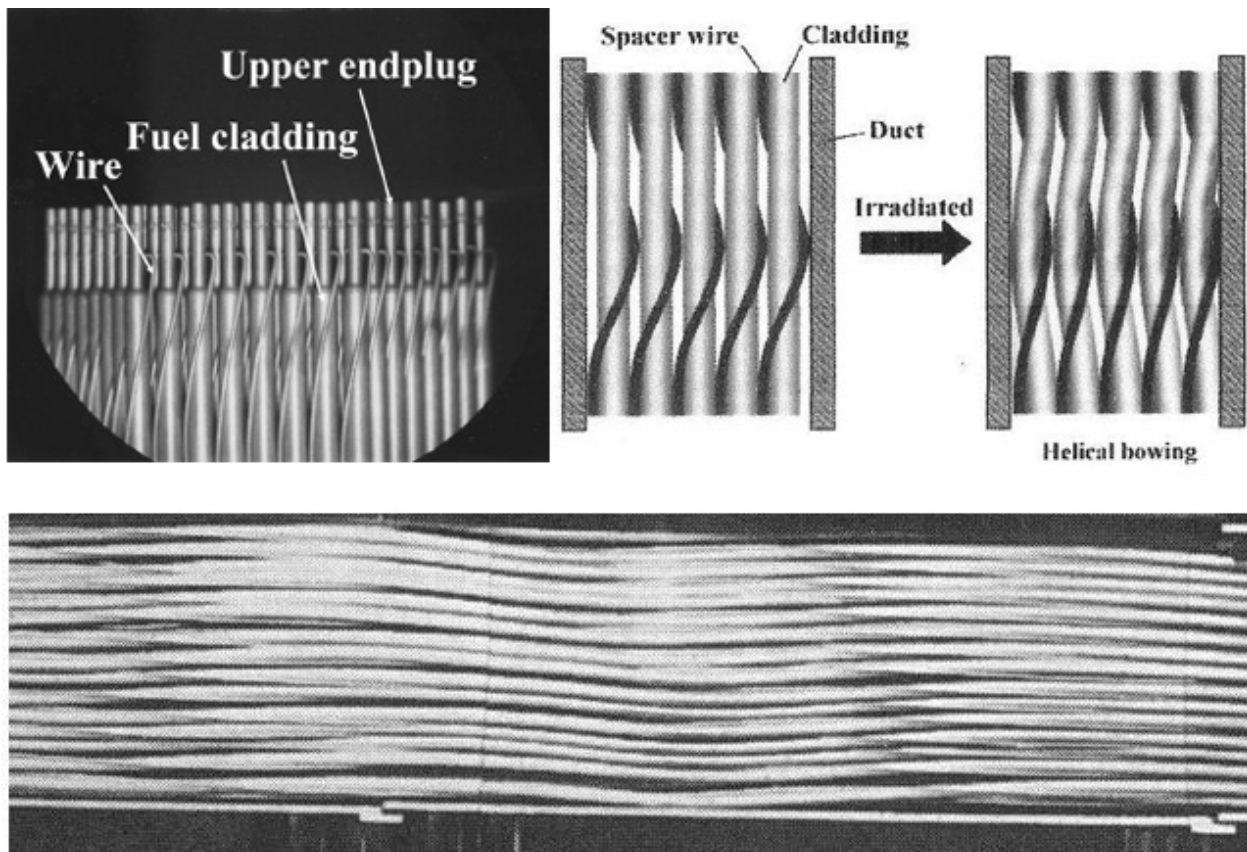


FIG. 2.12. Effect of spirally wrapped spacer wire to constrain swelling of fuel pins and produce spirally deformed pins [2.15]. The lower diagram shows distorted pins corresponding to the fuel assembly shown in Fig. 2.11(b) [2.14]. The wire swells less than the cladding in this example.

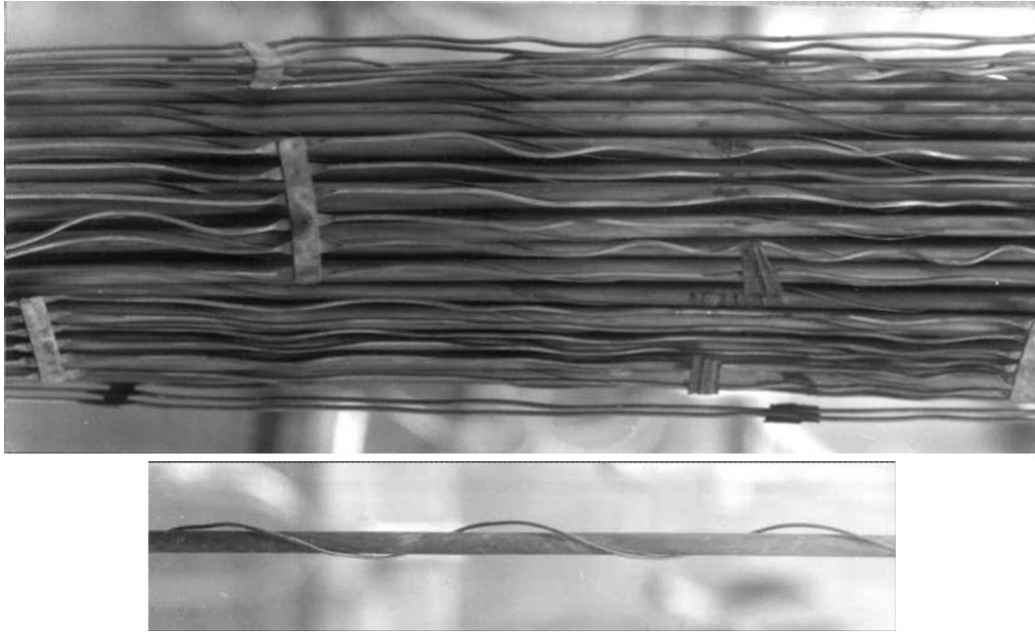


FIG. 2.13. Example of the wire swelling more than the cladding, from BN-600 [2.16].

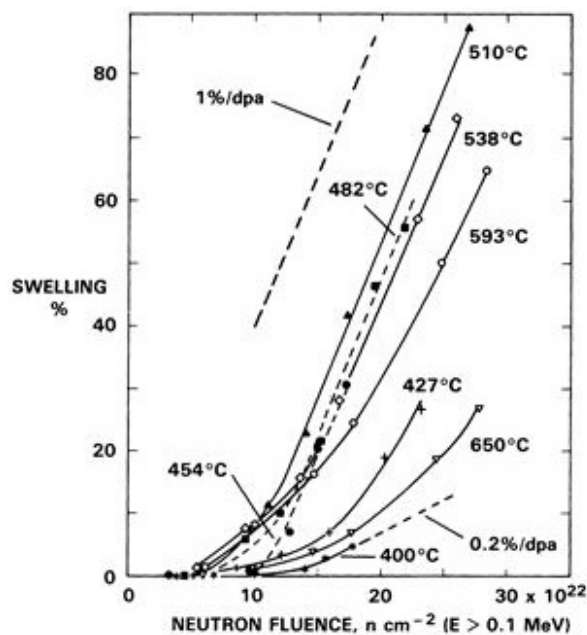


FIG. 2.14. Swelling observed at various combinations of temperature and dpa rate in 20% cold worked 316 during irradiation in EBR-II, demonstrating that the steady state swelling rate is $\sim 1\%/dpa$ over much of the temperature range [2.17].

2.3. VOID SWELLING OF FERRITIC–MARTENSITIC STEELS

There is much less data on the swelling of iron base body centred cubic (bcc) alloys, but in general, most data show significantly less swelling when compared with austenitic alloys at comparable irradiation conditions. A review of the limited data can be found in Ref. [2.18].

Perhaps the best way to demonstrate the promise of ferritic and ferritic–martensitic steels is to provide some examples, focusing on three alloys: HT9, EP-450 and MA957. Figure 2.15 shows an FFTF subassembly identical

to the austenitic assembly that was shown in Fig. 2.11(b). However, this second assembly was constructed from HT9, a 12Cr ferritic–martensitic steel, while the first assembly was constructed from D9 austenitic steel. Both assemblies reached the same maximum exposure of ~75 dpa. The HT9 assembly appears to have experienced no discernible distortion, whereas the D9 assembly experienced considerable distortion.

Figure 2.16 presents swelling and creep data on EP-450 from a series of four 37-pin fuel pin assemblies irradiated in BOR-60. EP-450 is a duplex alloy (~50% ferrite, ~50% tempered martensite) that is routinely used for wrappers in the fuel assemblies of BOR-60 and BN-600. In these highly enriched (~75%) assemblies, the swelling observed in the cladding was very small (~1.2% maximum at 163 dpa and ~30% burnup), with most of the swelling occurring in the ferrite grains [2.19]. The observed creep strains were significantly larger than

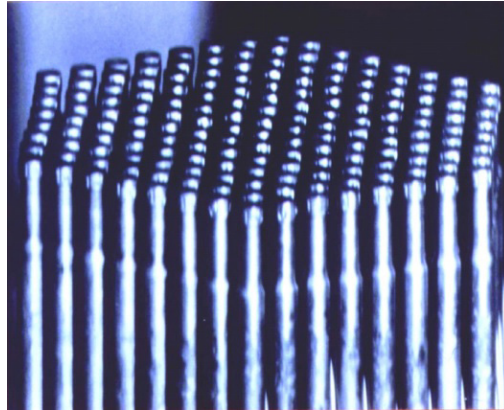


FIG. 2.15. Top of an FFTF fuel pin assembly irradiated to a maximum of 75 dpa, showing no discernible distortion [2.14].

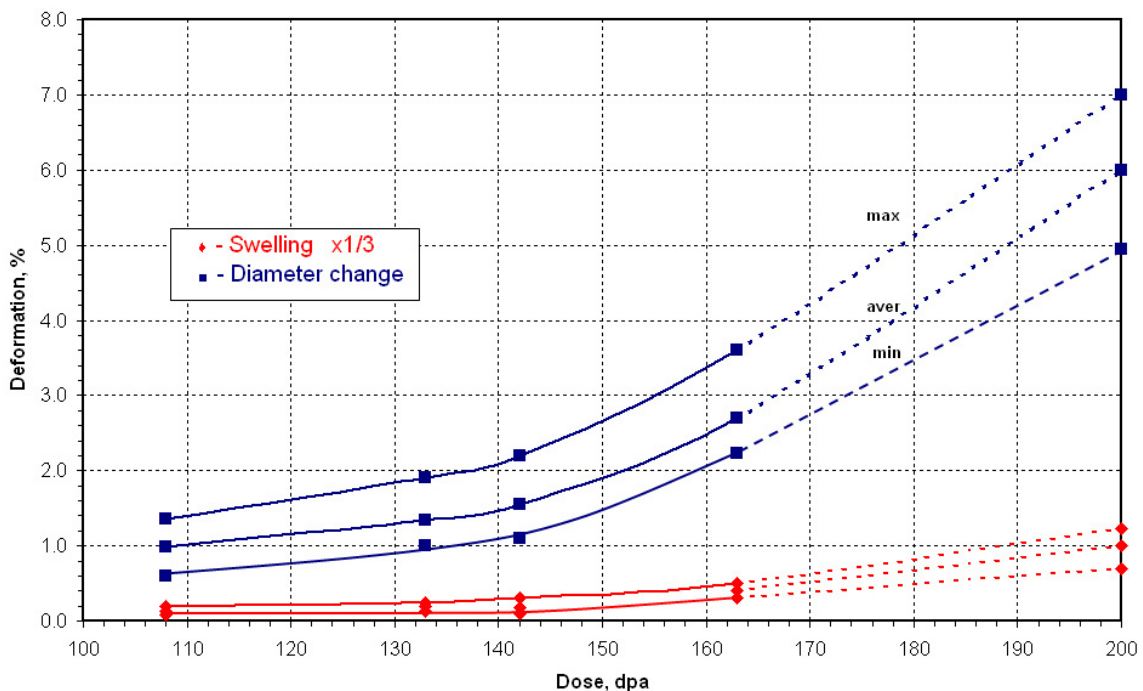


FIG. 2.16. Maximum diameter change measurements and swelling values determined by electron microscopy for four BOR-60 fuel assemblies with EP-450 used as cladding [2.19]. As there were 37 pins in each assembly, there was a range of strains for each assembly. The dotted lines represent the expectations of the Russian researchers for further strain had the last assembly been allowed to receive more exposure.

expected from fission gas pressure alone, being driven primarily by fuel clad contact due to fuel swelling at such high burnup. Most importantly, at 108–163 dpa, not a single one of the 148 pins had failed or leaked, demonstrating the potential of this steel to reach higher dpa levels.

An HT9 duct irradiated in FFTF to a maximum of ~155 dpa was examined and found to have very little swelling, although isolated areas bloomed with well-formed voids at several tenths of a per cent swelling [2.20, 2.21], indicating that swelling at ~155 dpa probably lies just below the average incubation dose. Figure 2.17 (top) shows an example of such an observation.

Figure 2.17 (bottom) shows two micrographs from pressurized tubes irradiated in FFTF at ~400°C to 208 dpa [2.22]. These two tubes were maintained at hoop stresses of 0 and 200 MPa with intermediate tubes at

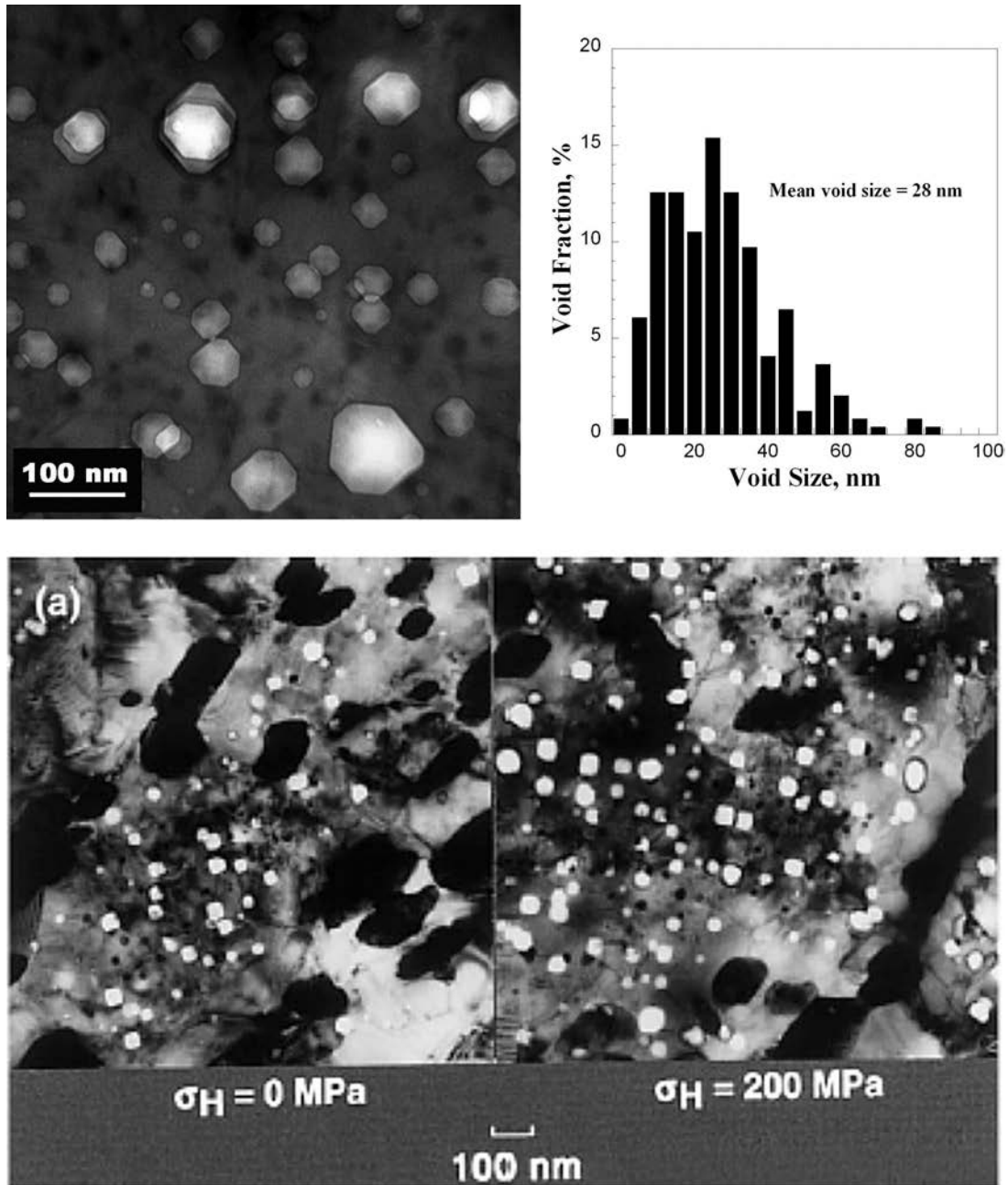


FIG. 2.17. (Top) Swelling observed in an HT9 duct irradiated in FFTF to 155 dpa at 450°C [2.20]. (Bottom) Swelling observed in walls of pressurized tubes irradiated in FFTF at ~400°C and 208 dpa [2.22]. The density changes at 0 and 200 MPa stress levels were ~0.9% and 2.6%, respectively.

stresses of 50, 100 and 150 MPa. Density measurements were made at all stress levels and increased linearly with stress from ~0.9% to 2.6% swelling. Austenitic experience shows that when a strong effect of stress on swelling is observed, then the end of the transient regime of swelling is approaching.

If this generality is also relevant to ferritic and ferritic–martensitic alloys, the swelling rate might be expected to accelerate by perhaps ~300 dpa. Under neutron irradiation, however, it has not yet been demonstrated that ferritic alloys display a bilinear swelling behaviour (incubation transient followed by a higher steady state swelling rate) as observed in austenitic alloys.

There is another generality developed from experience with austenitic alloys that might provide some guidance in forecasting the possibility of bilinear swelling in these alloys. Whenever a trend was observed in simple solute free model alloys, it was very likely that the same tendency would eventually assert itself in more complex solute modified and thermal–mechanically processed alloys.

Note in Fig. 2.18 that the Fe–Cr binary model alloys exhibit a bilinear swelling behaviour in both EBR-II and FFTF [2.23, 2.24]. Two features are of particular note. First, the eventual swelling rate appears to be on the order of ~0.2%/dpa. Second, the incubation transient regimes are much longer in FFTF than in EBR-II. This latter difference is thought to reflect the influence of two differences in the neutron flux spectra. FFTF has a softer spectrum and produces significantly less helium per dpa. FFTF also has a dpa rate that is about three times larger. Both of these factors are known to prolong the transient regime of swelling. Note that in Fig. 2.18(b), the transient regime also increases with increasing temperature and increasing dpa rate.

The tendency for the transient regime of austenitics to be shortened at lower dpa rates is well established for both model and complex alloys [2.25–2.28]. As shown in Fig. 2.19, a similar trend has been observed in EP-450 irradiated in three Russian fast reactors with significant differences in dpa rate. The most swelling per dpa was observed in reactor BR-10, with the lowest dpa rate.

ODS alloys are generally thought to be relatively immune to swelling due to the high density of stable microstructural sinks (dispersoids) serving as annihilation centres for point defects and as collection surfaces for helium so as not to assist in void nucleation. However, neither of these two concepts has been conclusively demonstrated experimentally.

There are not large amounts of swelling or creep data on ODS steels at very high exposure, but data developed on MA957 irradiated in FFTF at 80–110 dpa did not display any voids [2.30].

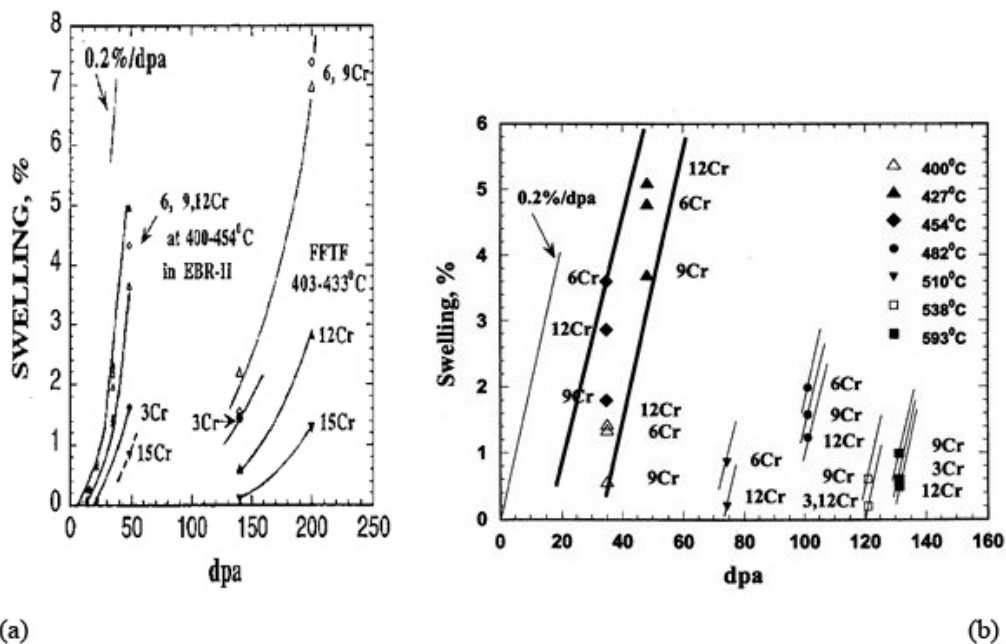
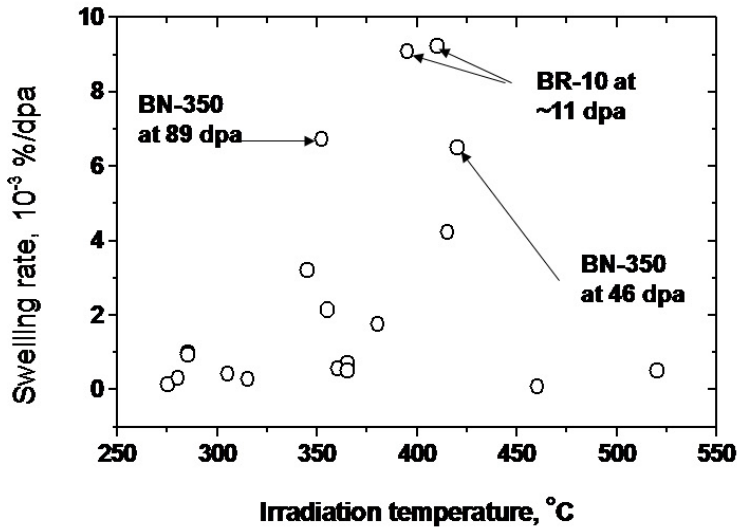
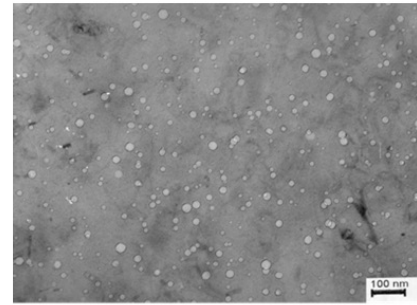


FIG. 2.18. Swelling measured by density change of model Fe–Cr binary alloys in: (a) EBR-II and FFTF at 400–454°C and (b) in EBR-II only, but over a wider range of temperatures [2.23, 2.24].

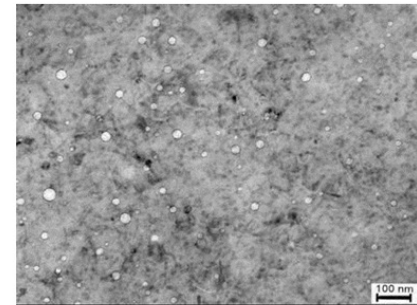


dpa rate in BR-10: 7×10^{-8} dpa/sec
dpa rate in BN-350: $1-2 \times 10^{-6}$ dpa/sec

Swelling is accelerated at lower dpa rates



89 dpa, 352°C



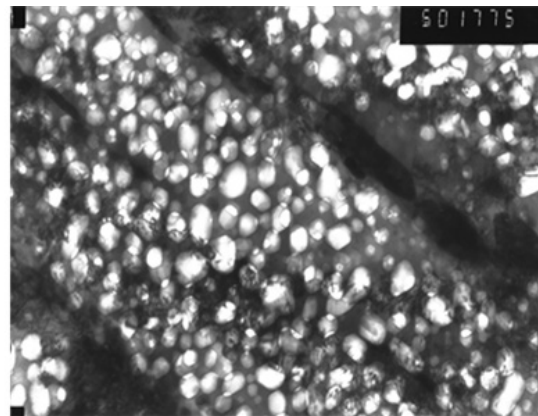
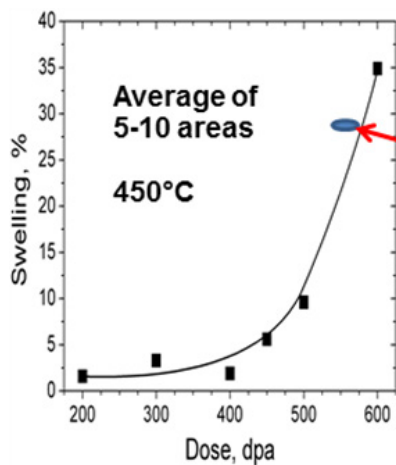
46 dpa, 420°C

FIG. 2.19. Average swelling rates (swelling/dpa) observed in EP-450 by microscopy for three Russian fast reactors. Note that voids have been observed down to the lowest inlet temperature found in BN-350 [2.29].

2.4. EARLY ION IRRADIATION RESULTS FOR COMPARISON WITH NEUTRON EXAMPLES

Chapter 3 shows some results for an ion irradiation facility capable of producing 1×10^{-2} dpa/s while minimizing the effects of surface influences and injected interstitials. Three unpublished results are presented in this section to demonstrate the potential for this ion irradiation facility to extend and supplement neutron data to higher exposures. In the following examples, there was no injection of either helium or hydrogen.

Figure 2.20 shows that HT9 with a tempered martensite matrix can eventually develop a bilinear swelling behaviour with a post-transient swelling rate of $\sim 0.2\%/dpa$, in agreement with the rate observed in Fe-Cr model alloys in EBR-II and FFTF. Section 3.6.6 shows that the ferrite phase of EP-450 also develops this swelling rate, but that it starts at a much lower dpa level of ~ 150 dpa.



28% swelling at 450°C and 550 dpa

FIG. 2.20. Swelling of cold worked HT9 at 450°C to 600 dpa [2.31, 2.32].

Figure 2.21 shows previously unpublished examples by Voyevodin and Garner of the pre-irradiation microstructure of an early heat of MA957 that had a very inhomogeneous distribution of yttria dispersoids, resulting in a very inhomogeneous distribution of void swelling at 400 dpa. It is important to note that MA957 has a ferrite rather than a tempered martensite matrix. Figure 2.22, from the unpublished study, shows that swelling at 450°C and 400 dpa is very inhomogeneous, most likely arising from the inhomogeneous dispersoid distribution.

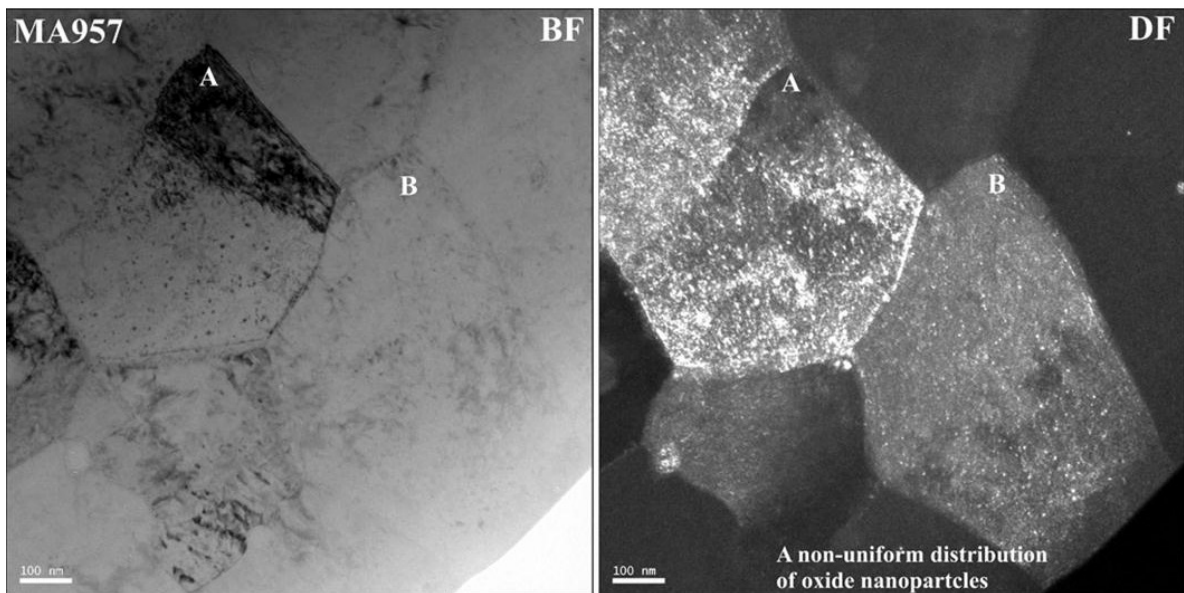
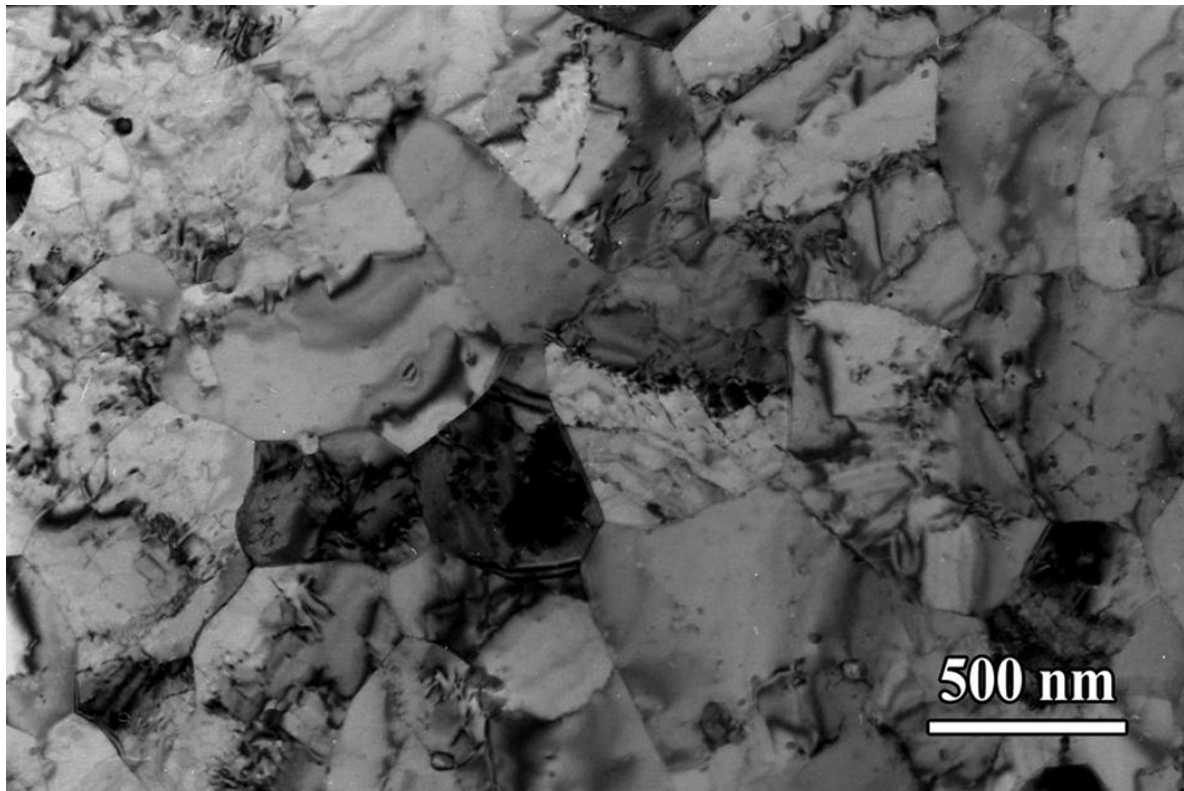


FIG. 2.21. Microstructure of an early heat of MA957 prior to irradiation (previously unpublished). The dark field (DF) image shows that two adjacent grains have yttria densities varying from 0.2×10^{22} to $1.7 \times 10^{22} \text{ m}^{-3}$ (the lower two micrographs were supplied by Luke Hsiung of Lawrence Livermore National Laboratory).

In another better prepared heat used to make pressurized tubes, swelling was more homogeneous at 450°C and 500 dpa and reached only ~3.5% average swelling, but it should be noted that a strong part of the swelling resistance appears to arise from denuded zone effects associated with the highly elongated grains [2.32, 2.33] (see Fig. 2.23).

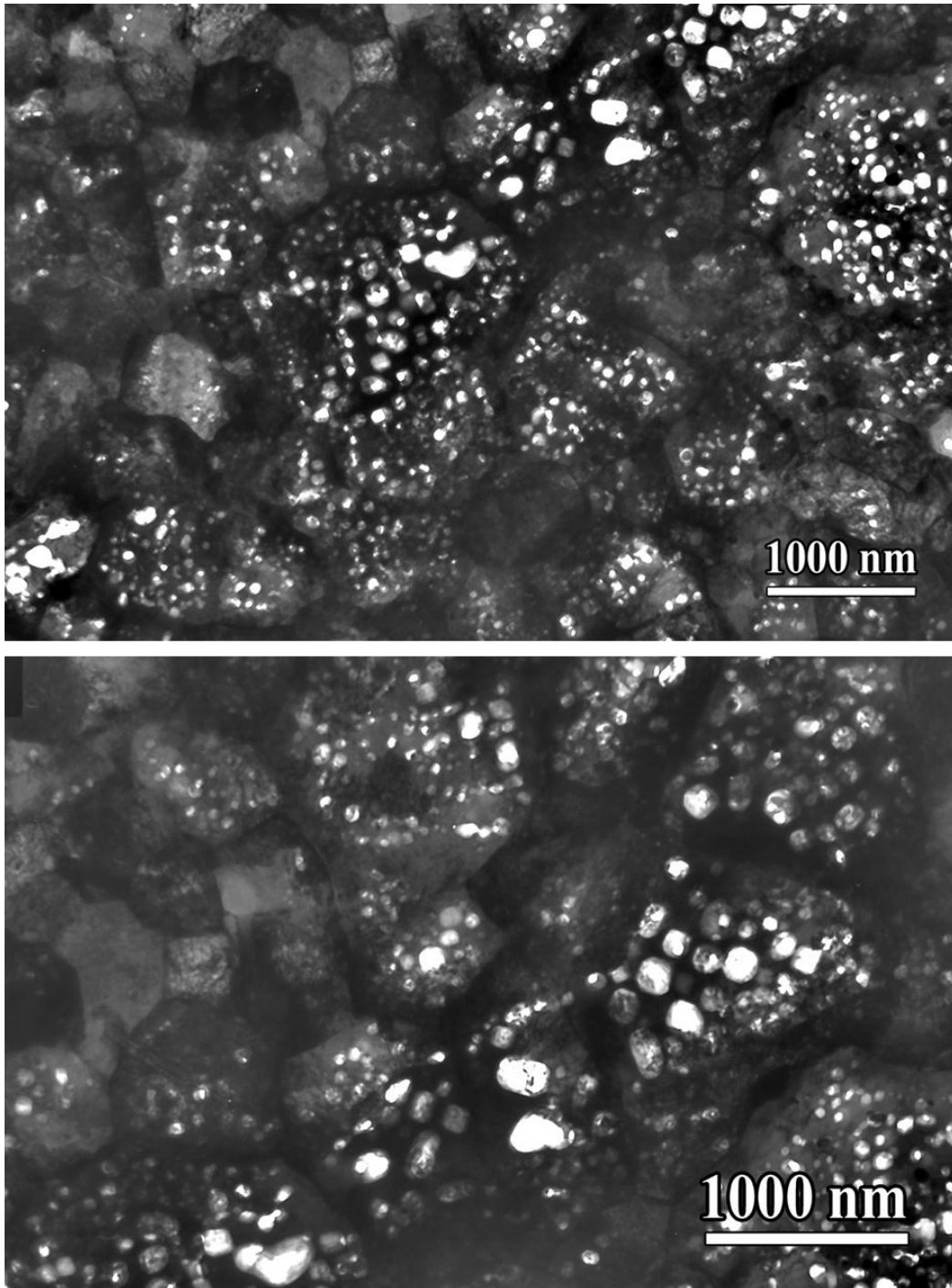


FIG. 2.22. Very heterogeneous swelling observed in MA957 at 450°C and 400 dpa (at a distance and in close-up), most likely as a consequence of insufficient homogeneity of dispersoid distribution (previously unpublished). The average swelling measured over a large area is ~8%.

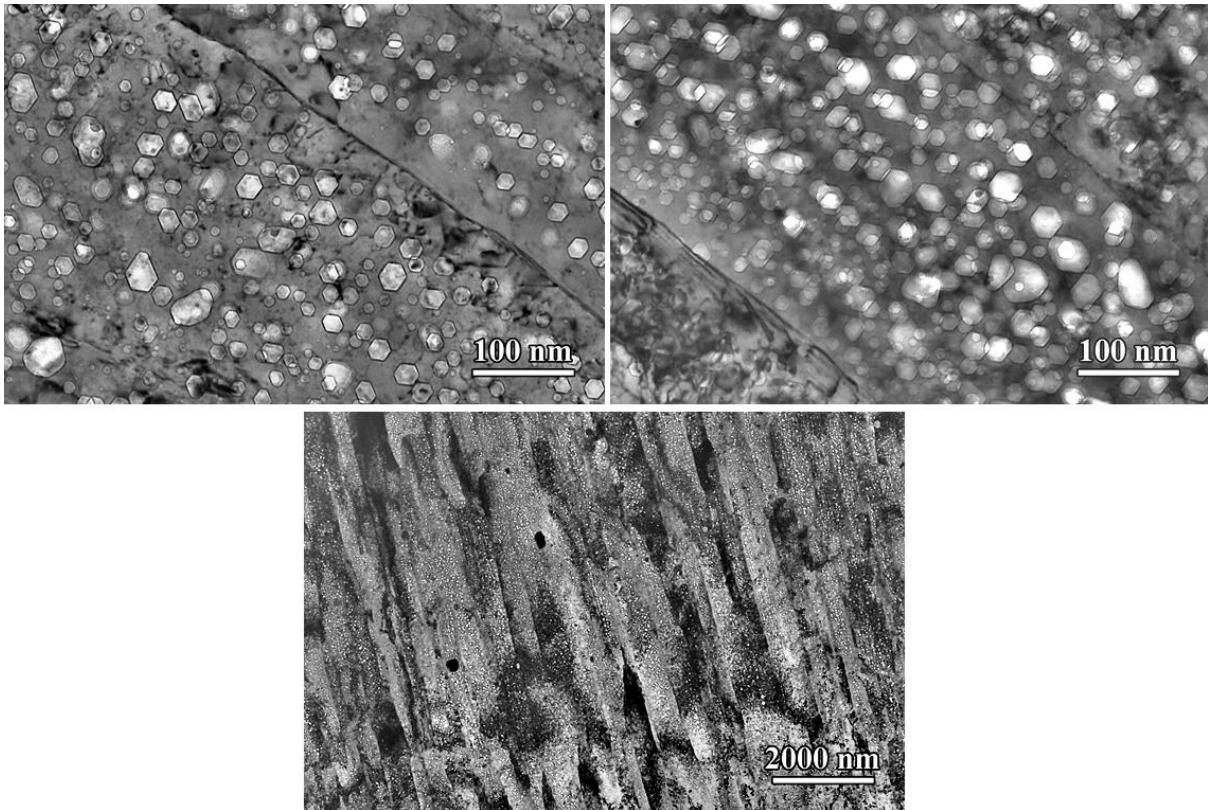


FIG. 2.23. Swelling in three separate areas observed in a tube heat of MA957 after ion irradiation 500 dpa at 450°C [2.33].

Several conclusions can therefore be drawn: first, swelling can be introduced in both ferritic and ferritic–martensitic alloys, even in the absence of helium or hydrogen; second, the eventual post-transient swelling rate might be $\sim 0.2\%/dpa$, as observed in model alloys irradiated in EBR-II and FFTF; and third, dispersoids in a ferrite matrix appear to delay but not preclude the onset of swelling, but only if the dispersoids are homogeneously distributed.

2.5. CONCLUSIONS

- Austenitic alloys cannot be used to reach very high dose levels (<150 dpa) without becoming very distorted by swelling–creep interactions and developing severe void induced embrittlement. Therefore, there is no possibility of increasing fuel burnup using this class of alloys.
- Limited neutron data developed on HT9, EP-450 and MA957 indicate that ferritic, ferritic–martensitic and ODS variants thereof develop significantly less swelling than austenitics and therefore have the potential to reach much higher dpa levels with resulting higher attainable levels of fuel burnup.
- Whereas the post-transient swelling rate of austenitics is $\sim 1\%/dpa$, that of ferritic and ferritic–martensitic alloys may be on the order of only $\sim 0.2\%/dpa$.
- Use of ion irradiation as a surrogate for neutron irradiation appears to offer great promise based on early results, allowing rapid turnaround on alloy improvement studies conducted even to very high doses.
- Given the differences between ion and neutron irradiation conditions, modelling efforts should continue to assess the effects of important variables, especially the dpa rate.

REFERENCES TO CHAPTER 2

- [2.1] GARNER, F.A., “Radiation damage in austenitic steels”, *Comprehensive Nuclear Materials*, Vol. 4 (KONINGS, R.J.M., ed.) Elsevier, Amsterdam (2012) 33–95.
- [2.2] GARNER, F.A., TOLOCZKO, M.B., High dose effects in irradiated face-centered cubic metals, *J. Nucl. Mater.* **206** (1993) 230–248.
- [2.3] ERHLICH, K., Deformation behaviour of austenitic stainless steels after and during neutron irradiation, *J. Nucl. Mater.* **133–134** (1985) 119–126.
- [2.4] GARNER, F.A., HAMILTON, M.L., PANAYOTOU, N.F., JOHNSON, G.D., The microstructural origins of yield strength changes in AISI 316 during fission or fusion irradiation, *J. Nucl. Mater.* **104** (1981) 803–807.
- [2.5] FISH, R.L., STRAALSUND, J.L., HUNTER, C.W., HOLMES, J.J., Swelling and tensile property evaluations of high fluence EBR-II thimbles, *ASTM STP529* (1973) 149–164.
- [2.6] BOND, G.M., et al., “Void swelling of annealed 304 stainless steel at ~370-385°C and PWR-relevant displacement rates”, *Proc. 9th Int. Symp. on Environmental Degradation of Materials in Nuclear Power Systems — Water Reactors*, Newport Beach, CA, 1999, Minerals, Metals & Materials Society, Warrendale, PA (1999) 1045–1050.
- [2.7] POROLLO, S.I., et al., Swelling and void-induced embrittlement of austenitic stainless steel irradiated to 73–82 dpa at 335–360°C, *J. Nucl. Mater.* **258–263** (1998) 1613–1617.
- [2.8] NEUSTROEV, V.S., et al., “Experimental studies of the failure of irradiated ducts in the BOR-60 reactor”, *Proc. 6th Russian Conf. on Reactor Materials Science*, Dimitrovgrad, Russian Federation, 2000 (in Russian).
- [2.9] NEUSTROEV, V.S., GARNER, F.A., Very high swelling and embrittlement observed in a Fe–18Cr–10Ni–Ti hexagonal fuel wrapper irradiated in the BOR-60 fast reactor, *J. Nucl. Mater.* **378** (2008) 327–332.
- [2.10] PORTER, D.L., GARNER, F.A., Irradiation creep and embrittlement of AISI 316 stainless steel at very high neutron fluences, *J. Nucl. Mater.* **159** (1988) 114–121.
- [2.11] MAKENAS, B.J., CHASTAIN, S.A., GNEITING, B.C., “Dimensional changes in FFTF austenitic cladding and ducts”, *Proc. LMR: A Decade of LMR Progress and Promise*, Washington, DC, 1990, American Nuclear Society, Washington, DC (1990) 176–183.
- [2.12] FISSOLO, A., et al., “Influence on irradiated CW titanium-modified 316 embrittlement”, *Proc. 14th Int. Symp. on Effects of Radiation on Materials*, ASTM STP1046, Vol. 2, Philadelphia, PA (1990) 700–713.
- [2.13] STRAALSUND, J.L., POWELL, R.W., CHIN, B.A., An overview of neutron irradiation effects in LMFBR materials, *J. Nucl. Mater.* **108–109** (1982) 299–305.
- [2.14] MAKENAS, B.J., CHASTAIN, S.A., Postirradiation Examination Report for FFTF Extended-Lifetime Fuel Assembly D9-4, Westinghouse Hanford Rep. WHC-SP-0901 (1992).
- [2.15] UWABA, T., ITO, M., UKAI, S., PELLETIER, M., Development of a FBR fuel bundle-duct interaction analysis code-BAMBOO: Analysis model and verification by Phenix high burn-up fuel subassemblies, *J. Nucl. Sci. Tech.* **42** (2005) 608–617.
- [2.16] ASTASHOV, S.E., et al., *Studies of the Structural Materials in the Core Components of Fast Sodium Reactors*, Russian Academy of Science, Ural Branch (1984) 48–84 (in Russian).
- [2.17] GARNER, F.A., GELLES, D.S., “Neutron-induced swelling of commercial alloys at very high exposures”, *Proc. 14th Int. Symp. on Effects of Radiation on Materials*, ASTM STP1046, Vol. 2, Philadelphia, PA (1990) 673–683.
- [2.18] KLUEH, R.L., HARRIES, D.R., High-chromium Ferritic and Martensitic Steels for Nuclear Applications, MONO3, ASTM, West Conshohocken, PA (2001).
- [2.19] FEDOSEEV, A., MAKAROV, O., POVSTYANKO, A., PROKHOROV, V., GARNER, F.A., Ferritic-martensitic steel EP450 as the structural material after irradiation to 108–163 dpa in the BOR-60 reactor, NIIAR Internal Report, *J. Nucl. Mater.* (in preparation).
- [2.20] SENCER, B.H., KENNEDY, J.R., COLE, J.I., MALOY, S.A., GARNER, F.A., Microstructural analysis of an HT9 fuel assembly duct irradiated in FFTF to 155 dpa at 443°C, *J. Nucl. Mater.* **393** (2009) 235–241.
- [2.21] SENCER, B.H., KENNEDY, J.R., COLE, J.I., MALOY, S.A., GARNER, F.A., Microstructural stability of an HT-9 fuel assembly duct irradiated in FFTF, *J. Nucl. Mater.* **414** (2011) 237–242.
- [2.22] TOLOCZKO, M.B., GARNER, F.A., EIHLZER, C.R., Irradiation creep and swelling of the US fusion heats of HT9 and 9Cr-1Mo to 208 dpa at ~400°C, *J. Nucl. Mater.* **212–215** (1994) 604–607.
- [2.23] GARNER, F.A., TOLOCZKO, M.B., SENCER, B.H., Comparison of swelling and irradiation creep behavior of fcc-austenitic and bcc-ferritic/martensitic alloys at high neutron exposure, *J. Nucl. Mater.* **276** (2000) 123–142.
- [2.24] SENCER, B.H., GARNER, F.A., Compositional and temperature dependence of void swelling in model Fe-Cr base alloys irradiated in the EBR-II fast reactor, *J. Nucl. Mater.* **283–287** (2000) 164–168.
- [2.25] OKITA, T., SATO, T., SEKIMURA, N., GARNER, F.A., GREENWOOD, L.R., The primary origin of dose rate effects on microstructural evolution of austenitic alloys during neutron irradiation, *J. Nucl. Mater.* **307–311** (2002) 322–326.

- [2.26] OKITA, T., WOLFER, W.G., SATO, T., SEKIMURA, N., GARNER, F.A., “Influence of composition, helium generation rate and dpa rate on neutron-induced swelling of Fe-15Cr-16Ni-0.25Ti alloys in FFTF at ~ 400°C”, Proc. 11th Int. Conf. Environmental Degradation of Materials in Nuclear Power Systems — Water Reactors, Stevenson, WA, 2003, American Nuclear Society, La Grange Park, IL (2003) 657–663.
- [2.27] BUDYLKIN, N.I., et al., The strong influence of displacement rate on void swelling in variants of Fe–16Cr–15Ni–3Mo austenitic stainless steel irradiated in BN350 and BOR60, *J. Nucl. Mater.* **329–333** (2004) 621–624.
- [2.28] GARNER, F.A., et al., “Microstructural analysis of an HT9 fuel assembly duct irradiated in FFTF to 155 dpa at 443°C”, Proc. 11th Int. Conf. on Environmental Degradation of Materials in Nuclear Power Systems — Water Reactors, Stevenson, WA, 2003, American Nuclear Society, La Grange Park, IL (2003) 647–656.
- [2.29] DVORIASHIN, A.M., POROLLO, S.I., KONOBEEV, Yu.V., GARNER, F.A., Influence of high dose neutron irradiation on microstructure of EP-450 ferritic-martensitic steel irradiated in three Russian fast reactors, *J. Nucl. Mater.* **329–333** (2004) 319–323.
- [2.30] TOLOCZKO, M.B., GARNER, F.A., MALOY, S.A., Irradiation creep and density changes observed in MA957 pressurized tubes irradiated to doses of 40–110 dpa at 400–750 °C in FFTF, *J. Nucl. Mater.* **428** (2012) 170–175.
- [2.31] BRYK, V.V., et al., “Ion issues of irradiation behavior of structural materials at high doses and gas concentrations”, Proc. 11th Int. Topical Mtg on Nuclear Applications of Accelerators, Bruges, 2013, Curran Associates, Red Hook, NY (2013).
- [2.32] GARNER, F.A., et al., Use of self-ion bombardment to study void swelling in advanced radiation-resistant alloys (Proc. 17th Int. Conf. on Environmental Degradation of Materials in Nuclear Power Systems — Water Reactors, Ottawa, 2015).
- [2.33] TOLOCZKO, M.B., et al., Ion-induced swelling of ODS ferritic alloy MA957 tubing to 500 dpa, *J. Nucl. Mater.* **453** (2014) 323–333.

3. ACCELERATORS FOR SIMULATION OF RADIATION DAMAGE

V.N. VOYEVODIN
National Science Center,
Kharkov Institute of Physics and Technology,
Kharkov, Ukraine

Abstract

The results of radiation simulation experiments on different metals and alloys are presented and analysed in this chapter. Using irradiation with charged particle beams, it is possible to reproduce and examine many of the known radiation effects and investigate the physical nature of these effects, in detail, under well-controlled conditions. Additionally, the characteristics of some radiation sources used for studies of radiation effects and some experimental procedures are presented. Accelerator systems, with accompanying high technology instrumentation and methodologies for analysis of experimental data, are shown to provide a comprehensive tool for the determination of mechanisms of radiation damage and the selection of materials with high radiation resistance.

3.1. INTRODUCTION

The worldwide use of nuclear power provides a strong option for production of low cost, long term electrical and thermal power with a guarantee of ecological safety. Nuclear development has proceeded in strong competition with traditional carbon and hydropower technologies, and also with alternative renewable energy sources. Currently, the most effective way to further improve the technical and especially economic characteristics of the nuclear fuel cycle is to increase the burnup of fuel as measured in percentage of heavy atoms (%ha) and in energy produced from a unit quantity of nuclear fuel, measured in gigawatt-day/metric tonnes (GW·d/t). Additionally, these quantities are frequently limited by the cladding of the fuel, not its nuclear characteristics, with exposure of the cladding expressed in units of dpa. Table 3.1 provides a summary of the current status and target goals for these quantities.

TABLE 3.1. CHARACTERISTICS OF PRESENT AND FUTURE REACTORS

Type of reactor	Electrical power (GW·d/t)	Burnup (%ha)	Damage dose (dpa)
<i>Current</i>			
Light water reactors	45–50	~5	8–10
Fast reactors	~75	10–12	80–90
<i>Target</i>			
Light water reactors	75–80 100	~8 ~10–11	12–15 18–20
Fast reactors	~200	20–25	>200

The behaviour of cladding and structural materials under irradiation has been studied for more than 50 years. Most experience has been in the area of thermal reactors, where core structural materials are subject to temperatures up to 400°C and damage levels up to 60 dpa for near-core austenitic internals and up to 10 dpa for typical light

water reactor (LWR) fuel cladding at a burnup rate of 40 GW·d/tU. Fast reactors have been under development for about 40 years and operate at much higher neutron fluxes where exposures reach as high as ~200 dpa for temperatures approaching 600°C.

Looking forwards, it is projected that structural components of Generation IV fission reactors will operate at 500–1000°C and reach damage levels of up to 100–200 dpa. For projected fusion devices with greatly differing neutron spectra arising from neutrons with 14 MeV of energy, there will be a wide range of dpa and temperature levels. For example, the International Thermonuclear Experimental Reactor (ITER) will experience temperatures of only 100–300°C and achieve maximum damage of ~3 dpa, while the prototype demonstration fusion power reactor DEMO is expected to operate in the range 500–1000°C and to reach ~150 dpa at the end of 5 years of full power operation. Radiation doses in future commercial fusion power reactors might be significantly higher than 150 dpa.

High irradiation doses and temperatures planned for advanced fission and future fusion reactors will almost certainly require the development of new, improved materials to reach these exposure levels [3.1]. Ambitious international programmes, such as the International Project on Innovative Nuclear Reactors and Fuel Cycles, Generation IV or the Global Nuclear Energy Partnership, need to address and solve materials problems that restrict or preclude the attainment of reaching higher dpa and thereby preclude higher burnup of fuel [3.2].

The limiting scientific and technical challenge is the lengthy time (20 or more years) required for developing improved materials, testing them in reactors, removing them and obtaining results before licensing can begin. Additionally, the cost of materials testing under neutron irradiation for these advanced nuclear systems is continuously increasing, while the availability of test reactors is steadily decreasing as nuclear facilities of all types continue to be shut down.

The production of radiation resistant materials is a very difficult problem due to insufficient understanding of the nature of radiation induced phenomena and materials damage in the previously uninvestigated ranges of high irradiation doses.

Materials development for operation under the unique conditions of high dose irradiation must therefore make use of existing irradiation facilities other than reactors, with a strong emphasis on using methods of charged particle simulation irradiation.

3.2. SIMULATION EXPERIMENTS

In 1969, Nelson and Mazey [3.3] performed research on specimens of M316 steel that were irradiated by ions of carbon, oxygen and iron, and that showed that the structure of ion irradiated specimens was very similar to the structure of neutron irradiated specimens. Since then, many studies have utilized ion irradiation as a reactor surrogate to study radiation damage. The range of such activities can be illustrated by briefly describing the historical activities of the author's laboratory.

In 1972, the Soviet governmental programme of activities on the physics of radiation damage and radiation material science was approved, focusing on both neutron and charged particle irradiation. This programme ensured scientific assistance with developing new structural materials and predicting their behaviour in operating fast reactors as well as future fusion reactors.

The use of accelerators in radiation materials science and the physics of radiation phenomena at the Kharkov Institute of Physics and Technology (KIPT) began in 1974, and KIPT was appointed the main organization in the Soviet Union for accelerator research on material issues. Over the past four decades, a great deal of experience in the use of charged particle accelerators in simulation technologies has been accumulated at KIPT. Ion irradiation technologies have been shown to considerably reduce the time and materials resources required for selection and optimization of chemical composition, and the thermal and thermal–mechanical treatment of structural materials.

Over the years, the following general observations and conclusions have been drawn:

- The main phenomena limiting the use of materials (embrittlement of reactor pressure vessels, low temperature swelling of austenitic steels in LWRs, growth and deformation of zirconium alloys, and swelling of claddings and wrappers of fast reactors) are interconnected by their common physics, manifested in specific conditions for each phenomenon and alloy.

- The possibility of the use of materials in nuclear power assemblies is determined by the irradiation conditions, especially by the energy spectra of the neutrons, the temperature of irradiation and the coolant environment. These conditions determine the behaviour of ensembles of point defects and transmutants responsible for the degradation mechanisms and for dimensional instability. In most cases, such conditions may be studied using ion simulation technologies.
- The desired goal of reaching high levels of dpa and therefore high nuclear fuel burnup may be realized only on the basis of modern scientific ideas concerning the role of physical mechanisms of radiation induced microstructural evolution that alter the initial physical–mechanical properties. Creation of radiation resistant materials is still very complicated due to insufficient knowledge of the nature of the radiation induced microstructure and the resultant material damage that will occur at the previously uninvestigated range of very high irradiation doses.

Development of theoretical models combined with accelerator simulation of the processes of radiation damage and the resulting microstructure therefore provide an opportunity to explore and possibly predict material behaviour at conditions of lengthy operation in the cores of nuclear reactors. It must be recognized that there is much complexity in the participating processes. The behaviour of point defects and their complexes produced under irradiation, and the high concentration and high diffusive mobility of defects, induce some processes (Fig. 3.1) that are not observed or only weakly demonstrated in conditions without irradiation.

The degradation of initial properties and the loss of radiation resistance are caused by the radiation induced evolution of both microstructure and microcomposition. Irradiation of structural materials at reactor operating temperatures creates the unprecedented possibilities of non-equilibrium changes of microstructure, of significant changes in mechanical properties and especially of changes in the external dimensions of structural components arising from void swelling, irradiation growth and irradiation creep.

The main mechanisms of degradation and dimensional instability arise from the following processes:

- Displacement of atoms from their lattice sites;
- Radiation induced segregation;
- Long range migration and clustering of defects;
- Preferential interaction of interstitial atoms with edge dislocations;
- Formation of transmutants and their interaction with point defects and phase evolution.

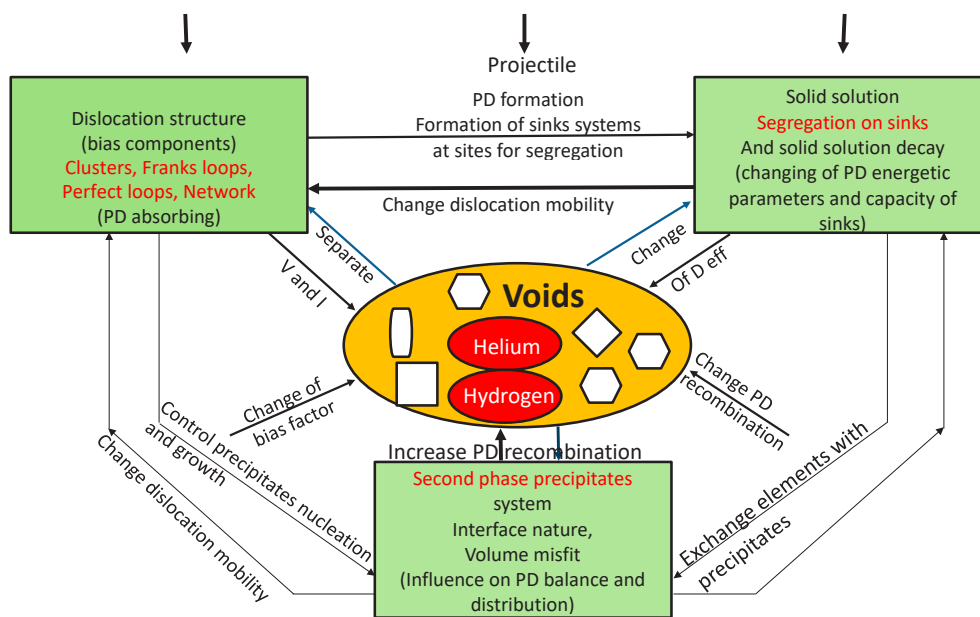


FIG. 3.1. Main relationships observed in structure and composition of austenitic stainless steels under irradiation. I — interstitial; PD — point defect; V — vacancy [3.1].

In this regard, the main tasks to be addressed using accelerators are listed below:

- Investigation of fundamental processes, for example, particle collisions, quantification of the kinetic properties of radiation defects, formation and growth of defects, and assessment of defect characteristics depending on radiation dose (type, size, density, etc.);
- Research and development of materials for fast reactors, especially the investigation of void swelling and embrittlement;
- Observation of radiation induced microstructure producing segregation and hardening;
- Microstructural prediction of possibilities of life extension for operating reactors, focusing on reactor pressure vessel steels, especially the effect of dpa rate on low temperature embrittlement;
- Investigation of the influence of gas on mechanisms of radiation damage, especially on the synergetic effects of helium and hydrogen in fusion, light water and spallation driven systems.

Simulation experiments in investigations of radiation damage have some obvious advantages compared with reactor tests:

- Precise continuous control of the experimental parameters of irradiation, particularly temperature and dpa rate;
- Possibility of direct investigation of different factors on structure phase evolution under irradiation, ideally suited for optimizing alloy composition;
- Absence of induced radioactivity, so that specimens can be handled safely;
- Low cost compared to reactor irradiation;
- Rapid turnaround times compared with reactor irradiation.

The use of accelerators allows researchers to:

- Conduct experiments under cyclic and other non-stationary regimes of irradiation;
- Conduct irradiation in pulsed regimes or concurrent with continuously implanted helium or other gases with variable relationships with the displacement rate;
- Reach exposure doses not yet achieved in nuclear plants;
- Change the rate of damage over large limits;
- Obtain extensive information on the influence of irradiation conditions such as the mass and energy of bombarding particles, dose rate, rate of gas implantation, pulsed beam effects on formation of radiation porosity, dislocation structure evolution and phase state of irradiated material.

Simulation experiments also have substantial disadvantages and limitations:

- Differences in recoil spectra and the structure of primary radiation damage;
- Phase stability differences at high dpa rates and increased temperatures;
- Changes in typical conditions for nucleation and growth of voids;
- Injected interstitial effects on suppression of void nucleation;
- Influences of ion incident surfaces acting as sinks for point defects;
- Difficulties in simulating transmutant accumulation, mainly helium and hydrogen, but also other neutron induced species (the problem with transmutant gases must be addressed using either multibeam or multi-ion accelerators);
- Stress states induced by irradiation compounded with surface proximity.

It is possible to minimize the disadvantages and limitations of simulation experiments by the use of new types of accelerators (dual or triple beam accelerators), by understanding the important effects, especially surface and injected interstitial effects, and by choosing irradiation and examination techniques that reduce the impact of each phenomenon. Additionally, modern high technology methods of investigation can be used to extract detailed information from the small volumes involved. Examples include: transmission electron microscopy (TEM) (loops, cavities and precipitates); scanning transmission electron microscopy (STEM) and energy dispersive X ray

spectrometry and electron energy loss spectrometry (segregation at grain boundaries); atom probe tomography (clusters of solutes); Auger electron spectroscopy and X ray photoelectron spectroscopy (segregations at surface); the use of focused ion beam (FIB) instruments (production of microspecimens); the use of nanoindenters (micromechanical properties); and extended X ray absorption fine structure spectroscopy and small angle neutron scattering (for study of structure evolution on the nanoscale). There are also nuclear physical methods such as Rutherford backscattering spectroscopy (RBS) and channelling (non-destructive analysis yielding the nature of point defects and their localization in lattice), which are covered in Chapter 5.

3.3. SELECTION OF IRRADIATION CHARACTERISTICS FOR SIMULATION EXPERIMENTS

During the study of radiation damage of materials, especially the important phenomenon of void swelling, it is necessary to use all available irradiation facilities (reactors and accelerators). This allows the effects of the structure of primary radiation damage, rate dose, surface influence and ion implantation on the development of radiation porosity (voids and bubbles) to be determined as well as the general and special mechanisms of void swelling. By selecting the type, energy and intensity of particle flux in simulation experiments, it is possible to minimize simulation effects and realize conditions similar to reactor irradiation.

The main criterion determining the selection of the particle type that reproduces the primary processes of material damage under reactor irradiation is the structure of the primary radiation damage. A preliminary conclusion about the degree of reproducibility of the primary event of reactor damage may be drawn by comparing the spectra of primary knocked out atoms. Calculations show that irradiation of metals by self-ions simulates the process of point defect production [3.4].

The advantage of irradiation by self-ions is that the irradiation of pure metals by self-ions at moderate doses does not produce significant alloying (although significant modification can occur in the deposition region at very high exposures). Therefore, for irradiation of composite alloys, it is preferable to use ions from one of the main components of the irradiated alloy.

Particle energy is selected by balancing the surface and ion implantation influences on the processes occurring in the irradiated material. The degree of reproducibility of the primary processes of ion interaction with the matter in the damage peak and in adjacent layers at ion energies higher than 0.5 MeV depends weakly on the primary energy of the ion [3.5]. At 800–1000 K and dose rates of 1×10^{-5} – 5×10^{-3} dpa/s, the surface effects in steel and nickel specimens reach depths of 200–300 nm. Ion beams of metals with energies in the range of 2–5 MeV are widely used, reaching acceptable limits for the effects of surface and ion implantation on the development of porosity in the investigated layer. The beam currently used at KIPT is shown in Fig. 3.2. Note that the shaded area

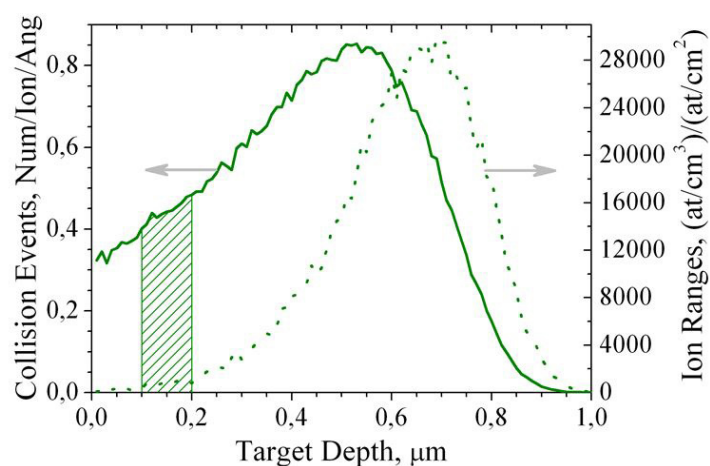


FIG. 3.2. Determination of the depth layer (shaded) that is optimal for microscopy investigation of void swelling. Profiles of damage and deposition of chromium ions with an energy of 1.8 MeV during ion irradiation of stainless steel 18Cr10NiTi [3.6] were calculated using the Kinchin–Pease option of SRIM (stopping and range of ions in matter) 2011 for correct comparison with neutron induced swelling of this steel [3.7].

is chosen as a compromise area for examination by electron microscopy, in order to minimize the effects of the injected interstitial and surface sink. At higher ion energies, intense ion beams deposit excessive energy, creating heat removal and temperature control problems.

The degree of reproduction of nuclear reaction products is determined from comparison of polarized neutron reflectivity spectra for comparable types of irradiation [3.8, 3.9]. In experiments with gas ion irradiation and with coincident beams, an area for investigation is selected in which gas atoms are implanted for the required ratio with number of dpa.

Selection of the particle flux intensity (dose rate) should take into account that changes induced by acceleration of damage must allow for the concept of temperature shift, arising during accelerated irradiation, where the swelling regime moves to higher temperatures as the dpa rate increases (see Fig. 3.3). The higher the difference in damage rates in reactor conditions and in simulation experiments, the lower the probability that variations in porosity development caused by an increase in the damage rate will be completely or adequately described by the temperature shift. In simple metals, such as nickel, such variations are not very pronounced, but in more complex metals and alloys, there are other rate sensitive processes involving phase stability (structure phase transformations) that may compete in the void swelling process.

For pure nickel, the following relationship between dose rate (Φ) and temperature (T) can be described by the following equation: $T_1/T_2 = A \ln(\Phi_2/\Phi_1)$ [3.10].

Structure phase transformations intrinsic for reactor irradiation can be implemented in two stage accelerator irradiation experiments. First, the structure phase transformations characteristic of reactor irradiation are introduced by initial accelerator irradiation at low rates of dose accumulation (10^{-7} – 10^{-5} dpa/s), followed by irradiation at higher dpa rates to generate swelling. Another approach is to use specimens previously irradiated in the reactor to produce reactor relevant structure phases, followed by ion irradiation to achieve higher doses. Experience accumulated to date shows that the simulation specific problems discussed earlier have been studied well, to allow understanding of most experimental results as well as the use of accelerators to investigate the behaviour of metals at very high doses.

The international accelerator community is rather diverse and dynamic, and is able to provide bright light sources, high dpa rates in particle generation and precise measurements of physical properties, as shown in Tables 3.2–3.4.

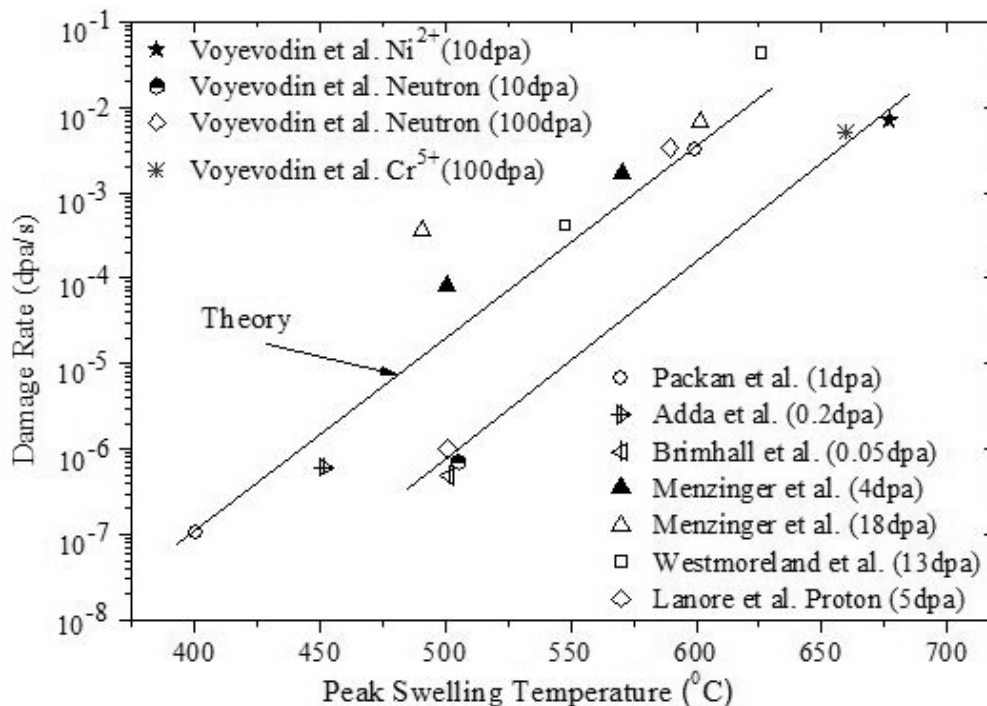


FIG. 3.3. Summary of available data on damage rate induced temperature shift of void swelling in pure nickel [3.1, 3.11]. Note that the peak swelling temperature tends to increase significantly as the dose rate increases.

Figure 3.4 shows that the higher damage rates available in accelerators as a result of higher cross-sections of charged particle interactions with materials (10^{-2} – 10^{-4} dpa/s) compared with rates of displacements in the different reactors (10^{-6} – 10^{-8} dpa/s) allow the necessary doses to be achieved much faster, often in only a few hours.

Heavy ions generate the highest defect production rate, but they possess very short penetration depths, as demonstrated in Fig. 3.2. Protons and electrons generate somewhat smaller dpa rates, but have larger penetration depths, unfortunately coupled with much larger heat deposition by electronic interactions. Therefore, heavy ion accelerators, with beam energies ranging from hundreds of kiloelectronvolts to a few megaelectronvolts, are mainly used for producing high levels of defect concentrations in thin layers of the irradiated material. Figure 3.5 shows the difference in damage efficiencies of various irradiating particles, demonstrating why the choice of particles for irradiation simulation experiments is very important.

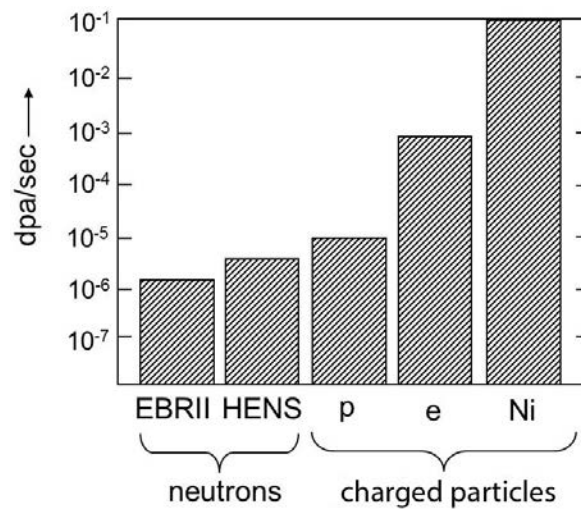


FIG. 3.4. Typical damage rate attainable by fast reactor neutrons and charged particles [3.12].

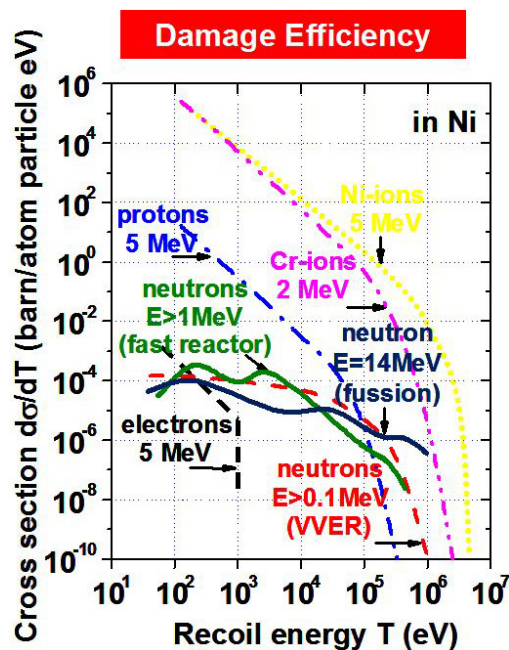


FIG. 3.5. Damage efficiencies of irradiating particles in pure nickel. 1 barn = 1×10^{-24} cm² [3.13].

TABLE 3.2. GLOBAL RESEARCH CENTRES DEDICATED TO IRRADIATION TECHNOLOGIES (DUAL AND TRIPLE BEAM ACCELERATORS)

Laboratory	Facilities	Ions used, damage rates and doses	Reference(s)
MSD, IGCAR, Kalpakkam, India	1.7 MV Tandetron 30–150 kV Ion implanter	Heavy ion or proton and light ion Damage rate 7×10^{-3} dpa/s Dose up to 200 dpa	[3.12, 3.14]
TIARA, Takasaki, Japan	Cyclotron accelerator AVF K110 3 MV Tandem accelerator 3 MV Single ended 400 kV Ion implanter	Heavy ion Light ion/proton Damage rate 10^3 dpa/s Dose 100 dpa	[3.15]
HIT, Tokyo, Japan	3.75 MV Van de Graaff 1 MV Tandetron	Heavy ion and He injection Damage rate 5×10^4 to 10^3 dpa/s Dose up to 10 dpa	[3.14, 3.16]
Nagoya University, Japan	2 MV Van de Graaff 200 kV Ion implanter		[3.14]
FZ, Rossendorf, Germany	6 MV Tandetron 3 MV Tandetron 500 kV Ion implanter	Heavy ion and He, H injection	[3.14]
FSU, Jena, Germany	3 MV Tandetron JULIA 400 kV Ion implanter ROMEO 10 kV Ion beam implanter LEILA	Range of ion fluences: Xe ion, 3×10^{12} to 4×10^{15} ; N ion, 8×10^{13} ions \cdot cm $^{-2}\cdot$ s $^{-1}$	[3.14, 3.17]
IAE, Kyoto, Japan	1.7 MV Tandetron 1 MV Van de Graaff 1 MV Singletron		[3.14]
DuET, Kyoto University, Japan	1.7 MV Tandem 1 MV Single end accelerator	Heavy ion or proton and light ion Damage rate 5×10^{-5} to 2×10^{-3} dpa/s Dose 60 dpa (nominal)	
JAERI, Takasaki, Japan	3 MV Tandem 3 MV Van de Graaff 400 kV Ion implanter		[3.14]
DMN, Saclay, France	3 MV Pelletron EPIMETHEE 2.5 MV Van de Graaff 2.25 MV Tandetron	Heavy ion and He, H injection Damage rate 5×10^{-3} dpa/s	[3.14]
KIPT NSC, Kharkov, Ukraine	1.8 MV Van de Graaff ESUVI and GiV	Heavy ion with He, H ions Damage rate 5×10^{-5} to 7×10^{-2} dpa/s Dose up to 500 dpa	[3.18]
KIPT NSC, Kharkov, Ukraine	ESU-2 1.6 MV Van de Graaff 50 kV Ion implanter 50 kV Ion implanter	Ions (He, Ne, Ar, Kr, Xe) Damage rate 2×10^{-3} to 2×10^{-1} dpa/s Dose up to 300 dpa Ions (He, H, N, O, D) Damage rate 4×10^{-6} to 8×10^{-4} dpa/s	[3.19]

Note: AVF — Azimuthally Varying Field; DMN — Département des Matériaux pour le Nucléaire; DuET — Dual-Beam Facility for Energy Science and Technology; ESU — electrostatic accelerator; ESUVI — electrostatic accelerator with external injector; FSU — Friedrich Schiller University; FZ — Forschungszentrum; GiV — gas ion source; HIT — high-fluence irradiation facility; IAE — Institute of Advanced Energy; IGCAR — Indira Gandhi Centre for Atomic Research; JAERI — Japan Atomic Energy Research Institute; KIPT NSC — Kharkov Institute of Physics and Technology National Science Center; MSD — Materials Science Division; TIARA — Takasaki Ion Accelerators for Advanced Radiation Application.

TABLE 3.3. SINGLE AND DUAL BEAM ACCELERATORS COUPLED TO TRANSMISSION ELECTRON MICROSCOPES

Laboratory	Facilities	Ions used, damage rates and doses	Reference(s)
<i>Mono or dual ion beams (>100 keV) coupled to a transmission electron microscope</i>			
CARET, Sapporo, Japan	1.3 MV High voltage transmission electron microscope 400 kV Ion implanter 300 kV Ion implanter	Electron damage rate 2×10^{-3} dpa/s 70–80 keV H, He injection	[3.15, 3.20]
Tohoku University, Japan	50 MV AVF Cyclotron	Ion (He) damage rate 10^{-3} dpa/s Dose up to 90 dpa	[3.20]
Argonne National Laboratory, USA	2 MV Tandem 650 kV Ion implanter 300 kV Transmission electron microscope		[3.14]
CSNSM, Orsay, France	2 MV Tandem/ Van de Graaff ARAMIS 150 kV Ion implanter IRMA 200 kV Transmission electron microscope	Flux He ion 10^{16} ions·cm ⁻² ·s ⁻¹ Pb ion 1.5×10^{11} ions·cm ⁻² ·s ⁻¹	[3.14, 3.21]
MIBL, University of Michigan, USA	2 MV Protons 5 MV Ion Tandetron	Ion damage rate 10^{-3} dpa/s Proton damage rate 10^{-5} dpa/s Dose up to 500 dpa	[3.22]
<i>Dual kiloelectronvolt ion beams coupled to a transmission electron microscope</i>			
IMR, University of Salford, UK (under construction)	200 kV Transmission electron microscope kV Ion implanter (5–100 kV, $A \leq 140$)	Ions from H to Xe Flux 10^{14} ions·cm ⁻² ·s ⁻¹	[3.14, 3.23]
JAERI, DMD, Takasaki, Japan	400 kV Transmission electron microscope 400 kV Ion implanter 40 kV Ion gun		[3.14]
JAERI, DMSE, Tokaimura, Japan	2×10 kV Ion guns 400 kV Transmission electron microscope		[3.14]

Note: AVF — Azimuthally Varying Field; CARET — Center for Advanced Research of Energy Technology; CSNSM — Centre de Sciences Nucléaires et de Sciences de la Matière; DMD — Department of Material Development; DMSE — Department of Nuclear Engineering and Management, School of Engineering; IMR — Institute of Materials Research; JAERI — Japan Atomic Energy Research Institute; MIBL — Michigan Ion Beam Laboratory.

TABLE 3.4. COMPARISON OF IRRADIATION PARAMETERS AND RADIATION INDUCED SEGREGATION FOR DIFFERENT PARTICLE TYPES

Particle type	Energy (MeV)	Dose rate (dpa/s)	Dose (dpa)	Dpa rate
Electrons	1	2×10^{-3}	28	
Protons	3.4	7×10^{-6}	7	1 dpa–1 day
Nickel ions	5	5×10^{-3}	25	10 dpa–1 hour

3.4. ELECTRON ACCELERATORS AND HIGH VOLTAGE ELECTRON MICROSCOPES

While self-ions are optimal choices for some purposes such as void swelling, electrons are better for other purposes, especially those associated with fundamental effects arising from simple defect configurations and early stages of radiation damage. Electrons are subject to many large angle scattering events, and so the range straggling is severe. In radiation damage studies, however, the primary concern is the passage of electrons through relatively thin targets in which the fractional energy loss is small. This loss can be estimated for many purposes using the following general prescription. Electrons with energy in the range of 1–10 MeV induce displacements of atoms and produce, in metals, defects as isolated Frenkel pairs [3.24]. Therefore, high voltage electron microscopes (HVEMs) with electron beams of energy 1 MeV and higher are widely used, not only as a high resolution research facility, but also as an irradiation accelerator of electrons.

The density of electron beams in modern electron microscopes reaches $2 \times 10^{24} \text{ m}^{-2} \cdot \text{s}^{-1}$ [3.25], producing rates of displacement in metals of 10^{-4} – 10^{-2} dpa/s, which is three to four orders higher than the rates of displacement observed in reactor conditions. The advantage of HVEMs is the possibility to irradiate relatively thick (3 μm) targets and study dynamically the process of development of radiation induced structural defects. This is of great importance for the study of mechanisms of nucleation and growth of dislocation loops, voids and precipitates [3.26, 3.27]; the understanding of the effects of gases and dislocation on the development of radiation porosity [3.28, 3.29]; and the determination of energetic characteristics of point defects and their agglomerates [3.30, 3.31]. Additionally, it is important for determining the relationship between porosity development and transformations in other components of the defect structure [3.32, 3.33]; the study of the behaviour of voids and dislocation loops near dislocations, twins and grain boundaries [3.34]; and finally for investigating voids and dislocation loops produced by preliminary neutron or ion irradiation [3.35, 3.36].

As noted earlier, electrons with energies of 1–10 MeV induce displacement of atoms and produce defects in metals as isolated Frenkel pairs. This has been of the utmost importance in developing the understanding of radiation damage, as it has allowed for studies of defect creation mechanisms.

At KIPT NSC, such irradiation was performed on the electrostatic electron accelerator ELIAS, manufactured by High Voltage Engineering Corporation, model KS/3000. The energy of electrons on the specimen surface was 2 MeV, with a beam current density of 10 mA/cm² and an area of irradiation of 10 mm \times 25 mm.

As an example, the process of point defect annealing in low alloyed Zr–Sc and Zr–Y after low temperature irradiation with electrons of energy 2 MeV has been investigated, and the temperature intervals of the main stages of irradiation successfully determined [3.37]. Figure 3.6 shows the difference curves of spectra of isochronous

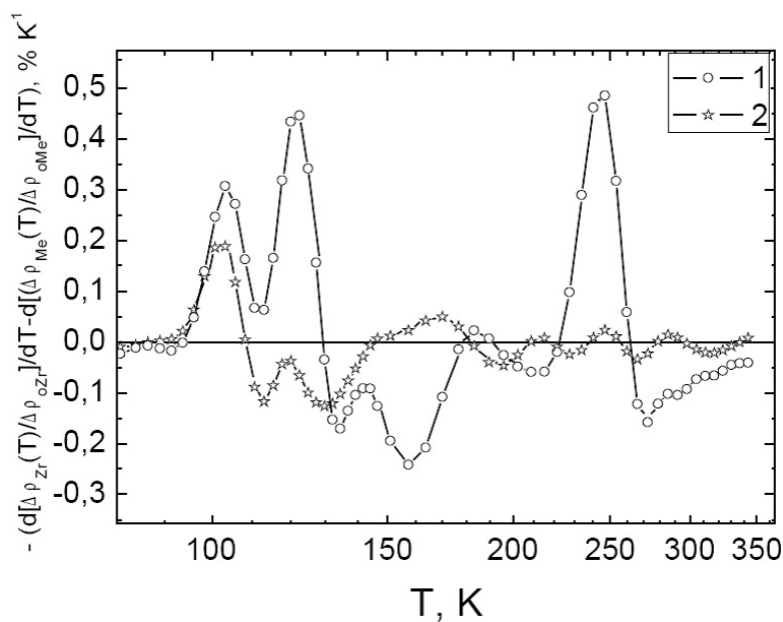


FIG. 3.6. Difference curves of isochronous annealing spectra of (1) Zr–Y and (2) Zr–Sc alloys versus annealing temperature [3.37].

annealing of zirconium and two alloys. In fact, these are the temperature ranges of formation of complexes of the radiation defect (interstitial–vacancy) atom of the alloying element. Spikes below the axis of abscissa indicate the intensification of annealing in alloys in comparison with pure zirconium and identify the temperature ranges of decay of early formed complexes.

Using low temperature (~80 K) irradiation with an electron energy of 2 MeV and measurements of electrical resistance, annealing of radiation point defects has been investigated in low doped alloys Zr–Gd, Zr–Dy and Zr–La. It was experimentally established that impurity atoms such as lanthanum, dysprosium and gadolinium interacted effectively with point defects in the zirconium matrix. Such interactions can result in the formation of interstitial–impurity and vacancy–impurity complexes. This influences considerably the processes of annihilation and redistribution of radiation defects and must be taken into account in the development and modification of zirconium based alloys for use in the cores of nuclear power reactors (Fig. 3.7) [3.38].

Irradiation with high energy electrons ($E > 8$ MeV) leads not only to the generation of Frenkel pairs, but also to the formation of complex radiation defects and nuclear reaction products. This allows for separation of the various mechanisms of radiation embrittlement. High temperature embrittlement exists under irradiation by electrons with γ quanta, with energies higher than the level of nuclear reactions [3.39].

The main reason for the difference in swelling under irradiation by neutrons, heavy ions and electrons with energies of 1 MeV is the difference in the primary processes of radiation damage. In the case of electron irradiation, only formation of isolated Frankel pairs of interstitial atoms and vacancies occurs, while irradiation by heavy ions and by neutrons causes the formation of cascades that then form vacancy loops, producing an excess of interstitial atoms, and simultaneous nucleation of vacancy and interstitial loops then proceeds.

At higher dose levels, the important difference in void evolution in iron based alloys under self-ion irradiation and under irradiation by 1 MeV electrons is the rate of void nucleation. Under ion irradiation, saturation of void concentration requires high irradiation doses (~60 dpa for 30% cold worked steel), but under electron irradiation, the void concentration stabilizes at considerably lower doses: usually 10 dpa or lower and only in special cases at 30 dpa.

The influences of vacancy loops nucleating in cascades under neutron or heavy ion irradiation on the processes of swelling and irradiation creep have been discussed in the literature [3.40]. Their main role during the steady state course of radiation damage processes is the intensification of processes of point defect recombination.

A plot of the swelling characteristics of various steels (Fig. 3.8) demonstrates that at an electron irradiation temperature of 575°C, the rates of swelling of annealed austenitic steel and of 10% cold worked steel became

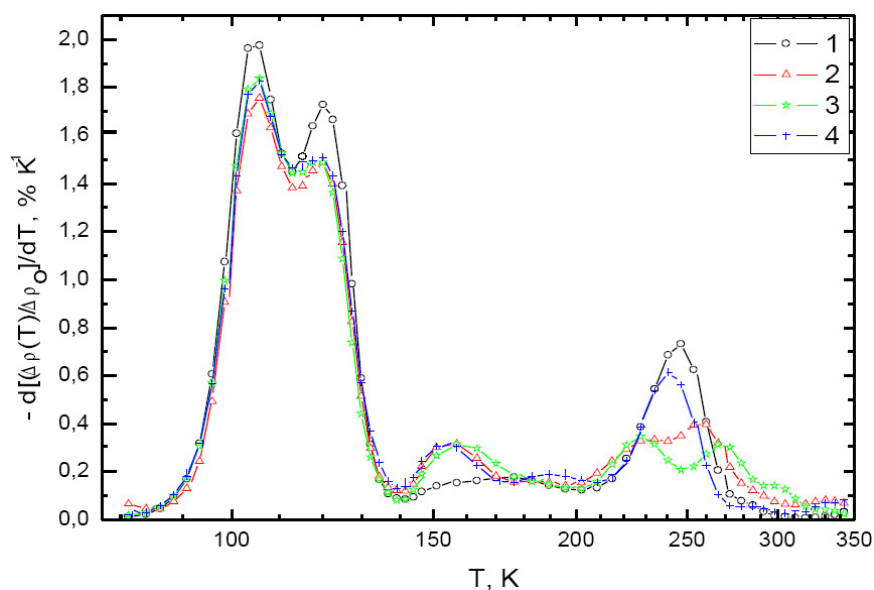


FIG. 3.7. Spectra of isochronous annealing of (1) pure Zr, (2) Zr–Dy, (3) Zr–Gd and (4) Zr–La alloys irradiated with electrons ($E=2$ MeV, $T_{irr}=82$ K, $D=1.4 \times 10^{19}$ e/cm²) [3.38].

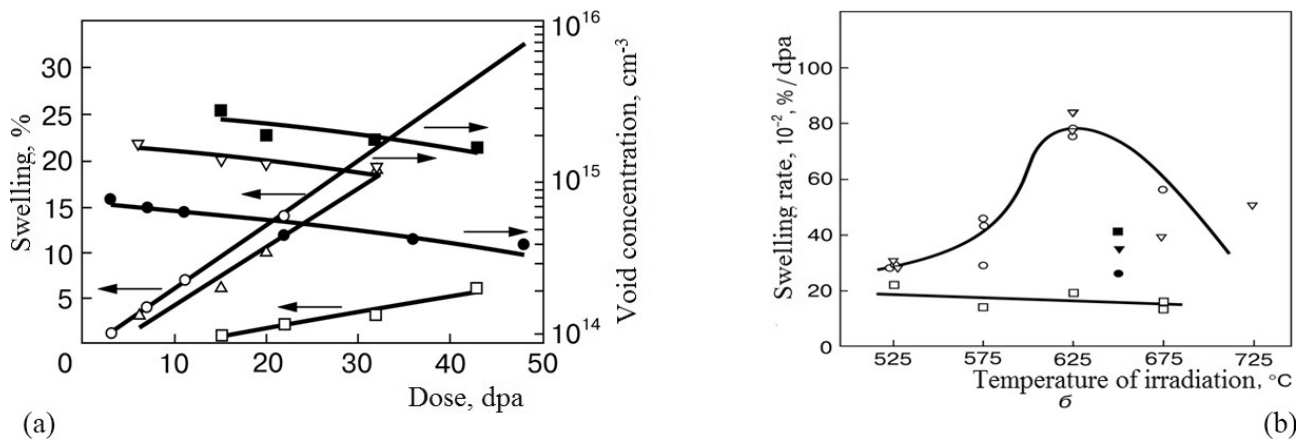


FIG. 3.8. Dependence of: (a) swelling and void concentration on dose in EI-847 steel under irradiation in a high voltage electron microscope ($T_{irr}=600^{\circ}\text{C}$; Δ — void concentration; \circ — solution annealed at 1050°C for 30 min; ∇ — 10% cold working; \square — 30% cold working); (b) rates of swelling on temperature at electron (1 MeV; \circ ; ∇ ; \square — high voltage electron microscope) and ion (3 MeV; \bullet ; \blacktriangledown ; \blacksquare — ion accelerator) irradiation of EI-847 steel in different structural states (\circ — solution annealed at 1050°C for 30 min; ∇ — 10% solution treated; \square — 30% solution treated).

approximately the same. Increasing the irradiation temperature to 625°C leads to a situation in which the swelling rate of 10% cold worked steel becomes higher than that in annealed steel [3.41].

Therefore, investigation of the swelling regime of austenitic steels under irradiation by 1 MeV electrons in HVEMs allows for monitoring of the void evolution during irradiation, and for obtaining additional information on the physics of the phenomena involved.

3.5. LIGHT ION ACCELERATORS: CYCLOTRONS

For investigations of radiation effects such as strengthening, embrittlement, creep and growth of materials, it is necessary to use charged particle beams, with the energy providing homogeneous damage throughout all the irradiated specimen thickness. Therefore, for radiation damage physics studies, high energy beams of protons, α particles, carbon or nitrogen ions, and the like, are used, which can produce a homogeneous defect structure throughout the entire thickness of the irradiated samples. The grain sizes in austenitic stainless steels are 20–30 μm and thus the maximum thickness of the samples for mechanical tests must be on the order of 100–250 μm in order to provide five or more grains across the thickness. Therefore, for these purposes, it is necessary to use charged particle beams with energies that provide a zone of homogeneous damage throughout the thickness of the irradiated specimen. High energy electron and γ beams do not exceed reactor neutron fluxes in displacement production rates, but with regard to helium accumulation, the high energy electron and γ beams are more effective than fast neutrons, by approximately two orders of magnitude. This makes it possible to simulate high temperature radiation.

Cyclotrons are very useful instruments for studying the different effects of radiation damage by use of light ions. Investigation of radiation damage of structural materials is one of the main uses of Cyclotron CV-28, currently located at KIPT NSC. Researchers at the Jülich Research Centre have developed methodologies that allow simulation of the evolution of mechanical properties of materials for nuclear reactors under bombardment by light ions generated in Cyclotron CV-28 [3.42]. They have also developed methods of working with miniaturized specimens and have presented recommendations to carry out mechanical testing of miniaturized irradiated specimens [3.43, 3.44]. Also presented was a method for simulating mechanical property changes in spallation targets by directly implanting helium.

Reference [3.45] presents a study of homogeneously α implanted specimens of a 9Cr–1Mo (EM10) martensitic steel at 550°C to a concentration of 5000 atomic parts per million (appm). The irradiation apparatus is located at a beamline of the Jülich Compact Cyclotron. The initial energy of the α beam (27.4 MeV) was degraded by a rotating wheel consisting of 24 aluminium foils of different thicknesses. In order to obtain a homogeneous implantation, the beam was scanned at saw tooth frequencies of typically 300 hertz (Hz) in both directions across

the specimen. The bubbles were found to be small (average diameter of 5–10 nm) and clearly faceted, as shown in Fig. 3.9.

The aim was to analyse the helium bubbles in an α implanted EM10 steel and to determine precisely the density and pressure by electron energy loss spectrometry. Two main results were obtained:

- The high quality data obtained allowed for the establishment of two linear relationships: one between the energy shift and the estimated helium density, and another between the pressure and the inverse bubble radius;
- By applying an equation of state, it was shown that the bubbles are underpressured and therefore not at equilibrium pressure.

Similar approaches were used at the Kurchatov Institute for cyclotron injection of helium ions into a typical water cooled, water moderated power reactor zirconium based specimen up to damage doses of 10–20 dpa and depths of 100 μm , with subsequent investigations of the structure (by TEM) and the corrosion properties [3.46]. Typical results of the numerical calculation of the distribution profile of the generation rate of point defects under irradiation of zirconium alloy by 15 MeV helium ions at an irradiation dose of 10^{17} cm^{-2} are presented in Fig. 3.10.

Under neutron irradiation, zirconium alloys are subject to structure transformations, elemental redistribution and acceleration of uniform corrosion, particularly for intermetallic type zirconium alloys. Correlation among these processes has long been of interest in the investigation of new zirconium materials for in-pile operation. Neutron irradiation in reactors and the difficulties associated with corrosion tests of irradiated samples therefore call for the use of charged particle accelerators to achieve high damage levels over shorter periods, making experiments both faster and cheaper.

Figure 3.11 shows the microstructural changes in neutron irradiated Russian zirconium alloy E635 up to a neutron dose of $0.5 \times 10^{26} \text{ n/m}^2$ and a damage dose of 2 dpa.

The obtained results show the distribution of precipitates and ordered a-type dislocation loops with an average diameter of 10–20 nm and a bulk density of loops of about 10^{16} cm^{-3} . The same physical picture has been observed after charged particle irradiation on the microstructure of zirconium alloy E635 irradiated on a cyclotron by protons of energy 4 MeV at 350°C and an irradiation dose of 1 dpa ($2 \times 10^{17} \text{ p/cm}^2$), where the ordered structure of dislocation loops was also observed. These experimental results confirm the good correlation between microstructural changes in irradiated zirconium alloys after neutron and charged particle irradiations at comparable dpa levels (1–2 dpa).

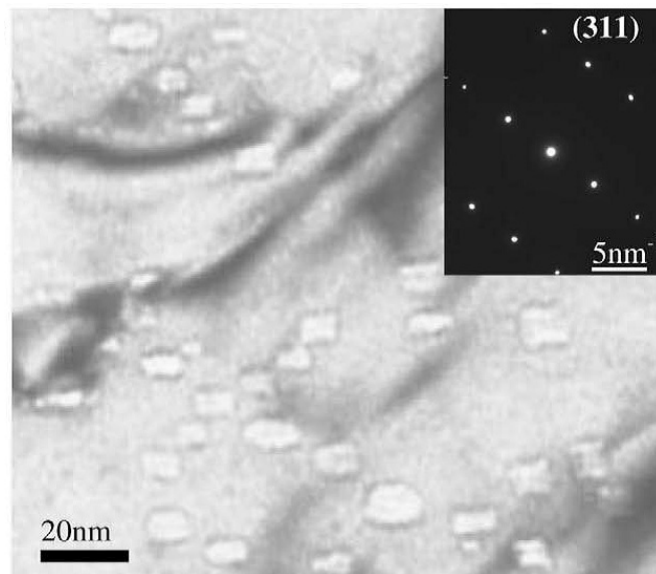


FIG. 3.9. Transmission electron micrograph obtained along the $[311]$ zone axis and the corresponding diffraction pattern of EM 10 martensitic steel after a implantation at 550°C to a concentration of 5000 appm [3.45].

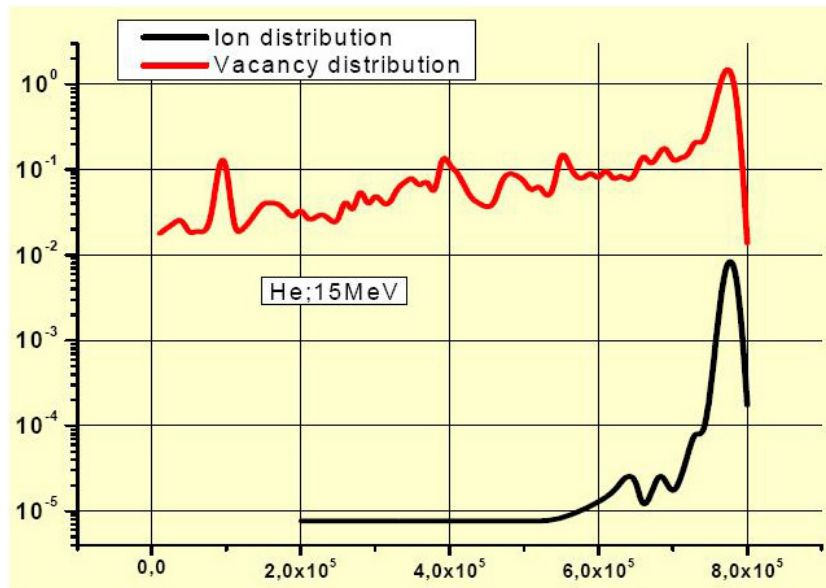


FIG. 3.10. Distribution profile (depth in Å) of generation rate of point defects (number per atom) during irradiation of Zr alloy by 15 MeV helium ions to an irradiation dose of 10^{17} cm^{-2} [3.46].

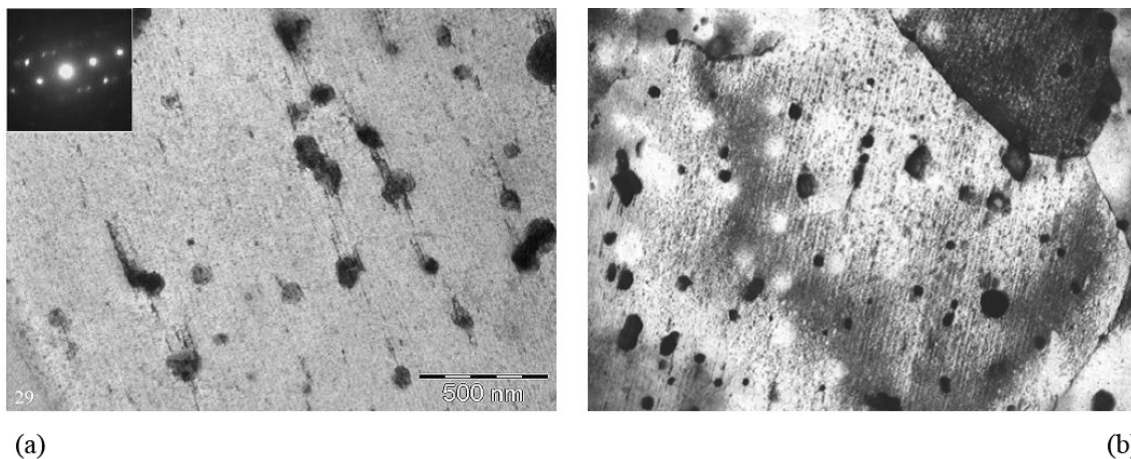


FIG. 3.11. Microstructure of Zr alloy E635 irradiated on a cyclotron by (a) neutrons and (b) helium ions up to a neutron dose of $0.5 \times 10^{26} \text{ n/m}^2$ and a damage dose of 2 dpa [3.15].

3.6. HEAVY ION IRRADIATION

Achieving high burnup (20–25%ha) in fast reactors demands a solution to the swelling problem of cladding and wrapper materials. Up until now, void swelling has been the main limiting factor to using structural materials for fast reactors and for reactors of future generations [3.20]. The advantages of accelerators are considerable because they allow comprehensive studies of different factors that influence void nucleation and growth. Many of these factors, such as the role of structure phase evolution, and the influences of crystal lattice, gaseous impurities, and the like, have already been studied [3.1, 3.47, 3.48]. The role of different alloying elements in the radiation behaviour of cladding for fuel elements has also been investigated [3.49].

The combination of *rate theory* (to approximate the temperature shift required to compensate for changes in dose rate in order to produce the same microstructural effect at a fixed dose) and *efficiency* in producing freely migrating defects can account for the effects of particle type and dose rate in particle beam experiments used to simulate neutron irradiation effects in austenitic stainless steels [3.50].

A standard practice for neutron radiation damage simulation by charged particle irradiation is provided in ASTM standard E521 [3.51].

Using the ASTM standard procedures and recommendations for irradiation with charged particle beams, it is possible to examine practically all known types of radiation effects and investigate the physical nature of these effects in detail under well-controlled conditions. Some successful examples from studies conducted at KIPT are presented below.

Under irradiation, not only does the initial structure change, but there are also changes in the initial solid solution composition. In addition, formation and modification of second phase precipitates are often observed as a result of the interaction of point defect fluxes and atoms in the solid solution. Irradiation modifies the structure phase state of steels and alloys via acceleration and modification of diffusion processes, often producing structure phase transformations that are impossible under conditions of thermal equilibrium [3.1].

Investigation of segregation on segments of the dislocation network has shown that the same tendencies revealed upon investigation of neutral sinks were preserved: enrichment by nickel and silicon and depletion by chromium and iron were often observed. Measurements of segregation profiles on large faulted Frank loops (Fig. 3.12) have shown considerable increases in nickel and silicon concentrations and also decreases in the concentrations of chromium and iron. Factors of enrichment/depletion changed as follows: Ni→1.5; Cr→0.78; Si→1.8; that is, nickel content was 1.5 times higher and silicon content was 1.8 times higher after irradiation.

The content of nickel in the plane of the stacking fault exceeded the content of iron, and nickel became the dominant element of microcomposition of the Frank loop, such that the dislocation loop was surrounded by the region of nickel microalloy with a composition that differed considerably from the composition of the matrix of the base steel. The level of segregation decreased moving away from the plane of the stacking fault, and at a distance greater than 50 nm, the segregation changed sign because the enrichment of the defected plane caused removal from the adjacent matrix. Similar behaviours of segregants with higher levels of segregation on defected Frank loops were detected in steel prime candidate alloy irradiated in the FFTF reactor to 15 dpa at 520°C [3.53].

A decrease in loop size decreases considerably the level of segregation of all elements. About 80% of dislocation loops with diameters greater than 80 nm showed detectable segregation, and loops of sizes smaller than 40 nm did not exhibit such segregation.

In another example, the evolution of metallic carbide (MC) precipitates under irradiation exhibited a relationship with swelling, such that with increasing dose, the concentration of fine dispersed metallic carbide precipitates decreased and their size increased, and the precipitates changed shape from spherical to globular and platelet. It was observed that the moment of precipitate shape change coincided with the onset of fast swelling (Fig. 3.13).

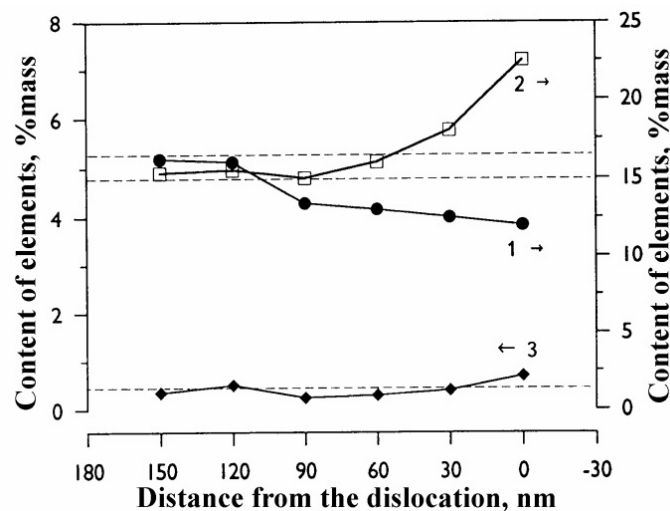


FIG. 3.12. Distribution of elements in the stacking fault plane of a Frank loop (dotted lines show the mean content of elements in the matrix): (1) Cr, (2) Ni, (3) Si (EI-847). Cr^{3+} , $E=3$ MeV, $T_{irr}=600^{\circ}C$, $D=25$ dpa [3.52].

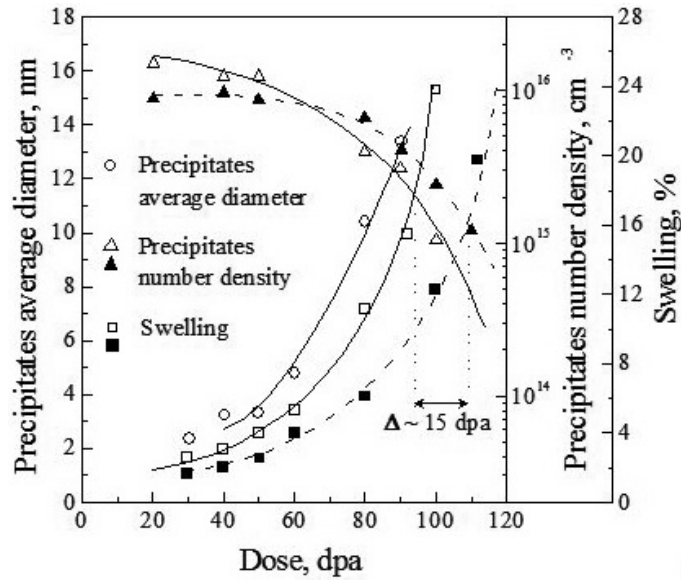


FIG. 3.13. Relationship of metallic carbide precipitate evolution with swelling of EI-847 steel (Cr^{3+} , $E=3\text{ MeV}$, $T_{\text{irr}}=650^\circ\text{C}$) [3.54].

The described modification of precipitate shape means the loss of coherency by metallic carbide precipitates. This initiated the mechanism of phase evolution discussed in Ref. [3.1] that led to heavy infiltration and accelerated growth of precipitates via the flux of solute atoms arriving from the matrix.

Irradiation by heavy ions is a unique method for the study of swelling behaviour of ferritic–martensitic steels, allowing super high irradiation doses to be attained. At KIPT NSC, the possibility of high dose irradiation is currently being realized with the study of swelling of ferritic–martensitic steels in the temperature range $430\text{--}550^\circ\text{C}$. An example is shown in Fig. 3.14, where Russian duplex alloy EP-450 was irradiated with 1.8 MeV Cr^{3+} ions to doses as high as 300 dpa. The maximum swelling of ferrite grains in EP-450 was at a temperature of $\sim 480^\circ\text{C}$. After a lengthy incubation period of ~ 150 dpa, a transition to steady state swelling proceeding at a rate of $\sim 0.2\%/dpa$ was observed. It has been shown that swelling of ferritic steel may reach $\sim 25\%$ [3.52, 3.55]. The tempered martensite grains in EP-450 resisted swelling at much higher doses.

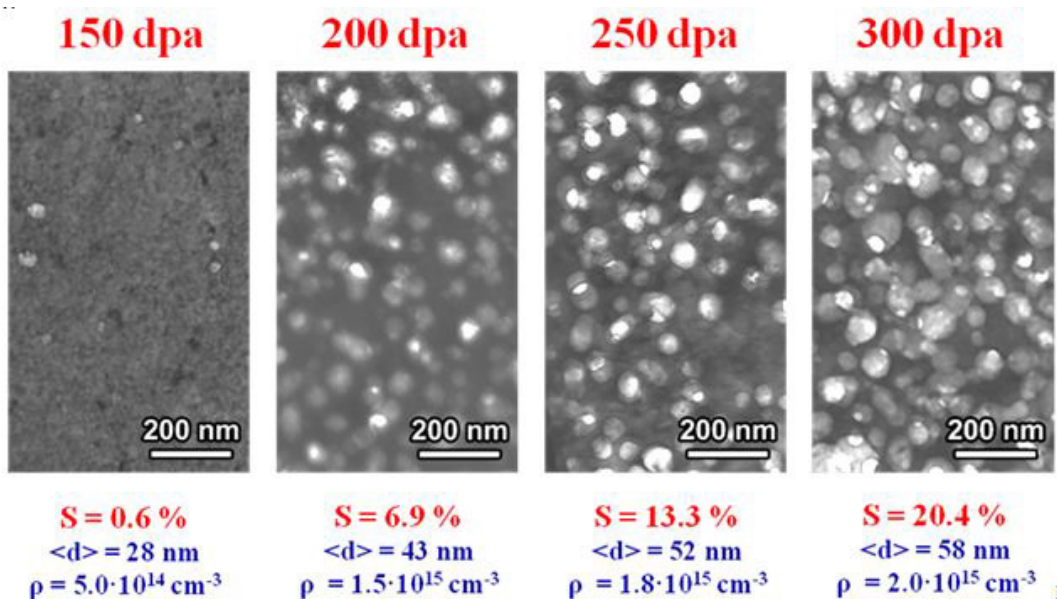
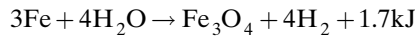
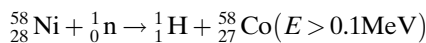
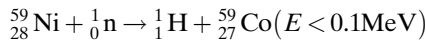
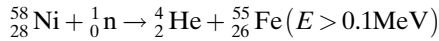
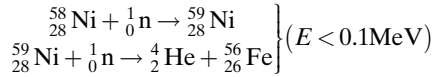


FIG. 3.14. Void volume fraction observed in ferrite grains of EP-450 after irradiation with 1.8 MeV Cr^{3+} ions. After calculating swelling from void volume fraction, swelling at 300 dpa is $\sim 25\%$, reached at a steady state swelling rate of $\sim 0.2\%/dpa$ [3.55].

3.7. MULTIBEAM TECHNIQUES

In nuclear plants, structural materials under neutron exposure are exposed to products, both chemical and nuclear in nature, which are produced simultaneously with radiation damage. The primary sources of helium and hydrogen in thermal reactors result from nuclear reactions in nickel isotopes, and hydrogen can also arise from corrosion, as shown below:



The relevance of investigating the behaviour of helium and hydrogen in metals has increased since results on the interaction of these gases with defects in the crystalline lattice have been obtained, the defected structure and microstructure have evolved, and the impacts of helium and hydrogen on the mechanical properties of structural materials have been observed. Many results have indicated the negative effects of helium and hydrogen after or during joint generation or implantation [3.56].

For instance, the radiation effects and tolerance of several steels under ion and electron irradiation on the hardening, phase stability and helium embrittlement were studied using helium implantation on nano ODS steels [3.57]. The experimental procedures used were ion beam irradiation in the DuET facility, using 6.4 MeV iron ions at 650°C and 5×10^{-4} dpa/s to ~60 dpa. The size distribution of complex oxides before and after ion irradiation was compared, but significant modification could not be detected. Microstructural evolution did not occur, indicating that the dispersed oxides in the ODS steels were stable under the tested conditions. Cavities in reduced activation ferritic steel formed on dislocations and at grain boundaries, but the cavities in the ODS steel were formed mainly at the interfaces of oxide particles with the matrix. Oxide particles obviously acted as trapping sites for helium, suppressing swelling and intergranular embrittlement as a result of preventing helium from gathering at grain boundaries.

Ongoing development of a special irradiation facility at KIPT will allow the simultaneous irradiation of metals with chromium ions, hydrogen and helium in any combination of deposition rates. Originally developed under the Science and Technology Centre in Ukraine's project 3663, evaluation of the performance of ferritic–martensitic steels under gas conditions relevant to advanced reactor concepts, this facility will be used to determine the full parametric performance of all ferritic–martensitic steels currently being developed in the global community for advanced reactor applications. Iron ions will be used to generate radiation damage without gas. The facility will also allow co-implantation of both helium and hydrogen at reactors specific levels using a novel concept of a three ion single beam rather than the usual three accelerator approach. Analysis has shown that good alignment of damage profiles and of profiles of hydrogen and helium ion paths is possible using 1.8 MeV Cr^{3+} ions, 20 keV hydrogen and 40 keV helium. The corresponding deposition profiles for 18Cr10NiTi steel are presented in Fig. 3.15.

A series of such experiments was performed on austenitic iron–chromium–nickel steel 18Cr10NiTi, which is the main material for the pressure vessel internals of water cooled, water moderated power reactors. The effects of synergistic irradiation of materials by gases and heavy ions on defect structure evolution were analysed using JEM-100CX and JEM-2100 microscopes, which revealed considerable influences of gases on swelling of studied steel [3.58, 3.59].

As shown in Fig. 3.16, the temperature dependence of swelling under irradiation only by heavy ions of chromium exhibited a narrow maximum at ~615°C, while maxima of swelling under irradiation by gases in any combination were observed at ~600°C. Under double and triple irradiations, voids were observed over a much

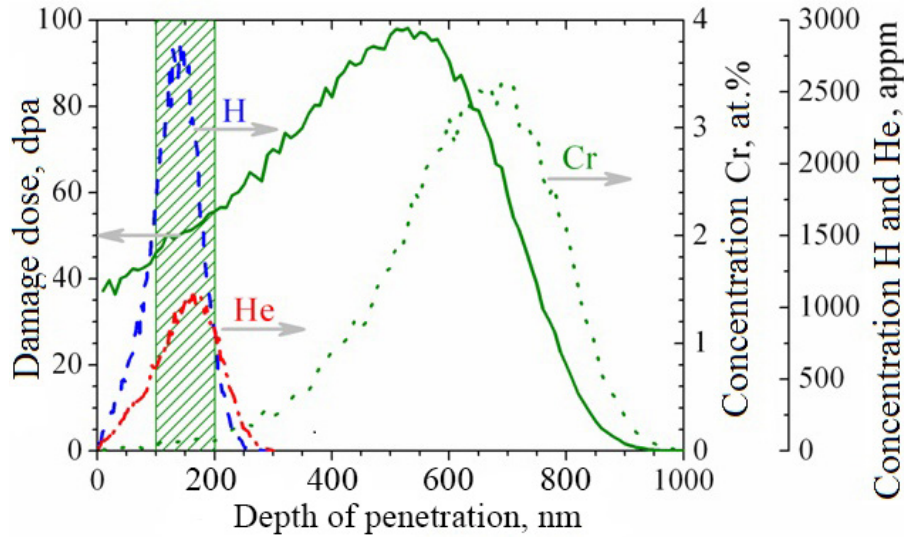


FIG. 3.15. Profiles of damage and range of 1.8 MeV Cr^{3+} in 18Cr10NiTi steel, together with range profiles of 20 keV H and 40 keV He with $n_{\text{Cr}} = 1 \times 10^{17}$ Cr ions/cm², $n_{\text{H}} = 2.4 \times 10^{15}$ H ions/cm², $n_{\text{He}} = 1.2 \times 10^{15}$ He ions/cm². The shaded area is the region investigated by electron microscopy.

wider range of temperatures not characteristic of irradiation by chromium ions only. While helium alone extended the temperature range of swelling, hydrogen was much more effective at increasing the swelling over the same range. When irradiated with both hydrogen and helium, the effects were more complex: decreasing swelling somewhat at lower temperatures, but increasing it at higher temperatures [3.59].

Under irradiation by heavy ions only, the dependence of void concentration on temperature followed the temperature curve of swelling, that is, the concentration increased at lower temperatures (ranging from 590 to 615°C) and decreased at higher temperatures. Helium significantly increased the void density, while hydrogen produced fewer and larger voids. It was also found that after co-irradiation by heavy ions and gaseous ions, grain

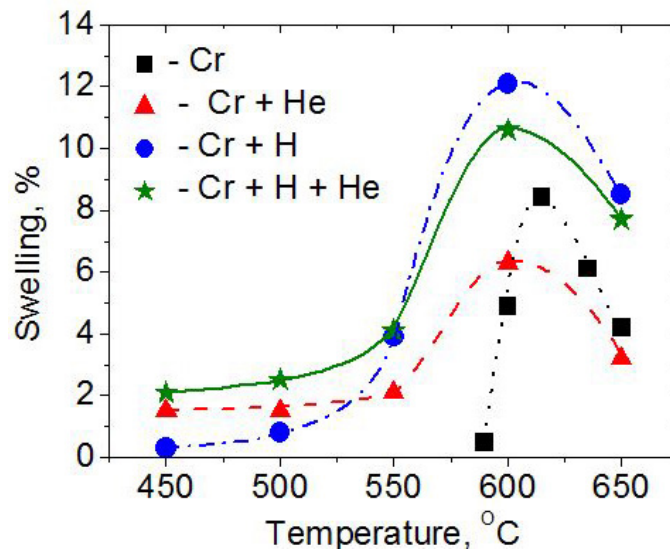


FIG. 3.16. Temperature dependence of swelling of 18Cr10NiTi after irradiation to 50 dpa: ■ — 1.8 MeV Cr^{3+} only; ▲ — 1.8 MeV Cr^{3+} and 60 keV He^+ at 1000 appm; ● — 1.8 MeV Cr^{3+} and 30 keV H^2+ at 2000 appm; ★ — 1.8 MeV Cr^{3+} with 30 keV H^2+ at 2000 appm and 60 keV He^+ at 1000 appm [3.59].

boundary surface influences on the development of radiation porosity were rather low, while areas free from voids along such surfaces were generally not observed.

3.8. CORRELATION OF RESULTS OF REACTOR AND ACCELERATOR EXPERIMENTS ON RADIATION SWELLING OF MATERIALS

During the development and conducting of simulation experiments, two purposes were pursued: first, to accelerate the process of understanding of swelling, and second, to achieve, in practice, the results of simulation experiments for predicting material behaviour under reactor irradiation.

As has been shown, simulation experiments have contributed greatly to the understanding of the phenomena associated with radiation damage, especially because a majority of the mechanisms of radiation porosity were found during the experiments. During irradiation of nickel and steels by ions of inert gases, the development of two systems of voids was detected [3.60]; similar behaviour was also detected under reactor irradiation.

During simulation experiments a hypothesis about the considerable role of the dislocation structure and its transformation in the development of porosity was confirmed [3.28, 3.60–3.62], the influence of gases on porosity development was also studied [3.60, 3.61, 3.63–3.67] and a new phenomenon (formation of a void lattice) was observed [3.67, 3.68].

Additionally, simulation experiments have shown promise in the use of some low swelling materials for fuel claddings and wrappers in fast reactors; these experiments have provided extensive information on the influence of thermal–mechanical treatment, composition and alloying on material behaviour under irradiation [3.69–3.72].

The introduction of simulation experiments in reactor materials science has determined, in a short time, the relationships among radiation swelling and other phenomena under irradiation, allowing for the programme of further reactor experiments to be adjusted or corrected, the mechanisms and phenomena revealed in simulation experiments to be identified and the preliminary classification of materials according to their tendency to high levels of swelling.

In a first approximation, it can be considered that for each type of particle, there is an effective dose (D_i) that determines the fraction of vacancies which were not subjected to annihilation and which were condensed as porosity. Theoretical and empirical development of dose relationships under which radiation induced swelling has the same value (or relationships of swelling values under the same dose) can therefore be realized.

Proton irradiation has undergone considerable refinement as a radiation damage tool [3.73]. Numerous experiments have been conducted and compared to equivalent neutron irradiation experiments in order to determine whether proton irradiations capture the effects of neutron irradiation on microstructure, microchemistry and hardening. In some cases, benchmarking exercises were conducted on the same native alloy heat as neutron irradiation in order to eliminate heat to heat variations, which could obscure comparison of the effects of the two types of irradiating particles.

Similarly, ion bombardment can be used to study swelling if its peculiarities and limitations are understood. In particular, it is necessary to minimize the surface influence and to avoid the influence of injected interstitials.

Using heavy ion irradiation at very high dpa rates (10^{-2} and 10^{-3} dpa/s) and doses (5–100 dpa) and coupling the results to available neutron data, a swelling equation for 18Cr10NiTi steel in Russian fast reactors has been developed within the framework of a single empirical model that specifically incorporates the effect of dpa rate on void swelling [3.74–3.77]:

$$S = (0.25 - 0.022 \ln k) \cdot \phi (D - 103 + 0.1T - 2.6 \ln k) \cdot \exp \left\{ - \frac{(T - 690 - 15.5 \ln k)^2}{2 \cdot (12.3 - 1.9 \ln k)^2} \right\} \quad (3.1)$$

where

- S is swelling (%);
- D is damage dose (dpa);
- T is irradiation temperature (°C);
- k is dose rate (dpa/s);

and the function $\phi(x)$ is defined by:

$$\phi(x) = x \cdot \theta(x)$$

where

$$\theta(x) = \begin{cases} 1, & x > 0 \\ 0, & x \leq 0 \end{cases}$$

Figure 3.17 shows some aspects of the refined behaviour of the ion and neutron datasets. Swelling maps constructed from this model allow forecasting of the behaviour of the steel in water cooled, water moderated power reactors under the required irradiation conditions, not only at already attained exposure doses, but more importantly at the higher dose levels that will be reached following plant life extension.

Figure 3.18 shows predicted dose temperature maps of 18Cr10NiTi swelling that were calculated using Eq. (3.1) at different dose rates typical of accelerator irradiation ($k = 10^{-3}$ dpa/s), fast reactor ($k = 10^{-6}$ dpa/s) and low flux thermal reactor ($k = 10^{-8}$ dpa/s) environments. Note that the swelling becomes progressively greater at lower dpa rates. The generality of this phenomenon is supported by other studies on a variety of austenitic steels, such as that of Budylnin et al. [3.78] and Seran and Dupouy [3.79]. In every case, the shortened incubation period at lower dpa rates leads to earlier and therefore more swelling at the lower dpa rates.

In one exceptional study, 18Cr10NiTi steel, when irradiated in the BR-10 fast reactor at a very low dpa rate (1.9×10^{-9} dpa/s), was observed at 350°C to be clearly swelling after accumulating only 0.6 dpa [3.80].

Figure 3.17 showed that with an increasing dose rate at a given dose, the temperature corresponding to the swelling peak rose. This temperature shift is due to the necessity of keeping constant the relationship between the

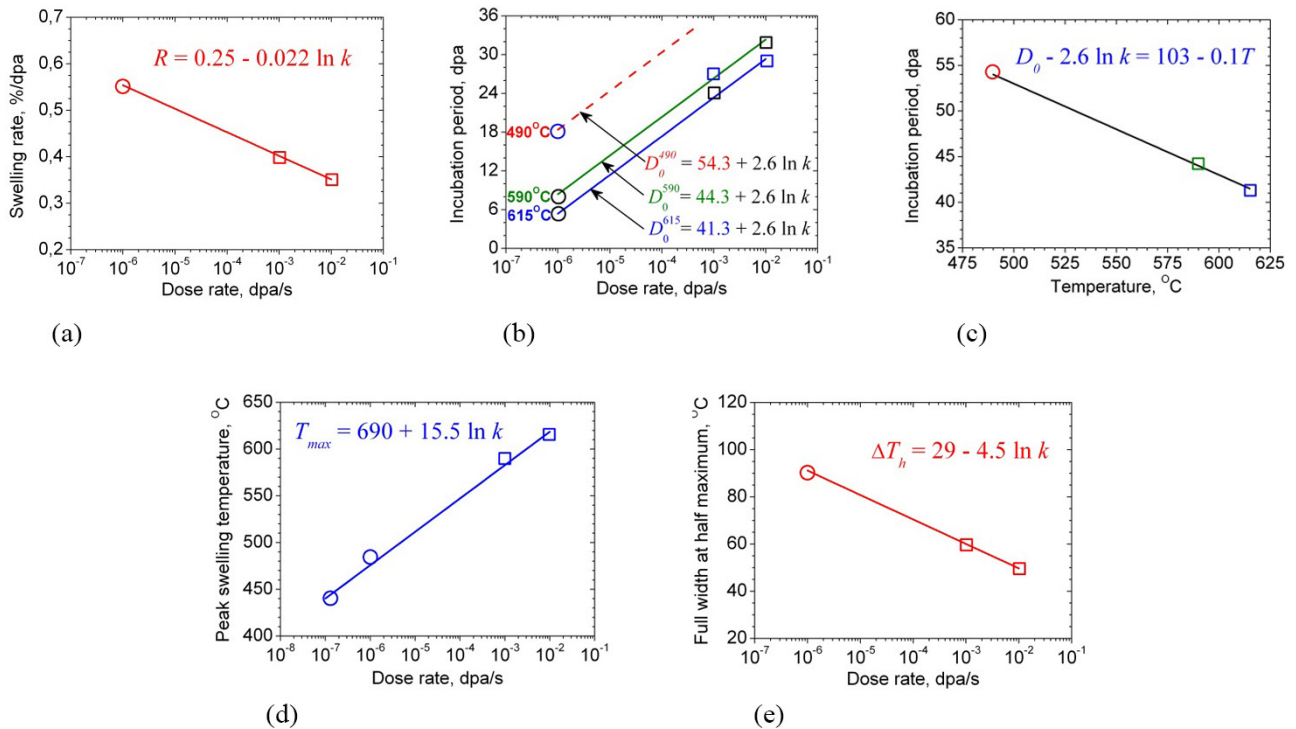


FIG. 3.17. (a) Peak swelling rate; (b) incubation period; (c) the coefficient entering into the approximating function versus irradiation temperature; (d) peak swelling temperature; (e) temperature distribution, all versus the dose rate, in 18Cr10NiTi steel. The symbols \circ and \square designate reactor and accelerator data, respectively R — approximating function; D_0 — incubation period of swelling; $T_{max}(k)$ — maximum temperature of swelling; ΔT_h — full width at half maximum (FWHM) [3.75].

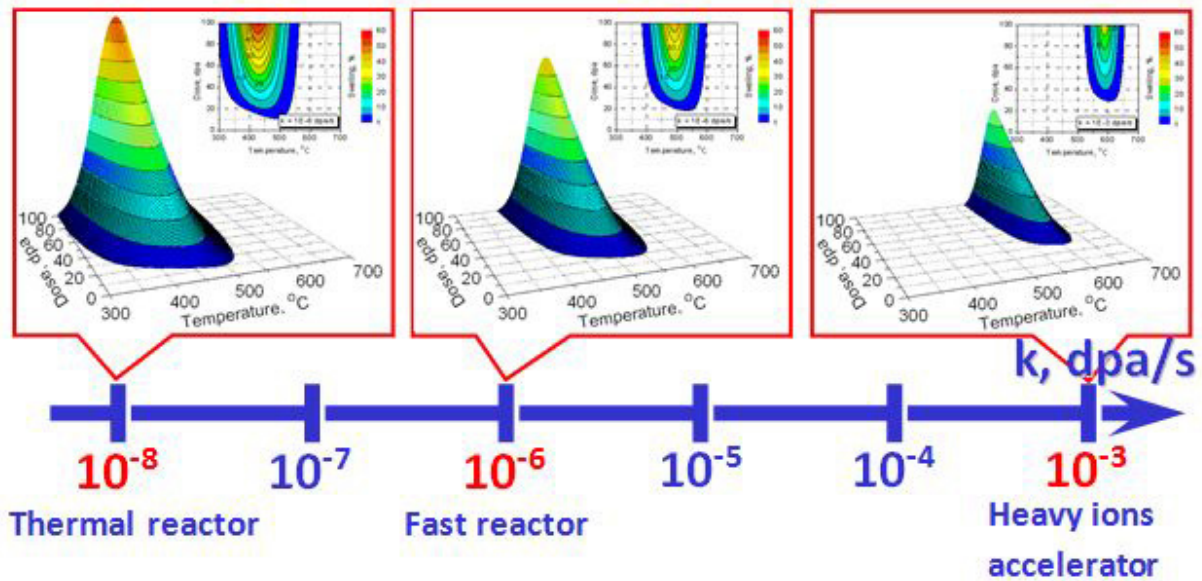


FIG. 3.18. Temperature dose maps of $18\text{Cr}10\text{NiTi}$ steel swelling for different dose rates, calculated using the fitting function of Eq. (3.1).

rates of point defect formation and disappearance at sinks so that the vacancy supersaturation level characteristic of charged particle irradiation conditions can be maintained at reactor relevant levels [3.81].

Therefore, an empirical function incorporating both ion bombardment and fast reactor data of annealed $18\text{Cr}10\text{NiTi}$ steel has been developed to predict the void swelling anticipated in the austenitic core internal components of water cooled, water moderated power reactors, especially under the conditions expected due to plant life extension. This function explicitly contains the dependence not only on the dpa level and irradiation temperature but also on the dpa rate, which is an approach not normally taken in earlier studies that produced equations containing no dose rate dependence.

3.9. PREDICTING RESULTS FOR PRACTICAL APPLICATIONS

What have we learned from the foregoing sections that can guide future studies?

- The results presented here for stainless steels may serve as an example of simulation use for technological purposes. Using irradiation of charged particles in accelerators at KIPT NSC, involving the monitoring of microstructure development, the understanding of the phenomena involved in the process of swelling has allowed for the formulation of scientific presumptions about the industrial levels of swelling resistance of these steels [3.4].
- The stability of the dislocation structure serves as a control in the distribution of fluxes of point defects and thereby determines the rate of further evolution as a result of different absorbing possibilities for point defects and possible segregation.
- The stability of the solid solution is determined by the possibilities of element segregation and by the characteristics of sinks.
- The role of precipitates as predominating mechanisms suppressing swelling depends on the alloying elements included in the precipitates and whether they are capable of changing the nature of the precipitates.
- The evolution of the defected structure in steel under irradiation represents the competition between surviving phases (MC , Fe_2P) and phases evolved as a result of solid solution decay (γ , G and M_6C). This competition may be extended by optimizing the composition and thermal–mechanical treatment.

- The task for future investigation of the synergetic effects of titanium, niobium, vanadium, phosphorus, boron and silicon is consideration of the possible formation of a system of fine stable precipitates under irradiation and the possible decrease of radiation induced segregation.
- One possible method of improving the radiation characteristics of austenitic materials may be the development of ODS–austenitic steels.

3.10. RADIATION RESISTANCE OF STAINLESS STEELS

Attainment of acceptably low levels of swelling is directly associated with formation of very stable microstructures under irradiation. The effects of alloying and treatment therefore involve the following:

- Formation of stable dislocation structures (preserving Frank loops with their inherent low mobility) and increases in point defect recombination. This may be achieved via cold deformation or by segregation of alloying elements on dislocation components that decrease their mobility.
- Preservation of fine carbide precipitates (TiC) and phosphides (Fe₂P) as a main factor of swelling suppression in these steels, shifting the dose range of formation of G phases and η carbides to higher doses.
- Delay of formation of G phases and η carbides will preserve, in a solid solution, sufficient quantities of elements such as nickel, silicon and phosphorus, which strongly influence the nucleation and growth of voids.

3.11. CONCLUSIONS

The current necessity of accelerator use to obtain data is dictated by the following main tasks:

- Provision of a proper understanding of the mechanisms of radiation damage in nuclear materials, obtaining information on the origin of point defects and on interactions among them.
- Determination of the correlations among radiation induced defects, structure phase evolution and mechanisms of material degradation.
- Study of the stability of systems with nano scaled properties that will provide the most promising materials for reactors of the next generation. In particular, it is important to pursue the development and prediction of the radiation behaviour of nano precipitates in ODS steels under high doses.
- Investigation of joint irradiation (reactor irradiation, followed by accelerator irradiation). The defected structure characteristic of reactor irradiation may be formed prior to subsequent irradiation in an accelerator. Despite the experimental complexities this method may present, it gives the best results for predicting radiation behaviour of materials under very high doses.
- Development of the procedure for predicting radiation behaviour of materials to doses characteristic of next generation reactors.

To achieve the goal of development of structural materials for safe and economic operation of existing and future nuclear power reactors, close collaboration of theoreticians, researchers and plant designers is necessary.

REFERENCES TO CHAPTER 3

- [3.1] VOYEVODIN, V.N., NEKLYUDOV, I.M., Evolution of the Structure Phase State and Radiation Resistance of Structural Materials, Naukova Dumka, Kiev (2006) 387 (in Russian).
- [3.2] GARNER, F.A., GREENWOOD, L.R., Neutron irradiation effects in fusion or spallation structural materials: Some recent insights related to neutron spectra, Radiat. Effects Defects Solids **144** (1998) 251–286.
- [3.3] NELSON, R.S., MAZEY, D.J., “Void formation in stainless steel during charged particle irradiation at elevated temperatures”, Proc. Radiation Damage in Reactor Materials, Vol. 2, IAEA, Vienna (1969) 157–163.
- [3.4] NEKLYUDOV, I.M., VOYEVODIN, V.N., Some issues related to making radiation resistant austenitic steels, Phys.-Chem. Mech. Mater. **42** (2006) 15.

- [3.5] GANN, V.V., YUDIN, O.V., “Investigation of the similarity degree of the PVA spectra using heavy ions to simulate neutron irradiation”, *Problems of Atomic Science and Technology, Radiation Damage Physics and Radiation Material Science Issue 3* (1982) 23–25.
- [3.6] BORODIN, O.V., et al., Radiation swelling of ferritic-martensitic steels EP-450 and HT-9 under irradiation by metallic ions to super-higher doses, *Issues of Atomic Science and Technology, Physics of Radiation Damages and Effects in Solids* **72** 2 (2011)10–15 (in Russian).
- [3.7] ZIEGLER, J.F., *The Stopping and Range of Ions in Matter* (2011), www.srim.org
- [3.8] KUZMENKO, V.A., SHILYAEV, B.A., YAMNYTSKYI, V.A., “The possibility to simulate helium accumulation using (p, a) reaction”, *Problems of Atomic Science and Technology, Radiation Damage Physics and Radiation Materials Science Issue 1* (1980) 54–56.
- [3.9] GANN, V.V., “Development of works on mathematical simulation of radiation damages in KIPT”, *Academy of Sciences USSR* **5** (1983) 67–71 (in Russian).
- [3.10] GARNER, F.A., Impact of the injected interstitial on the correlation of charged particle and neutron-induced radiation damage, *J. Nucl. Mater.* **117** (1983) 177–197.
- [3.11] PACKAN, N.H., FARRELL, K., STIEGLER, J.O., The influence of dose rate and injected helium on swelling in pure nickel, *J. Nucl. Mater.* **78** (1978) 143–155.
- [3.12] PANIGRAHI, B.K., et al., Heavy Ion Simulation of Void Swelling of Cold Worked D9, Indira Gandhi Centre for Atomic Research (2004).
- [3.13] ZELENSKIJ, V., et al., “Simulation of radiation damage in materials by charged particles (KIPT experience)”, *Proc. Eighth International Topical Meeting on Nuclear Applications and Utilization of Accelerators (AccApp’07)*, Pocatello, Idaho, 29 July–2 August 2007, American Nuclear Society, La Grange Park, IL (2007) 275–282.
- [3.14] BOUTARD, J.-L., “Combining experiments & modelling for effective pathways to develop new structural materials”, paper presented at the Joint IAEA–ICTP Advanced Workshop on Development of Radiation Resistant Materials, Trieste, 20–24 April 2009.
- [3.15] FLUSS, M., KING, W.E., Report on the Workshop for Science Applications of a Triple Beam Capability for Advanced Nuclear Energy Materials, 6–7 April 2009, Lawrence Livermore National Laboratory, Livermore, CA.
- [3.16] MIURA, T., FUJII, K., FUKUYA, K., “Interaction between dislocation sliding and damage structure in ion-irradiated stainless steels”, *Proc. 2008 Materials Research Society, Fall Mtg Boston, MA, 2008*, Salford University Microscopy Centre, Salford, UK (2008).
- [3.17] WESCH, W., Radiation Effects and Damage Formation in Semiconductors due to High Energy Ion Irradiation, Rep. of Friedrich Schiller University Jena, 7 November 2006.
- [3.18] ZELENSKIY, V.F., et al., Material science of heavy ion accelerator for simulation of reactor damages, *Issues of Atomic Science and Technology, Radiation Damage Physics and Radiation Material Science Issue 2* (1980) 20–23 (in Russian).
- [3.19] TOLSTOLUTSKAYA, G.D., RUZHYTSKIY, V.V., KARPOV, S.A., KOPANETS, I.E., Retention and features of deuterium detrapping from radiation-induced damages in steel, *Problems of atomic science and technology, Physics of Radiation Effect and Radiation Materials Science* **62** 4–1 (2009) 29–41.
- [3.20] TAKAHASHI, H., et al., “Behaviours of cascade damage structure under electron irradiation and annealing”, *Proc. Seventh China–Japan Symposium: Materials for Advanced Energy Systems and Fission and Fusion Engineering*, Lanzhou, China, 2002, World Scientific, London–Hong Kong (2003) 252–259.
- [3.21] SABATHIER, C., CHAUMONT, J., KRUPA, J.-C., Dose rate and temperature effects in radiation disorder creation in SrTiO₃, *Nuclear Instruments and Methods in Physics Research Section B: Beam Interactions with Materials and Atoms* **196**, 3–4 (2002) 308–314.
- [3.22] JIAO, G., WHARRY, J., YU, G., WAS, G.S., “High dose microstructures in ferritic martensitic alloys”, *Proc. 15th Int. Conf. on Fusion Reactor Materials (ICFRM-15)*, Charleston, SC, 2011.
- [3.23] PETKOV, N., In situ real-time TEM reveals growth, transformation and function in one-dimensional nanoscale materials: From a nanotechnology perspective, *ISRN Nanotechnology 2013* (2013) article ID 893060, 21 pages.
- [3.25] BONDARENKO, G.G., BYSTROV, L.N., IVANOV, L.I., PLATOVE, Y.M., Application of a high voltage electron microscopy in solid state physics, *Prog. Phys. Sci.* **116** 2 (1975) 303–314 (in Russian).
- [3.24] LEFFERS, T., SINGH, B.N., BUCKLEY, S.N., MANTHORPE, S.A., Void-swelling in cold-worked copper during HVEM irradiation, *J. Nucl. Mater.* **118** (1983) 60–67.
- [3.26] KIRITANI, M., “Electron radiation damage of metals and nature of point defects by high voltage electron microscopy”, in *Fundamental Aspects of Radiation Damage in Metals (Proc. Int. Conf. Gatlinburg, TN, 1975)*, Vol. 2, National Science Foundation, Oak Ridge National Laboratory, Oak Ridge, TN (1975) 695–721.
- [3.27] BOURRET, A., DAUTREPPE, D., Study of agglomerated defects in irradiated pure nickel by electron microscopy, *Phys. Stat. Sol.* **29** (1968) 283–298.
- [3.28] HARBOTTLE, J.E., The influence of dislocations on the nucleation of voids in nickel, *Philos. Mag.* **27** (1973) 147–157.

- [3.29] BUSWELL, J.T., FISHER, S.B., HARBOTTLE, J.E., NORRIS, D.I.R., “High voltage electron microscope studies of void swelling”, Proc. Int. Conf. on Physical Metallurgy of Reactor Fuels, Berkeley, UK, 1973, Central Electricity Generating Board Rep., London (1975) 170–174.
- [3.30] COCHRANE, B., FISHER, S.B., MILLER, K.M., GOODHEW, P.J., The quantitative analysis of loop-growth and void swelling in nickel, *J. Nucl. Mater.* **120** (1984) 79–87.
- [3.31] FISHER, S.B., WHITE, R.J., MILLER, K.M., Quantitative analysis of void swelling in pure copper, *Philos. Mag. A* **40** (1979) 239–255.
- [3.32] NORRIS, D.I.R., The growth of voids in nickel in a high voltage electron microscope, *Philos. Mag.* **23** (1971) 135–152.
- [3.33] KENIK, E., MITCHELL, T.E., Cooperative growth of dislocation loops and voids under electron irradiation, *Rad. Eff.* **24** (1975) 155–160.
- [3.34] THOMAS, L.E., FISHER, R.M., “HVEM studies of radiation swelling of reactor steels”, Proc. Int. Conf. on Physical Metallurgy of Reactor Fuels, Berkeley, UK, 1973, Central Electricity Generating Board Rep., London (1975) 161–169.
- [3.35] BUSWELL, J.T., FISHER, S.B., HARBOTTLE, J.E., NORRIS, D.I.R., WILLIAMS, K.R., “The application of high voltage electron microscopy to void studies”, CONF-710601, Proc. Int. Conf. on Radiation-induced Voids in Metals, Albany, NY, 1971, Oak Ridge National Laboratory, Oak Ridge, TN (1972) 533–549.
- [3.36] WOLFENDEN, A., A rapid method of deducing the nature of irradiation induced dislocation loops, *Micron* **9** 4 (1978) 211–214.
- [3.37] BORISENKO, V.N., PETRUSENKO, YU.T., BARANKOV, D.YU., VYUGOV, P.N., “Isochronal annealing of Zr-Sc and Zr-Y alloys irradiated by 2 MeV electrons”, *Issues of Atomic Science and Technology, Physics of Radiation Effect and Radiation Materials Science* **2** (2008) 10 (in Russian).
- [3.38] BORISENKO, V.N., PETRUSENKO, YU.T., BARANKOV, D.YU., VYUGOV, P.N., “Isochronal annealing of Zr-La, Zr-Dy and Zr-Gd alloys irradiated by 2 MeV electrons”, *Issues of Atomic Science and Technology, Physics of Radiation Effect and Radiation Materials Science* **6** (2007) 51–54 (in Russian).
- [3.39] ZELENSKIJ, V.F., et al., Utilization of electron accelerators for simulation and studies of radiation effects on mechanical properties of fusion reactor materials, *J. Nucl. Mater.* **207** (1993) 280–285.
- [3.40] BULLOUGH, R., QUIGLEY, T.M., “On the evolution of microstructure during irradiation”, *Point Defects and Defect Interactions in Metals* (TAKAMURA, J.I., et al., Eds), North Holland Publishing, Amsterdam (1982) 23.
- [3.41] VOYEVODIN, V.N., Structure Phase Changes in the Stainless Steels of Austenitic and Ferritic Types under Neutron and Charged Particles Irradiation, PhD Thesis, Kharkov Institute of Physics and Technology (1995).
- [3.42] YEGOROV, A.M., LYMAR, A.G., NEKLYUDOV, I.M., PETRUSENKO, Yu.T., A compact CV-28 cyclotron and prospects for its application, *Problems of Atomic Science and Technology, Nuclear Physics Investigations* **5** (2008) 12–15 (in Russian).
- [3.43] JUNG, P., ULLMAIER, H., “Miniaturized specimens for testing of irradiated materials”, Proc. IEA Int. Symp., Karlsruhe, 1994, KFA — Rep., Forschungszentrum, Jülich (1995).
- [3.44] JUNG, P., HISHINUMA, A., LUCAS, G.E., ULLMAIER, H., Recommendation of miniaturized techniques for mechanical testing of fusion materials in an intense neutron source, *J. Nucl. Mater.* **232** (1996) 186–205.
- [3.45] FRÉCHARD, S., et al., Study by EELS of helium bubbles in a martensitic steel, *J. Nucl. Mater.* **393** (2009) 102–107.
- [3.46] RYAZANOV, A., “Using of charge particle accelerators for investigation of physical mechanisms radiation resistance of fission and fusion structural materials”, *Problems of Atomic Science and Technology. Physics of Radiation Effect and Radiation Materials Science* **62** 4–1 (2009) 116–126.
- [3.47] GARNER, F.A., “Irradiation performance of cladding and structural steels in liquid metal reactors”, *Materials Science and Technology: A Comprehensive Treatment*, Vol. 10A, Nuclear Materials, Part 1 (CAHN, R.W., HAASEN, P., KRAMER, E.J., Eds), Wiley-VCH, Weinheim, Germany (1994) 420–543.
- [3.48] ZELENSKIJ, V.F., NEKLYUDOV, I.M., CHERNYAEVA, T.P., *Radiation Defects and Swelling of Metals*, Naukova Dumka, Kiev (1988) 293 (in Russian).
- [3.49] MITROFANOVA, N.M., et al., “The state of development and the prospect of using the complex alloy steel 07Cr16Ni19Mo2 (EK164) as a core for fuel element of the reactor BN”, *Problems of Atomic Science and Technology, Physics of Radiation Damage and Radiation Material Science* **73–74** (1999) 121–132.
- [3.50] WAS, G.S., et al., Emulation of neutron irradiation effects with protons: Validation of principle, *J. Nucl. Mater.* **300** (2002) 198–216.
- [3.51] American Society for Testing and Materials, Standard Practice for Neutron Radiation Damage Simulation by Charged-Particle Irradiation, ASTM E521-16, ASTM, West Conshohocken, PA (1996).
- [3.52] VOYEVODIN, V.N., AKASAKA, N., Analysis of irradiated structures of core component materials for FBR: Print Japanese Nuclear Corporation report TN 9400 2001-104, November 2001.
- [3.53] KENIK, E.A., HOJOU, K., Radiation-induced segregation in FFTF-irradiated austenitic stainless steels, *J. Nucl. Mater.* **191–194** (1992) 1331–1335.
- [3.54] VOYEVODIN, V.N., NEKLYUDOV, I.M., BRYK, V.V., BORODIN, O.V., Microstructural evolution and radiation stability of steels and alloys, *J. Nucl. Mater.* **271–272** (1999), 290–295.

- [3.55] VOYEVODIN, V.N., et al., "Use of ion irradiation to study swelling of ferritic martensitic alloy EP-450 to 200 dpa and higher", Proc. 15th Int. Conf. on Fusion Reactor Materials (ICFRM-15), Charleston, SC, 2011.
- [3.56] NEKLYUDOV, I.M., TOLSTOLUTSKAYA, G.D., "Helium and hydrogen in structural materials", Issues of Atomic Science and Technology, Physics of Radiation Effect and Radiation Materials Science **3** (2003) 3–14 (in Russian).
- [3.57] KIMURA, A., et al., "Nano sized oxide dispersion strengthening steels for high burnup fuel cladding", paper presented at the 6th Pacific Rim Int. Conf. on Advanced Materials and Processing, Session 14, Energetic Particles-Materials Interactions and Nuclear Materials, Jeju Island, Republic of Korea, 5–9 November 2007.
- [3.58] BORODIN, O.V., BRYK, V.V., VOYEVODIN, V.N., KALCHENKO, A.S., MELNICHENKO, V.V., "Investigation of the defective structure of X18H10T steel under simultaneous irradiation of two and three beam of Cr and He, H ions", paper presented at the XIX Int. Conf. on Physics of Radiation Effects and Radiation Material Science, Alushta, Ukraine, 2010.
- [3.59] BORODIN, O.V., et al., "Synergistic effects of helium and hydrogen on self-ion-induced swelling of austenitic 18Cr10NiTi stainless steel", Proc. 15th Int. Conf. on Fusion Reactor Materials (ICFRM-15), Charleston, SC, 2011.
- [3.60] ZELENSKYI, V.F., et al., On the presence of two void systems in nickel irradiated by xenon ions, Atomic Energy **45** (1978) 61–62.
- [3.61] LANORE, J.M., et al., "Studies of void formation in pure metals", in Fundamental Aspects of Radiation Damage in Metals (Proc. Int. Conf.), Vol. 2, Gatlinburg, TN, 1975, National Science Foundation, Oak Ridge National Laboratory, Oak Ridge, TN (1975) 1169–1180.
- [3.62] HOSSAIN, M.K., BROWN, L.M., Studies of irradiation damage using a high voltage electron microscope, Rad. Eff. **31** (1977) 203–211.
- [3.63] MAYER, R.M., MORRIS, E.T., Neutron irradiation of dilute aluminium alloys, J. Nucl. Mater. **71** (1977) 36–43.
- [3.64] SUNDQUIST, M.L., DONHOWE, J.M., Some effects of preinjected helium and irradiation temperature on void formation in aluminum irradiated with aluminum ions, Nucl. Tech. **31** (1976) 140–143.
- [3.65] BRIMHALL, J.L., SIMONEN, E.P., Effects of helium on void swelling in vanadium, Trans. ANS **22** (1975) 176.
- [3.66] WIEDERSICH, H., BURTON, J.J., KATZ, J.L., Effect of mobile helium on void nucleation in materials during irradiation, J. Nucl. Mater. **51** (1974) 287–301.
- [3.67] EVANS, J.H., Observations of a regular void array in high purity molybdenum irradiated with 2 MeV nitrogen ions, Nature **229** (1971) 403–404.
- [3.68] EVANS, J.H., Observations of a regular void array in high purity molybdenum and T.Z.M. irradiated at high temperatures with 2 MeV nitrogen ions, Rad. Eff. **10** (1971) 55–60.
- [3.69] JOHNSTON, W.G., ROSOLOWSKI, J.H., TURKALO, A.M., LAURITZEN, T., An experimental survey of swelling in commercial Fe–Cr–Ni alloys bombarded with 5 MeV Ni ions, J. Nucl. Mater. **54** (1974) 24–40.
- [3.70] APPLEBY, W.K., CHALLENGER, K.D., "Swelling of cold worked stainless steel — some effects of processing", Proc. Eur. Conf. on Irradiation Behaviour of Fuel Cladding and Core Component Materials, Karlsruhe, 1974, Gesellschaft für Kernforschung m.b.H., Karlsruhe, Germany (1974) 25–28.
- [3.71] WILLIAMS, T.M., ARKELL, D.R., Void-swelling in 20% cold-worked FV548 austenitic stainless steel irradiated with 22 MeV C²⁺ ions or 46.5 MeV Ni⁶⁺ ions, J. Nucl. Mater. **80** (1979) 79–87.
- [3.72] NELSON, R.S., HUDSON, J.A., MAZEY, D., Walters, G.P., Williams, T.M., "Void formation in metals during ion bombardment", CONF – 710601, Proc. Int. Conf. on Radiation-induced Voids in Metals, Albany, NY, 1971, US Atomic Energy Commission, Washington, DC (1972) 430–448.
- [3.73] WAS, G.S., "Dose rate effects in stainless steel and pressure vessel steel using different particle types", paper presented at the Int. Workshop on Influence of Atomic Displacement Rate on Radiation-induced Aging of Power Reactor Components: Experimental and Modelling, Ulyanovsk, Russian Federation, 2005.
- [3.74] KALCHENKO, A.S., BRYK, V.V., VOYEVODIN, V.N., LAZAREV, N.P., "Simulation of swelling in X18H10T steel under simulation and reactor conditions", Issues of Atomic Science and Technology, Physics of Radiation Effect and Radiation Materials Science **4** 2 (2009) 131–139 (in Russian).
- [3.75] KALCHENKO, A.S., et al., Prediction of swelling of 18Cr10NiTi austenitic steel over a wide range of displacement rates, J. Nucl. Mater. **399** (2010) 114–121.
- [3.76] KALCHENKO, A.S., BRYK, V.V., VOYEVODIN, V.N., LAZAREV, N.P., GARNER, F.A., "Analytical description of X18H10T steel swelling based on ion and reactor irradiation data", paper presented at the XIX Int. Conf. on Physics of Radiation Effects and Radiation Material Science, Alushta, Ukraine, 2010.
- [3.77] KALCHENKO, A.S., BRYK, V.V., VOYEVODIN, V.N., LAZAREV, N.P., GARNER, F.A., "Prediction of void swelling in the 18Cr10NiTi stainless steel baffle ring of the VVER-1000 reactor using ion and neutron data", paper presented at the 25th Symp. on Effects of Radiation on Nuclear Materials, Anaheim, CA, 2011.
- [3.78] BUDYLKIN, N.I., et al., The strong influence of displacement rate on void swelling in variants of Fe–16Cr–15Ni–3Mo austenitic stainless steel irradiated in BN-350 and BOR-60, J. Nucl. Mater. **329–333** (2004) 621–624.
- [3.79] SERAN, J.L., DUPOUY, J.M., "The swelling of solution annealed 316 cladding in Rapsodei and Phenix", Effects of Radiation on Materials (Proc. 11th Int. Symp.), ASTM STP782 (1982) 5–16.

- [3.80] POROLLO, S.I., et al., Microstructure and mechanical properties of austenitic stainless steel 12X18H9T after neutron irradiation in the pressure vessel of BR-10 fast reactor at very low dose rates, *J. Nucl. Mater.* **359** (2006) 41–49.
- [3.81] MANSUR, L.K., Void swelling in metals and alloys under irradiation: An assessment of the theory, *Nucl. Tech.* **40** (1978) 5–34.

4. MULTISCALE MODELLING IN NUCLEAR MATERIALS SCIENCE

L. MALERBA
Institute for Nuclear Materials Science,
Boeretang 200 – B-2400 Mol,
Belgium

Abstract

In this chapter, the multiscale nature of radiation effects in materials is illustrated, and the meaning and role of a multiscale modelling approach explained. The modelling tools used in the SMORE CRP are then overviewed as classified based on the processes the models deal with, namely atomic level phenomena, nanostructural and microchemical evolution and mechanical behaviour. The range of applications, strengths and weaknesses of each modelling tool is discussed.

4.1. INTRODUCTION

4.1.1. Radiation effects on materials as a multiscale problem

Radiation effects originate from the interaction of energetic particles (e.g. neutrons with energy >0.1 MeV) with the atoms of a material (here, explicit reference will be made to metals). The nuclear interaction takes only a fraction of a femtosecond (10^{-15} s), and, depending on the type of particle and its energy, may lead to activation, transmutation and atomic displacement [4.1, 4.2]. Only the latter effect is dealt with here. Atomic displacements occur when the particle bounces off the target nucleus (elastic scattering), making it recoil. If the energy transferred in the process is higher than a threshold for displacement, E_d , the corresponding atom is ejected from its initial position. Recoiling atoms lose energy by inducing electronic excitation, as well as in elastic and inelastic collisions with other atoms, which can be, in turn, displaced if they acquire energy in excess of E_d [4.2–4.4]. Thus, a branching atomic displacement sequence called a *displacement cascade* can be produced [4.5–4.8]. The overall lifetime of a displacement cascade is only a few picoseconds (10^{-12} s), and the region affected by it has a characteristic length of only a few nanometres (10^{-9} m). At the end of the process, some point defects (vacancies and self-interstitial atoms) are left in the affected region. These can either be isolated or form clusters. The distribution of defects at this time defines the *primary state of damage*, or *cascade debris* [4.4].

Cascades are produced continuously in the material during irradiation. Yet, it is mainly the further evolution of the defects left in the cascade debris, in interplay with the chemical elements that compose the material, that determines the material's property changes observed at the macroscopic level [4.9–4.17]. This is called *nanostructural evolution*, which occurs at the pace of the diffusion properties of the defects, ranging from microseconds to seconds [4.12, 4.13]. Self-interstitial type defects generally migrate faster than vacancy type defects [4.12, 4.13]. Defects migrate until they are absorbed at so-called *sinks*; therefore, the size and density of the sinks, together with the defect migration mechanism, determine the mean distance covered by migrating defects and their lifetime [4.9, 4.15–4.19]. A sink is any nanostructural or microstructural feature capable of absorbing a specific defect. For example, a cluster of point defects is a sink for point defects, and upon their absorption, it may grow, becoming a three dimensional (3-D) cavity (void) or a platelet (dislocation loop), or it may shrink. In turn, point defect clusters may migrate [4.20–4.26]. Dislocations, grain boundaries and free surfaces are extended sinks for both single point defects and migrating clusters [4.9, 4.18].

While migrating to sinks, defects cause redistribution of chemical elements by diffusion. Therefore, radiation generally assists lengthy diffusion processes [4.27] such as precipitation [4.28–4.31] or segregation [4.32, 4.33]. Radiation makes these processes possible at temperatures at which they would not take place otherwise (radiation *enhanced*, e.g. Refs [4.28–4.30]), or even induces them outside the thermodynamic temperature and concentration ranges (radiation *induced*, e.g. Ref. [4.31]). In turn, the interaction of the defects with chemical species, both impurities and solute atoms, influences their stability and mobility and thus the kinetics of defect cluster formation and defect recombination [4.34–4.37]. These processes, depending on temperature and other factors, develop over

timescales ranging from seconds to years, and produce features at the nanometre to micrometre scale that only a combination of advanced and often sophisticated experimental techniques can unambiguously detect [4.10, 4.11, 4.14, 4.38].

The radiation induced nanostructural and microchemical changes affect the macroscopic properties of the material. For example, cavities, dislocation loops, dislocation networks and precipitates formed due to irradiation act as additional obstacles to dislocation motion upon attempts to deform the material. The macroscopic effect is higher yield strength, that is, hardening [4.39, 4.40]. The difficulty of setting dislocations into motion also affects the ability to resist crack propagation in the material, which thus becomes more brittle [4.11, 4.14, 4.41]. Yet, embrittlement does not need to be accompanied by hardening: radiation induced segregation (RIS) of specific chemical elements, for example, phosphorus, at grain boundaries decreases their cohesion, promoting intergranular fracture [4.42]. Alternatively, embrittlement may be induced at high irradiation temperatures by precipitate coarsening, even though the material does not harden or even becomes softer [4.43]. Crack initiation and intergranular fracture may also be exacerbated by formation of voids and, above all, helium bubbles at grain boundaries [4.44–4.46]. At elevated temperatures, other phenomena also appear, such as swelling and irradiation creep, both leading the material to a loss of dimensional stability. Swelling is the main limiting factor to the long term use of austenitic steels in reactor internal components [4.47]. Finally, microchemical processes like RIS may also influence the onset of swelling and irradiation creep [4.48–4.51], while having an impact on properties such as susceptibility to stress corrosion cracking, because of the change in composition at grain boundaries and surfaces [4.52, 4.53].

These, and other macroscopic effects, all of them originating from the sudden production of defects in nanometric displacement cascades, but taking place over times that can reach the order of years, may seriously compromise the ability of a component to maintain its integrity during operation. These effects are clearly and inherently a multiscale problem. The multiscale nature of radiation effects makes their quantitative prediction especially challenging. The complexity of the problem, and the many variables involved, calls for the support of numerical tools.

4.1.2. What is multiscale modelling?

To create a model, the mechanisms governing the behaviour of the real physical system must first be understood. A model, by definition, does not need to include all details, but it must contain the important ones. A model is expected to be predictive, that is, to behave in the same way as the real system under comparable conditions. Different modelling approaches can be distinguished, ranging from fully empirical to physics based. All rely heavily on the interplay between the performance of experiments and the attempt at interpreting the experimental results, based on an evolving conceptual model. This, when consolidated, is used as a guide to produce the mathematical model, which will allow quantitative verification against experiments, as well as further refinement based on new experimental data. In the process of building a model, the use of a tool, commonly called a *thought experiment*, is instrumental. It is necessary to try to *imagine*, based on the conceptual model, how the system would react to certain experimental conditions, without actually *performing* the experiment, in order to either better design real experiments, or further refine the model, or both.

In the process of constructing a model in interplay with experiments, many unknowns appear, and many different mechanisms are possible. In a physical approach, the preparation of experiments to investigate these unknowns and to discriminate between mechanisms will require very refined thought experiments, because many of the experiments ideally needed will, in practice, be unfeasible. Thought experiments find their natural extension in the use of computer simulations. Computer simulations are, indeed, nothing other than virtual experiments, aimed at identifying and quantifying physical mechanisms, without actually performing the experiment (which might actually be impossible to perform), or in preparation of the performance of a real experiment. Computer experiments can be used for two purposes: (i) to assess quantities, or study processes, that are barely accessible, or totally inaccessible, to real experiments and (ii) to test possible physical mechanisms, in order to verify if they can explain the results of real experiments. Computer simulations turn out to be suitable tools to actually build the physical model that is sought. For this practical reason, computer modelling and physical modelling tend to coincide nowadays.

Moreover, if the problem at hand involves many different length scales and timescales (multiscale), as is the case for radiation effects, it becomes necessary to study the different processes of interest at the correct scales, with

the correct tools, be these experimental, theoretical or computational. A first definition of multiscale modelling can thus read: use of the proper experimental examination and modelling technique to study each phenomenon of interest at the correct scale. However, because of the inherently multiscale nature of the problem, this will generally not be sufficient. Not all details of a model dealing with one scale are needed to build a model at a higher scale. Therefore, it will be necessary to learn how to extract, from the model developed at one scale, the information that is needed either to bridge to a larger scale or to build a comprehensive conceptual model. A second definition of multiscale modelling can thus be: combination of experimental and modelling techniques specific for different scales to describe phenomena at all scales, or at the scale of practical interest. In this process, unavoidably, extensive (and intensive) use will be made of not only advanced theory and experimental techniques, but also, and especially, computer simulations.

In radiation effects, the scales involved range from the atomic level to the component level, passing through all the intermediate levels. Modelling approaches can be classified accordingly. In the following sections, the multiscale modelling tools used in this CRP are overviewed based on the processes that the models deal with, namely atomic level phenomena, nanostructural and microchemical evolution and mechanical behaviour.

4.2. ATOMIC LEVEL MODELLING

Atomic level models use density functional theory (DFT) calculations, energy minimization techniques, molecular dynamics (MD) simulations and Monte Carlo (MC) methods. DFT is a quantum mechanical approximation for solving the Schrödinger equation; the other techniques generally make use of classical interatomic potentials to calculate energy and describe interatomic forces.

Atomic level modelling is generally used to obtain information inaccessible to experiments, thus the experimental validation of these models may be problematic. Certain phenomena are mainly or only known through computer simulations with atomic level models, for example, displacement cascades. Here, the implicit standpoint is that the model is not developed to be compared with experiments: it is based on well-established physics and used in order to gain insight into processes that are known, or supposed, to occur in reality, even though they cannot be directly observed in experiments. These models are true computer experiments, and are meant to complement real ones and to help or enable the interpretation of the results obtained.

4.2.1. Density functional theory calculations and interatomic potentials

DFT is an exact one body reformulation of the many body quantum mechanical problem governed by the Schrödinger equation, which can be used effectively, with the introduction of approximations, to determine the ground state energy of a system of, for example, electrons and ions (see Refs [4.53, 4.54] for good introductions). DFT is currently the most reliable tool for describing the interactions between atoms, without any a priori restriction on the number and type of chemical elements. The main limitation is the high computer power required: as the algorithms scale as N^3 (N is the number of particles), in practice, only systems of about $\sim 10^3$ atoms can be studied. Methods for performing dynamic simulations do exist [4.55, 4.56], but their application is computationally too expensive. Thus, DFT calculations are mainly performed in a static manner, that is, the atomic positions may be relaxed to accommodate the strain due to defects or impurities (using energy minimization techniques such as conjugate gradient methods or others [4.57]), but, apart from this, they do not move during the simulation. Even so, the quantity of information that can be extracted from DFT calculations is enormous. Defects in pure elements or interacting with impurities and solute atoms can be studied in terms of formation and binding energy (for a good example, see Ref. [4.58]). Migration mechanisms and relevant energy values can be explored (e.g. [4.59]) using numerical techniques to search for saddle points in a given energy landscape along minimum energy paths, for example, nudged elastic bands [4.60] or dimer methods [4.61]. All these quantities are experimentally either extremely difficult or totally impossible to measure. But by just knowing these energy values for all the important elements of an alloy, it is often possible to build a qualitative picture (conceptual model) to interpret experimental results. Unfortunately, with DFT, only clusters of a few point defects, or a limited number of combinations of chemical elements, can be studied. Complicated solutions or oversimplified geometries must be adopted when studying extended defects, such as dislocations and grain boundaries (e.g. [4.62, 4.63]). Difficulties also arise when handling concentrated random alloys with limited amounts of atoms to reproduce a random distribution [4.64].

An important use of the results of DFT calculations is to fit classical interatomic potentials. These are mathematical functions of the relative positions of atoms, $U(r)$, with parameters to be fitted, that describe the potential energy landscape of the system. By deriving U with respect to the atomic positions r , the force acting on each atom can be obtained, $F=-\nabla U$. The use of potentials is the only practical way to simulate the dynamic behaviour and evolution of systems containing large numbers (millions) of atoms with some degree of realism. Knowing the forces, the Newtonian equations of motion can be written and solved for all atoms, so their evolution starting from given initial conditions can be predicted: this is the principle of MD. Moreover, suitable MC approaches can be developed given $U(r)$ to find equilibrium configurations of the system. Alternatively, characteristic energy values can be statically calculated, by means of energy minimization and saddle point search techniques [4.57, 4.60, 4.61], in exactly the same way as with ab initio calculations, but with much less stringent limitations as to the size of the system. The main limitation is that reliable potentials are relatively difficult to produce for pure elements, and, to date, potentials for at most quaternary alloys have been published [4.65]. Thus, only model alloys can be studied by means of interatomic potentials.

Potentials should predict acceptably the largest amount of physical properties possible for the material of interest, while requiring the minimum computing time possible. Many formalisms exist [4.66–4.68], generally derived either as approximations of first principle expressions, or based on heuristic considerations of some physical significance. For metals, many body potentials of the embedded atom method type [4.69–4.72] have been the state of the art for the last 25 years and are still widely used. A potential for Fe–Cr has been developed in this CRP; see the SMoRE report by Malerba et al. summarized in Section 6.1 and given in full in the accompanying CD-ROM.

4.2.2. Molecular dynamics

MD is a numerical method to trace the time evolution of a physical system by solving the classical Newtonian equations of motion of a set of N interacting atoms ($F_i=ma_i$; $i=1, \dots, N$; $a_i=d^2r_i/dt^2$), given the interaction potential and starting from assigned initial conditions. If needed, convenient constraints can be used to control thermodynamic variables, such as temperature and pressure, or impose given strain states. It is a powerful, highly flexible technique, and is used very widely to study innumerable physical problems in materials science. It is irreplaceable whenever the knowledge of atomic level details is required. An especially clear and succinct description of the technique can be found in Ref. [4.73], and the technique is explained in full detail in classic works on the subject [4.74, 4.75]. In contrast to MC methods, MD is a deterministic technique: given an initial set of positions and velocities, the subsequent evolution is, in principle, completely determined (in practice, rounding off numerical errors leads to a loss of memory of the initial conditions, but this is useful for statistical mechanics studies). However, in order for the equations of motion to be solved by respecting, for example, total energy conservation using finite difference methods, the time between the initial set of positions and velocities and the subsequent set (time step) has to be much shorter than the typical period of oscillation of atoms in condensed matter (i.e. ~ 1 fs). Hence, after one million time steps in a standard MD run, a simulated timespan of only 1 ns (10^{-9} s) has been covered. The limitation on the time span that can be simulated is the main shortcoming of MD, because many processes of practical interest, for example, diffusion, need times much longer than nanoseconds to develop. Another limitation is the size of the system: with current computers, sets of up to 10^7 atoms can be studied for times up to tens of nanoseconds, also owing to the fact that MD algorithms are easily parallelized. Larger sizes or longer times can be considered, but not simultaneously; that is, the extent of the method is a trade-off between size and time. Nevertheless, MD allows atomic level mechanisms to be identified and quantified, so it is irreplaceable for radiation effect studies. In addition, it naturally allows the study of both equilibrium and non-equilibrium conditions, thereby embracing systems in a stable phase or in a phase transition, ordered and disordered, in the presence of complex defects and so on. The physical reliability of the results relies only on the accuracy and acceptability of the interatomic potentials used.

The main applications of MD in radiation effect studies can be summarized as follows:

- (a) *Simulation of displacement cascades*, for which MD is the technique par excellence. As cascades cannot be directly observed in experiments, most available information about them comes from MD simulations. The literature on the subject is vast (for reviews, see Refs [4.4, 4.76–4.79]). In order to simulate a displacement cascade, after equilibration of the system at the desired temperature, an atom is given a kinetic energy equal

to the energy to be dissipated in displacement production (typically, tens of keV) and made to move in a randomly chosen direction. Special boundary conditions may or may not be applied in order to control temperature and (more rarely) pressure. The simulation volume must be large enough to contain all atoms affected by the cascade process (typically $\sim 10^6$ atoms, depending on the energy of the cascade). For good simulation tips, see Refs [4.80, 4.81].

- (b) *Simulation of point defects and point defect clusters*, especially to establish their stable configurations (formation energy, binding energy, etc.), how they interact with each other (reaction mechanisms) and how they diffuse (migration energies and mechanisms), also in interplay with alloying elements (e.g. [4.21, 4.23, 4.35, 4.36, 4.82–4.85]). This requires the defects of interest to be created in a sufficiently large simulation volume and the evolution of the system to be followed for times that may be especially long (tens of nanoseconds), in order to be statistically meaningful.
- (c) *Simulation of extended defects*, such as dislocations and grain boundaries, and their interactions with point defects, point defect clusters and different alloying chemical species [4.86, 4.87]. In this category, especially important are studies of the interactions of dislocations with hardening defects, such as voids, dislocation loops or precipitates.

4.3. NANOSTRUCTURAL AND MICROCHEMICAL EVOLUTION MODELLING

This section addresses two fairly different classes of modelling tools, namely atomistic MC and rate theory equations. The first retains the discrete nature of materials, describing them as sets of atoms that redistribute themselves in a volume following given physical rules; the second describes the material as a continuum in which concentrations of species, either defects or chemical elements, vary as dictated by the solution of a system of balance equations. Despite their differences, both can be used to study the nanostructural and microchemical evolution of a material under irradiation. Models that somehow intermediate between these two extremes also exist. In these models, which are generally known as object kinetic MC models [4.88, 4.89], atomic details are given up, but discrete defects and chemical species redistribute themselves in a simulation volume according to predefined physical rules. They are not described here because they were not used in the present CRP.

4.3.1. Metropolis and atomistic kinetic Monte Carlo methods

4.3.1.1. Metropolis Monte Carlo methods

MC methods are stochastic, statistical mechanics numerical tools used very widely in physics, especially in materials science. Metropolis Monte Carlo (MMC) methods are historically the first example of the latter application [4.90]: they sample the possible microstates of a system of atoms interacting according to a given cohesive model, for example, an interatomic potential. They therefore have a range of applications similar to MD, of which they can be seen as an alternative, or a prolongation, although in MMC models, energy can also be estimated using rigid lattice interactions [4.91–4.93]. Like MD methods, their reliability lies more in the cohesive model used than in the approximations made. MMC techniques and applications are explained in detail in several textbooks [4.74, 4.75, 4.94, 4.95].

MMC methods sample the phase space of N atoms through a random walk along a series of linked configuration changes, within a given statistical ensemble, which is defined by the thermodynamic state variables that remain constant, for example, energy (E), volume (V) and number of particles (N) in the microcanonical ensemble. The chain of states is built by considering possible changes (trials) to the atomic distribution, which, in turn, determine changes in the total energy of the system. After each trial, the energy of the system is calculated, and the decision whether to accept the new configuration is based on the ratio of the relative probabilities: $P_{\text{new}}/P_{\text{old}} = \exp(-\Delta E/kT)$, where ΔE is the energy difference between the old and the new configurations, k_B is the Boltzmann constant and T is the temperature. If this ratio exceeds unity, that is, the energy decreases after the trial, then the new configuration is always accepted; otherwise, it is accepted with probability $P_{\text{new}}/P_{\text{old}}$ and the decision is made by extracting a random number. Examples of trials are: (i) small displacement of an atom chosen at random from its initial position (equivalent to allowing atomic vibrations; possible only if the cohesive model is a continuous function of atomic positions); (ii) position swapping between two randomly chosen atoms of different

chemical species (or between an atom and a point defect); (iii) random, uniform volume changes (for constant pressure sampling); and (iv) transmutation of a randomly chosen atom into a different chemical species (specific to simulations in the semigrand canonical ensemble). Clearly, these trials do not correspond to physically possible mechanisms of atomic redistribution.

MMC methods are used mainly for two purposes: (i) to calculate thermodynamic averages in a system of atoms at finite temperatures, that is, to build the phase diagram of an alloy given a cohesive model (for this, the semigrand canonical ensemble with transmutation is especially suitable [4.96]) and (ii) to simulate the annealing of a system of atoms in order to find configurations corresponding to possible energy minima, for example, corresponding to segregation at extended defects, phase separation via precipitation, rearrangement of a grain boundary structure by diffusion, order–disorder transformations and so on [4.97–4.100]. The main disadvantages of MMC algorithms are that: (i) the final minimum energy states are not reached through real physical mechanisms, therefore, intermediate configurations are physically meaningless, so MMC methods are of no use for identifying and quantifying atomic level mechanisms and (ii) time is not a variable. The way to partially overcome these limitations is to resort to the use of atomistic kinetic Monte Carlo (AKMC) models.

4.3.1.2. Atomistic kinetic Monte Carlo method

Like MMC models, AKMC models include atoms of different chemical species, as well as defects, distributed within a volume, generally occupying predefined positions on a lattice. The system is made to evolve stochastically, by extracting random numbers to choose one out of many possible events. Differently from MMC, these events correspond to physical mechanisms, typically point defect diffusional jumps, for example, a position swap between a vacancy and a neighbouring atom, or a translation of an interstitial atom to a neighbouring position. The main purpose of AKMC models is thus to follow the *physical–kinetic* pathways leading the system to a steady state, characterized, for example, by the formation of new phases (precipitates), or the segregation of certain chemical species at extended defects [4.101, 4.102]. AKMC models are similar to MD in that they, too, allow the evolution of a system of atoms to be followed, as driven by specific atomic level mechanisms. However, in contrast to MD and MMC, atomic vibrations around the equilibrium position are not possible events, and in the majority of AKMC models, atoms are distributed on rigid lattices. This is both the main advantage and the main shortcoming of AKMC techniques. It is an advantage in terms of computing time, as vibrations are events that do not produce configuration changes: neglecting vibrations enables AKMC models to reach timescales of decades. It is a disadvantage because vibrational entropy effects are not spontaneously accounted for, nor are strain and relaxation effects included straightforwardly.

In AKMC simulations, atoms are redistributed via thermally activated processes, namely point defect jumps, i , characterized by specific frequencies:

$$\Gamma_i = \nu_i \exp(-\Delta E_i^m / k_B T) \quad (4.1)$$

Here, the exponential is a Boltzmann type probability that accounts for the effect of temperature, provided the migration energy barrier, ΔE_i^m , is given. The latter is the most important information needed, and determines most of the physical reliability of the model. ΔE_i^m depends on the migrating point defect, on the chemical nature of the migrating atom and on the local environment (chemical species and strain field). What distinguishes the different AKMC models is chiefly how the migration barriers ΔE_i^m are estimated [4.101–4.114]. The attempt frequency ν_i indicates how many times per unit time the point defect *tries* to jump: its order of magnitude equals the frequency of oscillation of atoms in materials ($\sim 10^{13} \text{ s}^{-1}$). This factor *replaces* the atomic vibrations of MD and MMC simulations. It depends on the local environment, as well, but this dependence is often neglected in practice, and ν_i is replaced by a constant value, ν_0 . In AKMC, the Γ_i values of Eq. (4.1) are used as probabilities to drive the evolution of the system. Each point defect can take a number of different jumps from the position occupied, each with a different Γ_i . Each jump probability is obtained by normalizing the specific Γ_i on the sum of all possible ones. These probabilities are then collapsed onto a segment of length 1 and, by extracting a random number between 0 and 1, depending on where the number falls, a jump (an event) is chosen (this is the essence of the MC algorithm). The use of frequencies as probabilities allows, in AKMC, a time increment to be associated with each defect jump, as follows:

$$\Delta t = \frac{-\ln R}{\sum_{i=1}^N \Gamma_i} \approx \frac{1}{\sum_{i=1}^N \Gamma_i} \quad (4.2)$$

where R is a random number between 0 and 1.

This is called the residence time algorithm [4.115, 4.116, 4.117]: the event at time t is chosen stochastically according to the MC algorithm and, subsequently, the clock is updated by adding Δt from Eq. (4.2). It is thus possible to ascertain, from a purely stochastic method, how long it takes the system to evolve, without solving the deterministic Newtonian equations of motion as in MD. AKMC simulations are hence regarded as a way to accelerate and prolong MD simulations. Reference [4.118] demonstrates that the time step is correctly sampled by Eq. (4.2). For a discussion of different possible kinetic MC methods and algorithms, see Ref. [4.118].

Despite the tremendous potential of AKMC simulations, limitations to their use remain [4.110]. One is the lengthy computational time required (days to weeks, even for volumes with characteristic lengths of only a few tens of nanometres). Another, specific to radiation effects, concerns how to treat self-interstitial atoms, which are characterized by an extended strain field, not included easily in a rigid lattice model. Self-interstitial atoms interacting with solute elements have been introduced in AKMC simulations [4.101, 4.106, 4.109, 4.119]. These simulations account for the diffusion of certain chemical species via self-interstitials [4.119], but the configuration and migration properties of self-interstitial clusters are not correct when compared to DFT or MD. Finally, AKMC models on rigid lattices are unable to reproduce phase changes involving crystallographic transformations, and the introduction of extended defects such as dislocations and grain boundaries represents a problem.

4.3.2. Rate theory

4.3.2.1. General

Rate equations are the traditional theoretical approach used to construct models of the nanostructural and microchemical evolution of materials under irradiation. Within this approach, the creation, diffusion and annihilation of radiation defects are described by a set of coupled differential equations of balance that contain reaction rates between defects and other microstructural features. Several references provide ample details [4.9, 4.12, 4.51, 4.120–4.122].

Rate theory models are based on the assumption that the material is a continuum. The discrete nature of materials as composed of atoms is given up, as well as largely the stochastic, inhomogeneous and localized nature of the process of radiation damage production (e.g. displacement cascades [4.123]) and evolution (e.g. correlated recombination [4.124]). In the continuum approximation, all infinitesimal volumes are equivalent: all of them contribute in the same manner to both the generation and the loss of mobile species. The variables handled by the equations are concentrations of defects and the model contains (and provides) no information concerning their atomic configuration and spatial position. If needed, rate theory models can give up partially the assumption of uniform space distribution, by introducing an explicit dependence of concentrations on position, hence assuming that species concentrations are uniform only within a volume located around a certain point in space, whose dimension is defined by the mesh used.

The great advantage of rate theory models is that solving a system of coupled differential equations is a task generally performed very efficiently by a computer, so computational time is not an issue, and the evolution of the system can be followed up to any timescale. However, in order to write the rate equations correctly, with all terms and factors made explicit, the mechanisms contributing to defect creation and annihilation must be known (the model does not provide them) and must be given a mathematical expression in terms of reaction rates. So, the key is the definition of the coefficients that appear in the different terms of the equations, which contain the actual physics of the problem. The advances made in rate theory applied to radiation effects over the past few decades correspond, essentially, to identifying the correct coefficients to describe the rate for the specific reactions (mechanisms) included in the equations [4.16, 4.19, 4.125]. Knowledge of diffusion coefficients, binding energies and reaction radii for all species involved is also a prerequisite of the model. These quantities can sometimes be measured experimentally, but most often, they can only be assessed using atomic level models. Alternatively, sensitivity studies can be performed to find the range of values that agree with experimental data, or to investigate

the influence of certain key parameters on the process studied. Even though this is feasible only for simplified models, involving relatively few equations and coefficients, rate equations are, in fact, particularly suitable for these types of exercises [4.120]. In the following subsections, the ideas behind the equations developed to describe specific processes addressed within the CRP are briefly illustrated.

4.3.2.2. Application to radiation induced segregation

Irradiation of materials leads to supersaturation of point defects and radiation enhanced diffusion. In alloys, this leads to RIS. Under uniform irradiation, RIS results in a considerable change in the alloy composition near point defect sinks: grain boundaries and surfaces, dislocations, incoherent precipitates, voids and gas bubbles (e.g. [4.126–4.128]). It can strongly affect the phase composition [4.48, 4.126–4.136], swelling [4.48–4.51], corrosion [4.137, 4.138], intergranular embrittlement [4.139–4.141] and other radiation phenomena in structural materials. In particular, RIS of nickel in Fe–Cr–Ni based alloys can result in the formation of austenite regions in ferritic alloys [4.129] or ferrite regions in austenitic alloys near voids and grain boundaries [4.130, 4.131]. The typical length of RIS regions near sinks may reach tens of nanometres. The temperature interval of RIS observation is $(0.2–0.6) T_m$, where T_m is the melting point. Two main mechanisms lead to RIS: (i) the inverse Kirkendall effect, that is, redistribution of elements in gradients of point defects due to differences in the diffusivities of elements by vacancy or interstitial mechanism and (ii) the formation of point defect solute complexes, due to the existence of a stable bond, especially in the case of undersized impurities such as phosphorus, silicon or sulphur.

RIS is usually modelled using various linear approximations of the thermodynamics of irreversible processes [4.142, 4.143]. The problem here is to determine the relationships between the coupling coefficients (the phenomenological coefficients L_{ij} of the Onsager matrix) and the point defect diffusivities. In dilute binary alloys, this has been done using atomistic models of point defect jump frequencies in the vicinity of impurity atoms [4.143, 4.144], for both face centred cubic (fcc) [4.145–4.147] and body centred cubic (bcc) [4.148, 4.149] lattices. Various approximations are related to the number of coordination spheres, in which the return of point defects to the impurity atom is accounted for [4.143]. In concentrated alloys, the random alloy model proposed by Manning [4.149] (continuum model) is usually used, thus accounting for the inverse Kirkendall effect. In such an approach, alloy component profiles near foil surfaces and grain boundaries, including moving ones, in binary and ternary alloys and near cylindrical (dislocations) and spherical (voids or precipitates) sinks in binary alloys have been obtained by numerical solution of diffusion equations for the concentrations of alloy components and point defects. Usually, in calculations of RIS in Fe–Cr–Ni alloys, only a difference in component diffusivities via vacancies is suggested. In most cases, a computer model developed by Perks et al. [4.150], as well as diffusivity ratios from the work of Rothman et al. [4.151], was used, and a satisfactory agreement of predictions with experimental data was achieved. In order to best fit the experimental data, some variations in parameters were allowed. Temperature dependent diffusivity ratios were adopted in Refs [4.137, 4.152]. Local composition dependent diffusivities were included in Ref. [4.33] using a simplified nearest neighbour pair potential approximation [4.153]. However, interaction energies between nearest neighbours were taken from experimental data on binary alloys, which have distinct interatomic spacing and sometimes another type of crystal lattice. An interstitial mechanism of RIS, including preferential association of undersized atoms with the interstitial flux, was proposed by Wiedersich et al. [4.153] and extended in Refs [4.134, 4.154–4.157]. RIS in Fe–Cr–Ni alloys near moving grain boundaries is modelled in Refs [4.158, 4.159] and near cylindrical and spherical sinks are discussed in the SMORE report by Pechenkin et al., summarized in Section 6.1 and given in full in the accompanying CD-ROM.

The disadvantages of rate theory models of RIS include difficulties in accounting for correlation effects, simplified treatment of self-interstitial atoms and the impossibility of describing the precipitation kinetics, including nucleation. However, estimates of radiation modified phase diagrams [4.48, 4.134–4.136] and kinetics of precipitate layer growth [4.160] are possible. One of the advantages of the rate theory models of RIS is the possibility of deriving analytical expressions for steady state component profiles near various point defect sinks in simple cases for binary [4.138, 4.161] and ternary [4.161] alloys and at grain boundaries for multicomponent alloys [4.162, 163], including Gibbsian adsorption. These models allow the physical mechanisms to take into account the effect of RIS on swelling [4.51, 4.137] and the estimation of segregation induced bias of sinks to interstitials or vacancies related to Kirkendall forces and drift forces caused by point defect migration and formation energy gradients near sinks [4.48, 4.137, 4.138]. Modelling of RIS along the projectile range of ions in alloys is possible by accounting for the effects of the sample surface and the non-uniformity of the point defect generation rate (e.g. Ref. [4.127]).

and the SMORE report by Pechenkin et al.). Further progress in application of these models could be related to MD calculations of point defect and component diffusivities and their dependence on temperature and alloy composition (e.g. Ref. [4.46] and the SMORE report by Pechenkin et al.). MD also allows atomic level mechanisms of this dependence to be identified and quantified.

4.3.2.3. Application to helium effects on nanodefects

Accumulation of helium atoms during irradiation can induce drastic changes of the mechanical properties of structural materials (swelling, radiation hardening and embrittlement [4.164]), because of bubble formation (controlled by helium diffusion via the interstitial or self-interstitial helium/replacement mechanisms [4.164]) and also because of enhanced dislocation loop formation at high concentrations of helium atoms, as helium interstitial clusters may act as nuclei for dislocation loops [4.165–4.173]. Radiation hardening therefore increases quickly with helium dose implantation [4.174–4.179].

Much theoretical work has been conducted on the kinetics of defect cluster formation under irradiation, including MD simulation of cluster formation in cascades ($t < 10^{-12}$ – 10^{-11} s) and later ($t > 10^{-11}$ s) [4.121, 4.179–4.185]. At low cascade energies and low concentrations of helium atoms and point defects, when the critical radii of defect clusters are large, this phenomenon can be described as a phase transition of first order, with the energy barrier at the critical point (critical radius) controlling the generation rate of defect clusters. For high concentrations of helium atoms (high production rates of helium) and at low temperatures ($T \leq 0.3T_m$), bubble nucleation is controlled by atomistically small critical clusters, where a few (as an extreme case, only two) helium atoms form a stable nucleus. In this case, the kinetics of nucleation of small defect clusters can be described by the diatomic (spontaneous) nucleation model [4.121, 4.182]. In the SMORE report by Ryazanov et al., summarized in Section 6.1 and given in full in the accompanying CD-ROM, a rate theory model based on the diatomic approximation is proposed, which can describe defect cluster formation, including helium bubbles and dislocation loops at high concentrations of helium. On the basis of this model, the main features of the kinetics of formation of helium vacancy clusters and small dislocation loops (both separately and in conjunction with helium bubble formation) are studied. The obtained theoretical results are compared with experimental data for density and mean size of defect clusters obtained by TEM after α implantation, as functions of helium concentration.

The theoretical description of helium vacancy cluster and dislocation loop kinetics is based on the rate equation approach [4.25, 4.27, 4.179–4.187]. One of the main parameters in these equations is the critical number of vacancies and helium atoms in the critical nucleus of helium vacancy clusters. For low helium generation rates and high temperatures, when the critical size of clusters is large, the continuous Fokker–Planck equation, where particle numbers in clusters (vacancies and helium atoms) are considered continuous variables, is a useful approach. The calculated generation rate for helium vacancy clusters in this case has a strong temperature dependence. The diatomic nucleation model of helium bubbles [4.121, 4.182] is used in the opposite case, at high helium generation rates and low temperatures, when the critical size of bubbles is small and, as an extreme case, only two helium atoms form a stable helium bubble nucleus. The diatomic model for cluster formation can thus be very useful for interpreting experimental results for radiation hardening of materials containing a high helium concentration, including the estimation of dose and temperature dependencies. This theoretical model allows simultaneous description of the formation of helium bubbles and dislocation loops in bulk irradiated materials.

4.3.2.4. Application to cascade effects on particle evolution

Forecasting the dynamics of precipitate growth under irradiation is important to estimate the stability of mechanical properties in different types of steels, from those used in pressure vessels of current reactors, to ODS steels for the cladding of future reactors. Many studies have investigated the influence of irradiation with different types of particles on the stability of precipitates [4.188–4.203]. The basic physical processes that occur during irradiation in an alloy containing precipitates are discussed in some detail in Ref. [4.188]. One of the suggestions there is that precipitates are destroyed by cascades. Experimental observations are not unequivocal in proving that this indeed happens; however, hints in this direction are found. Moreover, the interface is certainly affected, and clear evidence of amorphization of precipitates under irradiation exists.

A theoretical model of precipitate cascade interaction under fast particle irradiation of materials is proposed in the SMORE report by Ryazanov et al. Expressions describing concentration and size of precipitates as functions

of dose are produced based on this model, in which the contribution of precipitate evolution at high doses of fast particle irradiation due to collision cascades is comparable to the contribution of diffusion processes, or even exceeds it. The theoretical results obtained have been calibrated on experimental data for copper precipitates in pressure vessel steels for water cooled, water moderated power reactors, irradiated by fast neutrons [4.204]. This model can be generalized to describe the kinetics of precipitate evolution in irradiated ODS steels. Coarsening may occur at high irradiation doses, as a consequence of large precipitates growing at the expense of the dissolution of small ones, enhanced by the effect of collision cascades.

4.4. MECHANICAL PROPERTY MODELLING

The mechanical behaviour of metals is largely determined by how dislocations are created, move and interact with one another and with the existing microstructure when applying a load [4.205]. Thus, *physical* models describing the mechanical properties of metals are inherently *dislocation dynamics* (DD) models. In practice, however, DD models are only applicable to single crystals. Beyond this, continuum crystal plasticity models based on constitutive laws can be used. The proper physics can be retained by informing the continuum model of laws derived from DD. On the other hand, the interaction of dislocations with nanostructural features is an atomic level process best described by MD simulations, which are used to parameterize DD models. Combining these different techniques, a complete, multiscale description of the mechanical behaviour of materials from the atomistic level to the dislocation level can be obtained.

4.4.1. Molecular dynamics simulations of dislocation–defect interactions

The simulation by MD of dislocation motion and dislocation — defect interactions in systems containing several millions of atoms — has become a standard way to assess the mechanisms whereby the mechanical properties of metals are influenced by radiation induced nanostructural and microchemical changes [4.206–4.228]. To do this, acceptable boundary conditions and methods for simulating the shear of the crystallite have to be identified; see Ref. [4.206] for edge dislocations and Ref. [4.215] for screw dislocations (although no consensus exists in the latter case on the most suitable boundary conditions).

The methodology developed for edge dislocations [4.206] used within this CRP consists of the following, for bcc metals. The principal axes x , y and z of the simulated volume are oriented along the $[111]$, $[112]$ and $[110]$ directions, respectively (see Fig. 4.1). An initially straight edge dislocation with slip plane x – y is created along the y direction, with the Burgers vector, $\mathbf{b} = \frac{1}{2} [111]$, parallel to the x axis. Periodic boundary conditions are applied along the x and y directions. Different box sizes may be used, to consider different initial lengths of the dislocation segment. Any defect interacting with the dislocation will be placed at the midplane normal to the z direction, that is, on the dislocation glide plane. The box is divided into three parts along the z direction. The upper and lower

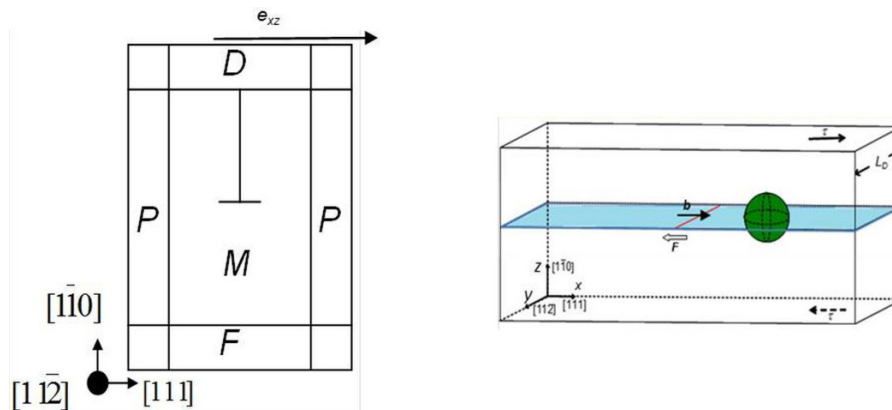


FIG. 4.1. Schematic representation of the simulation set-up for an edge dislocation; F — fixed atoms; D — rigidly displaced atoms; P — periodic boundary conditions; M — atoms where molecular dynamics simulation is performed.

parts consist of several atomic planes in which atoms are rigidly fixed in their original position, whereas atoms in the inner region are free to move during the MD runs. The dislocation is set in motion by the relative displacement of the upper rigid block in the x direction, which corresponds to simple shear strain $\varepsilon = e_{xz}$, where e_{xz} is the shear displacement in direction z on the surface normal to the x axis. The corresponding resolved shear stress induced by the applied deformation is calculated as $\sigma = F_x/A_{xy}$, where F_x is the total force in the x direction on the lower block of atoms due to all atoms in the inner region and A_{xy} is the xy cross-sectional area of the box. For analysis and visualization purposes, the dislocation line can be identified in different ways: by counting the number of first nearest neighbours [4.208], by checking the atomic registry in (112) planes [4.206] and by measuring the potential energy deviation per atom. The simulation set-up is illustrated in Fig. 4.1.

4.4.2. Dislocation dynamics and a bridge from molecular to dislocation dynamics

4.4.2.1. Dislocation dynamics simulations

Only the principal features of DD simulations used within the CRP are presented here. Full descriptions of how DD simulations are performed can be found in Refs [4.229, 4.230], and for more details on the method used to account for different crystallographic structures, see Refs [4.231, 4.232]. Line discretization and the definition of a 3-D lattice tiling an elastic continuum are the two essential features. Dislocation lines are decomposed into segments, constrained to lie on a lattice that discretizes the simulated volumes. Thus, by construction, the dislocation segments can only take a finite number of characters. In practice, only the edge, the screw and two mixed line directions are taken into account in each slip system. Line discretization decreases the number of degrees of freedom to be accounted for during the displacement of the dislocations; this results in a better computing efficiency without loss of accuracy. The incremental time steps of the simulation are divided into two parts. First, dislocations are treated as purely elastic defects. The effective force on each segment is computed at its midpoint as a superposition of several contributions. The latter include the Peach–Koehler forces derived from the applied stress, the stress fields of other dislocation segments and a local line tension term. To estimate the resulting displacement of the segments, a mobility law is required. The definition of mobility laws is an important input of DD simulations. Second, the positions of the dislocation segments are updated using a procedure that accounts for possible local events occurring during their displacement. These events include direct annihilation with other dislocations, junction formation with non-coplanar dislocations and cross-slip, for which specific local rules are implemented. Therefore, the DD simulations can treat cross-slip from the primary to the secondary slip system and allow for mutual interaction of these two slip systems.

Well-known limitations of DD simulations originate from the small value of the maximum plastic strain reachable. This is due to the rapid increase in the number of interacting dislocation segments during plastic straining. When cross-slip and dislocation climb are negligible, the quasi-static component of the precipitation hardening is a pure two dimensional (2-D) phenomenon. Hence, most treatments reported in the literature on the Orowan process are 2-D approaches. In the present CRP, dynamics is introduced by applying a fixed strain rate through 3-D simulations (see the SMoRE report by Monnet et al. summarized in Section 6.1 and given in full in the accompanying CD-ROM).

4.4.2.2. Mobility laws: A bridge from molecular dynamics to dislocation dynamics

To carry out DD simulations, the mobility laws for dislocations must first be established using MD simulations. But the results of MD simulation cannot be transferred *directly* into DD models, because in MD, unrealistic strain rates are applied. It is thus necessary to extract quantities that are *independent* of strain rate and any other specific features of each MD simulation, such as box size. Quantities that fulfil this requirement are friction stress, τ_f , critical effective stress opposed by an obstacle to dislocation motion, τ_c , and the activation energy for unpinning when the stress experienced by the obstacle is less than the effective stress, τ_{eff} , which depends not only on τ_c , but also on the length of the dislocation segment inside the obstacle, w , and on the distance between obstacles, l . Likewise, the activation energy for unpinning when the applied stress is below the unpinning stress fulfils this requirement. Methods to extract the relevant information from MD simulations have been developed and applied in Refs [4.215, 4.233–4.235]. So, MD simulations of dislocation motion for different alloy compositions need to be performed to deduce τ_f , which is identifiable when, above a certain temperature, the threshold stress for

dislocation motion reaches a thermal plateau. In the case of obstacles, an analysis is made to extract τ_C from τ_{eff} , exerted on dislocation segments in contact with the defect. Depending on temperature, the probability of unpinning is a function of the effective stress only. The activation energy per dislocation length versus effective stress is also obtained from MD simulations, and the thermally activated unpinning probability is then integrated into the DD code via an MC scheme.

In the DD simulation, precipitates or radiation defects can be represented by spherical volumes in the simulation space. For every spherical volume, a specific procedure for the dislocation mobility is considered as a function of τ_{eff} , to account for the resistance of the precipitate to dislocation penetration. This representation is appropriate for DD simulations, because τ_{eff} is always computed on the segment attempting to enter the precipitate. Therefore, it allows the concepts of pinning force and critical angle, which imply the use of an isotropic line tension model, to be avoided. If needed, the link with the classical pinning force F can be retrieved as $F = b d \tau_{\text{eff}}$, where b is the Burgers vector and d is the precipitate size. Only defects cutting the slip plane of a dislocation constitute obstacles. Thus, the number of defects introduced in the 3-D simulation box can be reduced to those cutting planes where dislocations were introduced, which allows the surface density C to be used in DD simulations. The connection with the volume density, Q , is $C = dQ$. In practice, the parameter used to deduce the number of precipitates is the average spacing between precipitates, l , which is also the fundamental parameter in theoretical models and is deduced directly from the volume density: $l \approx (dQ)^{-0.5} = C^{-0.5}$. In the athermal regime, the lattice friction is completely overcome by thermal activation. It is then assumed that a unique mobility law can describe the mobility of all dislocations:

$$v = \begin{cases} 0 & |\tau_{\text{eff}}| < \tau_F \\ B(\tau_{\text{eff}} - \text{sign}(\tau_{\text{eff}})\tau_F) & |\tau_{\text{eff}}| \geq \tau_F \end{cases} \quad (4.3)$$

where

v is the dislocation velocity

and B is a viscous drag coefficient.

When any portion of a segment located inside the interaction volume of a defect, Eq. (4.3) is replaced by the velocity deduced from the activation energy the motion of the dislocation segments becomes stochastic and dependent on the probability of thermal activation.

4.4.3. A bridge to finite element methods

Finite element methods (FEMs) are the widest employed numerical techniques to find the approximate solutions to continuum problems with given boundary conditions. At the micro and macro length scales, FEM solutions of material behaviour are obtained using advanced plasticity models such as crystal plasticity [4.236], Gurson micromechanical models [4.237], etc. FEMs are now even finding application in solving atomistic problems, where the constitutive input from the atomic level is coupled with that of the continuum, to tackle large domains. Here, a brief illustration of FEMs is given, focusing on structural problems: finding displacements and stresses in bodies under given loads. The solution to these problems is expected to be beneficial in terms of physical reliability from a link with DD models.

The goal here is to find the equilibrium configuration of a continuum body under given loads. The variable to be determined is the displacement at any point in the body given by $\mathbf{u} = \{u, v, w\}^T$. The body is subjected to various forces such as body force $\mathbf{F} = \{f_x, f_y, f_z\}^T$, surface traction $\mathbf{T} = \{T_x, T_y, T_z\}^T$ and point loads \mathbf{P}_i , as shown in Fig. 4.2(a).

The six independent stress components at any point are represented by the stress tensor $\boldsymbol{\sigma} = \{\sigma_x, \sigma_y, \sigma_z, \tau_{xy}, \tau_{yz}, \tau_{zx}\}^T$, where $\sigma_x, \sigma_y, \sigma_z$ are the normal stresses and $\tau_{xy}, \tau_{yz}, \tau_{zx}$ are the shear stresses. The corresponding strain tensor and its components are $\boldsymbol{\varepsilon} = \{\varepsilon_x, \varepsilon_y, \varepsilon_z, \gamma_{xy}, \gamma_{yz}, \gamma_{zx}\}^T$, where $\varepsilon_x, \varepsilon_y, \varepsilon_z$ are the normal strains and $\gamma_{xy}, \gamma_{yz}, \gamma_{zx}$ are the engineering shear strains, which are given in terms of displacement components as:

$$\{\boldsymbol{\varepsilon}\} = \left[\frac{\partial u}{\partial x}, \frac{\partial v}{\partial y}, \frac{\partial w}{\partial z}, \frac{\partial u}{\partial y} + \frac{\partial v}{\partial x}, \frac{\partial v}{\partial z} + \frac{\partial w}{\partial y}, \frac{\partial u}{\partial z} + \frac{\partial w}{\partial x} \right]^T \quad (4.4)$$

For linear elastic materials, the strain ε is related to the stress σ by constitutive equations given by Hooke's law. For isotropic materials, the two material properties are Young's modulus (or modulus of elasticity), E , and Poisson's ratio, ν . Thus, the strain-stress relationship in matrix notation is $\{\varepsilon\}=[C]\{\sigma\}$, and the inverse relationship is given by $\{\sigma\}=[D]\{\varepsilon\}$, where $[D]$ is the material matrix in terms of elastic constants.

The governing equilibrium equations for linear elastic problems and boundary conditions are given by $\nabla \cdot \sigma + F = 0$, with boundary conditions

$$\begin{aligned} n\sigma &= T \text{ on } S = S_f \\ u &= u_0 \text{ on } S = S_u \end{aligned} \tag{4.5}$$

where

- ∇ is the divergence operator;
- n is the outer unit normal to the volume surface S , i.e. the volume boundary;
- S_u is the surface portion to which a displacement is imposed as boundary condition;

and S_f is the surface portion to which a tension is imposed as boundary condition.

The step by step procedure to solve this boundary value problem using an FEM is as follows:

- (a) The continuum is divided into subdomains called finite elements, which are connected at the nodes, as shown in Fig. 4.2(b).
- (b) The displacements at any point within an element are interpolated in terms of unknown nodal displacement values, by using interpolation functions called shape functions $[N]$, that is, $\{u\}=[N]\{d\}$, where $\{d\}$ is the unknown nodal displacement vector. A typical 2-D quadrilateral element is shown in Fig. 4.2(c).

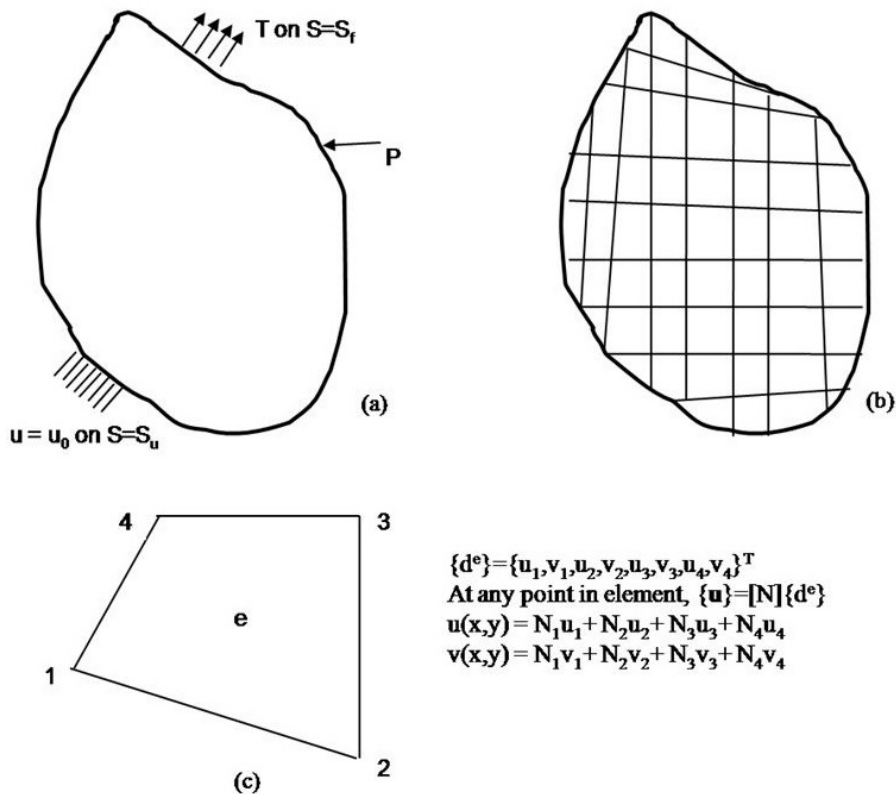


FIG. 4.2. (a) Continuum body with boundary values shown; (b) finite element discretization; (c) typical two dimensional quadrilateral element and interpolation of displacements in terms of nodal values.

- (c) Within the element, strains are related to the nodal displacements by $\{\varepsilon\}=[B]\{d^e\}$ and stresses are related to strains by Hooke's law as $\{\sigma\}=[D]\{\varepsilon\}$, where $[B]$ relates the strains at any point to nodal displacement values $\{d^e\}$.
- (d) Over each element, the relationships between primary field variables $\{u\}$ and secondary variables (forces f) are developed. This is achieved by taking the weak form of stress equilibrium equations, for example, the Galerkin weighted residual method.
- (e) This finally leads to a system of element level linear algebraic equations in terms of unknown nodal values $[K^e]\{d^e\}=\{Q^e\}$, where $[K^e]$ is the element level stiffness matrix and $\{Q^e\}$ is the element level load vector.
- (f) The element level equations are assembled by using the continuity of primary variables and balance of secondary variables at nodes, which leads to a global system of equations $[K^G]\{d^G\}=\{Q^G\}$.
- (g) Boundary conditions are applied and the system of equations is solved to obtain the displacements at nodes $\{d\}$. Strains and stresses are obtained from the displacements.

The above procedure is applicable for linear problems, where the stress–strain relationship is obtained using Hooke's law. For dealing with problems where material or geometrical non-linearities are involved, the constitutive input is provided by various plasticity models, and the solution is obtained in an incremental manner.

The goal of the multiscale methodology is to predict the stress–strain behaviour of materials at the continuum scale by bridging different length scale models. For example, in crystal plasticity FEMs, the material parameters used for representing kinetics of plastic flow and dislocation hardening can be computed numerically in DD simulations at the mesoscale. Similarly, parameters such as dislocation mobility rules used in DD can be obtained from the MD atomistic simulations at the nanoscale.

4.5. CONCLUDING REMARKS

This chapter illustrated the multiscale nature of radiation effects in materials and the meaning and role of the multiscale modelling approach and provided an overview of the modelling tools used in the present CRP, emphasizing their range of application, strengths and weaknesses. While explaining the meaning of multiscale modelling, the importance of building a conceptual model as a guide to developing a mathematical or computational model has been emphasized. The overview of the available modelling tools should have made it clear that the process of translating a conceptual model into a mathematical or computational one is far from straightforward. It turns out that, in order to properly implement in the actual model all the details that the conceptual model suggests, very sophisticated and time consuming developments are needed, whether theoretical, experimental or computational. This fact is the main bottleneck to the development of models, although it is not always immediately perceived as such. The application of multiscale, physics based models has certainly helped to interpret experimental results and has sometimes anticipated them. Yet, clearly, several challenges remain that limit the ability of these models to provide clear answers of scientific and technological relevance to the many open questions concerning the behaviour of materials in nuclear reactors. A few are listed below:

- Real materials contain many chemical elements. Yet, reliable atomistic simulations in multicomponent systems containing millions of atoms remain limited to three or four chemical elements with their specific interatomic potentials. Extending to more elements can be done only at the price of using strong approximations, as in AKMC models. Moreover, the interatomic potentials themselves should be further improved. The challenge is hence twofold: on the one hand, new potential formalisms should be developed, with deeper physical foundations (e.g. for alloys and magnetic materials), offering better accuracy and reliability, with computational efficiency similar to, or only slightly lower than, embedded atom methods; on the other hand, methods to effectively and reliably fit potentials for multicomponent alloys should be devised and applied. Although significant progress is being made in both directions, more needs to be done. However, it must probably be accepted that the full chemical complexity of real materials cannot be realistically included in models, whether they are *atomistic or not*. This implies that experimental work should be always foreseen to identify the chemical elements of primary importance for the problem of interest, in order to guide the development of models that will contain all (but also only) the necessary ingredients for the description of the phenomenon of interest.

- It remains difficult to describe simultaneously, in one model, both microchemical and nanostructural evolutionary processes under irradiation. Microchemical processes can be properly treated in atomistic MC models or in specific rate theory models, but it is difficult to describe with these the evolution of defects, especially self-interstitial defects, produced by irradiation in sufficient detail. Rate theory or object kinetic MC methods allow the evolution of irradiation defects to be described, including the correct physics of point defect clusters, but the *simultaneous* description of complex microchemical processes and point defect cluster evolution is not straightforward. Effort should be placed, therefore, on developing more sophisticated models of this type, be they atomistic, coarse grained or under the continuum assumption.
- With regard to mechanical property modelling, bridging between discrete and continuum models remains difficult. For instance, no fully established method exists yet to couple DD (which can reliably describe single crystal flow behaviour) with crystal plasticity and other continuum models that use finite element computation to describe the flow behaviour of polycrystals. Similarly, attempts at studying fracture mechanisms by coupling detailed atomistic descriptions at the crack tip with continuum finite element models in the remainder of the specimen have not yet reached any significant breakthrough that makes them routinely applicable. However, it is important to emphasize that significant progress has been made towards a full integration of MD studies for the construction of DD models.
- Finally, existing models still have trouble describing the irradiation processes that proceed to high dpa values and/or at high temperatures. Rate theory models can be used for this purpose, but only under specific assumptions, which basically exclude a full description of processes that occurred *before* reaching a certain dose, that is, defect nucleation is not described and the models are mainly steady state. As a consequence, it is also difficult to use models to help transfer data directly from ion irradiation experiments to neutron irradiation environments, except, of course, when referring to fundamental physical mechanisms. For example, while models describing steady state swelling have long been proposed, with different degrees of success, no model can describe the duration of the transient regime to reach steady state swelling, which is, in fact, for practical applications, the most important process to be understood and quantified.

ACKNOWLEDGEMENTS

Sections 4.3.2.2–4.3.2.4 and 4.4.2 are based on descriptions provided by V.A. Pechenkin, A. Ryazanov and G. Monnet, who are warmly thanked for their contributions.

REFERENCES TO CHAPTER 4

- [4.1] SEITZ, F., Radiation effects in solids, *Phys. Today* **5** 6 (1952) 6–9.
- [4.2] GREENWOOD, L.R., Neutron interactions and atomic recoil spectra, *J. Nucl. Mater.* **216** (1994) 29–44.
- [4.3] ROBINSON, M.T., Basic physics of radiation damage production, *J. Nucl. Mater.* **216** (1994) 1–28.
- [4.4] AVERBACK, R.S., DÍAZ DE LA RUBIA, T., “Displacement damage in irradiated metals and semiconductors, *Solid State Physics*, Vol. 51 (EHRENREICH, H., SPAEPEN, F., Eds), Academic Press, New York (1997) 281–402.
- [4.5] BRINKMAN, J.A., On the nature of radiation damage in metals, *J. Appl. Phys.* **25** 8 (1954) 961–970.
- [4.6] BRINKMAN, J.A., Production of atomic displacements by high-energy particles, *Amer. J. Phys.* **24** 4 (1956) 246–267.
- [4.7] SEITZ, F., KOEHLER, J.S., “Displacement of atoms during irradiation”, *Solid State Physics*, Vol. 2, *Advances in Research and Applications* (SEITZ, F., TURNBULL, D., Eds), Academic Press, New York (1956) 305–448.
- [4.8] SEEGER, A.K., “On the theory of radiation damage and radiation hardening”, *Proc. 2nd United Nations Int. Conf. on Peaceful Uses of Atomic Energy*, Vol. 6, IAEA, Vienna (1958) 250–273.
- [4.9] BULLOUGH, R., WOOD, M.H., “Theory of microstructural evolution”, *Physics of Radiation Effects in Crystals* (JOHNSON, R.A., ORLOV, A.N., Eds), Elsevier Science Publisher BV, North Holland (1986) 189–224.
- [4.10] EYRE, B.L., MATTHEWS, J.R., Technological impact of microstructural evolution during irradiation, *J. Nucl. Mater.* **205** (1993) 1–15.
- [4.11] PHYTHIAN, W.J., ENGLISH, C.A., Microstructural evolution in reactor pressure vessel steels, *J. Nucl. Mater.* **205** (1993) 162–177.
- [4.12] MANSUR, L.K., Theory and experimental background on dimensional changes in irradiated alloys, *J. Nucl. Mater.* **216** (1994) 97–123.

- [4.13] SINGH, B.N., et al., Aspects of microstructure evolution under cascade damage conditions, *J. Nucl. Mater.* **251** (1997) 107–122.
- [4.14] ENGLISH, C.A., PHYTHIAN, W.J., McELROY, R.J., “Microstructure and modelling of RPV embrittlement”, *Proc. Materials Research Society*, Vol. 439 (1996) 471–482.
- [4.15] SINGH, B.N., Impacts of damage production and accumulation on materials performance in irradiation environment, *J. Nucl. Mater.* **258–263** (1998) 18–29.
- [4.16] TRINKAUS, H., SINGH, B.N., GOLUBOV, S.I., Progress in modelling the microstructural evolution in metals under cascade damage conditions, *J. Nucl. Mater.* **283–287** (2000) 89–98.
- [4.17] GAN, J., WAS, G.S., STOLLER, R.E., Modeling of microstructure evolution in austenitic stainless steels irradiated under light water reactor condition, *J. Nucl. Mater.* **299** 1 (2001) 53–67.
- [4.18] BARASHEV, A.V., GOLUBOV, S.I., TRINKAUS, H., Reaction kinetics of glissile interstitial clusters in a crystal containing voids and dislocations, *Philos. Mag. A* **81** 10 (2001) 2515–2532.
- [4.19] TRINKAUS, H., HEINISCH, H.L., BARASHEV, A.V., GOLUBOV, S.I., SINGH, B.N., 1D to 3D diffusion-reaction kinetics of defects in crystals, *Phys. Rev. B* **66** (2002) 060105I.
- [4.20] TRINKAUS, H., SINGH, B.N., FOREMAN, A.J.E., Glide of interstitial loops produced under cascade damage conditions: Possible effects on void formation, *J. Nucl. Mater.* **199** 1 (1992) 1–5.
- [4.21] OSETSKY, Yu.N., BACON, D.J., SERRA, A., SINGH, B.N., GOLUBOV, S.I., One-dimensional atomic transport by clusters of self-interstitial atoms iron and copper, *Philos. Mag. A* **831** (2003) 61–91.
- [4.22] FU, C.-C., DALLA TORRE, J., WILLAIME, F., BOCQUET, J.-L., BARBU, A., Ab initio study of helium in α -Fe: Dissolution, migration, and clustering with vacancies, *Nat. Mater.* **4** 1 (2005) 68–74.
- [4.23] TERYTYEV, D., MALERBA, L., HOU, M., Dimensionality of interstitial cluster motion in bcc-Fe, *Phys. Rev. B* **75** (2007) 104108.
- [4.24] DJURABEKOVA, F.D., MALERBA, L., DOMAIN, C., BECQUART, C.S., Stability and mobility of small vacancy and copper-vacancy clusters in bcc-Fe: An atomistic kinetic Monte Carlo study, *Nucl. Instr. Meth. Phys. Res. B* **255** (2007) 47–51.
- [4.25] ANENTO, N., SERRA, A., OSETSKY, Yu.N., Atomistic study of multimechanism diffusion by self-interstitial defects in α -Fe, *Model. Simul. Mater. Sci. Eng.* **18** (2010) 025008.
- [4.26] PASCUET, M.I., CASTIN, N., BECQUART, C.S., MALERBA, L., Stability and mobility of Cu-vacancy clusters in Fe-Cu alloys: A computational study based on the use of artificial neural networks for energy barrier calculations, *J. Nucl. Mater.* **412** 1 (2011) 106–115.
- [4.27] SIZMANN, R., The effect of radiation upon diffusion in metals, *J. Nucl. Mater.* **69–70** (1978) 386–412.
- [4.28] SKLAD, P.S., MITCHELL, T.E., Radiation-enhanced precipitation in Al-4%Cu by high voltage electron microscopy, *Scr. Metall.* **8** (1974) 1113–1118.
- [4.29] ODETTE, G.R., On the dominant mechanism of irradiation embrittlement of reactor pressure vessel steels, *Scr. Metall.* **17** 10 (1983) 1183–1188.
- [4.30] MATHON, M.H., et al., A SANS investigation of the irradiation-enhanced α - α phases separation in 7–12 Cr martensitic steels, *J. Nucl. Mater.* **312** 2–3 (2003) 236–248.
- [4.31] BARBU, A., MARTIN, G., Radiation induced precipitation in nickel solid solutions: Dose rate effects, *Scr. Metall.* **11** 9 (1977) 771–775.
- [4.32] KAMEDA, J., BEVOLO, A.J., Neutron irradiation-induced intergranular solute segregation in iron base alloys, *Acta Metall.* **37** 12 (1989) 3283–3296.
- [4.33] ALLEN, T.R., WAS, G.S., Modeling radiation-induced segregation in austenitic Fe–Cr–Ni alloys, *Acta Mater.* **46** 10 (1998) 3679–3691.
- [4.34] COTTRELL, G.A., DUDAREV, S.L., FORREST, R.A., Immobilization of interstitial loops by substitutional alloy and transmutation atoms in irradiated metals, *J. Nucl. Mater.* **325** 2–3 (2004) 195–201.
- [4.35] TERYTYEV, D., MALERBA, L., BARASHEV, A.V., On the correlation between self-interstitial cluster diffusivity and irradiation-induced swelling in Fe–Cr alloys, *Philos. Mag. Lett.* **85** 11 (2005) 587–594.
- [4.36] TERYTYEV, D., OLSSON, P., MALERBA, L., BARASHEV, A.V., Characterization of dislocation loops and chromium-rich precipitates in ferritic iron–chromium alloys as means of void swelling suppression, *J. Nucl. Mater.* **362** 2–3 (2007) 167–173.
- [4.37] FU, C.-C., MESLIN, E., BARBU, A., WILLAIME, F., OISON, V., Effect of C on vacancy migration in α -iron, *Solid State Phen.* **139** (2008) 157–164.
- [4.38] CARTER, R.G., et al., Microstructural characterization of irradiation-induced Cu-enriched clusters in reactor pressure vessel steels, *J. Nucl. Mater.* **298** 3 (2001) 211–224.
- [4.39] BEMENT, A.L., “Fundamental materials problems in nuclear reactors”, *Proc. 2nd Int. Conf. on the Strength of Metals Alloys*, American Society for Metals **2** (1970) 693–728.
- [4.40] OLANDER, D.R., *Fundamental Aspects of Nuclear Reactor Fuel Elements*, Technical Information Center, Energy Research and Development Administration, Oak Ridge, TN (1976).

- [4.41] TANAKA, M., TARLETON, E., ROBERTS, S.G., The brittle-ductile transition in single-crystal iron, *Acta Mater.* **56** 18 (2008) 5123–5129.
- [4.42] NISHIYAMA, Y., ONIZAWA, K., SUZUKI, M., Phosphorus segregation and intergranular embrittlement in thermally aged and neutron irradiated reactor pressure vessel steels, *J. ASTM Int.* **4** 8 (2007) 1–12.
- [4.43] KLUEH, R.L., SHIBA, K., SOKOLOV, M.A., Embrittlement of irradiated ferritic/martensitic steels in the absence of irradiation hardening, *J. Nucl. Mater.* **377** 3 (2008) 427–437.
- [4.44] TRINKAUS, H., SINGH, B.N., Helium accumulation in metals during irradiation — where do we stand? *J. Nucl. Mater.* **323** 2–3 (2003) 229–242.
- [4.45] HENRY, J., MATHON, M.-H., JUNG, P., Microstructural analysis of 9% Cr martensitic steels containing 0.5 at.% helium, *J. Nucl. Mater.* **318** (2003) 249–259.
- [4.46] SCHÄUBLIN, R., HENRY, J., DAI, Y., Helium and point defect accumulation: (i) microstructure and mechanical behaviour, *C.R. Phys.* **9** 3 (2008) 389–400.
- [4.47] CHEON, J.S., et al., Sodium fast reactor evaluation: Core materials, *J. Nucl. Mater.* **392** 2 (2009) 324–330.
- [4.48] PECHENKIN, V.A., EPOV, G.A., STEPANOV, I.A., KONOBEEV, Yu.V., “Effect of radiation-induced segregation on precipitate stability and swelling in irradiated alloys”, *Proc. 18th Int. Symp. on Effects of Radiation on Materials*, ASTM STP1325 (NANSTAD, R.K., HAMILTON, M.L., GARNER, F.A., KUMAR, A.S., Eds), ASTM, West Conshohocken, PA (1999) 850–865.
- [4.49] WOLFER, W.G., Drift forces on vacancies and interstitials in alloys with radiation-induced segregation, *J. Nucl. Mater.* **114** 2–3 (1983) 292–304.
- [4.50] MARWICK, A.D., Calculation of bias due to solute redistribution in an irradiated binary alloy: Surfaces of a thin foil, *J. Nucl. Mater.* **135** 1 (1985) 68–76.
- [4.51] WAS, G.S., *Fundamentals of Radiation Materials Science — Metals and Alloys*, Springer-Verlag, Berlin, Heidelberg (2007).
- [4.52] CHATANI, K., et al., “Irradiation assisted stress corrosion cracking susceptibility of core component materials”, *Proc. 12th Int. Conf. on Environmental Degradation of Materials in Nuclear Power System — Water Reactors* (ALLEN, T.R., KING, P.J., NELSON, L., Eds), The Minerals, Metals and Materials Society (2005) 349–356.
- [4.53] HASNIP, P.J., “Advanced atomistic modelling”, *Introduction to Materials Modelling* (BARBER, Z.H., Ed.), Maney Publishing, London (2005) 29–44.
- [4.54] MARTIN, R.M., *Electronic Structure: Basic Theory and Practical Methods*, Cambridge University Press, Cambridge (2004).
- [4.55] CAR, R., PARRINELLO, M., Unified approach for molecular dynamics and density-functional theory, *Phys. Rev. Lett.* **55** 22 (1985) 2471–2474.
- [4.56] PAYNE, M.C., TETER, M.P., ALLAN, D.C., ARIAS, T.A., JOANNOPOULOS, J.D., Iterative minimization techniques for ab initio total-energy calculations: Molecular dynamics and conjugate gradients, *Rev. Mod. Phys.* **64** 4 (1992) 1045–1097.
- [4.57] PRESS, W.H., FLANNERY, B.P., TEUKOLSKY, S.A., VETTERLING, W.T., *Numerical Recipes in FORTRAN: The Art of Scientific Computing*, 2nd edn, Cambridge University Press, Cambridge, New York (1992).
- [4.58] OLSSON, P., KLAVER, T.P.C., DOMAIN, C., Ab initio study of solute transition-metal interactions with point defects in bcc Fe, *Phys. Rev. B* **81** 5 (2010) 054102.
- [4.59] OLSSON, P., Ab initio study of interstitial migration in Fe–Cr alloys, *J. Nucl. Mater.* **386–388** (2009) 86–89.
- [4.60] JÓNSSON, H., MILLS, G., JACOBSEN, K.W., “Nudged elastic band method for finding minimum energy paths of transitions”, *Classical and Quantum Dynamics in Condensed Phase Simulations* (BERNE, B.J., CICCOTTI, G., COKER, D.F., Eds), World Scientific, Singapore (1998) 385–404.
- [4.61] HENKELMAN, G., JÓNSSON, H., A dimer method for finding saddle points on high dimensional potential surfaces using only first derivatives, *J. Chem. Phys.* **111** 15 (1999) 7010–7022.
- [4.62] VENDELON, L., WILLAIME, F., Core structure and Peierls potential of screw dislocations in α -Fe from first principles: Cluster versus dipole approaches, *J. Comput.-Aided Mater. Des.* **14** (2007) 85–94.
- [4.63] WACHOWICZ, E., KIEJNA, A., Effect of impurities on grain boundary cohesion in bcc iron, *Comp. Mater. Sci.* **43** (2008) 736–743.
- [4.64] KLAVER, T.P.C., OLSSON, P., FINNIS, M.W., Interstitials in FeCr alloys studied by density functional theory, *Phys. Rev. B* **76** (2007) 214110.
- [4.65] BONNY, G., PASIANOT, R.C., CASTIN, N., MALERBA, L., Ternary Fe–Cu–Ni many-body potential to model reactor pressure vessel steels: First validation by simulated thermal annealing, *Philos. Mag.* **89** (2009) 3531–3546.
- [4.66] CARLSSON, A.E., Beyond pair potentials in elemental transition metals and semiconductors, *Solid State Phys.* **43** (1990) 1–91.
- [4.67] ROBINSON, M.T., “Interatomic potentials”, *Computer Simulation of Sputtering*, (*Mat. Fys. Medd. K. Dan. Vid. Selsk.*) **43** (1993) 39–71.
- [4.68] FINNIS, M.W., *Interatomic Forces in Condensed Matter*, Oxford University Press, Oxford (2003).
- [4.69] DAW, M.S., BASKES, M.I., Semiempirical, quantum mechanical calculation of hydrogen embrittlement in metals, *Phys. Rev. Lett.* **50** 17 (1983) 1285–1288.

- [4.70] FINNIS, M.W., SINCLAIR, J.E., A simple empirical N-body potential for transition metals, *Philos. Mag. A* **50** (1984) 45–55; Erratum, *Philos. Mag. A* **53** (1986) 161.
- [4.71] ERCOLESSI, F., TOSATTI, E., PARRINELLO, M., Au (100) surface reconstruction, *Phys. Rev. Lett.* **57** 6 (1986) 719–722.
- [4.72] JACOBSEN, K.W., NØRSKOV, J.K., PUSKA, M.J., Interatomic interactions in the effective-medium theory, *Phys. Rev. B* **35** 14 (1987) 7423–7442.
- [4.73] ERCOLESSI, F., A Molecular Dynamics Primer, (1997), <http://www.cems.uvm.edu/~gmirchan/classes/EE274/Images/Articles/MD%20Primer.pdf>
- [4.74] ALLEN, M.P., TILDESLEY, D.J., *Computer Simulation of Liquids*, Oxford Science Publications, Clarendon Press, Oxford (1987).
- [4.75] FRENKEL, D., SMIT, B., *Understanding Molecular Simulation: From Algorithms to Applications*, 2nd edn, Academic Press, Orlando, FL (2001).
- [4.76] ENGLISH, C.A., FOREMAN, A.J.E., PHYTHIAN, W.J., BACON, D.J., JENKINS, M.L., Displacement cascades in metals, *Mater. Sci. Forum* **97–99** (1992) 1–22.
- [4.77] BACON, D.J., GAO, F., OSETSKY, Yu.N., The primary damage state in fcc, bcc and hcp metals as seen in molecular dynamics simulations, *J. Nucl. Mater.* **276** 1–3 (2000) 1–12.
- [4.78] CROCOMBETTE, J.-P., “Cascade modelling”, *Handbook of Materials Modeling* (YIP, S., Ed.), Springer, Dordrecht (2005) 987–997.
- [4.79] MALERBA, L., Molecular dynamics simulation of displacement cascades in α -Fe: A critical review, *J. Nucl. Mater.* **351** 1–3 (2006) 28–38.
- [4.80] NORDLUND, K., et al., Defect production in collision cascades in elemental semiconductors and fcc metals, *Phys. Rev. B* **57** 13 (1998) 7556–7570.
- [4.81] VOSKOBOINIKOV, R.E., OSETSKY, Yu.N., BACON, D.J., Computer simulation of primary damage creation in displacement cascades in copper: I. Defect creation and cluster statistics, *J. Nucl. Mater.* **377** 2 (2008) 385–395.
- [4.82] MARIAN, J., et al., Dynamics of self-interstitial migration in Fe-Cu alloys, *Phys. Rev. B* **64** (2001) 094303.
- [4.83] MARIAN, J., WIRTH, B.D., PERLADO, J.M., ODETTE, G.R., DÍAZ DE LA RUBIA, T., Dynamics of self-interstitial cluster migration in pure α -Fe and Fe-Cu alloys, *Phys. Rev. B* **65** (2002) 144102.
- [4.84] PUIGVI, M.A., SERRA, A., DE DIEGO, N., OSETSKY, Yu.N., BACON, D.J., Features of the interactions between a vacancy and interstitial loops in metals, *Philos. Mag. Lett.* **84** 4 (2004) 257–266.
- [4.85] TERENCEV, D., MALERBA, L., KLAVER, P., OLSSON, P., Formation of stable sessile interstitial complexes in reactions between glissile dislocation loops in bcc Fe, *J. Nucl. Mater.* **382** 2–3 (2008) 126–133.
- [4.86] BACON, D.J., OSETSKY, Yu.N., Modelling dislocation-obstacle interactions in metals exposed to an irradiation environment, *Mater. Sci. Eng. A* **400–401** (2005) 353–361.
- [4.87] TERENCEV, D., HE, X., SERRA, A., KURIPLACH, J., Structure and strength of $\langle 110 \rangle$ tilt grain boundaries in bcc Fe: An atomistic study, *Comput. Mater. Sci.* **49** 2 (2010) 419–429.
- [4.88] DOMAIN, C., BECQUART, C.S., MALERBA, L., Simulation of radiation damage in Fe alloys: An object kinetic Monte Carlo approach, *J. Nucl. Mater.* **335** 1 (2004) 121–145.
- [4.89] BECQUART, C.S., et al., Modeling the long-term evolution of the primary damage in ferritic alloys using coarse-grained methods, *J. Nucl. Mater.* **406** 1 (2010) 39–54.
- [4.90] METROPOLIS, N., ROSENBLUTH, A.W., ROSENBLUTH, M.N., TELLER, A.H., TELLER, E., Equation of state calculations by fast computing machines, *J. Chem. Phys.* **216** (1953) 1087–1092.
- [4.91] LIU, C.L., ODETTE, G.R., WIRTH, B.D., LUCAS, G.E., A lattice Monte Carlo simulation of nanophase compositions and structures in irradiated pressure vessel Fe-Cu-Ni-Mn-Si steels, *Mater. Sci. Eng. A* **238** 1 (1997) 202–209.
- [4.92] VAN DER VEN, A., CEDER, G., Vacancies in ordered and disordered binary alloys treated with the cluster expansion, *Phys. Rev. B* **71** (2005) 054102.
- [4.93] INDEN, G., SCHÖN, C.G., Thermodynamic self-consistency issues related to the cluster variation method: The case of the bcc Cr-Fe (chromium-iron) system, *Comp. Coupling Phase Diag. Thermochem.* **32** (2008) 661–669.
- [4.94] BINDER, K., HEERMANN, D.W., *Monte Carlo Simulation in Statistical Physics: An Introduction*, 4th edn, Springer, Berlin (2002).
- [4.95] LANDAU, D.P., BINDER, K., *A Guide to Monte Carlo Simulations in Statistical Physics*, 2nd edn, Cambridge University Press, Cambridge (2005).
- [4.96] BONNY, G., PASIANOT, R.C., ZHURKIN, E.E., HOU, M., Determination of the phase diagram from interatomic potentials: The iron-chromium case, *Comp. Mat. Sci.* **50** 7 (2011) 2216–2220.
- [4.97] ZHURKIN, E.E., PEREIRA, R., CASTIN, N., MALERBA, L., HOU, M., “Metropolis Monte Carlo simulations of ordering and clustering in FeCr alloys”, *Materials for Future Fusion and Fission Technologies* (Proc. Materials Research Society Fall Mtg Warrendale, PA, 2008) 1125, R07–R37.
- [4.98] TERENCEV, D., HE, X., ZHURKIN, E.E., BAKAEV, A., Segregation of Cr at tilt grain boundaries in Fe–Cr alloys: A Metropolis Monte Carlo study, *J. Nucl. Mater.* **408** 2 (2011) 161–170.

- [4.99] ZHURKIN, E.E., HOU, M., KURIPLACH, J., OSSOWSKI, T., KIEJNA, A., Grain boundary segregation in low Cr Fe–Cr alloys: The effect of radiation induced vacancies studied by Metropolis Monte Carlo simulations, *Nucl. Instr. Meth. Phys. Res. B* **269** (2011) 1679–1683.
- [4.100] ZHURKIN, E.E., TEREITYEV, D., HOU, M., MALERBA, L., BONNY, G., Metropolis Monte-Carlo simulation of segregation in Fe–Cr alloys, *J. Nucl. Mater.* **417** 1–3 (2011) 1082–1085.
- [4.101] BECQUART, C.S., DOMAIN, C., Introducing chemistry in atomistic kinetic Monte Carlo simulations of Fe alloys under irradiation, *Phys. Status Solidi B* **247** 1 (2010) 9–22.
- [4.102] SOISSON, F., et al., Atomistic kinetic Monte Carlo studies of microchemical evolutions driven by diffusion processes under irradiation, *J. Nucl. Mater.* **406** 1 (2010) 55–67.
- [4.103] SOISSON, F., BARBU, A., MARTIN, G., Monte Carlo simulations of copper precipitation in dilute iron-copper alloys during thermal ageing and under electron radiation, *Acta Mater.* **44** 9 (1996) 3789–3800.
- [4.104] LE BOUAR, Y., SOISSON, F., Kinetic pathways from embedded-atom-method potentials: Influence of the activation barriers, *Phys. Rev. B* **65** (2002) 094103.
- [4.105] CERESO, A., HIROSAWA, S., ROZDILSKY, I., SMITH, G.D.W., Combined atomic-scale modelling and experimental studies of nucleation in the solid state, *Philos. Trans. R. Soc. Lond. A* **361** 1804 (2003) 463–476.
- [4.106] SOISSON, F., Kinetic Monte Carlo simulations of radiation induced segregation and precipitation, *J. Nucl. Mater.* **349** 3 (2006) 235–250.
- [4.107] SOISSON, F., FU, C.-C., Cu-precipitation kinetics in α -Fe from atomistic simulations: Vacancy-trapping effects and Cu-cluster mobility, *Phys. Rev. B* **76** (2007) 214102.
- [4.108] VINCENT, E., BECQUART, C.S., PAREIGE, C., PAREIGE, P., DOMAIN, C., Precipitation of the FeCu system: A critical review of atomic kinetic Monte Carlo simulations, *J. Nucl. Mater.* **373** 1–3 (2008) 387–401.
- [4.109] VINCENT, E., BECQUART, C.S., DOMAIN, C., Microstructural evolution under high flux irradiation of dilute Fe–CuNiMnSi alloys studied by an atomic kinetic Monte Carlo model accounting for both vacancies and self interstitials, *J. Nucl. Mater.* **382** 2–3 (2008) 154–159.
- [4.110] BONNY, G., TEREITYEV, D., MALERBA, L., VAN NECK, D., Early stages of [alpha-alpha'] phase separation in Fe-Cr alloys: An atomistic study, *Phys. Rev. B* **79** (2009) 104207.
- [4.111] XU, Q., VAN DER VEN, A., First-principles investigation of migration barriers and point defect complexes in B2–NiAl, *Intermet.* **17** 5 (2009) 319–329.
- [4.112] CASTIN, N., MALERBA, L., Prediction of point-defect migration energy barriers in alloys using artificial intelligence for atomistic kinetic Monte Carlo applications, *Nucl. Instr. Meth. Phys. Res. B* **267** (2009) 3148–3151.
- [4.113] CASTIN, N., MALERBA, L., BONNY, G., PASCUET, M.I., HOU, M., Modelling radiation-induced phase changes in binary FeCu and ternary FeCuNi alloys using an artificial intelligence-based atomistic kinetic Monte Carlo approach, *Nucl. Instr. Meth. Phys. Res. B* **267** (2009) 3002–3008.
- [4.114] CASTIN, N., MALERBA, L., Calculation of proper energy barriers for atomistic kinetic Monte Carlo simulations on rigid lattice with chemical and strain field long-range effects using artificial neural networks, *J. Chem. Phys.* **132** (2010) 074507.
- [4.115] YOUNG, W.M., ELCOCK, E.W., Monte Carlo studies of vacancy migration in binary ordered alloys: I, *Proc. Phys. Soc.* **89** 3 (1966) 735–746.
- [4.116] BORTZ, A.B., KALOS, M.H., LEBOWITZ, J.L., A new algorithm for Monte Carlo simulation of Ising spin systems, *J. Comp. Phys.* **17** (1975) 10–18.
- [4.117] FICHTHORN, K.A., WEINBERG, W.H., Theoretical foundations of dynamical Monte Carlo simulations, *J. Chem. Phys.* **95** 2 (1991) 1090–1096.
- [4.118] CHATTERJEE, A., VLACHOS, D.G., An overview of spatial microscopic and accelerated kinetic Monte Carlo methods, *J. Comput.-aided Mater. Des.* **14** (2007) 253–308.
- [4.119] NGAYAM-HAPPY, R., BECQUART, C.S., DOMAIN, C., MALERBA, L., Formation and evolution of MnNi clusters in neutron irradiated dilute Fe alloys modelled by a *first principle*-based AKMC method, *J. Nucl. Mater.* **426** 1–3 (2012) 198–207.
- [4.120] BARASHEV, A.V., GOLUBOV, S.I., Unlimited Damage Accumulation in Metallic Materials under Cascade-damage Conditions, Rep. ORNL/TM-2008/141, Oak Ridge Natl Lab., Oak Ridge, TN (2008).
- [4.121] MANSUR, L.K., “Mechanisms and kinetics of radiation effects in metals and alloys”, *Kinetics of Nonhomogeneous Processes* (FREEMAN, G.R., Ed.), Wiley, New York (1987) 377–463.
- [4.122] PICHLER, P., *Intrinsic Point Defects, Impurities, and their Diffusion in Silicon*, Springer, New York (2004).
- [4.123] BARBU, A., CLOUET, E., Cluster dynamics modeling of materials: Advantages and limitations, *Solid State Phenom.* **129** (2007) 51–58.
- [4.124] ORTIZ, C., CATURLA, M.J., Simulation of defect evolution in irradiated materials: Role of intracascade clustering and correlated recombination, *Phys. Rev. B* **75** (2007) 184101.
- [4.125] BRAILSFORD, A.D., BULLOUGH, R., The theory of sink strengths, *Philos. Trans. R. Soc. Lond. A* **302** (1981) 87–137.
- [4.126] RUSSELL, K.C., Phase stability under irradiation, *Prog. Mater. Sci.* **28** 3–4 (1984) 229–434.
- [4.127] NOLFI, F.V. (Ed.), *Phase Transformations during Irradiation*, Applied Science Publishers, London (1983).

- [4.128] KLUEH, R.L., HARRIES, D.R., High Chromium Ferritic and Martensitic Steels for Nuclear Applications, Monograph 3, ASTM International, West Conshohocken, PA (2001).
- [4.129] DUMBILL, S., WILLIAMS, M., "Irradiation-induced grain boundary segregation in neutron-irradiated Fe-Cr-Ni alloys", Materials for Nuclear Reactor Core Applications (Proc. Int. Conf. 27–29 October 1987), Vol. 1, British Nuclear Energy Society, London (1987) 119–123.
- [4.130] GARNER, F.A., "Irradiation performance of cladding and structural steels in liquid metal reactors", Materials Science and Technology: A Comprehensive Treatment, Vol. 10a (CAHN, R.W., HAASEN, P., KRAMER, E.J., Eds), Wiley-VCH, Weinheim (1994) 419–543.
- [4.131] MAZIASZ, P.J., Formation and stability of radiation-induced phases in neutron-irradiated austenitic and ferritic steels, *J. Nucl. Mater.* **169** (1989) 95–115.
- [4.132] HAMADA, S., SUZUKI, M., MAZIASZ, P.J., HISHINUMA, A., Microstructural evolution in austenitic stainless steels irradiated to 57 dpa in HFIR, *J. Nucl. Mater.* **179–181** (1991) 515–518.
- [4.133] MARTIN, G., BELLON, P., Driven Alloys, Solid State Physics, Advances in Research and Applications, Vol. 50 (EHRENREICH, H., SPAEPEN, F., Eds), Academic Press, New York (1996) 189–331.
- [4.134] BAKAI, A.S., TURKIN, A.A., "Radiation-modified phase diagrams of binary alloys", Proc. 15th Int. Symp. on Effect of Radiation on Materials, ASTM STP1125 (STOLLER, R.E., KUMAR, A.S., GELLES, D.S., Eds), ASTM, West Conshohocken, PA (1992) 709–730.
- [4.135] TURKIN, A.A., BAKAI, A.S., BUTS, A.V., "Phase diagrams of binary alloys in cascade-producing irradiation", Physics of Irradiation Effects in Metals (Proc. Int. Conf. on Physics of Irradiation Effects in Metals, Siofok, Hungary, 1991) (SZENES, G., Ed.), Mater. Sci. Forum **97–99** (1992) 343–350.
- [4.136] PECHENKIN, V.A., EPOV, G.A., The influence of radiation-induced segregation on precipitate stability in austenitic steels, *J. Nucl. Mater.* **207** (1993) 303–312.
- [4.137] NORRIS, D.I.R., BAKER, C., TITCHMARSH, J.M., "A study in radiation-induced sensitization in 20/25/Nb steel by compositional profile measurements at grain boundaries", Proc. Conf. on Materials for Nuclear Reactor Core Applications, Bristol, 1987, British Nuclear Energy Society, London, Vol. 1 (1987) 277–283.
- [4.138] BRUEMMER, S.M., Grain boundary composition and effects on environmental degradation, Mater. Sci. Forum **294–296** (1998) 75–82.
- [4.139] ENGLISH, C.A., ORTNER, S.R., GAGE, G., SERVER, W.L., ROSINSKI, S.T., "Review of phosphorus segregation and intergranular embrittlement in reactor pressure vessel steels", Proc. 20th Int. Symp. on Effects of Radiation on Materials, ASTM STP1405 (ROSINSKI, S.T., GROSSBECK, M.L., ALLEN, T.R., KUMAR, A.S., Eds), ASTM, West Conshohocken, PA (2001) 151–173.
- [4.140] FAULKNER, R.G., JONES, R.B., LU, Z., FLEWITT, P.E., Grain boundary impurity segregation and neutron irradiation effects in ferritic alloys, *Philos. Mag.* **85** 19 (2005) 2065–2099.
- [4.141] PECHENKIN, V.A., KONOBEEV, Yu.V., STEPANOV, I.A., NIKOLAEV, Yu.A., "On the mechanism of irradiation embrittlement enhancement in reactor pressure vessel steels at high neutron fluences", Proc. 21st Int. Symp. on Effects of Radiation on Materials, ASTM STP1447 (GROSSBECK, M.L., ALLEN, T.R., LOTT, R.G., KUMAR, A.S., Eds), ASTM, West Conshohocken, PA (2004) 138–148.
- [4.142] ALLNATT, A.R., LIDIARD, A.B., Statistical theories of atomic transport in crystalline solids, *Rep. Prog. Phys.* **50** (1987) 373–472.
- [4.143] ENGLISH, C.A., MURPHY, S.M., PERKS, J.M., Radiation-induced segregation in metals, *J. Chem. Soc. Faraday Trans.* **86** (1990) 1263–1271.
- [4.144] MURPHY, S.M., A model for segregation in dilute alloys during irradiation, *J. Nucl. Mater.* **168** 1–2 (1989) 31–42.
- [4.145] ALLNATT, A.R., Phenomenological coefficients for matter transport by vacancies from linear response theory: I. Derivation of Manning's equations for the impurity correlation factor, *J. Phys. C: Solid State Phys.* **14** (1981) 5453–5466.
- [4.146] ALLNATT, A.R., BARBU, A., FRANKLIN, A.D., LIDIARD, A.B., Atomic transport in dilute alloys containing interstitial defects, *Acta Metall.* **31** 9 (1983) 1307–1313.
- [4.147] BARBU, A., LIDIARD, A.B., Solute segregation in dilute bcc alloys under irradiation, *Philos. Mag. A* **74** (1996) 709–722.
- [4.148] OKAMURA, Y., ALLNATT, A.R., Calculations of phenomenological coefficients for matter transport by the matrix method of random walk theory, *J. Phys. C: Solid State Phys.* **16** 10 (1983) 1841–1862.
- [4.149] MANNING, J.R., Correlation factors for diffusion in nondilute alloys, *Phys. Rev. B* **4** 4 (1971) 1111–1121.
- [4.150] PERKS, J.M., MARWICK, A.D., ENGLISH, C.A., A Computer Code to Calculate Radiation-induced Segregation in Concentrated Ternary Alloys, Rep. AERE-R-12121, Harwell Lab., Oxford (1986).
- [4.151] ROTHMAN, S.J., NOWICKI, L.J., MURCH, G.E., Self-diffusion in austenitic Fe-Cr-Ni alloys, *J. Phys. F: Metal Phys.* **10** 3 (1980) 383–398.
- [4.152] ALLEN, T.R., WAS, G.S., "The effect of migration energies on reducing overprediction in radiation-induced segregation models", Microstructure of Irradiated Materials (Proc. 373, Materials Research Society Fall Mtg Symp. Y) (ROBERTSON, I.M., REHN, L.E., ZINKLE, S.J., PHYTHIAN, J., Eds), Materials Research Society, Pittsburgh, PA (1995) 101–106.

- [4.153] GRANDJEAN, Y., BELLON, P., MARTIN, G., Kinetic model for equilibrium and nonequilibrium segregation in concentrated alloys under irradiation, *Phys. Rev. B* **50** 6 (1994) 4228–4231.
- [4.154] WIEDERSICH, H., OKAMOTO, P.R., LAM, N.Q., A theory of radiation-induced segregation in concentrated alloys, *J. Nucl. Mater.* **83** 1 (1979) 98–108.
- [4.155] LAM, N.Q., KUMAR, A., WIEDERSICH, H., “Kinetics of radiation-induced segregation in ternary alloys”, Proc. 11th Int. Conf. on Effects of Radiation on Materials, ASTM STP782 (BRAGER, H.R., PERRIN, J.S., Eds), ASTM, West Conshohocken, PA (1982) 985–1007.
- [4.156] STEPANOV, I.A., PECHENKIN, V.A., KONOBEEV, YU.V., “The modeling of radiation-induced phosphorus segregation at point defect sinks in dilute Fe-P alloys”, Proc. 21st Int. Symp. on Effects of Radiation on Materials, ASTM STP1447 (GROSSBECK, M.L., ALLEN, T.R., LOTT, R.G., KUMAR, A.S., Eds) ASTM, West Conshohocken, PA (2004) 579–589.
- [4.157] PECHENKIN, V.A., STEPANOV, I.A., Modeling the radiation-induced segregation of undersized solutes near grain boundaries, *Mater. Sci. Forum* **294–296** (1999) 771–774.
- [4.158] STEPANOV, I.A., PECHENKIN, V.A., Calculation of radiation-induced segregation near moving grain boundaries in Fe-Cr-Ni alloys, *Mater. Sci. Forum* **294–296** (1999) 775–778.
- [4.159] STEPANOV, I.A., PECHENKIN, V.A., KONOBEEV, Yu.V., Modeling of radiation-induced segregation at grain boundaries in Fe-Cr-Ni alloys, *J. Nucl. Mater.* **329–333** (2004) 1214–1218.
- [4.160] PECHENKIN, V.A., STEPANOV, I.A., KONOBEEV, Yu.V., Analytical model of radiation-induced precipitation at the surface of dilute binary alloy, *J. Nucl. Mater.* **307–311** (2002) 998–1002.
- [4.161] PECHENKIN, V.A., EPOV, G.A., Analytical expressions for steady-state component profiles of irradiated substitutional alloys near point defect sinks, *J. Nucl. Mater.* **186** 3 (1992) 269–276.
- [4.162] PECHENKIN, V.A., STEPANOV, I.A., KONOBEEV, Yu.V., “Modeling of phosphorus accumulation on grain boundaries in iron alloys under irradiation”, Proc. 20th Int. Symp. on Effects of Radiation on Materials, ASTM STP1405 (ROSINSKI, S.T., GROSSBECK, M.L., ALLEN, T.R., KUMAR, A.S., Eds), ASTM, West Conshohocken, PA (2001) 174–187.
- [4.163] TERENTYEV, D., OLSSON, P., KLAVER, T.P.C., MALERBA, L., On the migration and trapping of single self-interstitial atoms in dilute and concentrated Fe-Cr alloys: Atomistic study and comparison with resistivity recovery experiments, *Computat. Mater. Sci.* **43** 4 (2008) 1183–1192.
- [4.164] ULLMAIER, H., TRINKAUS, H., Helium in metals: Effect on mechanical properties, *Mater. Sci. Forum* **97–99** (1992) 451–472.
- [4.165] CHOYKE, W.J., et al., Helium effects in ion-bombarded 304 stainless steel, *J. Nucl. Mater.* **85–86** (1979) 647–651.
- [4.166] PEDRAZA, D.F., MAZIASZ, P.J., KLUEH, R.N., Helium effects on the microstructural evolution of reactor irradiated ferritic and austenitic steels, *Rad. Eff. Def. Solids* **113** 1–3 (1990) 213–228.
- [4.167] CHEN, K.Q., et al., The analysis of microstructure of helium bubbles in 316L SS induced by 3.02 MeV He ion irradiation, *J. Nucl. Mater.* **191–194** (1992) 737–741.
- [4.168] NIWASE, K., EZAWA, T., TANABE, T., KIRITANI, M., FUJITA, F.E., Permutation of deuterium implanted into pure iron, *J. Nucl. Mater.* **203** 1 (1993) 56–66.
- [4.169] ZHANG, C.H., CHEN, K.Q., WANG, Y.S., SUN, J.G., SHEN, D.Y., Formation of bubbles in helium implanted 316L stainless steel at temperatures between 25 and 550°C, *J. Nucl. Mater.* **245** 2–3 (1997) 210–216.
- [4.170] SHIMIZU, J., YASUDA, K., KINOSHITA, C., Formation process of defect clusters in copper and nickel under irradiation with helium ions, *J. Nucl. Mater.* **212–215** (1994) 207–211.
- [4.171] JASUDA, K., KINOSHITA, C., KUTSUWADA, M., HIRAI, T., Microstructural evolution in Fe-Cr-Ni alloy irradiated with Ni ion under varying temperature, *J. Nucl. Mater.* **233–237** (1996) 1051–1061.
- [4.172] IWAKIRI, H., WAKIMOTO, H., WATANABE, H., YOSHIDA, N., Hardening behavior of molybdenum by low energy He and D ion irradiation, *J. Nucl. Mater.* **258–263** (1998) 873–878.
- [4.173] DAI, Y., et al., Microstructure of both as-irradiated and deformed 304L stainless steel irradiated with 800 MeV protons, *J. Nucl. Mater.* **296** 1–3 (2001) 174–182.
- [4.174] SINGH, B.N., LEFFERS, T., GREEN, W.V., VICTORIA, M., Nucleation of helium bubbles on dislocations, dislocation networks and dislocations in grain boundaries during 600 MeV proton irradiation of aluminium, *J. Nucl. Mater.* **125** 3 (1984) 287–297.
- [4.175] ULLMAIER, H., CARSUGHI, F., Radiation damage problems in high power spallation neutron sources, *Nucl. Inst. Meth. Phys. Res. B* **101** 4 (1995) 406–421.
- [4.176] ULLMAIER, H., CAMUS, E., Low temperature mechanical properties of steels containing high concentrations of helium, *J. Nucl. Mater.* **251** (1997) 262–268.
- [4.177] CHEN, J., et al., Mechanical properties of 304L stainless steel irradiated with 800 MeV protons, *J. Nucl. Mater.* **275** 1 (1999) 115–118.
- [4.178] LEE, E.H., HUNN, J.D., BYUN, T.S., MANSUR, L.K., Effects of helium on radiation-induced defect microstructure in austenitic stainless steel, *J. Nucl. Mater.* **280** 1 (2000) 18–24.
- [4.179] YACOUT, A., STUBBINS, J.F., Model for the kinetics of cluster nucleation in irradiated materials, *J. Nucl. Mater.* **141–143** 2 (1986) 677–681.

- [4.180] LUCAS, G.E., The evolution of mechanical property change in irradiated austenitic stainless steels, *J. Nucl. Mater.* **206** 2–3 (1993) 287–305.
- [4.181] HAYNS, H.R., The nucleation and early growth of interstitial dislocation loops in irradiated materials, *J. Nucl. Mater.* **56** 3 (1975) 267–274.
- [4.182] TRINKAUS, H., Modeling of helium effects in metals: High temperature embrittlement, *J. Nucl. Mater.* **133–134** (1985) 105–112.
- [4.183] TRINKAUS, H., Mechanisms controlling high temperature embrittlement due to helium, *Rad. Effects* **101** (1987) 91–107.
- [4.184] GHONIEM, N.M., Theory of microstructure evolution under fusion neutron irradiation, *J. Nucl. Mater.* **179–181** (1991) 99–104.
- [4.185] KATOH, Y., STOLLER, R.E., KOHYAMA, A., Rate theory investigation of influence of cascade formation and solute trapping on point defect agglomeration and extended defect evolution, *J. Nucl. Mater.* **212–215** (1994) 179–185.
- [4.186] VOLKOV, A.E., RYAZANOV, A.I., Theory of gas bubble nucleation in supersaturated solution of vacancies, interstitials and gas atoms, *J. Nucl. Mater.* **273** 2 (1999) 155–163.
- [4.187] BORODIN, V.A., RYAZANOV, A.I., SHERSTENNIKOV, D.G., Low-temperature swelling of metals and ceramics, *J. Nucl. Mater.* **202** 1–2 (1993) 169–179.
- [4.188] NELSON, R.S., HUDSON, J.A., MAZEY, D.J., The stability of precipitates in an irradiation environment, *J. Nucl. Mater.* **44** 3 (1972) 318–330.
- [4.189] GELLES, D.S., GARNER, F.A., An experimental method to determine the role of helium in neutron-induced microstructural evolution, *J. Nucl. Mater.* **85–86** (1979) 689–693.
- [4.190] ZINKLE, S., NESTEROVA, E.V., BARABASH, V.R., RYBIN, V.V., NABERENKOV, A.V., Effect of ion irradiation on the structural stability of dispersion-strengthened copper alloys, *J. Nucl. Mater.* **208** 1–2 (1994) 119–127.
- [4.191] ASANO, K., KOHNO, Y., KOHYAMA, A., SUZUKI, T., KUSANAGI, H.J., Microstructural evolution of an oxide dispersion strengthened steel under charged particle irradiation, *J. Nucl. Mater.* **155–157** (1988) 928–934.
- [4.192] HIDE, K., et al., “Microstructural change in ferritic steels under heavy ion irradiation”, *Proc. 14th Int. Symp. on Effects of Radiation on Materials*, Vol. 1, ASTM STP1046 (PACKAN, N.H., STOLLER, R.E., KUMAR, A.S., Eds), ASTM, West Conshohocken, PA (1988) 61–72.
- [4.193] LITTLE, E.A., “Influence of thermomechanical treatment on irradiation microstructures in an ODS ferritic steel”, *Proc. 17th Int. Symp. on Effects of Radiation on Materials*, Sun Valley, ID, 1994, ASTM STP1270 (GELLES, D.S., NANSTAD, R.K., KUMAR, A.S., LITTLE, E.A., Eds), ASTM, West Conshohocken, PA (1996) 739–752.
- [4.194] SAITO, J., et al., Void formation and microstructural development in oxide dispersion strengthened ferritic steels during electron-irradiation, *J. Nucl. Mater.* **258–263** (1998) 1264–1268.
- [4.195] KINOSHITA, H., AKASAKA, N., TAKAHASHI, H., SHIBAHARA, L., ONOSE, S., Microstructural change on electron irradiated oxide dispersion strengthened ferritic steels, *J. Nucl. Mater.* **191–194** (1992) 874–878.
- [4.196] AKASAKA, N., YAMASHITA, S., YOSHITAKE, T., UKAI, S., KIMURA, A., Microstructural changes of neutron irradiated ODS ferritic and martensitic steels, *J. Nucl. Mater.* **329–333** (2004) 1053–1056.
- [4.197] KIMURA, A., et al., High burnup fuel cladding materials R&D for advanced nuclear systems, *J. Nucl. Sci. Technol.* **44** 3 (2007) 323–328.
- [4.198] DUBUISSON, P., SCHILL, R., HIGON, M.-P., GRISLIN, I., SÈRAN, J.-L., “Behavior of an oxide dispersion strengthened ferritic steel irradiated in Phenix”, *Proc. 18th Int. Symp. on Effects of Radiation on Materials*, ASTM STP1325 (NANSTAD, R.K., HAMILTON, M.L., GARNER, F.A., KUMAR, A.S., Eds), Hyannis, MA, 1996, ASTM, West Conshohocken, PA (1999) 882–898.
- [4.199] MONNET, I., et al., Microstructural investigation of the stability under irradiation of oxide dispersion strengthened ferritic steels, *J. Nucl. Mater.* **335** 3 (2004) 311–321.
- [4.200] YAMASHITA, S., OKA, K., OHNUKI, S., AKASAKA, N., UKAI, S., Phase stability of oxide dispersion-strengthened ferritic steels in neutron irradiation, *J. Nucl. Mater.* **307–311** (2002) 283–288.
- [4.201] TANIGAWA, H., SAKASEGAWA, H., OGIWARA, H., KISHIMOTO, H., KOHYAMA, A., Radiation induced phase instability of precipitates in reduced-activation ferritic/martensitic steels, *J. Nucl. Mater.* **367–370** (2007) 132–136.
- [4.202] ALLEN, T.R., et al., Radiation response of a 9 chromium oxide dispersion strengthened steel to heavy ion irradiation, *J. Nucl. Mater.* **375** 1 (2008) 26–37.
- [4.203] UKAI, S., “Oxide dispersion strengthened steels”, *Comprehensive Nuclear Materials*, Vol. 4 (KONINGS, R.J.M., Ed.), Elsevier, Amsterdam (2012) 241–272.
- [4.204] KULESHOVA, E.A., GUROVICH, B.A., STROMBAKH, Ya.I., NIKOLAEV, Yu.A., PECHENKIN, V.A., Microstructural behaviour of VVER-440 reactor pressure vessel steels under irradiation to neutron fluences beyond the design operation period, *J. Nucl. Mater.* **342** 1–3 (2005) 77–89.
- [4.205] HULL, D., BACON, D.J., *Introduction to Dislocations*, 4th edn, Butterworth-Heinemann, Oxford (2001).
- [4.206] OSETSKY, Yu.N., BACON, D.J., An atomic-level model for studying the dynamics of edge dislocations in metals, *Model. Simul. Mat. Sci. Eng.* **11** 4 (2003) 427–446.

- [4.207] OSETSKY, Yu.N., BACON, D.J., Void and precipitate strengthening in α -iron: What can we learn from atomic-level modelling? *J. Nucl. Mater.* **323** 2–3 (2003) 268–280.
- [4.208] RODNEY, D., Molecular dynamics simulation of screw dislocations interacting with interstitial Frank loops in a model FCC crystal, *Acta Mater.* **52** 3 (2004) 607–614.
- [4.209] OSETSKY, Yu.N., STOLLER, R.E., MATSUKAWA, Y., Dislocation–stacking fault tetrahedron interaction: What can we learn from atomic-scale modelling, *J. Nucl. Mater.* **329–333** (2004) 1228–1232.
- [4.210] TAPASA, K., BACON, D.J., OSETSKY, Yu.N., Simulation of dislocation glide in dilute Fe–Cu alloys, *Mater. Sci. Eng. A* **400–401** (2005) 109–113.
- [4.211] OSETSKY, Yu.N., STOLLER, R.E., RODNEY, D., BACON, D.J., Atomic-scale details of dislocation–stacking fault tetrahedral interaction, *Mater. Sci. Eng. A* **400–401** (2005) 370–373.
- [4.212] OSETSKY, Yu.N., BACON, D.J., Comparison of void strengthening in fcc and bcc metals: Large-scale atomic-level modelling, *Mater. Sci. Eng. A* **400–401** (2005) 374–377.
- [4.213] NOMOTO, A., SONEDA, N., TAKAHASHI, A., ISHINO, S., Interaction analysis between edge dislocation and self interstitial type dislocation loop in BCC iron using molecular dynamics, *Mater. Trans.* **463** (2005) 463–468.
- [4.214] RONG, Z., MOHLES, V., BACON, D.J., OSETSKY, Yu.N., Dislocation dynamics modelling of dislocation–loop interactions in irradiated metals, *Philos. Mag.* **85** 2–3 (2005) 171–188.
- [4.215] DOMAIN, C., MONNET, G., Simulation of screw dislocation motion in iron by molecular dynamics simulations, *Phys. Rev. Lett.* **95** (2005) 215506.
- [4.216] OSETSKY, Yu.N., RODNEY, D., BACON, D.J., Atomic-scale study of dislocation–stacking fault tetrahedron interactions. Part I: Mechanisms, *Philos. Mag.* **86** 16 (2006) 2295–2313.
- [4.217] PROVILLE, L., RODNEY, D., BRECHET, Y., MARTIN, G., Atomic-scale study of dislocation glide in a model solid solution, *Philos. Mag.* **86** 25–26 (2006) 3893–3920.
- [4.218] SCHÄUBLIN, R., CHIU, Y.L., Effect of helium on irradiation-induced hardening of iron: A simulation point of view, *J. Nucl. Mater.* **362** 2–3 (2007) 152–160.
- [4.219] BACON, D.J., OSETSKY, Yu.N., RONG, Z., Computer simulation of reactions between an edge dislocation and glissile self-interstitial clusters in iron, *Philos. Mag.* **86** 25–26 (2006) 3921–3936.
- [4.220] NOGARET, T., ROBERTSON, C., RODNEY, D., Atomic-scale plasticity in the presence of Frank loops, *Philos. Mag.* **87** 6 (2007) 945–966.
- [4.221] TEREPTYEV, D., MALERBA, L., BACON, D.J., OSETSKY, Yu.N., The effect of temperature and strain rate on the interaction between an edge dislocation and an interstitial dislocation loop in α -iron, *J. Phys.: Cond. Matter* **19** (2007) 456211.
- [4.222] TEREPTYEV, D., BACON, D.J., OSETSKY, Yu.N., Interaction of an edge dislocation with voids in α -iron modelled with different interatomic potentials, *J. Phys. Cond. Matter* **20** (2008) 445007.
- [4.223] TEREPTYEV, D., GRAMMATIKOPOULOS, P., BACON, D.J., OSETSKY, Yu.N., Simulation of the interaction between an edge dislocation and a $\langle 1\ 0\ 0 \rangle$ interstitial dislocation loop in α -iron, *Acta Mater.* **56** 18 (2008) 5034–5046.
- [4.224] TEREPTYEV, D., MALERBA, L., Effect of Cr atoms on the formation of double kinks in screw dislocations in Fe and its correlation with solute hardening and softening in Fe–Cr alloys, *Comp. Mater. Sci.* **43** 4 (2008) 855–866.
- [4.225] TEREPTYEV, D., BACON, D.J., OSETSKY, Yu.N., Reactions between a $1/2 \langle 111 \rangle$ screw dislocation and $\langle 100 \rangle$ interstitial dislocation loops in alpha-iron modelled at atomic scale, *Philos. Mag.* **89** 9 (2009) 1–15.
- [4.226] TEREPTYEV, D., OSETSKY, Yu.N., BACON, D.J., Competing processes in reactions between an edge dislocation and dislocation loops in a body-centred cubic metal, *Scr. Mater.* **62** 9 (2010) 697–700.
- [4.227] TEREPTYEV, D., HAGHIGHAT, S.M.H., SCHÄUBLIN, R., Strengthening due to Cr-rich precipitates in Fe–Cr alloys: Effect of temperature and precipitate composition, *J. Appl. Phys.* **107** (2010) 061806.
- [4.228] HAGHIGHAT, S.M.H., TEREPTYEV, D., SCHÄUBLIN, R., Atomistic simulation of the influence of Cr on the mobility of the edge dislocation in Fe(Cr) alloys, *J. Nucl. Mater.* **417** 1–3 (2011) 1094–1097.
- [4.229] DEVINCRE, B., KUBIN, L., LEMARCHAND, C., MADEC, R., Mesoscopic simulations of plastic deformation, *Mater. Sci. Eng. A* **309–310** (2001) 211–219.
- [4.230] QUEYREAU, S., MONNET, G., DEVINCRE, B., Slip systems interactions in α -iron determined by dislocation dynamics simulations, *Int. J. Plast.* **25** 2 (2009) 361–377.
- [4.231] MONNET, G., DEVINCRE, B., KUBIN, L.P., Dislocation study of prismatic slip systems and their interactions in hexagonal close packed metals: Application to zirconium, *Acta Mater.* **52** 14 (2004) 4317–4328.
- [4.232] DURINCK, J., DEVINCRE, B., KUBIN, L.P., CORDIER, P., Modeling the plastic deformation of olivine by dislocation dynamics simulations, *Am. Miner.* **92** (2007) 1346–1357.
- [4.233] MONNET, G., Mechanical and energetical analysis of molecular dynamics simulations of dislocation–defect interactions, *Acta Mater.* **55** 15 (2007) 5081–5088.
- [4.234] MONNET, G., OSETSKY, Yu.N., BACON, D.J., Mesoscale thermodynamic analysis of atomic-scale dislocation–obstacle interactions simulated by molecular dynamics, *Philos. Mag.* **90** 7–8 (2010) 1001–1018.

- [4.235] MONNET, G., Determination of the activation energy by stochastic analyses of molecular dynamics simulations of dislocation processes, *Philos. Mag.* **91** 29 (2011) 3810–3829.
- [4.236] GROH, S., MARIN, E.B., HORSTEMEYER, M.F., ZBIB, H.M., Multiscale modelling of the plasticity in an aluminium single crystal, *Int. J. Plasticity* **25** 8 (2009) 1456–1473.
- [4.237] GURSON, A.L., Continuum theory of ductile rupture by void nucleation and growth: Part I — Yield criteria and flow rules for porous ductile media, *J. Eng. Mater. Technol.* **99**1 (1977) 2–15.

5. PRE- AND POST-IRRADIATION EXAMINATION TECHNIQUES ON ION BEAM IRRADIATED SPECIMENS

P. HOSEMANN
University of California,
Berkeley, CA,

O. ANDEROGLU
Los Alamos National Laboratory,
Los Alamos, NM,
United States of America

E. STERGAR
SCK•CEN,
Belgian Nuclear Research Centre,
Mol,
Belgium

Abstract

This SMORE CRP has used a wide variety of microanalytical tools to extract data from ion beam simulations of neutron damage to reactor structural materials. While some of these tools have been used for many years, others are very new and are undergoing continuous evolution and refinement. These tools have significant advantages but also have unique limitations and disadvantages. This chapter reviews the major techniques and their characteristics, especially those that require reporting significantly more experimental details than might usually be included in general publications.

5.1. INTRODUCTION

As ion beam irradiation and subsequent materials analysis are receiving increasing attention in nuclear materials science (see Fig. 5.1), a summary of characterization techniques used in this CRP and which can be applied to future studies is presented here.

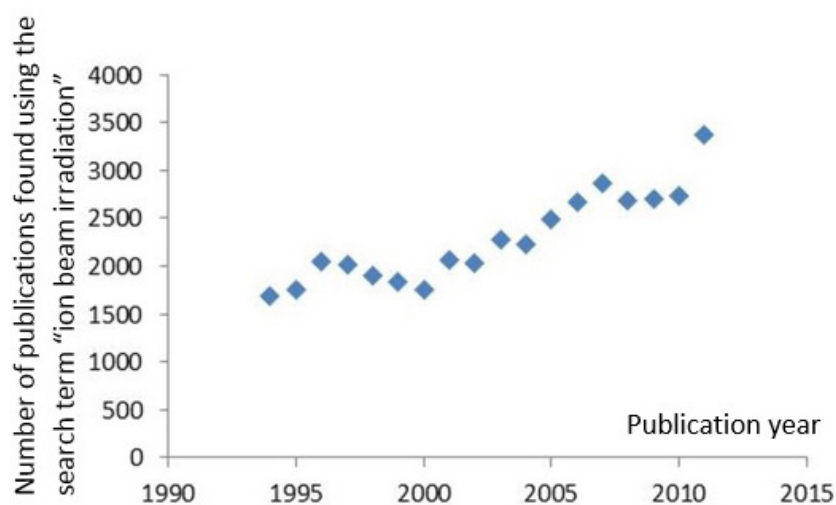


FIG. 5.1. Number of publications per year on sciencedirect.com containing the search term 'ion beam irradiation'.

While a large amount of work has been done to conduct the actual irradiation, data extraction techniques are becoming increasingly sophisticated, and it becomes ever more important to pay detailed attention to the post-irradiation examination (PIE), especially as PIE is the actual step where the data are generated. As illustrated in Fig. 5.1, there is an increasing publication rate of scientific articles on ion beam irradiation. It is therefore becoming more important to point out the difficulties associated with the PIE of such materials. It has to be noted that ion beam irradiation conducted on structural materials for nuclear applications is only as good as the PIE available. While large amounts of specimens can be irradiated to reasonably moderate doses utilizing ion beam techniques, PIE is usually the rate controlling step or bottleneck taking the most time and effort.

For example, the use of novel instruments such as the focused ion beam (FIB instrument or the local electrode atom probe (LEAP) allows unprecedented amounts of data and details from an irradiated specimen to be gained. However, no experimental technique is perfect, and every technique has its drawbacks and limitations. These have to be recognized and utilized by scientists who understand the trustworthiness of any applied technique. This chapter does not claim to cover all techniques, difficulties, or advantages, and does not favour one technique over another. Instead, it should be seen as a brief review of some of the PIE techniques available to scientists and engineers working on ion beam irradiated specimens.

The following sections discuss selected techniques, their advantages and disadvantages, and the limits to obtaining trustworthy data from them. Significant emphasis is placed on the importance of conscientious and thorough reporting of how the data were obtained, as this information determines the confidence and error estimates of the measurements.

5.2. SOME TECHNIQUES USED TO PERFORM POST-IRRADIATION EXAMINATION

5.2.1. Focused ion beam specimen preparation for atom probe tomography, micromechanical specimens and transmission electron microscopy

The availability of FIB specimen manufacturing methods has made specimen preparation an easier and more time efficient task for a variety of analysis techniques. FIB-based microstructural specimen manufacturing has quickly found a wide user community in the field of radiation damage studies in materials, although it does have some drawbacks. In this subsection, the procedure of how these types of specimens are prepared will be described, as well as the difficulties and scientific challenges associated with this novel method.

Most FIB specimen fabrication procedures, regardless of their final shape, be it for transmission electron microscopy (TEM), micropillar testing of micromechanical specimens or LEAP tomography, start with a standard trenching procedure involving energetic gallium ions. For specimens prepared for microstructural analysis (e.g. TEM and LEAP tomography), ion beam damage induced near the surface by gallium ions needs to be considered and mitigated. In order to protect the sensitive surfaces from excessive damage, a layer of platinum or carbon is deposited on top of the region of interest. For TEM and LEAP specimens, square shaped trenches are usually cut into the material, leaving a ~ 1 μm wide and maybe 10–20 μm long foil standing up in the original material, as shown in Fig. 5.2(a). More details about site specific atom probe tomography specimen preparation for various materials and applications can be found in Refs [5.1–5.5]. For LEAP specimen preparation, often just a V-cut is made, as described elsewhere [5.4].

Modern FIB instruments allow the time it takes to perform this task to be reduced to 20–40 min due to high beam currents and stable beam conditions. This step can be performed unattended. A subsequent finishing cut with a low beam current such as 1–3 nA makes the subsequent lift out procedure simpler. The U-shape undercutting to free the specimen is performed by having an angle between the specimen surface and the incoming beam, allowing for an angled cut underneath the foil. The angle depends on the ion gun arrangement and the maximum tilt of the specimen on the stage. The lift out procedure is conducted using a micromanipulator, which requires patience and skill in order to not lose the foil. The specimen can be extracted by welding the specimen onto the lift out needle using platinum/carbon deposition or a gripper device offered by some manipulator manufacturers.

The specimen is then transported to the specimen holder, which can be either a prefabricated atom probe holder or a TEM grid. Unfortunately, atom probe vendors do not standardize holders and specimen grips with commonly used electron microscopy holders, so adapters have to be either purchased or manufactured in house. Up to now, scientists built their own mechanical solutions, thereby contributing to non-standardization, leading to

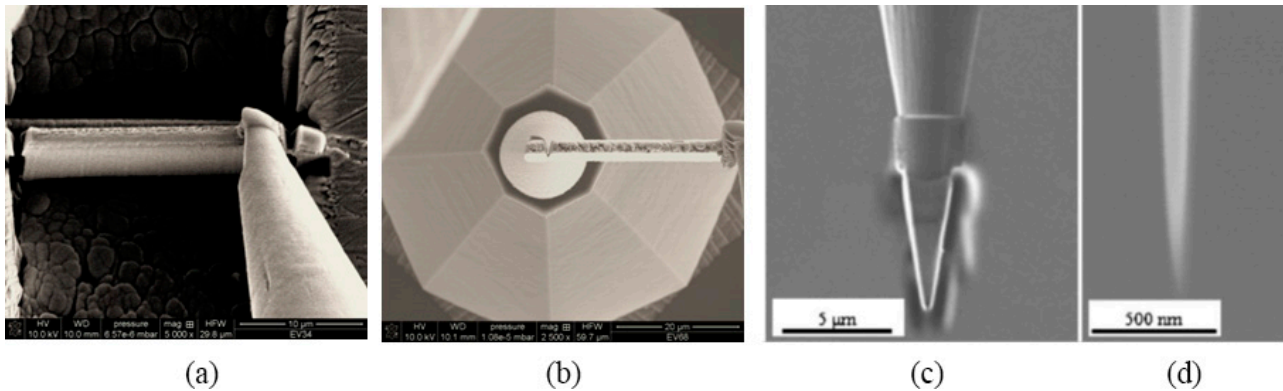


FIG. 5.2. (a) Lifting out of the specimen from the focused ion beam manufactured trench; (b) mounting of a specimen on the pre-shaped specimen holder; (c) initial shaping of the tip; (d) final tip. (Adapted from *J. Nucl. Mat.* **417** (2011) 274–278.)

the wide variety of holders, clamps and grippers used today. However, for TEM specimen manufacturing, the entire foil is usually mounted on an appropriate TEM grid using a platinum deposition tool. For atom probe specimen manufacturing, only one end of the specimen is welded to silicon stubs and a 1 μm long slice is cut out of the foil while the remaining foil, still mounted on the needle, is transported to the next stub, until the silicon grids are filled (Fig. 5.2) [5.2, 5.3].

After the specimens are mounted on either a TEM grid or a LEAP stub, the fine preparation starts, requiring skilled scientists and accumulated experience. In the following subsections, the standard procedures of specimen manufacturing are listed. These procedures are to be viewed as guidelines and not as a recipe; they therefore have to be adjusted accordingly for each specimen type, problem or instrument.

5.2.1.1. Transmission electron microscopy

A medium current of ~1.0 nA is used to reduce the foil thickness to approximately 500 nm from both sides of the specimen. Frequently, the material's microstructure becomes visible in the scanning electron microscopy image using proper beam settings. The beam current is reduced as the specimen becomes thinner in order to ensure good specimens with little FIB induced damage. The material and especially the skill of the operator determine the time required and beam settings needed.

For materials for which specimen curling due to internal stresses in the material can be an issue, window cuts are performed by thinning only a small area of the specimen to the final thickness while leaving the majority of the specimen hundreds of nanometres thick or by mounting the specimen in between two copper holders.

If available, a low (2 keV) ion beam energy and low current are desirable for final specimen cleaning, which removes the remaining FIB damage. Kiener et al. have analysed the damage occurring due to specimen preparation via FIB in copper [5.6]. For high resolution imaging, low kiloelectronvolt argon milling can help to reduce even further any potential ion beam damage, and recently developed nanomill tools have also proven their usefulness for that purpose. Post-FIB flash electro-polishing is used by several groups to mitigate the issue of FIB damage. However, as every material behaves differently in electrochemical environments, and copper holder and specimen (often steel) interaction cannot be predicted easily, the potential loss of the specimen hinders the widespread use of this technique.

5.2.1.2. Local electrode atom probe tomography

For LEAP analysis, a needle shaped specimen with an atomically sharp tip is required. In order to get as close as possible to this desired shape, annular milling is conducted on the square shaped starting material. Great care has to be taken to not accidentally create double needles, which can influence the subsequent measurements. Skilled operators can manufacture needles out of individual grain boundaries and other specified locations, resulting in very specific specimens. The beam current is progressively reduced as the specimen increasingly approaches the desired needle shape. Good operators can manufacture well shaped specimens within 40–60 min. Low kiloelectronvolt

ion milling (2 keV) is mandatory in order to remove any gallium irradiation damage in the specimen. Not all FIB instruments have this setting, and therefore the remaining gallium can be seen in the LEAP measurements.

The biggest concern with using FIB to manufacture ion irradiated PIE specimens is the resultant FIB damage. This fear is clearly justified, but it can be mitigated by skilled workers and low kiloelectronvolt milling. The FIB tool can also be used to manufacture microsized mechanical test specimens such as pillars, bend bars or even tensile specimens. FIB induced surface damage is also a concern for production of such specimens, and final cleaning steps need to be performed before specimen testing proceeds.

5.2.2. Microstructural characterization techniques

5.2.2.1. Transmission electron microscopy

TEM is one of the standard techniques used for pre- and post-irradiation characterization of ion irradiated materials. It is used for detailed microstructural characterization, including determination of composition, phase identification, crystallographic information, defect production and evolution. TEM has been revolutionized due to several technological developments, including advances in testing in situ and the application of aberration corrections to improve image resolution.

The bright field diffraction contrast images presented in Fig. 5.3 show a through focus series of Cu–Nb alternating layers with a bilayer period of 200 nm [5.7]. Cross-sectional TEM images are taken after irradiation with 150 keV He⁺ ions to a dose of $1 \times 10^{17} \text{ cm}^{-2}$. Small cavities and gas bubbles are easily visible with the images slightly out of focus and under kinematical diffraction conditions. Generally, in an under focus condition, the cavities or gas bubbles are bright relative to the background, and the image has a dark rim, as seen in Fig. 5.3(c). The reverse is true of an over focus condition, when the void is a dark image with a faint bright rim [5.8]. Figure 5.3(c) shows a large number of helium bubbles in both copper and niobium layers with a greater bubble concentration along layer interfaces. A slightly defocused high resolution (also known as phase contrast) transmission electron

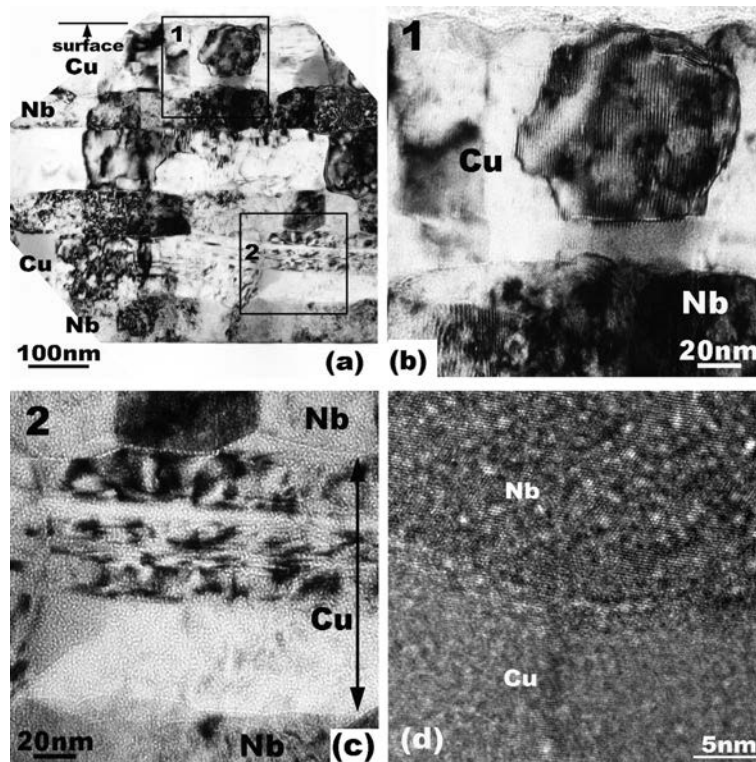


FIG. 5.3. (a) Cross-sectional transmission electron microscopy image of Cu–Nb multilayers subjected to He implantation; (b) no bubbles are detected; (c) large numbers of bubbles are seen; (d) high resolution transmission electron microscopy image showing 1–2 nm bubbles [5.7].

microscopy (HRTEM) image of Cu–Nb interfaces shows helium bubbles in each constituent at ~1–2 nm in diameter and aligned along the interface, as shown in Fig. 5.3(d).

A dark field weak beam image of the defect microstructure of proton irradiated copper is shown in Fig. 5.4, together with the derived size distributions of the two major components: loops and stacking fault tetrahedra [5.9]. The mean defect cluster size in copper is ~2 nm, and the majority of the defect clusters observed are stacking fault tetrahedra arising from low stacking fault energy. As the stacking fault energy increases, small loops form the majority of defects in bcc materials such as iron. However, loops are also seen in austenitic stainless steel with low stacking fault energy. Figure 5.5 shows an HRTEM image of stacking faults in proton irradiated copper [5.10].

Techniques based on Z-contrast imaging are also useful for pre- and post-irradiation analysis of microstructure. Figure 5.6(a) shows an STEM high angle annular dark field image of alloy 14YWT demonstrating lighter oxide particles in darker contrast [5.11]. The size, distribution and morphology of the particles can be deduced from the dark field images. The atomic scale characterization of a nano-oxide reveals the orientation relationship between the particle and the matrix [5.12]. HRTEM allows determination of coherency, strain and misfit dislocation spacing

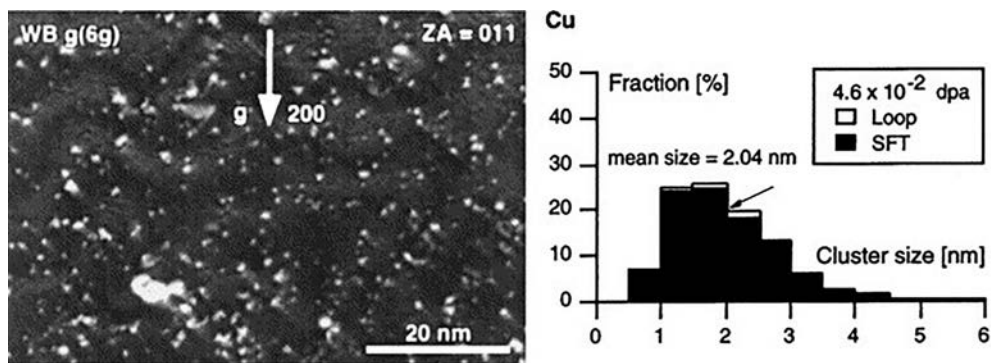


FIG. 5.4. Defect microstructure of copper (Cu) after proton irradiation at 320 K to 4.6×10^{-2} dpa and the derived defect size distribution [5.9]. SFT—stacking fault tetrahedra.

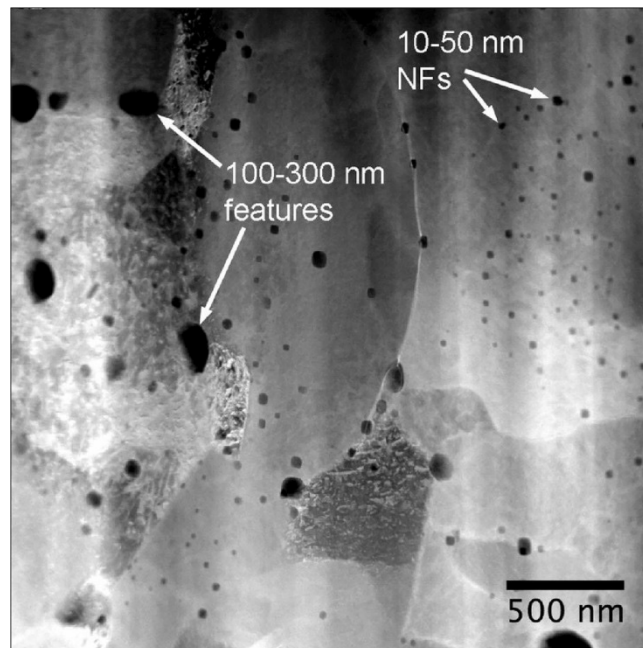


FIG. 5.5. High resolution transmission electron microscopy image of stacking faults in proton irradiated copper [5.10]. NF — nano features.

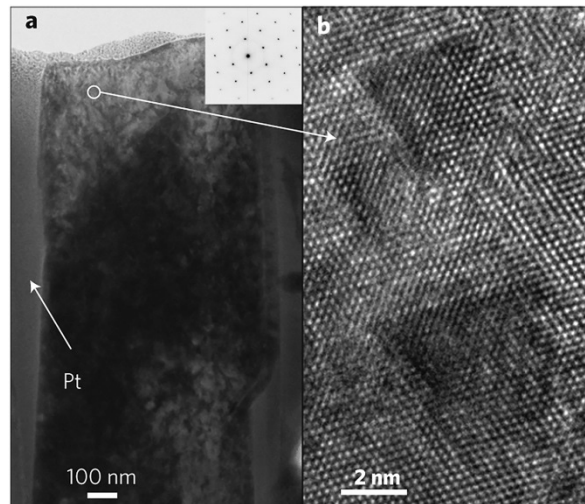


FIG. 5.6. (a) Scanning transmission electron microscopy dark field image of oxide particles in 14YWT [5.6]. (b) High resolution transmission electron microscopy image and corresponding diffraction pattern of a nano-oxide embedded ferrite in matrix [5.12].

at the interface. Such information is crucial in predicting the helium/dpa response of the bulk alloy. In addition, state of the art aberration corrected instruments show that some of the nanoclusters have a defective sodium chloride structure, with a high lattice coherency with the bcc steel matrix [5.13]. It has been suggested that the abundance of point defects, as well as the strong structural affinity of nanoclusters with the steel matrix, are important reasons for the unusual stability of the nano features under irradiation. Aberration corrected instruments are capable of high resolution STEM mapping as well as energy filtered imaging. Therefore, it is possible to resolve the type of atom at the interface [5.14].

STEM is also commonly used to study segregation and precipitation behaviour under ion irradiation. For instance, in austenitic steels where silicon and nickel segregate to grain boundaries, chromium and iron deplete, altering the grain boundary structure significantly [5.15]. For in situ testing, ion accelerators have been attached to TEM columns to enable study of the effects of ion irradiation on materials, similar to other techniques discussed later in this chapter.

5.2.2.2. Three dimensional atom probe tomography

In a three dimensional atom probe (3-DAP), a cryogenically cooled 50–100 nm diameter needle shaped specimen is analysed. A positive voltage is applied to this needle. By sufficiently increasing the voltage, surface atoms are removed from the specimen in the form of ions. This process is called field evaporation. To control the field evaporation process and also measure the time of departure, a standing field below the ionizing threshold is established, and short voltage pulses up from this field are applied. The pulses are typically about 10–20% of the applied standing voltage, and the pulse frequency for modern atom probes is approximately 200 kHz, leading to evaporation of atoms from the needle in a well-controlled manner. As the exact time of the electrical pulse is known, the time it takes the removed ions to reach the detector (as shown in Fig. 5.7) can be measured, allowing establishment of a time of flight (TOF) spectrum for the field evaporated ions.

This TOF spectrum can then be related to a mass to charge ratio of the detected ions, thus allowing identification of the ion species. The locations of where the ions hit the detector can be related to their original positions in the specimen. Therefore, a 3-D image can be reconstructed, allowing display of the types of atom at their original locations in three dimensions.

A 3-DAP relies on a combination of field evaporation, TOF spectroscopy and position sensitive detection. Essentially, an atom probe produces a sequence of atomic coordinates and the mass to charge ratio of each collected ion. Today's modern instruments allow the creation of atom probe tomography datasets containing several million atoms. The spatial resolution and searchable quality of the measurement is highly dependent on the assumptions made about evaporation (e.g. tip shape, evaporation order or evaporation fields). Common reconstruction procedures assume a hemispherical tip shape and ignore local variations of the evaporation field originating from

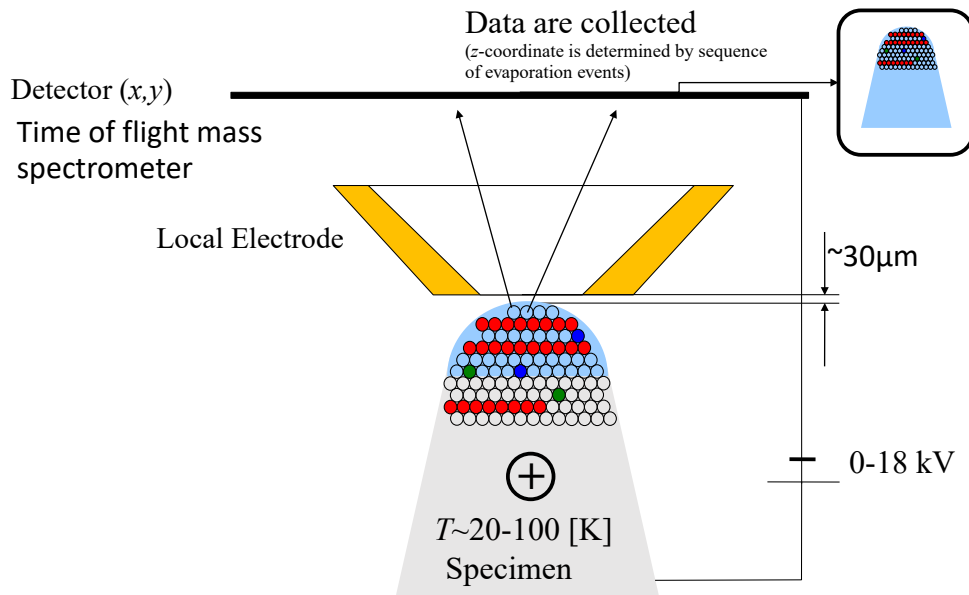


FIG. 5.7. Schematic diagram of a local electrode atom probe.

crystallography, chemical composition, etc., which can lead to difficult data interpretation as actual specimens do not usually follow all of these assumptions.

Figure 5.8 illustrates two different cases of high and low field phases and the overlap occurring. The extent of the overlap of various ions hitting the detector is dependent on the evaporation behaviour of both the matrix and the precipitate and also on the size of the precipitate. A further example, where a relative shift between the matrix and precipitate occurs due to variations in field evaporation of different elements, can be found in Ref. [5.16]. Owing to different evaporation fields of various phases in a material, incorrect representations of particle shapes can occur (e.g. precipitates become elongated or compressed in the analysis direction). The reconstruction algorithms used today are still very basic, even for simple materials, because of a lack of understanding of the field evaporation

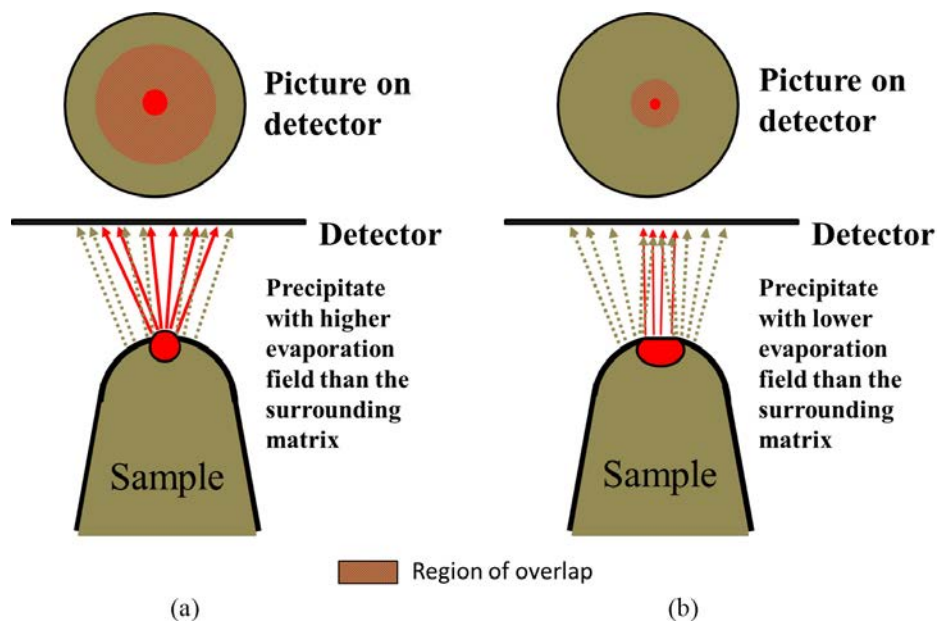


FIG. 5.8. Illustrations of evaporation of: (a) high field and (b) low field precipitates.

behaviour of different materials and alloys. A thorough description of these effects and related problems can be found in Ref. [5.17].

Compositional analysis is based on the analysis of a mass spectrum and therefore depends on the mass resolving power of the atom probe. Special care has also to be taken when peaks are assigned to elements and ranges, which is not always a straightforward task and requires experience with the technique and the analysed material. Possible limitations are noise level, insufficient mass resolution around peaks of interest, molecular ions (M_2 , M_3 , etc.) and overlap of peaks of interest (e.g. ^{54}Fe and ^{54}Cr , or ^{58}Fe and ^{58}Ni). An example where special care has to be taken is when the composition of carbides needs to be determined because carbon can occur in the forms C^{++} , C^+ , C_2^+ , C_3^{++} , C_3^+ , C_4^+ , etc., leading to a spectrum with multiple peaks of carbon, thus increasing the potential for peak overlap with other elements.

5.2.2.3. Laser assisted atom probe tomography

Although Kellogg and Tsong [5.18] introduced the first laser assisted 3-DAPs in 1980, they did not become commercially available until 2006 [5.19]. While the principal set-up is the same as for a voltage atom probe, laser, rather than voltage, pulses are used to trigger field evaporation of the specimen at a given time, thus allowing measurement of the TOF. This technique is usually used to analyse higher resistivity materials and those that show a brittle behaviour under high voltage and cryogenic conditions. With regard to reconstruction issues, in addition to the influence of crystallography and chemical composition described above, there is also an influence of the laser itself [5.20]. The mass resolution of this variant of 3-DAP is strongly dependent on how fast the heat introduced by the laser pulse can be removed from the apex region of the specimen. If the heat is not sufficiently well removed, field evaporation may occur in the tail of the thermal pulse, leading to a significantly deteriorated mass to charge spectrum characterized by significantly high mass tails in all the peaks of the spectra. For example, yttrium, a major component of the nano features in oxide dispersion strengthened (ODS) steels, has its peak in the mass spectrum within the thermal tail of iron, making an accurate measurement of yttrium content rather difficult.

Owing to the difference in the evaporation mechanism, there is also a shift in the occurrence of the charging states of the elements. While in voltage mode (due to the higher electric field necessary for field evaporation), almost all iron (in iron based alloys) occurs as Fe^{2+} , leading to an increase in temperature due to laser irradiation on the tip apex, owing to a shift from Fe^{2+} to Fe^+ . This ratio can be used to optimize the parameters for the measurement and also as a quality control check on the actual measurement. Large thermal tails and the occurrence of significant amounts of low charging states are typical signs of not having properly chosen the experimental parameters. Therefore, it is strongly recommended to always display the actual spectrum with the measurement, thus allowing others to evaluate the quality and accuracy of the data displayed. As a general rule, for laser assisted 3-DAP measurements, a mass to charge spectrum as similar as possible to that received from a measurement performed in voltage mode is desirable, as are cross comparisons. Applying such a critical view to the measurements and allowing continuous questioning of the results leads to more trustworthy results.

Careful voltage mode measurements have the potential to resolve the interatomic spacing between lattice planes, if the specimen is oriented along a zone axis; laser assisted measurements usually do not have this capability.

The most widely used method to detect clusters is the maximum separation method, described, for example, by Cerezo and Davin [5.21]. This method works on the principle that second phase precipitates represent a region where solute atoms are concentrated. Therefore, the spacing between these atoms will be smaller than within the matrix. Consequently, this method groups together atoms that are not separated by a distance larger than a defined distance d_{max} . All atoms connected this way are then defined as a cluster (see Fig. 5.9).

Clusters containing less than a certain number (usually referred to as N_{min}) of solute atoms are considered to be the result of random fluctuations and are therefore ignored. For clusters containing more than N_{min} atoms, all solute atoms within a separately defined distance L , which is usually the same value as or slightly larger than d_{max} , are also associated with the cluster. This leads to the incorporation of matrix atoms into the cluster, and also to a 'shell' of matrix clusters on the cluster–matrix interface (Fig. 5.10).

To eliminate this effect, all atoms are removed in the vicinity (defined by d_{err}) of a matrix atom (Fig. 5.11).

Choosing the right values for d_{max} , L and d_{err} for this type of search is still a process of trial and error, but newer versions of atom probe analysis software (e.g. IVAS from Cameca) are able to provide some guidance utilizing computer simulations. Newer versions of cluster detection algorithms combine the maximum separation method with density based analysis, as described, for example, in Ref. [5.22].

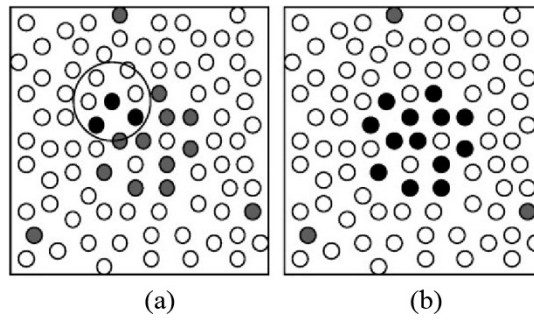


FIG. 5.9. (a) Grouping together solute atoms within a distance d_{max} ; (b) result of solute selection (after [5.21]).

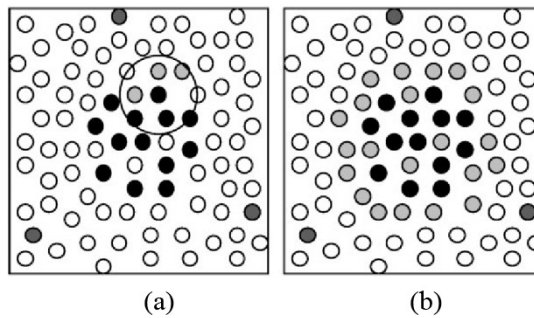


FIG. 5.10. (a) Selection of other than solute atoms; (b) result of atom selection (after [5.21]).

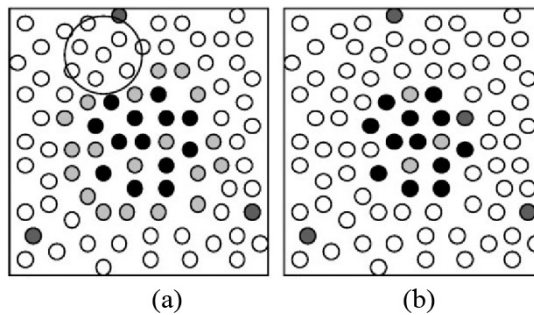


FIG. 5.11. (a) Erosion of atoms at the cluster-matrix interface; (b) result of the erosion process (after [5.21]).

Currently, only one vendor for 3-DAP exists (Cameca), which leads to typical problems arising from a lack of competition (very high prices, poor user support, etc.). While, for the microscope itself, the choice of instruments is limited to one vendor, it is possible to use different analysis software instead of IVAS. Excellent, freely available software such as 3Depict (threedepict.sourceforge.net) for data analysis can be applied. The benefit of 3Depict is its use of an open source code, allowing users to modify the code to their particular problem and so enhance the scientific outcome and rate of progress.

5.2.3. Microscale and mesoscale mechanical testing

As one of the main purposes of structural materials in nuclear applications is to maintain stability under applied stresses, thereby ensuring the structural integrity of a component, scientists are always interested in changes of mechanical properties due to irradiation. Therefore, analysis of microstructural evolution and its consequences on mechanical properties is an essential component of examining ion beam irradiated materials.

Since the beginning of ion beam irradiation studies, hardness testing has been an essential tool to evaluate changes in mechanical properties. Several studies have been conducted utilizing micro hardness testing on ion beam irradiated materials [5.23–5.25]. While it is essential to know what the change in hardness is, the ultimate goal is to determine the full stress–strain tensile test curve and the fracture toughness, which hardness data alone do not provide. The main limiting factor is the shallow irradiation depth in typical ion beam irradiated specimens. In recent times, nano indentation has become a popular tool for investigating mechanical property changes of ion beam irradiated materials [5.26–5.29]. Owing to the development of instrumented small scale hardness measurements, called nano indentation measurements, the thin near surface irradiation region of ion irradiated material has become accessible for testing.

While surface indentation (i.e. indentation in the same direction as the incident ion beam) has been applied in the past [5.30, 5.31], cross-section indentation has become available, allowing more accurate indenter positioning. If surface indentation is performed, great care has to be taken in how the measurement is taken in order to avoid an overlap of different effects. These effects are demonstrated in Fig. 5.12, which shows the overlaying of a varying dose profile, the indentation size effect, surface sputtering or deposition and end of ion range implantation [5.32]. Therefore, care needs to be taken with regard to what the indentation experiment is actually sampling, considering the size of the plastic zone around the indenter.

Cross-section indentation (i.e. indentation that is perpendicular to the irradiation direction) avoids several of these effects. It also might provide a way to estimate a yield strength value from the hardness value, by using a factor of approximately 3 [5.33].

However, when performing cross-section indentation, polishing artefacts have to be considered, and specimen preparation can be an issue. Figure 5.13 presents TEM images of indents performed in cross-section on an ion beam irradiated material. The hardness change due to ion beam irradiation can be seen clearly in the data plot, while the TEM pictures reveal the defects causing the hardness. However, in most cases, interest lies more in the change of a property due to irradiation than in its absolute, numerical value. Spherical indentations can also be used to evaluate the yield strength. A direct measurement of yield strength after irradiation can be achieved with microscale mechanical testing, such as microcompression testing or microtensile testing, as shown in Fig. 5.14 [5.5].

Recently, tensile testing on small FIB pillars has become available and is currently being used to investigate ion beam irradiated materials. While small scale mechanical test devices are built for compression, it is rather difficult to modify them for tensile testing. Two approaches being developed are push to pull devices and direct tensile testing (Fig. 5.15) [5.34].

However, when performing these types of measurements, it is essential to keep in mind what property is being sought. Absolute engineering values of yield stress obtained from using these techniques are sometimes questionable, as the influences of the size effects and the strength determining length scales need to be noted.

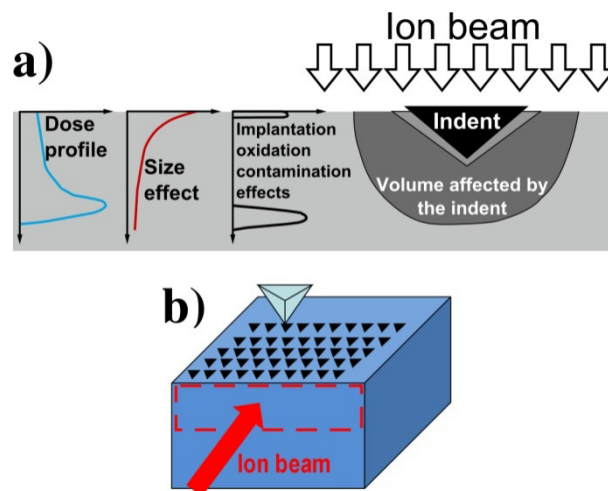


FIG. 5.12. (a) Effects to consider when performing post-irradiation surface indentation; (b) schematic cross-section of nano indentation on ion beam irradiated material [5.26].

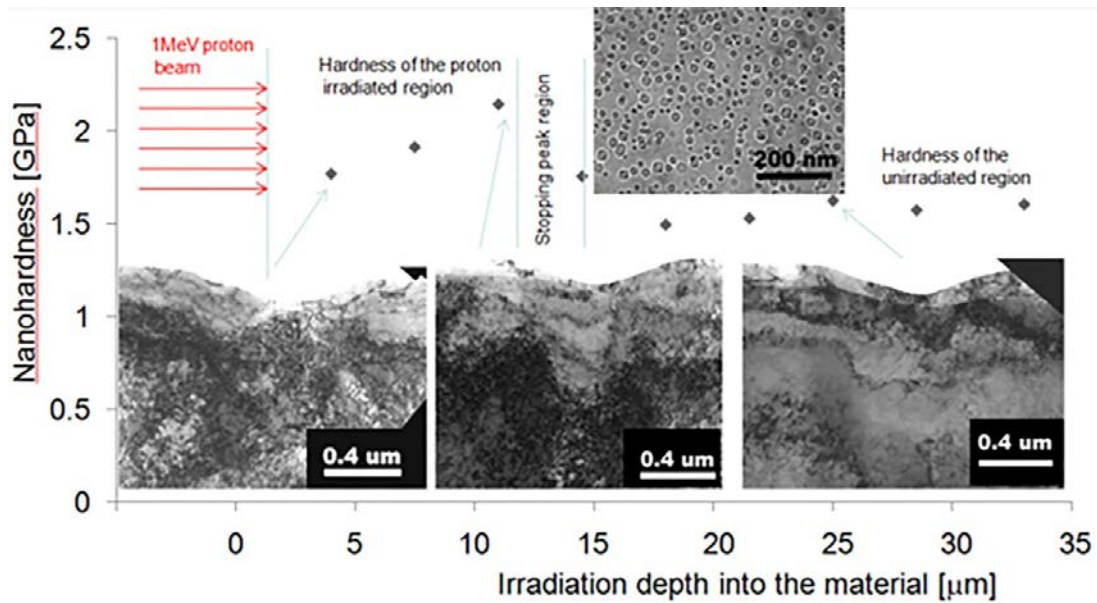


FIG. 5.13. Hardness measurements on ion beam irradiated copper (Cu) and transmission electron microscopy images of the indents. Insert shows the voids in the ion beam stopping area.

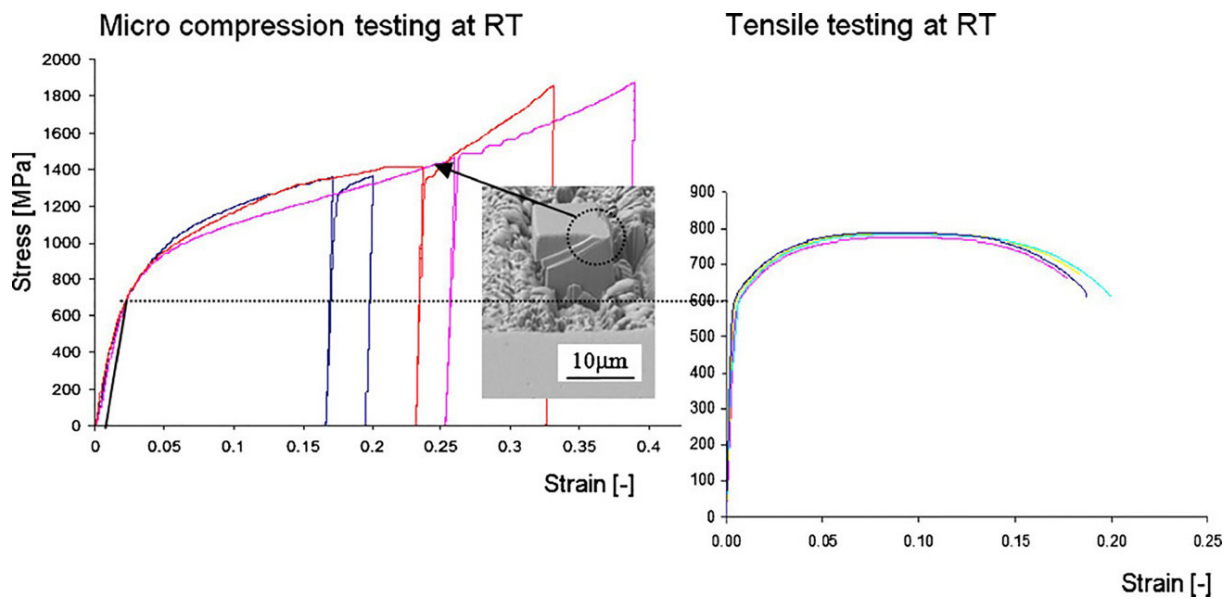


FIG. 5.14. Microcompression testing on a ferritic-martensitic steel (HT-9) in direct comparison with a regular tensile test (after [5.5]). RT — room temperature.

It has been found that nano structured materials have little to no size effects in compression testing, as long as the strength determining features are significantly smaller than the specimen size.

Therefore, ODS alloys [5.35] are prime candidates for testing with small scale techniques, while large grained materials are more difficult. Fracture toughness measurements are significantly more difficult to access on these scales. However, scientists have attempted to perform these measurements with small scale materials testing on rather brittle materials or interfaces, as shown in Fig. 5.16 [5.36, 5.37]. In this work, performed by Matoy et al., bend bars were manufactured to measure fracture toughness of amorphous silicon [5.36, 5.37]. It will be only a matter of time until scientists apply this method to irradiated materials.

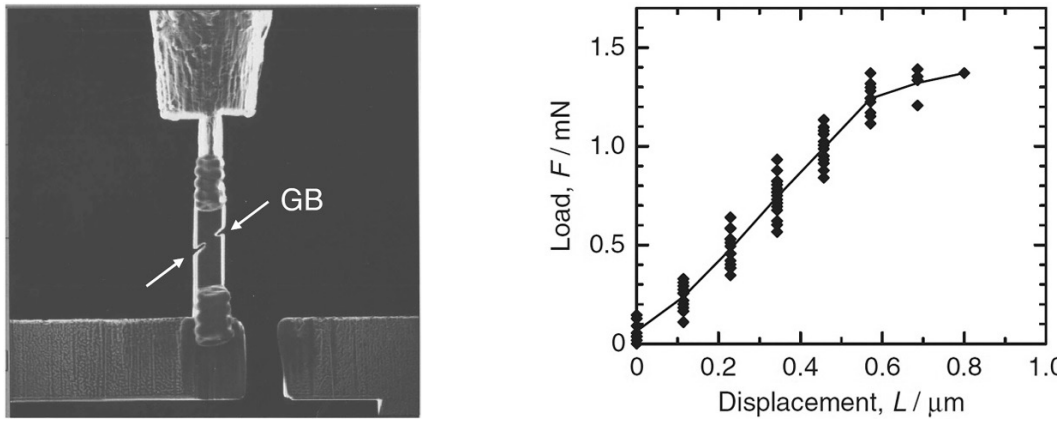


FIG. 5.15. Microtensile testing and the resulting tensile curve (after [5.34]). GB — grain boundary.

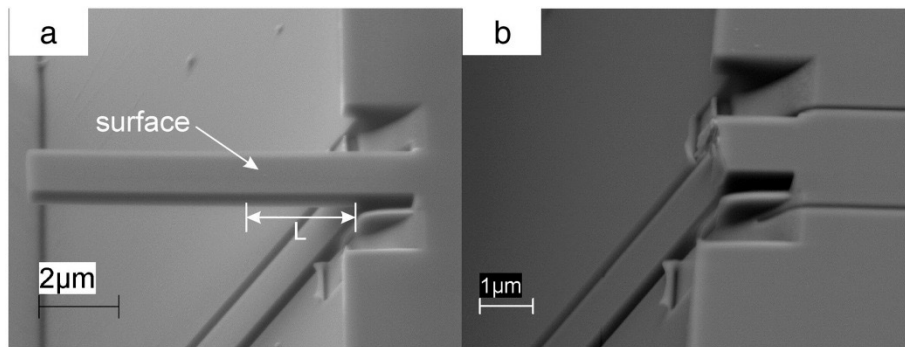


FIG. 5.16. Manufactured focused ion beam bend bars to measure fracture toughness on interfaces: (a) before testing; (b) after testing [5.37].

How small is too small? In recent work performed by Kiener et al. [5.6], a scaling study was performed in situ in the transmission electron microscope. It was found that microcompression tests on single crystal copper in the unirradiated state showed a pronounced size effect at diameters ranging from several micrometres to nanometres. Irradiated specimens with nanoscale defects (stacking fault tetrahedra), on the other hand, did not experience the same behaviour and showed a size effect only at dimensions <400 nm. Also, it has been found that nanostructured materials have little to no size effect in compression testing, as long as the strength determining features are significantly smaller than the specimen size. Therefore, ODS alloys [5.35] are prime candidates for testing using small scale techniques, while tests on large grained materials are more difficult to interpret.

5.2.4. Swelling measurements on ion beam irradiated materials

Radiation induced swelling is of significant concern in nuclear applications. Scientists have attempted to measure swelling using ion beam irradiation. However, evaluating swelling during the PIE is complex, as volumetric changes are difficult to measure. Today, most scientists publishing swelling results extract the data using TEM examination, as described earlier. The voids induced by radiation are measured and counted, leading to a calculated swelling number, but not an actual macroscopic swelling value gained by volumetric measurements. While this is a widely accepted and accurate method, it has the limitation of all TEM measurements of extremely small probing volume.

Some groups have attempted to measure swelling using atomic force microscopy or other surface profiling methods on masked and irradiated specimens [5.38]. While these types of measurements are possible, special care has to be taken on what is measured using atomic force microscopy on the ion beam irradiated specimens. As atomic

force microscopy is only a surface sensitive technique, the measurement of the step height increase due to swelling can be overlapped by measurements of the step height increase due to surface deposition or to other phenomena. As surface sputtering or the deposition of carbon can occur, these measurements have to be cross-calibrated with TEM investigations in which the void density is observed and the resulting volume changes are calculated [5.39].

5.2.5. Positron annihilation spectroscopy

Positron annihilation spectroscopy (PAS) has been used for decades to evaluate the defect structure of materials before and after irradiation. In this technique, the positron–electron pair annihilation process is utilized, whereby a radioactive decay event emits gamma rays of a specific wavelength [5.40] (Fig. 5.17).

Typically, positron sources such as ^{22}Na , ^{64}Cu or ^{58}Co are utilized, which have end point energies of <1 MeV and a range of <100 μm in a solid specimen. Additionally, accelerator devices are sometimes used, allowing for a wide range of positron energies and therefore an ability to attain a specific penetration depth.

After the emitted positron enters the solid, it is thermalized (in picoseconds), leading to ionizing collisions, plasmon electron hole excitation and phonon interaction. The positron interacts with an electron, annihilating the particle and antiparticle, usually emitting two gamma rays (one and three rays are possible as well, but are rare events). In areas of lower electron concentration in a material, the positron can be trapped and therefore annihilation is delayed, leading to an extended lifetime of this positron. Defects affecting the positron lifetime can be vacancies, small vacancy clusters, voids, dislocation lines and/or jogs. Therefore, PAS can be used to differentiate between the earliest stages of vacancy and interstitial clustering in irradiated metals not otherwise accessible by electrical resistometry or TEM.

Usually, the lifetime of an untrapped positron is on the order of 100–400 ps, depending on whether it is an ionic or metal crystal, and a significant number of these annihilation events are measured utilizing energy sensitive gamma detectors. Figure 5.18 [5.41] presents a positron lifetime spectrum for pure alpha iron before and after electron irradiation and subsequent annealing. A shift to longer lifetimes is clearly visible due to the defects produced under radiation.

While the positron lifetime spectrum reveals the basic number of defects in a material, implementation of a Doppler broadening measurement of the angular correlation of the gamma rays emitted from the annihilation process gives additional information.

Using PAS for ion beam irradiated specimens can be challenging. Most ion beam irradiations are conducted with a maximum energy of 1–2 MeV, leading to a 20–40 μm proton penetration depth or even significantly less if heavy ions are used. As most PAS systems use ^{22}Na or other isotopes with fixed positron energy, leading to a

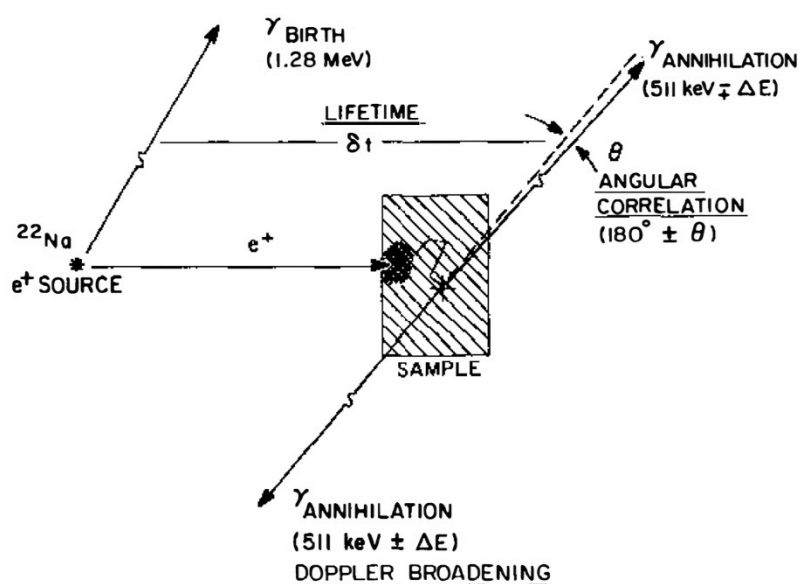


FIG. 5.17. Schematic sketch of the positron annihilation spectroscopy principle [5.30].

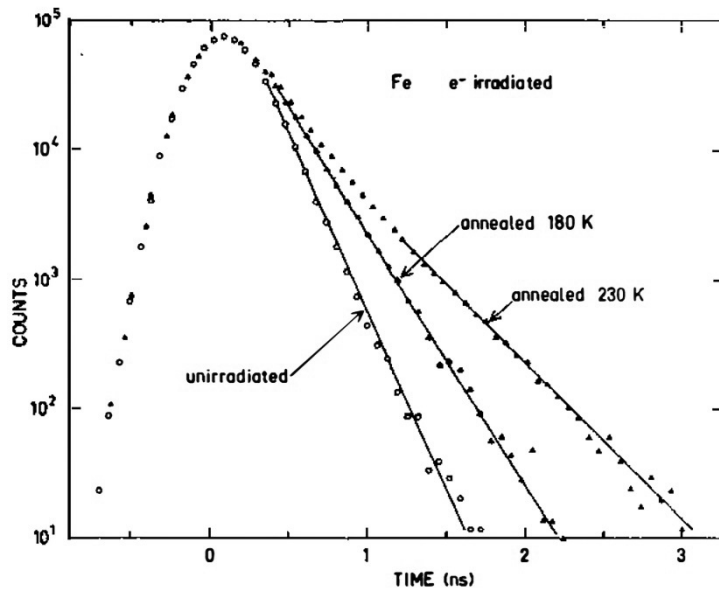


FIG. 5.18. Positron annihilation spectroscopy of pure alpha iron before and after electron irradiation and subsequent annealing at different temperatures [5.41, 5.42].

penetration depth of 100 μm , the signal is mixed based on dose range, dose rate range, interstitial implantation (stopping range) and unirradiated material, making it difficult to say what the defect density is at any given condition. Accelerator systems allowing a choice of target oriented positron energy might be more desirable for ion beam irradiated materials.

5.2.6. Ion beam analysis

While ion beams are used for ion beam irradiation to produce displacement damage, they can also be used for materials analysis. In fact, ion beam analysis methods are very common techniques for all types of basic and applied science studies. A detailed description of ion beam analysis can be found in Ref. [5.43].

Within the SMORE CRP, ion beam analysis methods were not utilized extensively, but a brief introduction was included in order to guide future programmes. Of the various methods found to be applicable to SMORE, the channelling and Rutherford backscattering spectroscopy (RBS) techniques are the most useful.

5.2.6.1. Rutherford backscattering spectroscopy

RBS utilizes ions with megaelectronvolt energies to determine elemental areal density, stoichiometry and impurity content on near surface regions. The number and energy of backscattered ions from a surface are evaluated in order to investigate the atomic mass and distribution of elements in the material. Figure 5.19 illustrates the experimental set-up and the spectrum obtained. In order to gain quantitative numbers based on this technique, it is necessary to understand and study energy losses in matter [5.43].

Most of the time ^4He ions are used, for historical and experimental reasons, but the technique can be conducted with any other type of ion beam. The main benefits of RBS are that it is comparatively easy to use, is an absolute measurement with no need for standards, is considered to be non-destructive and examines surface regions, which is important for the PIE of ion irradiated specimens. Its main drawback is the insensitivity to trace elements and light elements in a heavy matrix. In addition, as with all spectroscopy techniques, issues such as peak overlapping and fitting can lead to difficulties.

However, it is also necessary to consider that the use of ions for investigation can lead to the fact that the ions also end up in the material, and the finding of helium, utilizing other PIE techniques afterwards, can be attributed to this. Also, it is not a technique useful for deep ion beam irradiated materials. Irradiated materials several micrometres deep cannot easily be investigated using RBS. Only very shallow irradiations can be investigated, making it difficult to use other PIE techniques in addition to RBS.

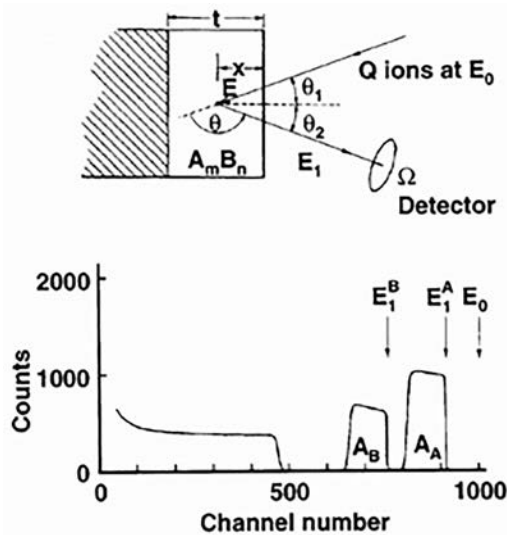


FIG. 5.19. Schematic of a Rutherford backscattering spectroscopy set-up and results attained on a two element metal [5.43]. E_0 , E_1^A and E_1^B indicate the energy of the incoming ion and outgoing ions, giving a signal for elements A and B, respectively. Q is the number of incoming ions, θ_1 and θ_2 the angle of the ion's flight. $A_m B_n$ is the composition of the metal and A_A and A_B signal on the Rutherford backscattering spectroscopy describing the metal. Ω is the angle at which the ions arrive at the detector.

5.2.6.2. Channelling

Channelling is the focused and oscillating travel of ion beams in the relatively open spaces between lattice planes in a crystal. Therefore, only crystalline materials can be investigated with this method. The channelling ions can interact with the host atoms in several different ways such as large angle Rutherford collisions, nuclear reactions and inner shell X ray excitation. However, any of these reactions will result in an interaction of the channelling ions and the host lattice, as illustrated in Fig. 5.20.

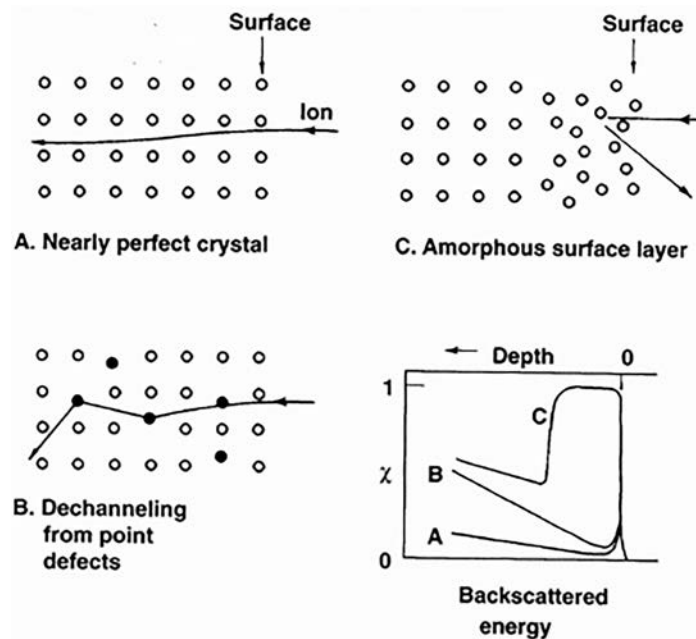


FIG. 5.20. Schematic of the different mechanisms of ion scattering in the host lattice: (a) little scattering in a nearby perfect crystal; (b) dechannelling by multiple scattering from point defects; (c) direct backscattering from an amorphous surface; (d) resulting channelling spectrum of each mechanism [5.43].

The normalized yield χh is proportional to the atoms not aligned with the channel (displaced host atoms). Ions travelling at small angles to the closed packed lattice planes have little interaction with atoms in the crystalline structure. The position of interstitial or substitutional atoms can be determined directly from channelling experiments. For substitutional atoms, $\chi h = \chi s$ for any angle ψ . If the substitutional atom sticks out of the lattice and interacts with the incoming ion, then χs is larger. However, if an interstitial atom is present, χs peaks at $\psi=0$. By performing a triangulation procedure, the exact position of a solute atom can be determined with high precision (0.005 nm). Figure 5.21 illustrates this mechanism.

While channelling is a powerful tool for determining the exact position of atoms in a lattice, its applications to the PIE of ion irradiated specimens can be rather limited. Owing to the fact that only shallow areas and single crystal materials can be investigated, its use is limited to very fundamental studies.

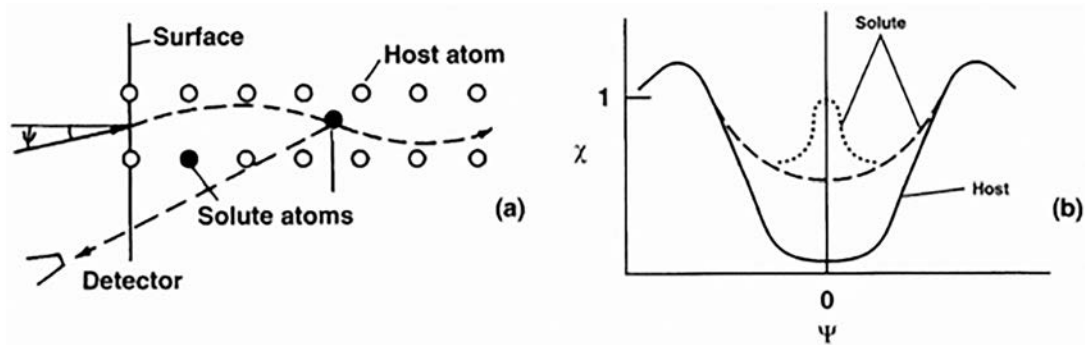


FIG. 5.21. Mechanism of ion and matrix atom interaction in a channelling experiment [5.43].

5.3. SUMMARY

This chapter has presented a brief introduction to some of the techniques used to perform PIE on structural materials after ion beam irradiation. It is not possible to list and discuss every method available, but widely used techniques such as TEM and ion beam analysis, as well as recently emerging techniques such as small scale mechanical testing and atom probe tomography, have been highlighted. One technique has not been valued over another, and not all benefits and drawbacks of each technique have been mentioned.

Other techniques such as beam broadening analysis from synchrotron X ray studies, resistivity measurements and many other techniques are available, but these were not utilized in the context of the SMORE CRP.

Given the complexities, especially for newly emerging techniques, it is desirable that reporting scientists are explicit with regard to the detailed methods used and the associated uncertainties. This will allow others to determine their confidence in such conclusions, and will especially allow them to reconcile the inevitable differences that will arise from different studies using nominally similar techniques.

REFERENCES TO CHAPTER 5

- [5.1] MILLER, M., RUSSELL, K., THOMPSON, G., Strategies for fabricating atom probe specimens with a dual beam FIB, *Ultramicroscopy* **102** 4 (2005) 287–298.
- [5.2] MILLER, M.K., RUSSELL, K.F., THOMPSON, K., ALVIS, R., LARSON, D.J., Review of atom probe FIB based specimen preparation methods, *Microscopy Microanalysis* **13** 6 (2007) 428–436.
- [5.3] RACHBAUER, R., MASSL, S., STERGAR, E., FELFER, P., MAYRHOFER, P.H., Atom probe specimen preparation and 3D interfacial study of Ti–Al–N thin films, *Surf. Coat. Technol.* **204** 11 (2009) 1811–1816.
- [5.4] THOMPSON, K., et al., In situ site specific specimen preparation for atom probe tomography, *Ultramicroscopy* **107** (2007) 131–139.
- [5.5] HOSEMANN, P., et al., Large and small scale materials testing of HT-9 irradiated in the STIP irradiation programme, *Exp. Mech.* **51** (2011) 1095–1102.

- [5.6] KIENER, D., MOTZ, C., RESTER, M., JENKO, M., DEHM, G., FIB damage of Cu and possible consequences for miniaturized mechanical tests, *Mater. Sci. Eng. A* **459** 1–2 (2007) 262–272.
- [5.7] ZHANG, X., et al., Nanostructured Cu/Nb multilayers subjected to helium ion-irradiation, *Nucl. Instrum. Methods Phys. Res. Sect. B: Beam Interact. Mater. Atoms* **261** (2007) 1129–1132.
- [5.8] LANDUYT, J.V., GEVERS, R., AMELINCKX, S., Diffraction contrast from small voids as observed by electron microscopy, *Phys. Stat. Sol. B* **10** 1 (1965) 319–335.
- [5.9] VICTORIA, M., et al., The microstructure and associated tensile properties of irradiated fcc and bcc metals, *J. Nucl. Mater.* **276** 1–3 (2000) 114–122.
- [5.10] KIENER, D., HOSEMANN, P., MALOY, S.A., MINOR, A.M., In situ nanocompression testing of irradiated copper, *Nat. Mater.* **10** (2011) 608–613.
- [5.11] BHATTACHARYYA, D., Los Alamos National Laboratory, personal communication, 2008.
- [5.12] RIBIS, J., CARLAN, Y.D., Interfacial strained structure and orientation relationships of the nanosized oxide particles deduced from elasticity driven morphology in oxide dispersion strengthened materials, *Acta Mater.* **60** 1 (2012) 238–252.
- [5.13] HIRATA, A., et al., Atomic structure of nanoclusters in oxide dispersion strengthened steels, *Nat. Mater.* **10** 12 (2011) 922–926.
- [5.14] HWANG, H.Y., et al., Emergent phenomena at oxide interfaces, *Nat. Mater.* **11** (2012) 103–113.
- [5.15] ROBERTSON, I.M., et al., Towards an integrated materials characterization toolbox, *J. Mater. Res.* **26** (2011) 1341–1383.
- [5.16] MARQUIS, E.A., VURPILLOT, F., Chromatic aberrations in the field evaporation behavior of small precipitates, *Microscopy Microanalysis* **14** (2008) 561–570.
- [5.17] MARQUIS, E.A., HYDE, J., Applications of atom-probe tomography to the characterisation of solute behaviours, *Mater. Sci. Eng.* **69** (2010) 37–62.
- [5.18] KELLOGG, G.L., TSONG, T.T., Pulsed laser atom-probe field ion microscopy, *J. Appl. Phys.* **51** (1980) 1184.
- [5.19] KELLY, T., MILLER, M., Atom probe tomography, *Rev. Sci. Instrum.* **78** 3 (2007) 031101.
- [5.20] GAULT, B., FONTAINE, A.L., MOODY, M.P., RINGER, S.P., MARQUIS, E.A., Impact of laser pulsing on the reconstruction in an atom probe tomography, *Ultramicroscopy* **110** 9 (2010) 1215–1222.
- [5.21] CEREZO, A., DAVIN, L., Aspects of the observation of clusters in the 3-dimensional atom probe, *Surf. Interf. Anal.* **39** (2007) 184–188.
- [5.22] STEPHENSON, L.T., MOODY, M.P., LIDDICOAT, P.V., RINGER, S.P., New techniques for the analysis of fine scaled clustering phenomena within atom probe tomography (APT) data, *Microscopy Microanalysis* **13** 6 (2007) 448–463.
- [5.23] POGREBNJAK, A.D., et al., A comparison of radiation damage and mechanical and tribological properties of [alpha]-Fe exposed to intense pulsed electron and ion beams, *Vacuum* **58** 1 (2000) 45–52.
- [5.24] MIURA, T., FUJII, K., FUKUYA, K., ITO, Y., Characterization of deformation structure in ion-irradiated stainless steels, *J. Nucl. Mater.* **386–388** (2009) 210–213.
- [5.25] GUPTA, G., JIAO, Z., HAM, A., BUSBY, J., WAS, G., Microstructural evolution of proton irradiated T91, *J. Nucl. Mater.* **351** 1–3 (2006) 162–173.
- [5.26] HOSEMANN, P., et al., An exploratory study to determine applicability of nano-hardness and micro-compression measurements for yield stress estimation, *J. Nucl. Mater.* **375** 1 (2008) 135–143.
- [5.27] HOSEMANN, P., MALOY, S., GRECO, R., SWADENER, J., ROMERO, T., Oxygen effects on irradiated tantalum alloys, *J. Nucl. Mater.* **384** 1 (2009) 25–29.
- [5.28] RICE, P., STOLLER, R., The effect of solutes on defect distributions and hardening in ion-irradiated model ferritic alloys, *J. Nucl. Mater.* **244** 3 (1997) 219–226.
- [5.29] HOSEMANN, P., et al., Nanoindentation on ion irradiated steels, *J. Nucl. Mater.* **389** 2 (2009) 239–247.
- [5.30] LI, N., et al., He ion irradiation damage in Fe/W nanolayer films, *J. Nucl. Mater.* **389** 2 (2009) 233–238.
- [5.31] LI, N., et al., He ion irradiation damage in Al/Nb multilayers, *J. Appl. Phys.* **105** 12 (2009) 123–522.
- [5.32] HOSEMANN, P., KIENER, D., WANG, Y., MALOY, S.A., “Issues to consider using nano indentation on shallow ion beam irradiated materials”, *J. Nucl. Mater.* **425** (2012) 136–139.
- [5.33] BUSBY, J.T., HASH, M.C., WAS, G.S., The relationship between hardness and yield stress in irradiated austenitic and ferritic steels, *J. Nucl. Mater.* **336** 2–3 (2005) 267–278.
- [5.34] FUJII, K., FUKUYA, K., Development of micro tensile testing method in an FIB system for evaluating grain boundary strength, *Mater. Trans.* **52** (2011) 20–24.
- [5.35] POUCHON, M., CHEN, J., GHISLENI, R., MICHLER, J., HOFFELNER, W., Characterization of irradiation damage of ferritic ODS alloys with advanced micro-sample methods, *Exp. Mech.* **50** (2010) 79–84.
- [5.36] MATOY, K., DETZEL, T., MÜLLER, M., MOTZ, C., DEHM, G., Interface fracture properties of thin films studied by using the micro-cantilever deflection technique, *Surf. Coat. Technol.* **204** 6–7 (2009) 878–881.
- [5.37] MATOY, K., et al., A comparative micro-cantilever study of the mechanical behavior of silicon based passivation films, *Thin Solid Films* **518** 1 (2009) 247–256.
- [5.38] TERASAWA, M., MITAMURA, T., LIU, L., TSUBAKINO, H., NIIBE, M., Metal surface swelling by heavy charged particle irradiation, *Nucl. Instrum. Methods Phys. Res., Sect. B* **193** 1–4 (2002) 329–335.

- [5.39] JOHNSTON, W., ROSOLOWSKI, J., TURKALO, A., LAURITZEN, T., An experimental survey of swelling in commercial Fe-Cr-Ni alloys bombarded with 5 MeV Ni Ions, *J. Nucl. Mater.* **54** 1 (1974) 24–40.
- [5.40] SIEGEL, R.W., Positron annihilation spectroscopy, *Annu. Rev. Mater. Sci.* **10** 1 (1980) 393–425.
- [5.41] VEHANEN, A., HAUTOJÄRVI, P., JOHANSSON, J., YLI-KAUPPILA, J., MOSER, P., Vacancies and carbon impurities in α -iron: Electron irradiation, *Phys. Rev. B* **25** 2 (1982) 762–780.
- [5.42] SZPALA, S., et al., Defect identification using the core-electron contribution in Doppler-broadening spectroscopy of positron-annihilation radiation, *Phys. Rev. B* **54** 7 (1996) 4722.
- [5.43] TESMER, J., NASTASI, M., BARBOUR, J.C., MAGGIORE, C.J., MAYER, J., *Handbook of Modern Ion Beam Analysis*, 1st edn, Materials Research Society, Warrendale, PA (1995).

6. SUMMARIES AND DISCUSSION OF THE RESULTS OF THE ACCELERATOR SIMULATION AND THEORETICAL MODELLING OF RADIATION EFFECTS COORDINATED RESEARCH PROJECT

6.1. SUMMARIES OF PARTICIPANT SUBPROJECTS

Full and final reports of all participants of the SMoRE CRP are compiled on the accompanying CD-ROM. Brief summaries are given below.

ATOMIC LEVEL MODELLING AND MODELLING ORIENTED EXPERIMENTS IN Fe–Cr ALLOYS,
L. Malerba, G. Bonny, N. Castin, M. Lambrecht, D. Terentyev [Belgium]

Fe–Cr alloys are model materials suitable for the study of the processes governing radiation effects in high chromium ferritic–martensitic steels, which are candidate structural materials for several components of future nuclear reactors. This report overviews the work performed at SCK•CEN as a contribution to the SMoRE CRP, to develop multiscale models describing nanostructural evolution and radiation hardening processes in Fe–Cr alloys. The report is divided into four parts: (i) development of an advanced interatomic potential for Fe–Cr alloys suitable for radiation damage studies; (ii) application of the interatomic potential in MD simulations of dislocation–defect interactions; (iii) application of the interatomic potential in advanced AKMC models for thermal ageing simulations and calculation of diffusion coefficients of radiation defects; and (iv) PAS characterization of neutron irradiated Fe–Cr model alloys, as part of a programme of modelling oriented experiments.

**VERY HIGH DOSE IRRADIATION INDUCED RADIATION DAMAGE AND SYNERGISTIC
EFFECTS ON THE FORMATION OF VACANCY CLUSTERS IN CHINA LOW ACTIVATION
MARTENSITIC STEEL,** S. Zhu, Y. Zheng, Y. Zuo, D. Yuan, P. Fan, D. Zhou, Q. Zhang, B. Cui, L. Chen,
W. Jiang, Y. Wu, Q. Wang, L. Peng, X. Cao, B. Wang, L. Wei [China]

A triple beam irradiation facility, a double stop positron lifetime spectrometer with four LaBr₃ scintillation detectors and a coincidence Doppler broadening energy spectrometer have been established, which will play an important role in investigating radiation damage in nuclear energy structural materials. Simultaneous and sequential irradiations of gold, hydrogen and helium ions were performed on China low activation martensitic steel. The dose and temperature dependencies of radiation damage in the steel were measured after ion irradiation, and showed that the size of vacancy clusters increased with an increasing irradiation dose up to 85 dpa and that the variation of the vacancy cluster size with irradiation temperature peaked at ~500°C. The obtained results show clearly the synergistic effects of displacement damage and hydrogen and helium on the formation of radiation damage.

**SYNERGISTIC EFFECTS ON SWELLING IN MODEL FERRITIC STEELS UNDER HIGH DOSE
IRRADIATION,** A. Barbu, L. Beck, E. Bordas, D. Brimbail, B. Décamps, C.C. Fu, J. Henry, H. Martin,
E. Martinez, E. Meslin, S. Miro, Y. Serruys, P. Trocellier, F. Willaime [France]

This report presents the work performed by the Commissariat à l'énergie atomique (France) in the framework of the SMoRE CRP concerning model ferritic steels under irradiation. It is based, on the one hand, on irradiations using the Jannus multiple ion beam irradiation facility and subsequent structural characterization of ferritic steels (ranging from pure iron to ODS ferritic steels) and, on the other hand, on the multiscale modelling of Fe and model Fe–Cr alloys using ab initio methods and kinetic models.

MULTISCALE MODELLING OF THE MECHANICAL BEHAVIOUR OF Fe–Cr ALLOYS: FROM THE ATOMIC TO THE CONTINUUM LEVEL, G. Monnet, France, D. Terentyev [Belgium]

The results of a multiscale modelling of mechanical properties of Fe–Cr alloys starting from the atomistic level and ending with the continuum level are reported. The multiscale modelling scheme aims at the construction of a complete characterization of the material's behaviour in order to establish a crystalline law accounting for the available physical data. First, MD simulations were used to investigate the dislocation motion in Fe–Cr solid solution, varying the chromium content. These simulations enabled the determination of the critical stress for the motion of a dislocation as a function of chromium content and temperature. Second, the interaction of dislocations with chromium precipitates, induced by irradiation at elevated temperatures, was studied using MD and DD simulations. The applied multiscale simulation approach allowed MD results to be used directly in DD simulations to predict the corresponding strengthening in the range of experimental strain rates. This report shows how MD output can be used to determine: (i) the absolute resistance of a chromium precipitate as a function of its size and (ii) the thermal activation parameters enabling the introduction of temperature effects on dislocation unpinning. These results are then used in DD simulations to compute the strengthening associated with a random array of chromium precipitates. Results show strong effects of temperature and spatial distribution on the strengthening induced by chromium precipitates.

NUMERICAL MODELLING OF MECHANICAL BEHAVIOUR OF IRRADIATED STRUCTURAL MATERIALS: A MULTISCALE APPROACH, P.V. Durgaprasas, B.K. Dutta, R. Kapoor, A.K. Pawar [India]

A multiscale material modelling methodology has been used to understand the properties of irradiated materials, with a focus on ferritic–martensitic steels. The complete description of failure and its numerical modelling requires knowledge of length scales ranging from nano to meso to micro length scales. For the irradiated materials, there are other governing defects, such as irradiation induced defect clusters that control the motion of dislocations under external loads. At the atomic scale, the motion and interaction of dislocations with irradiation induced defects in Fe, Fe–Cr and Fe–Cr–He systems was studied using MD simulations. The output of MD simulations, such as friction stress and critical resolved shear stress, was passed on to the next higher length scale DD simulations. With the DD simulations, the flow stress for Fe and Fe–Cr alloys in the presence of voids and bubbles was determined. Finally, at the micro length scale, a combined numerical and experimental methodology showing the use of small punch tests is presented, which can be used to understand the fracture behaviour of irradiated materials. Small punch tests have been carried out on T91 material, and micromechanical Gurson parameters have been determined.

IRRADIATION TOLERANCE AND ION IRRADIATION EFFECTS ON NANO-OXIDE DISPERSION STRENGTHENED STEELS, A. Kimura [Japan]

The radiation tolerance of nano ODS steels was assessed by investigating phase stability and helium bubble formation behaviour under irradiation at elevated temperatures. Ion irradiation experiments were performed with 6.4 MeV iron ions at 650°C up to a nominal displacement damage of 60 dpa, which corresponded to 180 dpa at the peak position. Microstructural examinations were carried out using TEM and energy dispersive X ray analysis. No significant change in grains and grain boundaries, as well as morphologies of complex oxides, was detected after ion irradiation up to 60 dpa at 650°C. The complex oxides of the ODS steels were considered to be highly stable in the irradiation environment. Energy degraded helium ions were simultaneously implanted into the steels at 1000 appm. Microstructural observations showed that helium cavities formed on dislocations, precipitations, lath boundaries and prior austenitic boundaries in F82H implanted with 1000 appm helium. On the other hand, helium cavities were distributed in the matrix of 9Cr–ODS steel. It was found that oxide particles in the 9Cr–ODS steel acted as effective trapping sites for helium. Helium implantation was carried out by a cyclotron with a beam of 50 MeV α particles, up to 1000 appm at ~550°C. In the case of F82H, a ferritic–martensitic steel, the ductile–brittle transition temperature shift induced by the helium implantation was about 60°C, and the brittle fracture mode changed from cleavage to grain boundary fracture in the helium implanted area. In contrast, no ductile–brittle transition temperature shift or fracture mode change was observed in helium implanted 9Cr–ODS and 14Cr–ODS

steels. It can be concluded that the radiation tolerance of ODS steels stems from their high capacity for trapping point defects and defect clusters and also helium at interfaces of the oxide particles and the matrix. Fine dispersion morphology increased the interface area and therefore trapping sites, which may account for the observed radiation tolerance of the ODS steels.

SIMULATION OF NEUTRON DAMAGE EFFECTS IN EXPERIMENTS ON STEELS IRRADIATED WITH NEUTRONS OR KRYPTON IONS, O.P. Maksimkin [Kazakhstan]

Irradiation induced changes in microstructure, density and micro hardness of ferritic–martensitic steel 12Cr13Mo2NbVB, also designated as EP-450, were studied. The obtained results showed that radiation and thermal exposure led to phase recrystallization of this initially two-phase or duplex steel and also showed the dissolution of pre-existing carbides. As a result, optical micrographs showed an increase in volume fraction of ferrite with increasing irradiation temperature, with the volume fraction of ferrite increasing threefold compared to the unirradiated condition. Also observed were strongly correlated changes of density, micro hardness and irradiation induced swelling of steel, which showed maximum values at 380°C and 61 dpa. Investigations were then conducted on the stainless steel 12Cr18Ni10Ti in the original, strained and irradiated states using ^{84}Kr ions, $E=1.56$ MeV/nucleon, at doses of 1×10^{15} ions/m² and 4×10^{15} ions/m² using magnetometry, X ray structure analysis and scanning electron microscopy with electron backscatter diffraction analysis. Application of the electron backscatter diffraction technique allowed determination of the microstructural differences in non-irradiated and irradiated samples, especially the α phase and ϵ phase formed in the near surface layer.

COMPUTATIONAL AND EXPERIMENTAL APPROACH TO RADIATION EFFECTS ON Fe–Cr MODEL ALLOYS, J. Kwon, C. Shin, H.-H. Jin, Y. Lee [Republic of Korea]

Microstructural evolution of Fe–Cr model alloys irradiated by various particles was studied using an electron microscope, a positron annihilation technique and an atom probe. Also, changes in the mechanical properties were measured by a nano indentation test. Additionally, computer simulations were used to derive the damage mechanism due to irradiation. The simulation techniques included MD, MC methods, DD and FEMs. The methods developed in this work will enable prediction of the mechanical properties of alloys irradiated by any kind of radiation.

NON-DESTRUCTIVE CHARACTERIZATION OF OXIDE DISPERSION STRENGTHENED STEELS, V. Krsjak, Z. Szaraz, P. Hähner [Netherlands]

This report discusses the application of various non-destructive testing methods on the microstructural characterization of ODS steels with possible nuclear applications. Emphasis is put on a multi-technique approach and mutual correlation of results as well as on the validation and interpretation of the results obtained by destructive mechanical tests. The results of positron lifetime spectroscopy, small angle neutron scattering and thermoelectric power measurements on the thermally aged ODS steels are discussed. Interpretation of the results was based on previously published papers on nuclear structural materials, as well as on the preliminary TEM and X ray diffraction experiments performed in collaboration with the Nuclear Research Centre Negev, Israel.

INFLUENCE OF IRRADIATION EFFECTS ON THE MECHANICAL PROPERTIES OF AUSTENITIC STAINLESS STEEL, W. Szteke, J. Wasiak, W. Biłous, E. Hajewska, T. Wagner [Poland]

The influence of irradiation with heavy ions and electrons on the mechanical properties of stainless steel was studied. A small punch method was used in the experiments. It was found that the small punch method was not useful for specimens with thicknesses of only 0.05 mm. Good results were obtained for specimens with thicknesses of 0.25 mm. Whereas swift heavy ions were sufficient for penetration of 0.05 mm foils, the use of 0.25 mm foils

required the use of high energy electrons to conduct studies on radiation embrittlement. It was determined that the small punch method could be successfully applied to determine crack toughness of metals, but the technique was not very precise for evaluating tensile and yield strengths.

IRRADIATION OF STRUCTURAL MATERIALS BY HEAVY IONS AND THEORETICAL MODELLING OF SWELLING AND RADIATION INDUCED SEGREGATION PHENOMENA,

V. Pechenkin, Yu. Konobeev, V. Romanov, G. Lysova, A. Chernova, A. Dvoriashin, G. Epov, S. Obraztsov, K. Chernov, V. Molodtsov, V. Ryabov [Russian Federation]

RIS in alloy samples along the projected range of metal ions was modelled, accounting for the non-uniformity of the point defect generation rate. It was shown that RIS induces significant changes in alloy composition not only near the sample surface, but also in a wide region near the peak point defect generation rate. The sample regions with minimum changes in composition of austenitic and ferritic–martensitic steels were recommended for TEM investigation of microstructural evolution at high damage doses under 7 MeV Ni²⁺ and 1.8 MeV Cr³⁺ ion irradiations. MD calculations of self-interstitial atom diffusion coefficients as well as of iron and chromium atom self-diffusion coefficients in Fe–(5–25)Cr alloys at temperatures from 600 to 1000 K were performed. The interatomic potentials used indicate the possibility of matrix enrichment in chromium near point defect sinks via an interstitial mechanism in Fe–Cr alloys at chromium contents up to 15%.

INVESTIGATION OF THE PHYSICAL MECHANISMS OF RADIATION INDUCED PROCESSES IN STRUCTURAL MATERIALS FOR FISSION AND FUSION REACTORS USING ACCELERATORS OF CHARGED PARTICLES AND THEORETICAL MODELLING,

A.I. Ryazanov, O.K. Chugunov, V.S. Koidan, B.I. Khripunov, S.T. Latushkin, R. Lindau, A. Möslang, M.A. Petukhov, K.E. Prikhodko, E.V. Semenov, M.V. Sorokin, V.N. Unezhev, P. Vladimirov [Russian Federation and Germany]

This report reviews the contributions of the KI NRC to the SMoRE CRP. The main aim of the project was the joint theoretical and experimental investigation of the physical mechanisms of radiation induced processes in graphite materials, tungsten and ODS materials for fission and fusion reactors using fast charged particle irradiation in the cyclotron at KI NRC. Similar to fast neutron irradiation in atomic reactors, fast particle irradiation of materials in accelerators results in considerable changes of their physical and mechanical properties. Fast particles can be used for fast tests of new radiation resistance materials in the cyclotron at KI NRC. This report consists of three parts: (i) investigation of the changes in the physical–mechanical properties of tungsten and carbon materials after fast particle irradiation in the cyclotron at KI NRC, including irradiation by helium and carbon ions and investigation of the effects of high levels of radiation damage produced in these materials following their interaction with deuterium plasma; (ii) determination of the effects of irradiation and high concentrations of helium atoms (up to 1000 appm) on the microstructure and mechanical property changes of ODS materials after uniform helium implantation in the KI NRC cyclotron at energies up to 30 MeV; (iii) theoretical investigation of the stability and growth of precipitates in irradiated materials (Y–Ti–O particles) under neutron or charged particle irradiation at high irradiation doses, taking into account the generation rates of atomic collision cascades; and (iv) development of diatomic models for investigations of helium atom effects on helium bubbles and interstitial dislocation loop formation at low temperatures and high helium generation under irradiation, and of the theoretical models of helium bubble growth in irradiated materials, taking into account the growth kinetics of helium bubbles in the volume and on Y–Ti–O precipitates in ODS materials under high doses of neutron or charged particle irradiation.

DIFFERENT CHROMIUM CONTENT AND THERMAL ANNEALING INFLUENCES ON ION IMPLANTED

Fe–Cr MODEL ALLOYS, S. Sojak, V. Slugeň, V. Kršjak, W. Egger, L. Ravelli, M. Petriska, S. Stanček, M. Skarba, P. Priputen, K. Vitázek, M. Stacho, J. Veterníková, V. Sabelová [Slovakia]

Reduced activation ferritic–martensitic steels represented by binary Fe–Cr alloys, with different chromium contents, were studied in the as-received state, as well as after helium ion implantation. In order to study the

changes in dependence on temperature, thermal annealing of helium ion implanted Fe–11.62%Cr specimens was performed. Measurements taken by a pulsed low energy positron system were then performed at the Garching, Germany, campus of the Technische Universität München. Annealing out of defects at lower temperatures was not significant, as expected, and some uncertainties were present. Extensive decrease of the positron lifetime of defects was observed in specimens annealed at a temperature of 600°C.

STUDY OF RESIDUAL STRESS AND VACANCY DEFECTS IN OXIDE DISPERSION STRENGTHENED STEELS, V. Slugeň, J. Veterníková, S. Kilpeläinen, F. Tuomisto [Slovakia]

This study focused on commercial ODS steels — MA956 (20%Cr), ODM751 (16%Cr) and ODS Eurofer (9%Cr) — developed for fuel cladding of Generation IV reactors. The ODS steels are described in order to compare their microstructure features. Vacancy defects were observed by Doppler broadening spectroscopy and positron annihilation lifetime spectroscopy. Residual stress proportional to all types of defects was investigated by magnetic Barkhausen noise measurement. Doppler broadening spectroscopy results found the highest defect presence for ODS Eurofer. This was followed by MA956, and ODM751 demonstrated the lowest presence of defects. The positron annihilation lifetime spectroscopy measurements confirmed the Doppler broadening spectroscopy results. The lowest defect density belonged to ODM751, although these defects were the largest (three or four vacancy clusters). MA956 had two or three vacancies and ODS Eurofer had the highest defect density with two vacancies. Magnetic Barkhausen noise results were in good accordance with positron techniques. The highest residual stress was found for ODS Eurofer, followed by MA956, and the lowest residual stress proportional to hardness was found for ODM751.

DEFECT FORMATION AND BINDING ENERGIES IN Fe–Cr ALLOYS AS A FUNCTION OF Cr CONCENTRATION: A SIMULATION STUDY, E. Del Rio, J.M. Perlado [Spain]

Significant progress has been made in modelling the formation and stability of defects and clusters in Fe–Cr alloys as a function of chromium content. A new version of the concentration dependent model potential can be used in the study of defects in Fe–Cr alloys. Vacancy formation energy showed a linear dependence, with the concentration for concentrations above 6% between the vacancy formation energy in iron and the vacancy formation energy in chromium, while it was almost constant for smaller concentrations. Formation energies for <100>, <110> and <111> self- and mixed interstitials converged to a unique value with chromium concentration independently of the starting geometry. The <100> geometry was the most stable. A change in the stability of <110> interstitials was observed: Fe–Cr interstitial was more stable for concentrations below 5% chromium, while Fe–Fe was the most stable for concentrations above 10% chromium. The <110> Fe–Fe interstitial formation energy showed a very weak dependence on the chromium position. A strong dependence of the formation energy on the chromium position for the case of <110> Fe–Cr interstitials was observed, and could be explained by the strong repulsion between the two chromium atoms at short distances. This was the same for the vacancies. The stability of vacancy clusters increased with the cluster size for the studied sizes (up to five units), and it differed slightly between two potentials for higher chromium concentrations. However, binding energies were shown to be not dependent on the chromium concentration for both potentials.

EXPERIMENTAL STUDIES OF FUNDAMENTAL MATERIALS PROPERTIES AND IRRADIATION BEHAVIOUR USING SUBSIZED SAMPLES AND MICROTTESTING, M.A. Pouchon [Switzerland]

Micromechanical testing is a powerful method to address local features within a large sample, or to test subsized samples. In this report, two major aspects are elaborated on: the change in the mechanical properties of an ion beam irradiated surface layer and the extraction of single grains within a polycrystalline material with adjacent mechanical testing. In order to address the surface layer modification, existing data from single ion beam irradiated samples were treated in a new way. A new calculation method was envisaged in order to achieve a better understanding of the indenter response within shallow surface layers, as they appear in ion irradiations. This new

analysis was performed in collaboration with the Korea Atomic Energy Research Institute, which was developing models for finite element calculations. The data of two ODS ferritic steels were treated in such a way that the models could be validated. The validation is ongoing. The single grain mechanical characterization was performed on technical austenitic steels. If the grain orientation relative to the load is known, the relative slip plane angles are also known and the corresponding Schmid factor can be determined. Therefore, the critical resolved shear stress can be experimentally determined and compared to modelling results. The experimental technique applied for the single grain testing was the fabrication of micropillars, followed by mechanical testing using a nano indenter with a flat punch. Two austenitic steels were tested this way, and the corresponding data delivered to Électricité de France, where the corresponding DD models were validated.

SIMULATION AND STUDIES OF HIGH DOSE RADIATION DAMAGE IN CORE STRUCTURAL MATERIALS WITH THE USE OF CHARGED PARTICLE ACCELERATORS AND HIGH TECHNOLOGY INSTRUMENTATION, V. Voyevodin, V. Bryk, O. Borodin, A. Turkin, N. Lazarev, G. Tolstolutskaia [Ukraine]

Problems of life extension for working nuclear reactors and the development of new types of reactors require that much data on the behaviour of fuel and core structural materials under irradiation need to be obtained. As part of several basic materials science programmes, such data have been generated using charged particles accelerators. This report overviews the work performed at KIPT NSC as its contribution to the SMORE CRP, to carry out a comprehensive programme of simultaneous irradiation by self-ions and by helium and/or hydrogen ions of ferritic, ferritic–martensitic and austenitic steels. These alloys are attractive for use in advanced reactors, with work focusing on high doses, high temperatures and gas producing concepts. This report highlights three accomplishments: (i) the development and use of triple ion irradiation to study the simultaneous introduction of displacement damage, helium and hydrogen on void swelling of austenitic steel, and the application of the results to provide a predictive swelling equation for application to water cooled, water moderated power reactor internals; (ii) the demonstration that even in the absence of helium and hydrogen, ferritic–martensitic steel EP-450 and an ODS variant of the steel will swell significantly when irradiations are conducted to hundreds of dpa, but that ferrite grains begin to swell earlier than do tempered martensite grains; and (iii) the achievement of the results of some fundamental studies directed towards interaction and trapping of helium and hydrogen by radiation induced microstructural sinks.

ION BEAM IRRADIATIONS ON STRUCTURAL MATERIALS FOR NUCLEAR APPLICATION, P. Hosemann, S.A. Maloy, D. Kiener, E. Stergar, Y. Wang, M. Pouchon, C. Hofer, A.M. Minor [United States of America]

This report is a summary of all activities at the University of California at Berkeley and Los Alamos National Laboratory related to the SMORE programme. Results of the ion beam irradiations conducted are presented. The focus of this work was to perform ion beam irradiations on candidate structural materials, as well as on basic simple materials, in order to understand their effects, leading to a path forwards for using these techniques for accelerated materials testing and prescreening of materials that can be used in nuclear applications. The work presented is centred around small scale mechanical testing after irradiation to assess property changes on materials due to ion beam irradiation, properties which are needed for a comparison with neutron irradiation data. This testing allows investigation of the extent to which these novel techniques can be useful in the study of large neutron irradiated materials, so that more radioactive materials can be avoided, while acquiring additional data to enhance the statistical value. As a result of these activities, the University of California at Berkeley and Los Alamos National Laboratory began several national and international collaborations on this topic.

DUAL AND TRIPLE ION BEAM IRRADIATION OF Fe, Fe(Cr) AND Fe(Cr)–OXIDE DISPERSION STRENGTHENED STEEL, M.J. Fluss, L.L. Hsiung, J. Marian [United States of America]

The structures of nanoparticles in Fe–16Cr–4.5Al–0.3Ti–2W–0.37Y₂O₃(K3) and Fe–20Cr–4.5Al–0.34Ti–0.5Y₂O₃(MA956) ODS ferritic steels produced by mechanical alloying and followed by hot extrusion have been studied using HRTEM techniques to gain insight about the formation mechanism of nanoparticles in these ODS steels. Observations of Y–Al–O complex oxide nanoparticles in the ODS steels imply that Y₂O₃ decomposed during mechanical alloying along with internal oxidation of aluminium. While the majority of oxide nanoparticles formed in both steels comprises Y₄Al₂O₉, a few oxide particles of YAlO₃ were also occasionally observed. These results revealed that titanium (0.3 wt%) played an insignificant role in forming oxide nanoparticles in the presence of aluminium (4.5 wt%). HRTEM observations of crystalline nanoparticles larger than ~2 nm and amorphous or disordered cluster domains smaller than ~2 nm provided an insight into the formation mechanism of oxide nanoparticles in these ODS steels. The observations appeared to infer a solid state amorphous precursor followed by recrystallization. Dual ion beam irradiation using He⁺+Fe⁸⁺ ions were employed to gain detailed insight into the role of nanoparticles in suppressing radiation induced swelling. This was elaborated through TEM examinations of cavity distributions in ion irradiated Fe–14Cr and K3–ODS ferritic steels. HRTEM observations of helium filled cavities (helium bubbles), preferably trapped at nanoscale oxide particles and clusters in ion irradiated K3–ODS, are presented. Finally, the results of triple ion beam irradiation using H⁺+He⁺+Fe⁸⁺ ions to emulate fusion first wall radiation effects are described. Preliminary work is reported that confirms the existence of significant hydrogen synergistic effects described elsewhere for Fe(Cr) and for F82H reduced activation ferritic–martensitic steel. These previous results combined with data suggest a complex new catalytic mechanism whereby hydrogen interacts with the steady state population of defects and the embryonic cavities so as to accelerate cavity (void) growth in Fe(Cr) and, under special conditions, in ODS steels.

The work described above was performed in part under the auspices of the United States Department of Energy by Lawrence Livermore National Laboratory under contract DE-AC52-07NA27344.

6.2. DISCUSSION AND SUMMARY

6.2.1. Structural materials for present and future reactor designs: Trends and challenges

This discussion of the many varied activities and results featured in the reports summarized in the preceding section restates the situation and goals, though in a somewhat different manner than in the first chapter of this publication.

If the nuclear community is comfortable with the deployment of current, well-accepted, reactor technologies, primarily light water power generation units and sodium cooled fast reactors, then it must accept that these reactors will have their economic, lifetime and safety considerations determined by the weaknesses of the structural components that house the fuel and support the fuel assemblies, and not by the characteristics of the nuclear fuel itself. As fuel is the most expensive portion of the fuel assembly, it would be better economically to maximize its burnup. In previous or current operating fast reactors, the maximum burnup that can be attained reliably is 10–12%, which is limited primarily due to distortion, volume change and associated fragility arising from void swelling and irradiation creep of the austenitic steels used for cladding and structural materials.

However, from a neutronic limitation viewpoint, ~30% burnup of the fuel is an economically better target, extracting the most energy effectively before accumulating fission products at levels that interfere with further power generation. Such burnups, however, would require that structural alloys experience doses on the order of ~300 dpa and perhaps even higher.

Therefore, the challenge is not so much to improve the fuel as to decrease the vulnerability of the structural steels. A large amount of work has been directed towards incremental improvement of austenitic steels, especially with respect to their tendency to swell and creep under irradiation. All international fast reactor programmes basically reach a barrier at about 150 dpa, beyond which void swelling, swelling enhanced creep and swelling induced fragility become unmanageable. Moving to other reactor concepts involving different neutron spectra (LWRs, fusion, acceleration driven spallation) does not escape this barrier, and may actually move the barrier

downwards in dpa as a result of different flux spectra and the influence on dpa rate, transmutation and especially gas production.

Therefore, to overcome this barrier, it is necessary to use another material regime. After large amounts of irradiation testing, it has become clear that some classes of alloy were less suitable compared to austenitic alloys for high (or, in some cases, even low) neutron exposures, sometimes because they swelled more, but often because other forms of degradation arose, involving transmutation, radioactivation and, particularly, changes in mechanical properties, including other modes of radiation induced fragility not experienced by austenitic alloys. On this basis, for instance, all refractory alloys were found to be unsuitable because of their excessive embrittlement and ductile to brittle shift behaviour.

Towards the end of various Western and Asian LMR programmes, it became clear that while fcc iron based alloys were prone to void swelling, bcc iron based alloys were much more resistant to swelling and irradiation creep. However, the reactors in which this feature might be studied have been progressively decommissioned. Only in the Russian Federation, where the two fast reactors BOR-60 and BN-600 continue to operate, was it possible to prove successfully the use of bcc iron based alloys on a routine basis. Even in the Russian Federation, however, the maximum exposure reached in EP-450 alloy was ~160 dpa in BOR-60. In this case, swelling of several tenths of a per cent or less was observed, whereas fcc iron based alloys would display swelling on the order of several tens of a per cent at the same dose and temperature [6.1].

Therefore, the radiation materials community has moved to ferritic and ferritic–martensitic alloys, hoping that the swelling resistance can be extended to hundreds of dpa, but without any supporting reactor data. Additionally, ferritic and ferritic–martensitic alloys have a known weakness in that they rapidly lose strength in both thermal and radiation environments at temperatures well below the desired maximum temperatures associated with efficient power production. However, by developing ODS variants of these alloys, it is known that, at least in thermal environments, strength is maintained, and it is hoped that such strength will be retained during irradiation, but once again, there are very limited neutron data to support such an expectation.

It has also long been suggested that high densities of small dispersoids would suppress void swelling by acting as recombination centres for vacancies and interstitials. Additionally, it has been proposed that dispersoids in ODS alloys may serve as surface dominated sinks to collect and remove helium and hydrogen from the alloy matrix, thereby reducing the possibility of gas activated bubble promotion to active void growth.

6.2.2. Summary of overall results and the path forwards

So, where to go from here? The first phase of the SMoRE project proposed and pursued a path based on the use of surrogate irradiation devices, primarily the path of charged particle irradiation at highly accelerated displacement rates relative to those experienced in fast reactors. It also focused on ferritic, ferritic–martensitic and ODS variants thereof, where there were insufficient or no neutron data for ion–neutron comparisons.

Knowing that there are serious deficiencies in knowledge, both for accelerated charged particle testing and the basic processes of radiation induced alteration in bcc iron based alloys, the SMoRE CRP addressed these deficiencies head on. This was done with some confidence based on the earlier, often successful use of charged particle irradiation of fcc iron based alloys in the US LMR programme, where many trends of swelling and embrittlement with composition and fabrication variables were observed in neutron data.

The SMoRE CRP activities in the first phase therefore involved the following seven categories of studies and activities:

- (1) Use of new studies involving neutron irradiation to rather low doses, concentrating on simple model alloys that exhibit responses at very low doses. Fundamental rather than technological data were sought here.
- (2) Developing new tools and expanding the use of existing tools that are capable of extracting the data needed in interpretation of low fluence neutron data, and then applying these tools to ion generated data.
- (3) As ion irradiation involves a very small volume of material with potentially significant perturbations associated with such small volumes, SMoRE sought to optimize the tools developed in item (2), above, to be compatible with ion studies. Such optimization should address not only fundamental physical and chemical properties, but also void swelling and irradiation induced fragility issues arising at higher damage exposures.
- (4) As ion irradiations have some features that are atypical of the neutron environment, attention must be and was paid to such features, especially cascade characteristics, damage versus depth distributions, surface

effects and injected interstitial effects, in order to confidently apply ion data to neutron predictions. Another issue addressed in this category was the phase evolution that proceeded at such vastly different dpa rates and therefore at different timescales. This is important because phase evolution determines the eventual matrix composition, and thereby the onset of swelling and sometimes fragility arising from phase instabilities.

- (5) Use of ion irradiations at moderately low doses to study important physical properties involving the stability of naturally occurring and radiation induced phases, as well as various oxide dispersoids, focusing not only on irradiation induced direct damage, but also on the effect of transmutant gases helium and hydrogen.
- (6) Use of ion irradiation to explore material responses to the very high doses required for extended service, focusing especially on technological issues such as void swelling and changes in physical and mechanical properties, especially strengthening and fragility.
- (7) As there are rather large unknowns in conducting the above studies, modelling played a very large and significant role in the SMORE CRP, to help bridge knowledge gaps. Modelling was conducted in a number of categories, ranging from fundamental defect production, defect transport and agglomeration, and elemental segregation, followed by processes involving defect structure interaction to produce swelling, creep, strengthening, fragility and phase stability. Additionally, modelling was required to address the effect of the atypical variables cited in item (4), above, and to assess the effects of specimen size to allow the development of size effects and the property–property correlations needed for application of SMORE produced data to reactor environments. The wide range of modelling efforts and their utility to SMORE objectives is well demonstrated in this publication and the contributed reports of the subprojects (see Section 6.1 and accompanying CD-ROM).

6.3. CONCLUSIONS AND RECOMMENDATIONS

6.3.1. Assessment of the results

Nineteen separate laboratories and several consultants contributed to this CRP (see accompanying CD-ROM), producing large amounts of insight and data, as well as raising new questions to be addressed in ongoing and future efforts. Most laboratories addressed more than one of the seven categories of studies listed in Section 6.2.2, thereby providing the first stage of linkages necessary to successfully apply surrogate ion irradiations to a reliable reactor application. Most important, however, are the extended linkages and collaborations developed by various subsets of participants in the SMORE community, allowing faster overall progress as a community in meeting its goal.

While it would be impractical to discuss all of the various results of the SMORE CRP in this section, there were some common features and significant derived insights that demonstrate the cumulative value of the results of the activities listed in this main report and the accompanying CD-ROM:

- The development of experimental analytical tools capable of exploring fundamental properties of Fe–Cr alloys, both model and complicated commercial and ODS variants, especially in very small volumes of unirradiated and irradiated specimens, appears to be making significant progress and warrants continued future emphasis and funding by supporting entities of the various SMORE participants.
- The miniaturization of various mechanical property tests appears to be making progress, establishing boundaries for confident testing and understanding of the effects of specimen size, orientation, etc., that are necessary to develop size effects and property–property correlations for use of shear punch, small punch and minitensile tests. In particular, micropillar activities at several laboratories offer the promise of determining fundamental properties, also with some promise of providing input on trends to be expected in engineering properties on larger specimens and higher doses. However, additional improvement of these techniques will be required before the results of such techniques are accepted by the engineering community.
- Experimental efforts generating neutron and ion data, and several of the modelling efforts, indicate that the simple Fe–Cr system is rather more complex than that of the simple fcc Fe–Cr–Ni system, especially in the composition dependence of point defect production, migration, segregation and microstructural interaction over the 0–14% range of chromium. In particular, the issue of chromium influence on magnetic properties, with an impact on point defect behaviour, also appears to need further addressing. Additional experimental and modelling activity is required to move forwards in this area.

- Some ion irradiation facilities have been developed that are capable of addressing both fundamental and technological questions relevant to SMORE activity. Some operate at relatively low dose rates, suitable for addressing fundamental issues, and others operate at higher dose rates where swelling and fragility issues become paramount. Most importantly, most of these facilities involve dual or triple beam systems to study the separate and synergistic effects of both helium and hydrogen in order to cover a wide range of reactor concepts. These facilities continue to evolve in their capabilities, but additional support is required.
- Several of the experimental and modelling studies draw attention to the stability of the ODS dispersoids during irradiation. There appear to be processes operating that are related to radiation induced amorphization and self-healing, apparently dependent on the initial state of the dispersoid, how it was produced and various compositional influences. It also appears that the introduction of hydrogen may interact with the surface of the dispersoid in a chemical sense to produce compounds, rather than just acting as a gas to be sequestered. Experimental observations also support the role of dispersoids as gas collection devices that might restrict the onset of swelling. More studies are required in this area, especially as new ODS alloy concepts are developed.
- Several modelling efforts also appear to support the role of dispersoids serving as collection centres for both point defects and gas atoms, providing confidence that dispersoids will not only strengthen the alloy at high temperatures, but also delay the onset of swelling and the swelling acceleration of creep.
- The suppression of swelling in ODS alloys by dispersoids requires that they be uniformly distributed on a scale that is commensurate with the diffusion lengths of point defects and gases, or there will be no benefit to retarding the swelling. Examples of ion induced swelling of ODS alloy MA957 shown in Chapter 2 clearly demonstrate in one non-homogeneously distributed heat that ODS distribution is a critical criterion. Otherwise, swelling in low density dispersoid grains surges to very high levels. In another heat of MA957, with better dispersoid distribution, the swelling was significantly delayed, but was not totally suppressed. This work also showed that other microstructural features arising from dispersoid introduction, such as to produce a finer and elongated grain structure, can have an impact on void swelling, namely via grain boundary denuded zones to suppress swelling locally.
- The high dose (100–600 dpa) ion results shown in Chapters 2 and 3 have provided some of the most exciting data from this CRP. It was shown that swelling of ferritic and ferritic–martensitic alloys and their ODS variants can occur even in the absence of gas introduction, and that gas addition does indeed accelerate the onset of swelling, at least in alloy EP-450. It was also shown that swelling follows a bilinear or steady state after incubation behaviour, with an eventual steady state swelling rate of $\sim 0.2\%/dpa$, a rate that was previously predicted in earlier neutron studies on Fe–Cr binary alloys. Most importantly, it was possible to reach swelling levels in ferritic–martensitic alloys that are as high as 20–30% before the ion irradiation was terminated. This latter finding indicates that although swelling can be delayed and will proceed at lower rates, it cannot be suppressed forever, thereby remaining a limitation on damage exposure.
- One very encouraging result of the 100–600 dpa studies was that there is definitely a chemical and structural dependence of the transient duration of swelling. In Russian duplex alloy EP-450, the ferrite grains started to swell much earlier than the adjacent tempered martensite grains. Also, various heats of HT9 appeared to have different transient durations for both ferrite and tempered martensite grains. This inspires confidence that composition and fabrication modifications will allow optimization of the swelling resistance, and that such modification can be studied effectively using ion irradiation.
- Several studies addressed the stability and distribution of dispersoids. This is an area that deserves increased attention, because, currently, most ODS alloys put dispersoids into a ferrite matrix, and not into a tempered martensite matrix. As shown in EP-450, tempered martensite presents the first line of defence to resist swelling; this line of defence has been abandoned in a ferrite only alloy, requiring that dispersoids carry all the weight in determining the swelling resistance. Future studies should concentrate on dispersoids in tempered martensite as a potential improvement in alloy design.
- Finally, several researchers in the SMORE CRP addressed new variants of ODS alloys, paving the way to explore, with ion irradiation, a wide field of compositional and structural space to reach high dpa levels with increasing radiation tolerance. These alloys should be irradiated as soon as possible to identify the path forwards for future SMORE activities.

6.3.2. Recommendations for future activities

The distinguishing features of the SMoRE CRP are the wide diversity of techniques, skills and laboratories involved, and the high levels of integration and cooperation. However, given the long term time horizon of the SMoRE objective, this CRP is not a stand-alone, completed project. It should be continued in some form to provide a platform upon which to ensure that the advances and insights attained are preserved and extended. No country or group of countries can fully provide or cover the large range of interactive prospects addressed by the SMoRE CRP.

In addition to continuing progress towards the long term goal of providing credible candidate alloys for high exposure reactor service, there are some areas where improvements could be made:

- The programme's accomplishments should be aggressively promoted with a view to providing additional resources for some of the participating laboratories with sparse funding opportunities. In particular, the very high dpa rates attainable at KIPT represent one of the most valuable resources, but are being conducted in an ageing facility that needs upgrades and enhanced ancillary equipment for data extraction. Such promotion can also be focused on creating new facilities or upgrading existing accelerator laboratories, especially in universities, to increase opportunities to produce additional data. The currently available ion irradiation facilities may be adequate for the beginning stages of SMoRE activities, but will soon be insufficient to meet the inevitably growing demand for ion irradiation.
- There is a need to expand participation in SMoRE follow-on efforts in two subject matter areas. In particular, the involvement of experts in earlier fast reactor irradiation programmes and in charged particle studies conducted in now discontinued national programmes is required. These experts are largely retired persons located in Japan, the Russian Federation and the United States of America, who can bring a wider perspective to the neutron side of SMoRE activities, especially in the engineering rather than solely scientific aspects of the SMoRE long term goals.
- Stronger emphasis needs to be placed on developing further the mechanics of ion irradiation, especially addressing details of beam current, rastering or stationary beams, dose definition and choice of volumes from which to confidently extract data.
- The IAEA might consider using its capabilities to facilitate wider international access to some facilities where neutron irradiation can still be conducted at relatively high dpa rates. Existing facilities such as BN-600 are not easily accessed in competition with their power producing mission, but might be able to make space available if national and international interests are addressed. The national fast reactor programmes of India and China might be encouraged to host international collaborations in their reactors. The soon to be operated/built fast reactor facilities in the Russian Federation, especially the Multipurpose Fast-neutron Research Reactor (MBIR), BN-800 and BREST, could be made more available within IAEA CRPs or other initiatives such as international centres of excellence, which are being planned now.
- Some of the issues restricting acceptance of ion data are related to the very different timescales for phase evolution in reactor and accelerator irradiations. These issues cannot be addressed in accelerators alone, but a hybrid approach employed in earlier fast reactor studies should be encouraged. This approach involved the use of previously reactor irradiated specimens for continued irradiation with ion beams. Such specimens were referred to as being *neutron preconditioned* and had the advantage that the majority of the segregation and phase evolution was well under way and more closely representative of the neutron case before the ion beam was turned on. While perhaps not possessing completely the correct microstructure, the results using such specimens will produce data that are much closer to the right answer.

Such an approach requires facilities and protocols that will allow the use of radioactive material in previously non-radioactive material facilities, although some laboratories, including several participants in the SMoRE CRP, can currently conduct such experiments involving radioactive specimens. With the encouragement of the IAEA and other international entities, the number of such facilities might be expanded.

REFERENCE TO CHAPTER 6

- [6.1] POVSTYANKO, A.V., FEDOSEEV, A.Ye., MAKAROV, O.Yu., PROKHOROV, V.I., “A study of four experimental fuel subassemblies using EP-450 FM pin claddings and hexagonal ducts after irradiation to 108–163 dpa in the BOR-60 reactor”, Proc. 2010 American Nuclear Society Winter Mtg, Las Vegas, NV (2010).

Annex

CONTENTS OF THE ATTACHED CD-ROM:

REPORTS FROM THE INDIVIDUAL COORDINATED RESEARCH PROJECT MEMBER ORGANIZATIONS

The case studies in the Annex have been prepared from the original material as submitted for publication and have not been edited by the editorial staff of the IAEA. The case studies remain true to the original reports submitted by the Member State.

The contents of the CD-ROM are available on the IAEA Publications web site. To download, please visit www-pub.iaea.org/books/IAEABooks

ATOMIC-LEVEL MODELLING AND MODELLING-ORIENTED EXPERIMENTS IN Fe–Cr ALLOYS

L. Malerba, G. Bonny, N. Castin, M. Lambrecht, D. Terentyev

VERY HIGH DOSE IRRADIATION INDUCED RADIATION DAMAGE AND SYNERGISTIC EFFECT ON FORMATION OF VACANCY CLUSTERS IN CLAM

Shengyun Zhu, Yongnan Zheng, Yi Zuo, Daqing Yuan, Ping Fan, Dongmei Zhou, Qiaoli Zhang, Baoqun Cui, Lihua Chen, Weisheng Jiang, Yican Wu, Qunying Wang, Lei Peng, Xinzhong Cao, Baoyi Wang, Long Wei

SYNERGISTIC EFFECTS ON SWELLING IN MODEL FERRITIC STEELS UNDER HIGH-DOSE IRRADIATION

A. Barbu, L. Beck, E. Bordas, D. Brimbal, B. Décamps, C.C. Fu, J. Henry, H. Martin, E. Martinez, E. Meslin, S. Miro, Y. Serruys, P. Trocellier, F. Willaime

MULTISCALE MODELLING OF MECHANICAL BEHAVIOUR OF Fe–Cr ALLOYS: FROM THE ATOMIC TO THE CONTINUUM LEVEL

G. Monnet, D. Terentyev

NUMERICAL MODELLING OF MECHANICAL BEHAVIOUR OF IRRADIATED STRUCTURAL MATERIALS: A MULTI-SCALE APPROACH

P.V. Durgaprasas, B.K. Dutta, R. Kapoor, A.K. Pawar

IRRADIATION TOLERANCE AND ION-IRRADIATION EFFECTS ON NANO-OXIDE DISPERSION STRENGTHENED STEELS

A. Kimura

SIMULATION OF NEUTRON DAMAGE EFFECTS IN EXPERIMENTS ON STEELS IRRADIATED WITH NEUTRONS OR KRYPTON IONS

O.P. Maksimkin

COMPUTATIONAL AND EXPERIMENTAL APPROACH TO RADIATION EFFECTS ON Fe–Cr MODEL ALLOYS

J. Kwon, C. Shin, H-H. Jin, Y. Lee

NON-DESTRUCTIVE CHARACTERIZATION OF OXIDE DISPERSION STRENGTHENED STEELS

V. Krsjak, Z. Szaraz, P. Hähner

INFLUENCE OF IRRADIATION EFFECTS ON MECHANICAL PROPERTIES OF AUSTENITIC STAINLESS STEEL

W. Szteke, J. Wasiak, W. Biłous, E. Hajewska, T. Wagner

IRRADIATION OF STRUCTURAL MATERIALS BY HEAVY IONS AND THEORETICAL MODELLING OF SWELLING AND RADIATION-INDUCED SEGREGATION PHENOMENA

V. Pechenkin, Yu. Konobeev, V. Romanov, G. Lysova, A. Chernova, A. Dvoriashin, G. Epov, S. Obraztsov, K. Chernov, V. Molodtsov, V. Ryabov

INVESTIGATION OF PHYSICAL MECHANISMS OF RADIATION-INDUCED PROCESSES IN STRUCTURAL MATERIALS FOR FISSION AND FUSION REACTORS USING ACCELERATORS OF CHARGED PARTICLES AND THEORETICAL MODELING

A.I. Ryazanov, O.K. Chugunov, V.S. Koidan, B.I. Khripunov, S.T. Latushkin, R. Lindau, A. Möslang, M.A. Petukhov, K.E. Prikhodko, E.V. Semenov, M.V. Sorokin, V.N. Unezhev, P. Vladimirov

EXAMINATION OF Fe–Cr BINARY AND ODS ALLOYS BY POSITRON ANNIHILATION SPECTROSCOPY AND OTHER TECHNIQUES

V. Slugeň

PAPER 1. DIFFERENT CHROMIUM CONTENT AND THERMAL ANNEALING INFLUENCE ON ION IMPLANTED Fe–Cr MODEL ALLOYS

S. Sojak, V. Slugeň, V. Kršjak, W. Egger, L. Ravelli, M. Petriska, S. Stanček, M. Skarba, P. Priputen, K. Vitázek, M. Stacho, J. Veterníková, V. Sabelová

PAPER 2. STUDY OF RESIDUAL STRESS AND VACANCY DEFECTS IN OXIDE DISPERSION STRENGTHENED STEELS

V. Slugeň, J. Veterníková, S. Kilpeläinen, F. Tuomisto

DEFECT FORMATION AND BINDING ENERGIES IN Fe–Cr ALLOYS AS A FUNCTION OF Cr CONCENTRATION: A SIMULATION STUDY

E. Del Rio, J.M. Perlado

EXPERIMENTAL STUDIES OF FUNDAMENTAL MATERIALS PROPERTIES AND IRRADIATION BEHAVIOR USING SUB-SIZED SAMPLES AND MICRO-TESTING

M.A. Pouchon

SIMULATION AND STUDIES OF HIGH DOSE RADIATION DAMAGE IN CORE STRUCTURAL MATERIAL WITH THE USE OF CHARGE PARTICLE ACCELERATORS AND HIGH-TECH INSTRUMENTATION

V. Voyevodin, V. Bryk, O. Borodin, A. Turkin, N. Lazarev, G. Tolstolutsкая

ION BEAM IRRADIATIONS ON STRUCTURAL MATERIALS FOR NUCLEAR APPLICATION

P. Hosemann

DUAL AND TRIPLE ION-BEAM IRRADIATIONS OF Fe, Fe(Cr) AND Fe(Cr)–ODS FINAL REPORT: IAEA SMORE CRP#

M.J. Fluss, L.L. Hsiung, J. Marian

ABBREVIATIONS

AISI	American Iron and Steel Institute
AKMC	atomistic kinetic Monte Carlo
ATR	advanced test reactor
bcc	body centred cubic
CRP	coordinated research project
DD	dislocation dynamics
DFR	Dounreay Fast Reactor
DFT	density functional theory
dpa	displacements per atom
EBR	Experimental Breeder Reactor
fcc	face centred cubic
FEM	finite element method
FFTF	Fast Flux Test Facility
FIB	focused ion beam
HFIR	High Flux Isotope Reactor
HRTEM	high resolution transmission electron microscopy
HVEM	high voltage electron microscope
ITER	International Thermonuclear Experimental Reactor
KI NRC	Kurchatov Institute National Research Center
KIPT	Kharkov Institute of Physics and Technology
KIPT NSC	Kharkov Institute of Physics and Technology National Science Center
LEAP	local electrode atom probe
LMR	liquid metal reactor
LWR	light water reactor
MBIR	Multipurpose Fast-neutron Research Reactor
MC	Monte Carlo
MD	molecular dynamics
MMC	Metropolis Monte Carlo
ODS	oxide dispersion strengthened
PAS	positron annihilation spectroscopy
PFR	Prototype Fast Reactor
PIE	post-irradiation examination
RBS	Rutherford backscattering spectroscopy
RIS	radiation induced segregation
SMoRE	Accelerator Simulation and Theoretical Modelling of Radiation Effects

SRIM	Stopping and Range of Ions in Matter
STEM	scanning transmission electron microscopy
2-D	two dimensional
3-D	three dimensional
3-DAP	three dimensional atom probe
TEM	transmission electron microscopy
TOF	time of flight

CONTRIBUTORS TO DRAFTING AND REVIEW

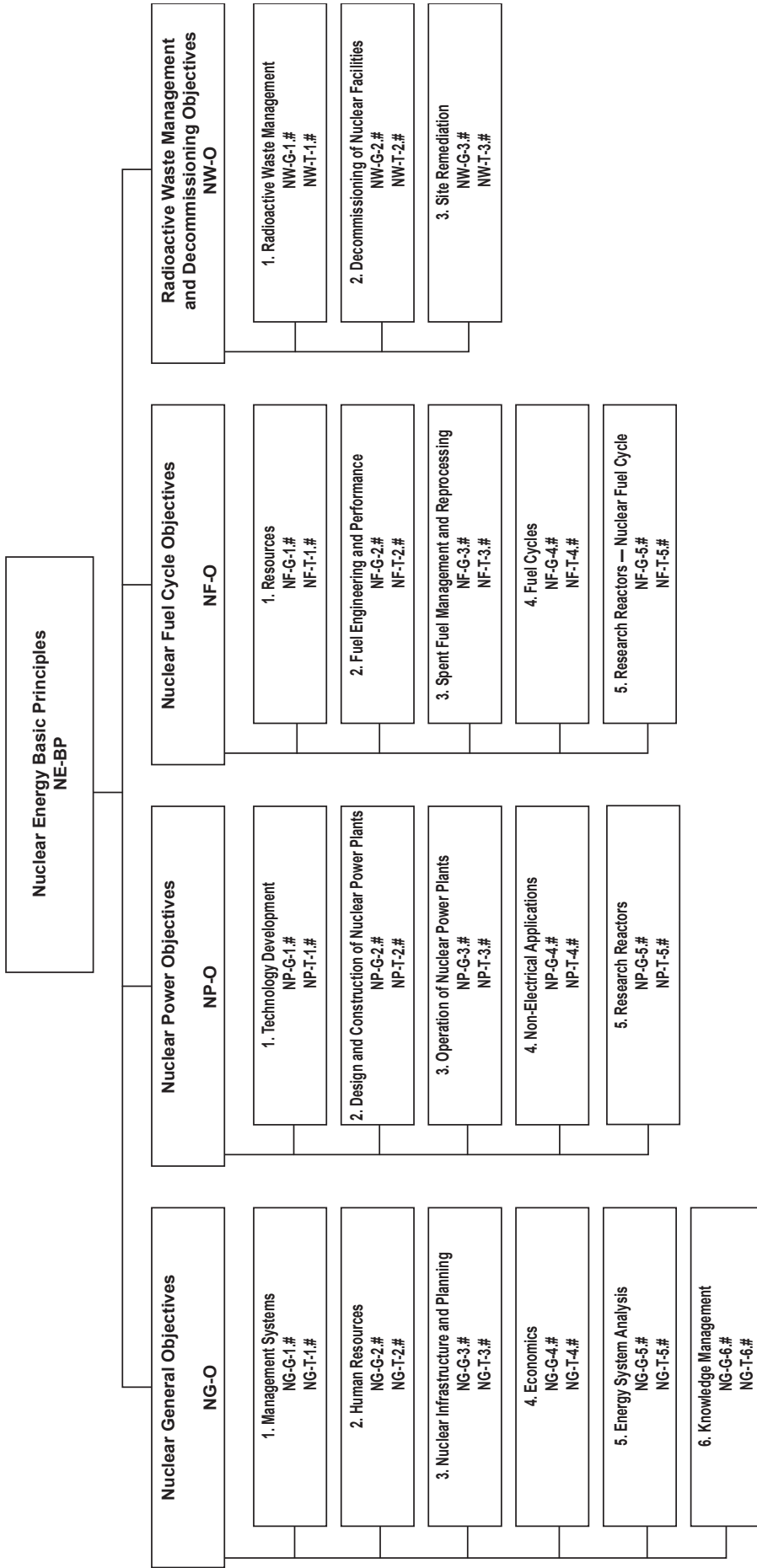
Del Rio, E.	Technical University of Madrid, Spain
Durgaprasad, P.	Bhabha Atomic Research Centre, India
Fluss, M.	Lawrence Livermore National Laboratory, United States of America
Garner, F.	Radiation Effects Consulting, United States of America
Hosemann, P.M.	Los Alamos National Laboratory, United States of America
Kimura, A.	Kyoto University, Japan
Kwon, J.	Korea Atomic Energy Research Institute, Republic of Korea
Maksimkin, O.	National Nuclear Center, Kazakhstan
Malerba, L.	Belgian Nuclear Research Centre, Belgium
Monnet, G.	Électricité de France, France
Pechenkin, V.	State Scientific Center of the Russian Federation, Russian Federation
Pouchon, M.A.	Paul Scherrer Institute, Switzerland
Ryazanov, A.	Kurchatov Institute, Russian Federation
Sojak, S.	Slovak University of Technology in Bratislava, Slovakia
Szteke, W.	Institute of Atomic Energy, Poland
Voyevodin, V.	Kharkov Institute of Physics and Technology, Ukraine
Willaime, F.	Commissariat à l'énergie atomique, France
Zhu, S.	China National Nuclear Corporation, China

Research Coordination Meetings

Vienna, Austria: 25–28 November 2008; 28 November–2 December 2011

Paris, France: 31 May–4 June 2010

Structure of the IAEA Nuclear Energy Series



Key

- BP:** Basic Principles
- O:** Objectives
- G:** Guides
- T:** Technical Reports
- Nos 1-6:** Topic designations
- #:** Guide or Report number (1, 2, 3, 4, etc.)

Examples

- NG-G-3.1:** Nuclear General (NG), Guide, Nuclear Infrastructure and Planning (topic 3), #1
- NP-T-5.4:** Nuclear Power (NP), Report (T), Research Reactors (topic 5), #4
- NF-T-3.6:** Nuclear Fuel (NF), Report (T), Spent Fuel Management and Reprocessing (topic 3), #6
- NW-G-1.1:** Radioactive Waste Management and Decommissioning (NW), Guide, Radioactive Waste (topic 1), #1



ORDERING LOCALLY

In the following countries, IAEA priced publications may be purchased from the sources listed below or from major local booksellers.

Orders for unpriced publications should be made directly to the IAEA. The contact details are given at the end of this list.

CANADA

Renouf Publishing Co. Ltd

22-1010 Polytek Street, Ottawa, ON K1J 9J1, CANADA
Telephone: +1 613 745 2665 • Fax: +1 643 745 7660
Email: order@renoufbooks.com • Web site: www.renoufbooks.com

Bernan / Rowman & Littlefield

15200 NBN Way, Blue Ridge Summit, PA 17214, USA
Tel: +1 800 462 6420 • Fax: +1 800 338 4550
Email: orders@rowman.com Web site: www.rowman.com/bernan

CZECH REPUBLIC

Suweco CZ, s.r.o.

Sestupná 153/11, 162 00 Prague 6, CZECH REPUBLIC
Telephone: +420 242 459 205 • Fax: +420 284 821 646
Email: nakup@suweco.cz • Web site: www.suweco.cz

FRANCE

Form-Edit

5 rue Janssen, PO Box 25, 75921 Paris CEDEX, FRANCE
Telephone: +33 1 42 01 49 49 • Fax: +33 1 42 01 90 90
Email: formedit@formedit.fr • Web site: www.form-edit.com

GERMANY

Goethe Buchhandlung Teubig GmbH

Schweitzer Fachinformationen
Willstätterstrasse 15, 40549 Düsseldorf, GERMANY
Telephone: +49 (0) 211 49 874 015 • Fax: +49 (0) 211 49 874 28
Email: kundenbetreuung.goethe@schweitzer-online.de • Web site: www.goethebuch.de

INDIA

Allied Publishers

1st Floor, Dubash House, 15, J.N. Heredi Marg, Ballard Estate, Mumbai 400001, INDIA
Telephone: +91 22 4212 6930/31/69 • Fax: +91 22 2261 7928
Email: alliedpl@vsnl.com • Web site: www.alliedpublishers.com

Bookwell

3/79 Nirankari, Delhi 110009, INDIA
Telephone: +91 11 2760 1283/4536
Email: bkwell@nde.vsnl.net.in • Web site: www.bookwellindia.com

ITALY

Libreria Scientifica "AEIOU"

Via Vincenzo Maria Coronelli 6, 20146 Milan, ITALY
Telephone: +39 02 48 95 45 52 • Fax: +39 02 48 95 45 48
Email: info@libreriaaeiou.eu • Web site: www.libreriaaeiou.eu

JAPAN

Maruzen-Yushodo Co., Ltd

10-10 Yotsuyasakamachi, Shinjuku-ku, Tokyo 160-0002, JAPAN
Telephone: +81 3 4335 9312 • Fax: +81 3 4335 9364
Email: bookimport@maruzen.co.jp • Web site: www.maruzen.co.jp

RUSSIAN FEDERATION

Scientific and Engineering Centre for Nuclear and Radiation Safety

107140, Moscow, Malaya Krasnoselskaya st. 2/8, bld. 5, RUSSIAN FEDERATION
Telephone: +7 499 264 00 03 • Fax: +7 499 264 28 59
Email: secnrs@secnrs.ru • Web site: www.secnrs.ru

UNITED STATES OF AMERICA

Bernan / Rowman & Littlefield

15200 NBN Way, Blue Ridge Summit, PA 17214, USA
Tel: +1 800 462 6420 • Fax: +1 800 338 4550
Email: orders@rowman.com • Web site: www.rowman.com/bernan

Renouf Publishing Co. Ltd

812 Proctor Avenue, Ogdensburg, NY 13669-2205, USA
Telephone: +1 888 551 7470 • Fax: +1 888 551 7471
Email: orders@renoufbooks.com • Web site: www.renoufbooks.com

Orders for both priced and unpriced publications may be addressed directly to:

Marketing and Sales Unit
International Atomic Energy Agency
Vienna International Centre, PO Box 100, 1400 Vienna, Austria
Telephone: +43 1 2600 22529 or 22530 • Fax: +43 1 26007 22529
Email: sales.publications@iaea.org • Web site: www.iaea.org/books

**INTERNATIONAL ATOMIC ENERGY AGENCY
VIENNA
ISBN 978-92-0-107415-7
ISSN 1995-7807**